Drosophila as a tool to identify genes and mechanisms involved in Amyotrophic Lateral Sclerosis

Andrea Ying Ying Chai

Thesis presented for the degree of Doctor of Philosophy

University of Edinburgh

2009

Declaration

I declare that this thesis and the work described in it is my own except where indicated and have not been submitted for any other degree.

Andrea Chai

August 2009

Acknowledgements

First and foremost, I offer my sincerest gratitude to my supervisor, Dr Giusy Pennetta, who has supported me throughout my Masters and Ph.D with her patience and knowledge. Above all, I am thankful for her encouragement and unflinching support both personally and professionally. Her scientific intuition and passion for science has made the past five years a truly enriching experience. I am indebted to her more than she knows and one simply could not wish for a better or friendlier supervisor

In my daily work, I have been blessed with a friendly and cheerful group of colleagues and I would like to thank all past and present members of the lab for their advice, technical help and encouragement. Among all, I am especially thankful to Kat Parry, Bin Yu and Hayley Patterson.

I would like to acknowledge Prof. Vivian Budnik and Dr. Young Ho Koh for performing the Ultrastructural analysis, Drs Bing Zhang and Giusy Pennetta for performing the electrophysiological analysis and Kat Parry for sharing the yeast two hybrid data. I also thank Steve Mitchell for his help with the SEM and the Scottish Motor Neurone Disease Association for funding this project.

A special thank you to James Withers for designing the eye quantification software, advice on statistical analysis and help with the morphometric analysis. I really appreciate his patience and for being ever so supportive.

Finally, I would like to thank my family, especially my parents for their love and unwavering support, my siblings for putting up with my idiosyncrasies and our family dog, Snow White for just being the great family pet that she is.

This thesis is dedicated to my grandfather.

Abstract

Motor neuron diseases (MNDs) are progressive neurodegenerative disorders characterized by selective death of motor neurons leading to spasticity, muscle wasting and paralysis. Human VAMP-associated protein B *(hVAPB)* is the causative gene of a clinically diverse group of MNDs including amyotrophic lateral sclerosis (ALS), atypical ALS and late-onset spinal muscular atrophy. The pathogenic mutation is inherited in a dominant manner. *Drosophila* VAMP-associated protein of 33 kDa A (DVAP-33A) is the structural homologue of hVAPB and regulates synaptic remodeling by affecting the size and number of boutons at neuromuscular junctions (NMJs). Associated with these structural alterations are compensatory changes in the physiology and ultrastructure of synapses, which maintain evoked responses within normal boundaries. *DVAP-33A* and *hVAPB* are functionally interchangeable and transgenic expression of mutant DVAP-33A in neurons recapitulates major hallmarks of the human disease including locomotion defects, neuronal death and aggregate formation. Aggregate accumulation is accompanied by a depletion of the endogenous protein from its normal localization. These findings pinpoint to a possible role of hVAPB in synaptic homeostasis. To elucidate the patho-physiology underlying motor neuron degeneration in humans, we also generated a *Drosophila* model of ALS8 in the adult eye. Targeted expression of mutant DVAP-33A in the *Drosophila* compound eye causes a degenerative phenotype characterized by a smaller eye containing missing or aberrantly oriented bristles and fused ommatidia. In a F1 deficiency screen, we performed a genome-wide survey aimed at identifying enhancers and suppressors of the degenerative eye phenotype. Several interacting regions have been found and the identification of these interacting genes will shed new light on the molecular mechanisms underlying VAP-induced ALS.

Table of Contents

List of Figures

List of Tables

Abbreviations

25OH	25-hydroxycholesterol
Aβ	β-Amyloid
AD	Alzheimer's Disease
ALS	Amyotrophic Lateral Sclerosis
AOA2	Autosomal recessive ataxia-oculomotor apraxia 2
APP	Amyloid precursor protein
AR-JP	Autosomal recessive juvenile parkinsonism
Arf1	ADP-ribosulation factor 1
BMP	Bone morphogenetic protein
Bnb	Bangles and beads
CBP	CREB binding protein
CCS	Copper chaperone for SOD1
Cdk-5	Cyclin-dependent kinase-5
CERT	Ceramide transfer protein
CRAL-TRIO	Cellular retinaldehyde-binding/triple function
Cy3	Cyanine
DAB	3,3-diaminobenzidine tetrahydrochloride
DARK	*Drosophila* Apaf-1-related killer
dCtBP	*Drosophila* C-terminal binding protein
DIAP	*Drosophila* Inhibitor of Apoptosis Protein
DRPLA	Dentatorubral Pallidoluysian Atrophy
DVAP-33A	*Drosophila* VAMP-associated protein of 33 kDa A
EAATs	Exitatory amino acid transporters
EJP	Evoked junctional potential
FALS	Familial Amyotrophic Lateral Sclerosis
FFAT	diphenylalanine (FF) in an acidic tract
FITC	Fluorescein isothiocyanate
FMR	Fragile X mental retardation
FTD	Fronto-temporal dementia

FTDP-17	Fronto-temporal dementia with Parkinsonism linked to chromosome 17
FTLD-U	Frontotemporal lobar degeneration with ubiquinated inclusions
FUS	Fused in sarcoma
GAP-43	Growth Associated Protein 43
GluRIIA	Glutamate Receptor IIA
GluRIIB	Glutamate Receptor IIB
GluRIII	Glutamate Receptor III
GluRIID	Glutamate Receptor IID
GluRIIE	Glutamate Receptor IIE
GSK-3	Glycogen synthase kinase 3
GST	Glutathione-S-transferase
HD	Huntington's Disease
HDAC	Histone deacetylase
HRP	Horseradish peroxidase
HSP40	40 kilodalton heat shock protein
HSP70	70 kilodalton heat shock protein
Htt	Huntingtin
hVAPB	Human VAMP-associated protein B
Hz	Hertz
Ig	Immunoglobulin
MARK	Microtubule affinity regulating kinase
MeCP2	Methyl-CpG-binding protein 2
mEJPs	Miniature excitatory junctional potentials
min	Minutes
MJDs	Machado-Joseph Disease
MNDs	Motor neuron diseases
MSP	Major Sperm Protein
NFT	Neurofibrillary Tangle
NGS	Normal Goat Serum
NMJs	Neuromuscular Junctions

OSBP	Oxysterol-binding protein
P56S	Proline to Serine substitution
PA	Phosphatidic acid
PAGE	Polyacrylamide gel electrophoresis
PBS	Phosphate Buffer Solution
PBT	Phosphate Buffer Solution with Triton
PD	Parkinson's Disease
PH	Pleckstrin homology
PtdCho	Phosphatidylcholine
PtdIns	Phosphatidylinositol
PtdIns-4-P	Phosphatidylinositol-4-phosphate
polyQ	Polyglutamine
RCCI	Regulator of chromatin condensation
RRM	RNA recognition motif
Sac1	Suppressor of Actin 1
SAHA	Suberoylanilide hydroxamic acid
SBMA	Spinobulbar Muscular Atrophy
SCA1	Spinocerebellar Ataxia type 1
SCA2	Spinocerebellar Ataxia type 2
SCA3	Spinocerebellar Ataxia type 3
SCA8	Spinocerebellar Ataxia type 8
SCAs	Spinocerebellar Ataxias
SCS2	Suppressor of choline sensitivity 2
SD	Standard Deviation
SDS	Sodiom dodecyl sulfate
s.e.m	Standard error of the mean
SEM	Scanning Electron Microscopy
SMA	Spinal muscular atrophy
SMARD	Spinal muscular atrophy with respiratory distress
SOD1	Cu/Zn Superoxide Dismutase 1
SUMO	Small uniquitin-like modifier

TARDBP/ TDP-43	43kDa TAR DNA-binding protein
TBS	Tris Buffer Solution
TBST	Tris Buffer Solution with Tween
TEM	Transmission Electron Microscopy
TLS	Translocation in liposarcoma
TMD	Transmembrane domain
TUNEL	Terminal deoxynucleotidyl transferase dUTP nick end labeling
VAPs	VAMP-associated proteins
VAPB	VAMP-associated protein B
wt	Wild Type
yip2	yippee interacting protein 2
ml	millilitre
µm	micron
µl	microlitre

Chapter 1: Introduction

1.1 Modeling neurodegenerative diseases in *Drosophila*

Amyotrophic Lateral Sclerosis (ALS) is a devastating neuromuscular degenerative disease that is the most common form of motor neuron disease in adults. Although modern genetics has identified several mutations as a primary cause of the disease and has implicated other ones as potential contributors, the mechanisms underlying the characteristic selective degeneration and death of motor neurons in ALS have remained a mystery (Mulder, D.W., 1986; Talbot, K., 2002). Since there is still no effective treatment for this progressive and fatal disorder, creating a powerful and versatile experimental model of ALS is important to provide a better understanding of the molecular mechanisms responsible for ALS. This in turn, will open up the possibility to identify new targets for more effective therapeutic interventions.

Comprehensive cross genomic analysis of human and the fly genome has shown that 50% of fly genes exhibit apparent homology to human genes, including conservation of entire genetic pathways and that 75% of all human disease genes have an orthologue in *Drosophila* (Rubin *et al.*, 2000; Fortini *et al*, 2000; Reiter *et al*, 2001). Given the high degree of evolutionary conservation among genes that control neuronal function, *Drosophila* makes an ideal system to study human neurodegeneration. Fly models have been successfully developed for a number of different neurodegenerative diseases (Warrick *et al.*, 1998; Jackson *et al.*, 1998; Struhl & Greenwald, 1999; Feany & Bender, 2000; Fernandez-Funez *et al.*, 2000; Jackson *et al.*, 2002; Iijima *et al.*, 2004), and the neurodegenerative field has begun to harness the power of *Drosophila* genetics in dissecting pathways of disease pathogenesis to identify targets for therapeutic intervention.

The adult fly eye has proven to be a favourable system for genetically dissecting various cellular processes, including receptor tyrosine kinase signaling, cell cycle progression, and cell death pathways (Agapite & Stellar, 1997; Tanenbaum *et al*, 2000; Wolff *et al.*, 1997). It has also been the tissue of choice to direct the expression of aberrant human genes in many neurodegenerative disease models

(Jackson *et al*, 1998; Warrick *et al*, 1998; Fernandez-Funez *et al*, 2000). The *Drosophila* eye is composed of about 800 regularly packed ommatidia, and numerous defects in cell-fate determination and differentiation produces a rough eye phenotype, the severity of which reflects the number or ommatidia affected (St Johnston, 2002).

Typically, expression of the disease genes is driven in cells of the eye using the UAS/Gal4 system (Brand and Perrimon, 1993) and neurotoxicity is monitored by the disruption of ommatidia or loss of photoreceptors. Gross analysis of the fly eye can easily be observed under the dissecting microscope in live flies by looking at the size and at the roughness of the eye. Such easily assayed, nervous system specific and degenerative phenotype, coupled with the dispensability of the eye for viability and fertility in the adult fly also makes the fly eye an ideal system to conduct genetic screens. Compared with experiments in vertebrates, large screens are facilitated in *Drosophila* by the low cost, the short generation time, the capacity for experiments with large numbers of animals and the availability of large collections of loss-of-function and overexpression mutant strains. Together with a wide variety of genetic tools available, this has made the fly eye one of the most popular system to study neurodegeneration in *Drosophila*.

1.2 Polyglutamine Diseases

The *Drosophila* eye has been fully exploited to study the pathogenesis of polyglutamine diseases. This diverse group of late-onset, dominantly inherited neurodegenerative diseases is caused by expansions of polyglutamine (polyQ)-encoding CAG trinucleotide repeats within coding regions of specific proteins. Polyglutamine-expansion disorders characterized thus far in *Drosophila* are: Huntington disease (HD) (Jackson *et al*, 1998) , spinobulbar muscular atrophy (SBMA) (Takeyama *et al*., 2002), dentatorubral pallidoluysian atrophy (DRPLA) (Zhang *et al*., 2002) and spinocerebellar ataxias (SCAs, also known as Machado-Joseph disease, MJD) (Fernandez-Funez *et al*., 2000; Warrick *et al*., 1998). The

mechanisms underlying polyglutamine-induced neuronal cell death remain poorly understood; however, using several *Drosophila* models, they were able to substantially improve our knowledge of the process. The expanded polyglutamine sequence confers a dominant gain-of-function on the encoded protein and there is a critical threshold for glutamine repeat number. The disease does not occur if the polyglutamine repeats are below a certain threshold, while number of repeats above a certain threshold triggers the disease. The severity of the disease is also correlated with the extent of CAG expansion, with long tracts conferring earlier onset and an increased severity in the symptoms (Jackson *et al.* 1998; Warrick *et al.*, 1998; Fernandez-Funez *et al.*, 2000).

In these *Drosophila* models, mutant huntingtin (Htt) fragment including 120 glutamine residues (Jackson *et al*, 1998), mutant MJD fragment including 78 glutamine repeats (Warrick *et al.*, 1998) and full-length ataxin-1 with 82 glutamine residues (Fernandez-Funez *et al.*, 2000) were expressed exclusively in the developing fly eye. The respective number of repeats/residues expressed in the eye corresponds to the number of repeats that will cause each disease while the number of repeats/residues triggering each disease differs from one another. In every case, expression of the mutant huntingtin, mutant MJD fragments and full-length ataxin-1 caused disruption of rhabdomere structure and loss of photoreceptor neurons; disruption of the external crystalline lattice of the eye (a so-called 'rough eye') and abnormal external eye respectively. Analysis on the internal structures of the eye also revealed several abnormalities: retinal sections of the eye showed decreased retinal thickness (Fernandez-Funez *et al.*, 2000), disrupted retinal pseudopupil (Warrick *et al.*, 1998), and loss of rhabdomeres (Jackson *et al.*, 1998).

1.3 Modifiers of Polyglutamine diseases

These *Drosophila* polyglutamine disease models have created a platform for candidate-based and unbiased genetic screens to identify polyglutamine modifiers. The basis of a modifier screen is to find the missing components of a given pathway

and to achieve that, one would carry out a screen for dominant enhancers or suppressors of a particular phenotype (St. Johnston, D., 2002). The rough-eye phenotype observed when expression of expanded polyglutamine tracts are expressed in the developing fly eye allows a nervous system specific, easily assayed and detectable phenotype for carrying out such modifier screens. Moreover, the dispensability of the eye for viability and fertility in the adult fly would facilitate the identification of modifiers.

The first of these polyglutamine modifiers to be reported was Hsp70 (70 kilodalton heat shock protein). Retinal coexpression of Hsp70 dramatically suppresses the eye phenotype of SCA3 (Spinocerebellar ataxia type 3) flies (Warrick *et al.*, 1999). Subsequently, *Drosophila* HDJ1, an Hsp40 (40 kilodalton heat shock protein), was also identified in an unbiased transposon-based screen. Misexpression of HDJ1 strikingly suppressed a polyglutamine phenotype (Kazemi-Esforjani and Benzer, 2000). Other disease models of polyglutamine diseases expressing truncated and full-length proteins have also identified Hsp40 as a suppressor of their associated cellular toxicity (Fernandez-Funez *et al.*, 2000; Takeyama *et al.*, 2002).

Hsp70 and Hsp 40 both belong to a family of molecular chaperones and aid in the proper folding of proteins. They are known to act under stress conditions to influence the processing of abnormally folded proteins (Bukau and Horwich, 1998). Since being identified as suppressors of polyglutamine toxicity, these molecular chaperones have been found to extend their suppressor activities to other human neurodegenerative models such as Parkinson's disease (PD) (Auluck *et al.*, 2002).

Other modifiers have also been identified in genetic screens of polyglutamine diseases. Not only is the effect of protein-folding important, so is the clearance of the disease protein. Enhancement of polyglutamine toxicity in flies has been shown to be caused by mutations in components of the proteosome pathway such as ubiquitin (Fernandez-Funez *et al.*, 2000; Chan *et al.*, 2002). Several other cellular pathways have also been implicated by genetic screens such as small ubiquitin-like modifier

(SUMO) pathways (Chan *et al.*, 2002), genes implicated in neoplasia (Kazemi-Esfarjani and Benzer, 2002), in addition to pathways associated with mRNA regulation, cellular detoxification and transcriptional regulation (Fernandez-Funez *et al.*, 2000; Steffan *et al.*, 2001).

Glutathione-S-transferase (GST) was uncovered as one of the suppressors of the Ataxin-1 phenotype. GSTs are enzymes that have a principal role in cellular detoxification as they catalyze the conjugation of reduced glutathione, which in turn detoxifies the products of chemical and oxidative stress. This suggests that cellular detoxification pathways are of great importance in polyglutamine diseases (Fernandez-Funez *et al*, 2000).

The mechanism of cell death in polyglutamine-induced degeneration is not yet known and so far, apoptosis related genes have not been recovered as modifiers in genetic screens. P35, a baculoviral caspase inhibitor, was reported to be a poor suppressor of both Ataxin-3 and Huntingtin-induced retinal degeneration (Jackson *et al.*, 1998; Warrick *et al.*, 1998). However, a candidate-based approach to assess the role of specific cell-death regulators revealed a common role of Dark (*Drosophila* Apaf-1-related killer) in polyglutamine pathogenesis. Dark is the fly homologue of Apaf-1, a key regulator of mammalian apoptosis. Sang and colleagues reported that polyglutamine-induced cell death was drastically suppressed in flies lacking Dark in addition to a suppression in caspase activation and aggregate formation (Sang *et al.*, 2005). Furthermore, Apaf-1 was found to colocalize to aggregates in brains of a mouse model of Huntington's disease and patients. These observations suggest that Dark/Apaf-1 may play a role in the formation of pathogenic polyglutamine-containing aggregates and a common role in polyglutamine pathogenesis (Sang *et al.*, 2005).

The success of *Drosophila* genetic screens in neurodegenerative diseases and the identification of several modifiers has already led to the possibility of preclinical trials for many of these diseases. Polyglutamine modifiers that have generated

special interest are those involved in transcriptional pathways, with several transcriptional cofactors reported as genetic modifiers in flies such as CREB binding protein (CBP), Sin3A, Rpd3 and *Drosophila* C-terminal binding protein (dCtBP) (Fernandez-Funez *et al.*, 2000, Steffan *et al.*, 2001). This finding shows that the loss of CBP or other transcriptional activities might be involved in polyQ disease progression. CBP has intrinsic histone acetyltransferase activity which can be inhibited by binding to a fragment of Huntington disease protein with expanded polyQ repeats. In flies, histone deacetylase (HDAC) inhibitors such as butyrate and suberoylanilide hydroxamic acid (SAHA) were also shown to arrest ongoing progressive neural degeneration induced by polyglutamine repeat expansion (Steffan *et al.*, 2001). Furthermore, expression of Huntington and androgen receptor with expanded polyQ repeats in cultured cells reduces the level of acetylated histones H3 and H4, and this reduction can be reversed by administering inhibitors of HDAC (Steffan *et al.*, 2001; McCampbell *et al.*, 2001). This line of evidence indicates that HDAC inhibitors might be a useful class of agents to ameliorate the transcriptional changes in HD and has lead to SAHA being tested in preclinical trials in mouse models of Huntington disease (Hockly *et al.*, 2003).

Another potential target for therapeutic intervention was uncovered by Chen and colleagues when they investigated the role of protein phosphorylation in SCA1 (Spinocerebellar ataxia type 1) pathogenesis, as it has been shown previously that substitution of ataxin-1 phosphorylation site greatly diminishes the ability of ataxin-1 to aggregate (Emamian *et al.*, 2003). It was found that the 14-3-3 protein, a multifunctional regulatory molecule, mediates the neurotoxicity of ataxin-1 by binding to and stabilizing ataxin-1, thereby slowing its normal degradation. The association of ataxin-1 with 14-3-3 is regulated by Akt phosphorylation and in a *Drosophila* model of SCA1, both 14-3-3 and Akt were shown to modulate ataxin-1-induced neurodegeneration, thus identifying 14-3-3 and phosphatidylinositol 3-kinase/Akt signalling as potential targets for therapeutic interventions (Chen *et al.*, 2003).

Recent pathological and molecular analyses have even revealed common attributes between what have been normally thought as distinct diseases based on syndromic classifications of neurodegenerative disorders. In particular, a functional link between seemingly unrelated neurodegenerative diseases has been reported for Ataxin 1, the gene responsible for SCA1 and Ataxin 2, the gene causing SCA2 (Spinocerebellar ataxia type 2) (Al-Ramahi *et al.*, 2007). In addition, it has been shown that Ataxin 2 also contributes to the pathogenesis of Ataxin 3, the causative gene of Spinocerebellar Ataxia 3 (Lessing and Bonini, 2008).

The poly-glutamine diseases mentioned above involved the expansion of trinucleotide repeat which leads to toxic protein production. However, there are other diseases caused by trinucleotide repeat expansion within noncoding regions of mRNAs. An example of trinucleotide repeat expansion within noncoding regions of mRNAs is SCA8 (Spinocerebellar ataxia type 8). The human SCA8 gene, which encodes a noncoding RNA, when expressed in fly eye induces a late-onset, progressive neurodegeneration phenotype. Both wild-type and trinucleotide-expanded SCA8 induced neurodegenerative eye phenotypes. A genetic screen was carried out using the SCA8 model in the *Drosophila* eye which identified four neuronally expressed RNA-binding proteins (Staufen, muscle blind, split ends and CG3249) as modifiers of SCA-8-induced neurodegeneration (Mutsuddi *et al.*, 2004). This screen provided potential candidates for designing therapeutic interventions for the treatment of SCA-8 and understand the mechanism of noncoding-region trinucleotide repeats–induced neurodegeneration.

Fragile X mental retardation (FMR) is another disease caused by trinucleotide repeat expansion within noncoding regions of mRNAs. rCGG repeats in the 5'UTR of the FMR gene cause neurodegeneration in premutation carriers. Expressing 90 noncoding rCGG repeats (an intermediate repeat number between repeat numbers found in patients and normal individuals) in the fly eye was sufficient to cause retinal degeneration. HSP70- and ubiquitin-positive neuronal inclusion bodies were found in the degenerating neurons even though no mutant protein was produced from this

repeat sequence. In addition, overexpression of HSP70 suppressed rCGG repeat–induced neuronal cell death. It is possible that the expanded RNAs cause neuronal toxicity by sequestering away essential RNA-binding proteins and molecular chaperones (Jin *et al.*, 2003).

1.4 Alzheimer's disease and modifier screens

A key event in the pathogenesis of Alzheimer's disease (AD) is the deposition of senile plaques consisting largely of a peptide known as β-amyloid (Aβ) that is derived from the membrane bound amyloid precursor protein (APP) and it is the cleaving of APP that generates pathogenic peptides (Tanzi & Bertram, 2005). The *Drosophila* eye has been used in this instance to study the effects of human Aβ peptide overexpression. $A\beta_{40}$ and $A\beta_{42}$, were expressed throughout eye development and strains containing $A\beta_{42}$ transgenes showed different degrees of eye disorganization ranging from slight abnormalities to more pronounced eye defects characterized by fusion of ommatidia and missing inter-ommatidia bristles. In the most severely affected strains, the eyes were 'glazed' and reduced in size. This phenotype was then used in a genetic modifier screen, where it was found that a mutation in a *Drosophila* neprilysin gene suppresses the $A\beta_{42}$ rough-eye phenotype by lowering the levels of $A\beta_{42}$ peptide, supporting the role of neprilysin in the catabolism of $A\beta_{42}$ peptides in vivo (Finelli *et al.*, 2004). Neprilysin has previously been implicated in Aβ degradation (Iwata *et al.*, 2001); this supports the use of *Drosophila* to identify other factors involved Aβ metabolism and toxicity to help in the search of a potential therapeutic target for the treatment of AD.

β- and γ-secretase are responsible for generating pathogenic Aβ peptides. γ-secretase cleavage of APP in the transmembrane domain underlies the majority of early onset, familial AD. γ-secretase resides in a large multi-protein complex, of which Presenilin, Nicastrin, APH-1 and PEN-2 are four essential components (De Trooper, 2003). Because the pathogenesis of AD results from increased deposition of Aβ, Guo and colleagues generated flies that function as living reporters for APP γ-

secretase activity. This sensitized genetic system utilizes a small eye phenotype to identify components or regulators of γ-secretase activity. A genetic screen carried out by the same group identified a suppressor of the reduced eye phenotype that was mapped to the 23C1–3 chromosomal region which contains 10–15 annotated genes whose products may promote γ-secretase activity. Once the modifier gene is identified, it may provide another therapeutic target for AD treatment.

1.5 Tauopathies and modifiers

Neurofibrillary tangle (NFT) that is mainly made up by tau proteins is the second key feature of AD pathology. Nevertheless, neurofibrillary pathology is also seen in a number of disorders collectively known as tauopathies. These disorders include fronto-temporal dementia with Parkinsonism linked to chromosome 17 (FTDP-17), progressive supranuclear palsy and corticobasal degeneration (Lee *et al.*, 2001).

Tau proteins are microtubule-associated proteins that are thought to stabilize axonal microtubules and increasing tau phosphorylation in regions flanking the microtubule binding repeats, negatively regulates microtubule binding. It is thought that tauopathies occur due to the dysregulation of tau phosphorylation and hence microtubule binding. Hyperphosphorylated and abnormally phosphorylated tau is thought to occur early in the cascade of events leading to the formation of insoluble tau protein that is seen in AD and tauopathies (Lee *et al.*, 2001).

A genetic model of tauopathy was reported where wild type and mutant forms (R406W and V337M) of human tau were expressed in *Drosophila* that recapitulates the key features of the human disorders even though no neurofibrillary pathology was observed. However, when human mutant tau (R406W) was expressed in the developing *Drosophila* eye, a mild decrease in eye size and rough-eye phenotype was observed (Wittmann *et al.*, 2001). This phenotype in the eye is significant because it would greatly facilitate a modifier screen.

Another *Drosophila* model was able to show that overexpression of wild-type human tau in the developing eye resulted in degeneration (reduced eye size and rough eye phenotype), without apparent accumulation of NFT as observed in other models (Williams *et al*, 2000, Wittmann *et al*., 2001). However, enhanced tau-induced neurodegeneration accompanied by formation of NFT-like filamentous tau aggregates was observed when tau was hyperphosphorylated by co-expression of GSK-3β homolog Shaggy. Perturbations in the expression of downstream components of Shaggy such as Armadillo (*Drosophila* homolog of β-catenin) and *Drosophila* T Cell Factor in the Wingless pathway also modulate tau-induced neurodegeneration. Furthermore, it was also shown that inhibitors of apoptosis suppressed tau-induced neurodegeneration. These findings suggest that Wnt/Wingless pathway could be a mediator of tau-induced neurodegeneration and factors other than phosphorylation can modulate neurodegeneration associated with tau dysregulation (Jackson *et al*., 2002).

Using the *Drosophila* model for tauopathy reported by Wittmann and colleagues, a screen for genetic modifiers of tau-induced neurodegeneration identified modifiers largely consisted of kinases and phosphatases including MARK kinase and the PP1 and PP2A phosphatases that have previously been shown to phosphorylate or dephosphorylate tau in vitro (Goedert *et al.* 1995 ; Liao *et al.* 1998 ; Sontag *et al.* 1999). In addition, several tau kinases such as CDK5, PKA and the JNK pathway were also reported to enhance tau toxicity in vivo. Despite some clinical and pathological similarities among neurodegenerative disorders and suggestions that disorders might share similar mechanisms of pathogenesis related to abnormal protein folding and aggregation, a direct comparison of modifiers between polyglutamine disorders and tauopathies revealed distinct mechanisms controlling tau and polyglutamine toxicity (Shulman and Feany, 2003).

Tau phosphorylation occurs on numerous residues and several kinases have been shown to be involved, leading to the conundrum of exactly which one contributes most to the formation of NFTs. In an elegant study carried out by

Nishimura and colleagues, they were able to show that the PAR-1/MARK kinase is the chief culprit in tau-related neurodegeneration. *Drosophila* PAR-1 and its mammalian homolog MARK (Microtubule affinity regulating kinase) are required for cellular processes involving microtubule organization and cytoskeletal dynamics. Phosphorylation of microtubule-binding proteins including tau by MARK, leads to microtubule disruption (Drewes *et al.*, 1997). Using the *Drosphila* eye as a model system, they have been able to show that *Drosophila* PAR-1 initiates tau-toxicity by triggering a temporally ordered phosphorylation process by directly phosphorylating its two PAR-1/MARK-dependent phosphorylation sites, S262 and S356. This phosphorylation event is a pre-requisite for action of downstream kinases such as glycogen synthase kinase 3 (GSK-3) and cyclin-dependent kinase-5 (Cdk-5) to phosphorylate several other sites and generate disease associated phosphor-epitopes. Coincidently, studies using transgenic mice overexpressing Cdk5 or GSK-3 have implicated these two kinases in tau phosphorylation and aggregation (Lucas *et al.*, 2001; Noble *et al.*, 2003). These studies strongly suggest an initiator role for PAR-1, where its phosphorylation acts as a trigger for subsequent multistep phosphorylation of tau by other tau kinases to form hyperphosphorylated, aggregate-prone tau. These findings provide yet more potential therapeutic targets of tauopathies by differentiating the effects on various phosphorylation events of tau-toxocity (Nishimura *et al.*, 2004).

1.6 Parkinson's disease and modifiers

Parkinson's disease is a common movement disorder affecting about 1% of the population above the age of 65 and exists also as a juvenile onset form. The neuropathological hallmarks of this condition are progressive degeneration of dopamine neurons in the substantia nigra pars compacta, and the presence of cytoplasmic neuronal inclusions known as Lewy bodies (Lang and Lozano, 1998). Although Parkinson's disease is generally sporadic, familial forms have been characterised. Mutations in α-synuclein have been found in families with autosomal-dominant Parkinson's disease (Polymeropoulos *et al.*, 1997, Kruger *et al*, 1998).

Genomic triplication of the α-synuclein locus has also been found to cause dominantly inherited Parkinson's disease (Singleton *et al.*, 2003). Incidentally, α-synuclein is also a component of Lewy bodies and Lewy neurites in the brains of patients with both familial and sporadic Parkinson's disease (Spillantini at al., 1997, Kruger at al., 1998).

Not all *Drosophila* models of neurodegeneration have been modeled in the adult eye. Feany and Bender were the first to model Parkinson's disease in *Drosophila* with pan-neural expression of normal human α-synuclein and two familial mutant forms. Both wild type and mutant forms of α-synuclein induced adult onset loss of tyrosine hydroxylase in dopaminergic neurons. Similar to human Parkinson's, Lewy body-like accumulations of α-synuclein and progressive motor impairment are observed in this fly model. In this instance, very mild degeneration in the *Drosophila* eye is observed in aged flies expressing wild type α-synuclein (Feany and Bender, 2000).

Chaperones such as HSP70 are up-regulated in stress responses to refold misfolded proteins (Glover and Lindquist, 1998) and HSP70 has been shown to suppress neurotoxicity of abnormal polyglutamine proteins in a fly model of SCA 3 (Warrick *et al*, 1999). Given the pathological similarities between polyglutamine- and α-synuclein-mediated neurodegeneration the role of chaperones in Parkinsons's have been examined using *Drosophila* models (Auluck *et al.*, 2002). Coexpression of Hsp70 in the dopaminergic neurons rescues α-synuclein induced toxicity whereas compromising levels of HSP70 enhances toxicity in flies. Hsp70 and its co-chaperone HSP40 have also been found to localize to Lewy bodies in the fly model of α-synuclein and human patient tissues from Parkinson's disease and other synucleinopathies. This suggests that altered chaperone activity by sequestration of chaperone may be involved in progression of Parkinson's disease (Auluck *et al.*, 2002). The role of chaperone activity in α-synuclein toxicity is further empasized when protection against α-synuclein neurotoxicity in dopaminergic neurons is

observed when feeding flies with the drug geldanamycin, which acts to upregulate heat shock response (Auluck and Bonini, 2002).

Whilst these findings emphasize the significance of chaperones in Parkinson's disease pathology, the abnormal motor behaviour with the expression of α-synuclein reported by Feany and Bender could not be reproduced (Auluck *et al.*, 2002). Furthermore, the significance of the α-synuclein model (Feany and Bender, 2000) has been called into question when tyrosine hydroxylase stainings in the brain could not detect any neurodegeneration, abnormal motor behaviour and retinal degeneration that has been reportedly induced by α-synuclein (Pesah *et al.*, 2005). Pesah and colleagues used whole mount immuno-histochemistry techniques instead of sequential paraffin sections used by Feany and Bender to study the number of dopaminergic neurons in the missexpression of α-synuclein. However, the same Gal4 drivers and α-synuclein transgenic lines were used in these two studies. Therefore, the antibodies and whole mount method could account for the discrepancies.

Loss of function mutations in the *parkin* gene, which encodes a ubiquitin-protein ligase, was also found to underlie a familial form of Parkinson's disease known as autosomal recessive juvenile parkinsonism (AR-JP) (Kitada *et al.*, 1998). The finding that Parkin functions as an ubiquitin protein ligase indicates that failure to label specific cellular targets with ubiquitin could be responsible for dopaminergic neuron loss in AR-JP (Greene *et al.*, 2003). Loss of function mutants of Parkin in flies have been reported to cause cell death of sperm and indirect fly muscles, reduction in cell size. Moreover, mitochondria defects and increased susceptibility to oxidative stress implicates disturbed mitochondrial function in the pathogenic mechanism of Parkinson's disease (Greene *et al.*, 2003; Pesah *et al.*, 2004).

The identification of autosomal recessive mutations in Pink1, which encodes a Ser/Thr kinase with a mitichondrial-targeting signal potentially associates mitochondrial dysfunction with the pathogenesis of Parkinson's disease (Velente *et*

al., 2004). Removal of *Drosophila* Pink1 function results in degeneration of muscles via apoptosis, mitochondrial morphological defects, increased sensitivity to oxidative stress, male sterility and mitochondrial dysmorphology (Clark *et al.*, 2006). Similarly in other studies, mitochondrial associated dopaminergic neuronal degeneration accompanied by locomotor defects and indirect flight muscle degeneration were reported (Park *et al.*, 2006; Wang *et al.*, 2006; Yang *et al.*, 2006). In addition, neurodegeneration in these flies can be suppressed by the expression of human SOD1 and antioxidant treatment, further supporting the role of oxidative stress and mitochondrial dysfunction in the disease (Wang *et al.*, 2006). Another encouraging finding that mitochondrial dysfunction could be a cause of Parkinson's disease is that Pink and Parkin appear to act in a common pathway that influences mitochondrial integrity (Clark *et al.*, 2006).

1.7 Amyotrophic Lateral Sclerosis, ALS

Amyotrophic Lateral Sclerosis (also known as Lou Gehrig disease) is the best characterised of all motor neuron diseases (MNDs). It was first described by the French neurologist Jean-Martin Charcot in 1869 and is a progressive and usually lethal neurodegenerative disorder caused by the degeneration of motor neurons. The hallmarks of the disease is the selective dysfunction and death of motor neurons in the brain and spinal cord, leading to spasticity, hyperreflexia, generalised weakness, muscle atrophy and paralysis of voluntary muscles (Mulder, D.W., 1986; Talbot, K., 2002).

ALS is the most prevalent motor neuron disease and strikes about 5 per 100,000 individuals. Most cases (about 90%) of ALS occurs without any genetic linkage and is known as sporadic ALS while the remaining 10% of ALS cases are familial (FALS), manifesting a variety of inheritance patterns with linkage to multiple independent chromosome loci (Bruijn *et al.*, 2004).

The pathological hallmark of ALS is selective atrophy and death of

cortocospinal and corticobulbar neurons in the motor cortex and motor neurons in the brain stem and spinal cord (Leigh and Garofolo, 1995). Affected neurons and axons often have cytoskeletal pathology with accummulations of neurofilaments (mainly hyperphosphorylated neurofilament subunits and peripherin) and aggregates of ubiquinated proteins (Leigh *et al.*, 1991; Sobue *et al.*, 1990).

In both sporadic and familial ALS, the typical age of disease onset is between 45-60 years with a disease course of about 5 years. Progressive manifestations and selective dysfunction of lower motor neurons (atrophy, cramps and fasciculations) and cortical motor neurons (spasticity and pathological reflexes) in the absence of sensory symptoms can be seen in patients. However, muscles controlling eye movements and the urinary sphincter are spared from degenerating. Denervation of the respiratory muscles and diaphragm towards the end of the disease course is generally the fatal event. In the majority of ALS patients this occurs within 2 to 5 years of the onset of clinical symptoms (Mulder, D.W., 1986; Talbot, K., 2002).

1.7.1. Superoxide Dismutase 1 (SOD1)

Understanding ALS pathogenesis began with the identification of dominant mutations in the gene encoding *Cu/Zn Superoxide Dismutase 1* (*SOD1*) in ~20% of familial ALS and ~1% of sporadic ALS cases (Rosen *et al.*, 1993). SOD1 is a homodimer of an ubiquitously expressed 153-amino acid polypeptide that catalyzes the dismutation of the superoxide radical anion ($O_2^{\cdot}$) generated by mitochondrial respiration to hydrogen peroxide, which will then be converted to less harmful substances such as water and oxygen (Eisen, A., 2000). More than 100 disease causing mutations can be found scattered throughout the primary and three-dimensional structure of the protein (Andersen, P.M., 2000; Gaudette *et al.*, 2000).

Several transgenic mouse models of SOD1 have been generated to study the pathogenesis of ALS. Transgenic mouse models overexpressing ALS-associated mutant forms of SOD1 results in motor-neuron disorder that recapitulates most

features of ALS such as paralysis, motor neuron loss and ultimately death. Neurofilament-rich spheroids, Lewy body-like neurofilament inclusions, and accumulation of SODl-protein were also found in motor neurons (Gurney *et al.*, 1994; Wong *et al.* 1995). On the other hand, mice that overexpress normal human SOD1 and *SOD1* null mice do not develop motor neuron disease (Dal Canto *et al.*, 1995; Reaume *et al.*, 1996). It remains unclear how mutant SOD1 leads to motor neuron degeneration. It was initially thought that decreased free-radical scavenging activity results in the toxicity of different SOD1 mutant proteins, however, it is now well established that SOD1 mediated toxicity in ALS is due to a gain of function instead of a loss of function mechanism. This fact is established though several lines of evidence: Firstly, *SOD1* knockout mice do not develop motor neuron disease (Reaume *et al.*, 1996); secondly, transgenic mice expressing familial linked mutants $SOD1^{G93A}$, $SOD1^{G37R}$, or $SOD1^{G85R}$ exhibited loss of motor neurons despite unchanged or enhanced SOD1 enzymatic activity (Bruijn *et al.*, 1997; Gurney *et al.*, 1994; Wong *et al.*, 1995). Thirdly, ablation or overexpression of wild-type SOD1 in mutant mice did not affect disease progression (Bruijn *et al.*, 1998). Furthermore, SOD1 activity levels do not correlate with disease in mice or humans, it has been shown that some mutant enzymes actually retain full dismutase activity (Borchelt *et al.*, 1994; Bowling *et al.*, 1995). Lastly, there is either no effect on the disease or acceleration of the disease when levels of wild-type SOD1 and dismutase activity are chronically increased (Bruijn *et al.*, 1998; Jaarsma *et al.*, 2000).

Since *SOD1* was the first gene to be identified in ALS and 20% of all familial cases of ALS are caused by dominantly inherited mutations in *SOD1*, most research efforts to understand ALS pathogenesis have subsequently focused on the study of the ubiquitously expressed SOD1. The following is an overview of proposed disease mechanisms of ALS.

1.7.2. Oxidative damage

Studies have suggested that structural changes and pro-oxidant properties of mutant SOD protein are involved in pathogenicity of FALS. It was proposed that misfolding of SOD1 induced by mutations would allow the access of abnormal substrates (Beckman *et al.*, 1993). The peroxidase activity hypothesis suggests that SOD1 mutant proteins can damage cellular targets including DNA, protein, and lipid membranes due to their enhanced ability to use hydrogen peroxide as a substrate to generate toxic hydroxyl radicals, hence promoting a cascade of oxidative damage. (Wiedau-Pazos *et al.*, 1996). Increased levels of oxidized products in parallel with disease progression have been reported in $SOD1^{G93A}$ transgenic mice (Bruijn *et al.*, 1997). Another candidate substrate is peroxynitrite, where the nitration of tyrosine residues in target proteins could occur (Beckman *et al.*, 1993). This is consistent with the increased levels of free 3-nitrotyrosine detected in the spinal cord of human ALS patients (Beal *et al.*, 1997) and in mouse models of ALS (Bruijin *et al.*, 1997). However, there is no evidence of increased levels of nitrotyrosine bound to proteins in ALS patients or in mutant SOD1 mice as compared to controls (Bruijin *et al.*, 1997; Strong *et al.*, 1998).

Experiments manipulating the SOD1 activity in mouse model of ALS have emerged, challenging the oxidative damage hypothesis. The absence of wild-type SOD1 in the $SOD1^{G85R}$ mutants would predict an increase in superoxide levels and its product peroxynitrite or hydroxyl radicals while the elevation of normal SOD1 activity would do the opposite in $SOD1^{G85R}$ mice either in a SOD1 knockout background or in a transgenic background overexpressing wild-type SOD1. However, the disease progression in $SOD1^{G85R}$ mice was not affected by either the elimination of endogenous SOD1 or addition of wild-type SOD1. The role of copper mediated oxidative damage is a commonality between the peroxynitrate and peroxidase activity hypotheses. While copper chaperone for SOD1 (CCS) is required for the delivery of copper to SOD1 enzymes in motor neurons, gene ablation of CCS had no effect on disease onset or progression in SOD1 mutant mice. This suggest that

SOD1 mutant toxicity is not mediated by CCS-dependent copper loading (Subramaniam *et al.*, 2002). Hence these results are inconsistent with mechanisms of disease involving superoxide-mediated oxidative damage (Bruijin *et al.*, 1998).

1.7.3. Protein instability and SOD1 aggregation

Intracellular aggregates is a common feature of neurodegenerative diseases and represent another mechanism of SOD1 toxicity in motor neurons (Bruijn *et al.*, 1998). In mutant SOD1 transgenic mice, and human ALS cases, aggregates that are immunoreactive to SOD1 are detected in motor neurons, neuropil and astrocytes. These aggregates coincide with disease onset and accumulates with disease progression (Bruijn *et al.*, 1998; Johnston *et al.*, 2000). These intracellular aggregates have been proposed to mediate motor neuron degeneration through sequestration of essential cellular components (Bruijn *et al.*, 1998; Pasinelli *et al.*, 2004), impairment of chaperone activity and ubiquitin proteasome pathway (Niwa *et al.*, 2002; Shinder *et al.*, 2001).

1.7.4 Axonal transport defects

An efficient and functional axonal transport system is presumably a particularly important aspect for the survival of motor neurons, which are among the largest and longest in the body. The presence of abnormal neurofilament inclusions together with the reduction in activity of axonal transport in ALS patients and mouse models supported the possibility that defects in axonal transport may play a role in the demise of motor neurons in ALS. Both fast and slow anterograde transport are slowed in SOD1 mutant mice prior to disease onset and exacerbated with the progression of the disease. Furthermore, retrograde transport is also impaired in SOD1 mutant mice (Sasaki *et al.*, 2005; William and Cleveland., 1999).

Further prove of defective axonal transport involved in ALS comes from mutations in the p150 subunit of dynactin, a major component of retrograde transport that elicit lower motor neuron disease in humans (Puls *et al.*, 2003). Similarly in

mice, reduced activity in axonal transport results in motor neuron disease. Forced expression of a subunit of dynactin called dynamitin disrupts the dynein-dynactin complex for retrograde transport and elicits late onset motor neuron disease (LaMonte *et al.*, 2002) while mutations in dynein have been shown to cause progressive motor neuron degeneration and the formation of Lewy-like inclusion bodies (Hafezparast *et al.*, 2003). Introduction of dynein mutations into *SOD1* mutant mice however, significantly ameliorates the motor neuron disease and the slowing of axonal transport initiated by mutant SOD1 protein. How this occurs is not fully understood but it has been suggested that cytotoxicity due to mutant SOD1 could require dynein-based transport (Teuchert *et al.*, 2006).

Neurofilaments have also been implicated as modulators of axonal transport as they play important roles in stimulating axonal growth and regulating axonal calibre. Transgenic mice with point mutations or overexpression of neurofilament subunits exhibit neurofilament accumulation and selective motor neuron dysfunction (Xu *et al.*, 1993; Lee *et al.*, 1994). Surprisingly, the overexpression of wild-type human and mouse neurofilament proteins did not exacerbate disease progression, but instead ameliorated motor neuron degeneration and extended the longevity of transgenic mice expressing mutant SOD1 ^{G37R} and SOD1^{G93A} respectively (Couillard-Després *et al.*, 1998; Kong & Xu, 2000). In addition, motor neuron disease still occurred in transgenic mutant SOD1 mice strains lacking axonal neuronal filaments and lead to an increase in lifespan (Williamson *et al.*, 1998; Eyer *et al.*, 1998).

1.7.5. Mitochondrial dysfunction

Several studies have focused on the role of mitochondria in ALS pathogenesis. Evidence of mitochondrial dysfunction in ALS patients includes the clustering of abnormal mitochondria and morphological defects within mitochondria found in skeletal muscles and intramuscular nerves in human sporadic ALS cases (Atsumi *et al.*, 1981; Afifi *et al.*, 1966). In addition, impaired mitochondria function and elevated levels of mitochondrial calcium have been observed in spinal cord and

muscles of sporadic ALS patients (Wiedemann *et al.*, 1998; Siklos *et al.*, 1996). Similarly, in mouse models of SOD1 transgenic mutants, swelling and vacuolization of mitochondria is observed (Kong and Xu., 1998; Sasaki *et al.*, 2004).

It has been proposed that mutant SOD1 that is found localized to the mitochondria forms insoluble aggregates that directly damage the mitochondria through fusion with peroxisomes and the outer membrane, which in turn form pores and lead to the release of cytochrome c and activation of caspases (Higgins *et al.*, 2003). The aggregates also impair mitochondrial function by disrupting the protein translocation machinery and abnormal interactions with BCL2, eventually activating mitochondrial apoptotic pathways (Pasinelli *et al.*, 2004). However, the notion of toxic mitochondrial mutant SOD1 has been suggested to be simply the result of the overexpression of mutant SOD1 that does not normally localize to the mitochondria (Bergemaim *et al.*, 2006).

1.7.6. Exocitotoxicity

Excessive glutamate induces stimulation of postsynaptic glutamate receptors which activates massive influx of calcium through glutamate receptors. Calcium influx to the cells will potentially lead to detrimental calcium-activated processes and molecules such as proteases, lipases and nucleases, causing exocitotoxicity. Therefore, excitatory amino acid transporters (EAATs) are present in the astrocytes to transport extra glutamate from the synaptic space to the surrounding astrocytes after glutamate release during neurotransmission (Fairman *et al.*, 1995). Glutamate-mediated neurotoxicity was first proposed as a possible mechanism of motor neuron degeneration when levels of glutamate were discovered to be increased in ALS patients. This was found to be apparent in about 40% of nearly 400 sporadic ALS patients that correlated with severity (Rothstein *et al.*, 1990; Spreux-Voroquaux *et al.*, 2002).

Interestingly, in about 65% of sporadic ALS cases and in transgenic murine models of ALS, a significant reduction in the expression and activity of EAAT2 in the cortex and spinal cords have been observed (Bruijn *et al.*, 1997; Howland *et al.*, 2002) EAAT2 has also been suggested to be a target of SOD1 toxicity when hydrogen peroxide was found to inactivate EAAT2. Similarly, the reduction of EAAT2 expression and activity could result from cleavage of the transporter by active Caspase 3 (Boston-Howes *et al.*, 2006). Indeed, overexpression of EAAT2 in mutant SOD1 mice delayed the onset of motor deficits, decreased caspase-3 activation and aggregate formation (Guo *et al.*, 2003). Therefore, in motor neurons, clearance of glutamate from the synaptic cleft by astrocytic glutamate transporter EAAT2 is imperative in preventing such glutamate excitotoxicity (Rothstein *et al.*, 1996).

These studies collectively suggest that glutamate excitotoxicity resulting from impaired glial glutamate transporter EAAT2 mediates motor neuron degeneration. Since most mutant gene products of ALS are ubiquitously expressed, the toxic cascade is achieved in part by mutant protein action in adjacent non-neuronal cells, impling that neuronal degeneration is also a non-cell autonomous process.

1.7.7. Non-cell autonomous effect on the degeneration of motor neurons

Whilst progressive paralysis in ALS is initiated by degeneration and death of motor neurons, several studies have demonstrated that toxicity to motor neurons derives from damage to cell types beyond motor neurons. Restricted expression of mutant SOD1 within motor neurons (Lino *et al.*, 2002) or astrocytes (Gong *et al.*, 2000) alone failed to induce motor neuron degeneration of death. With the caveat that mutant SOD1 expression exclusively in motor neurons might have been too low to initiate disease, the general view is that motor neuron death in SOD1 transgenic mice is non cell autonomous.

More definitive experiments from analyses of chimeric mice with mixed populations of cells expressing either wild type or mutant SOD1 demonstrate the non cell autonomous toxicity of mutant SOD1 proteins. Expressing mutant SOD1 in motor neurons fail to induce degeneration if the motor neurons are adjacent to a large number of supporting cells such as glia and astrocytes without the mutant SOD1. Reciprocally, motor neurons without mutant SOD1 degenerate when surrounded by non-neuronal cells expressing mutant SOD1 (Clement *et al.*, 2003). In addition, reducing the levels of mutant SOD1 in microglial and peripheral macrophages dramatically slowed late disease progression and extending survival of transgenic mice while expression of mutant SOD1 in microglial accelerates the late phase of murine ALS models (Boillée *et al.*, 2006).

Further proof of non cell autonomous effect on motor neurons come from studies on mutant SOD1 transgenic rodent models where astroglia-specific glutamate transporters were found to be defective (Bruijn *et al.*, 1997; Howland *et al.*, 2002). SOD1 inclusions in astrocytes precede symptom onset and increase with disease progression (Bruijn *et al.*, 1997). These experiments demonstrated that while SOD1 mutant action primarily determines the onset and early disease, mutant SOD1 within the supporting cells of the motor neuron accelerates disease progression.

Figure 1.1 summarize the possible mechanisms that might contribute to the pathogenesis of SOD1-induced ALS: A healthy motor neuron is triggered to fire with the release of glutamate from an upstream neuron. The firing of action potentials stimulate the release of acetylcholine at its axon terminus, causing muscle contraction. However, in neurons and astrocytes, mutant SOD1 aggregates form either by an inherently unstable conformation or by self-induced oxidative damage and accumulates in ALS patients over time. The misfolded mutant SOD1 subsequently triggers aberrant mitochondrial function, endoplasmic reticulum stress pathways, axonal transport defects, inhibition of chaperone and proteasome activity, and activation of caspases. Similar damage in astrocytes suppresses the accumulation and activity of glutamate transporters (EAAT2) that are necessary for recovering

synaptic glutamate and for preventing repetitive motor neuron firing. Disproportionate firing causes excessive calcium entry through calcium-permeable glutamate receptors, activating cell death pathways that contribute to motor neuron death through the degradation of key cellular components.

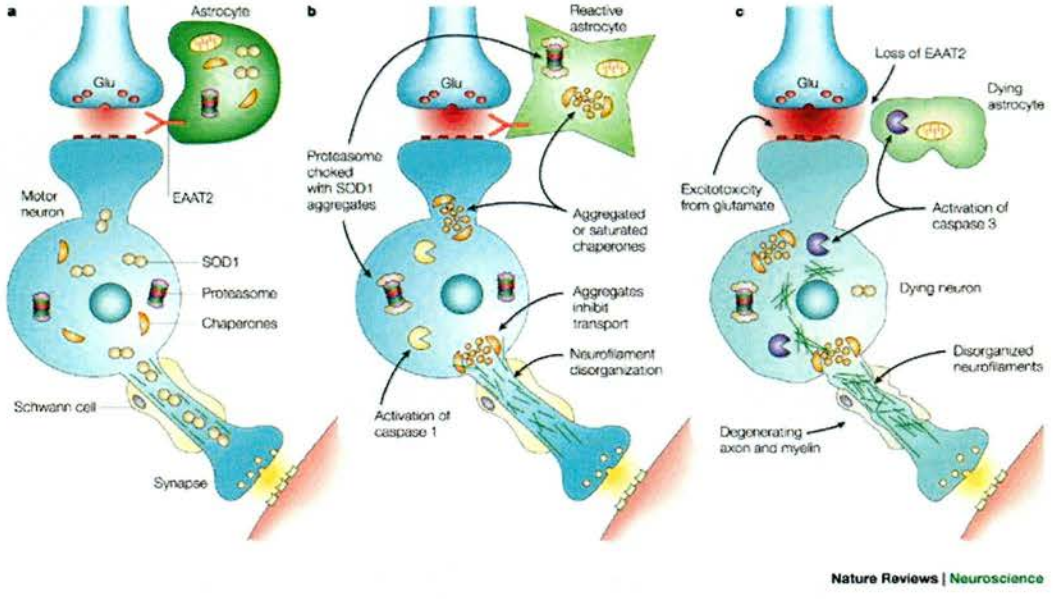

Figure 1.1. The specificity of the toxic effect of SOD1 mutations on motor neurons arises from the convergence of several factors.
Mutant SOD1 impairs multiple cellular functions and death of motor neurons is made up of a complex interplay between cell autonomous and non cell autonomous mechanisms. Diagram adapted from Cleveland and Rothstein, 2001.

1.7.8 *Drosophila* models of SOD1

Elia and colleagues used the G41S missense substitution in a human FALS *SOD* allele and the wildtype human *SOD*, and targeted the expression of the individual proteins in motor neurons of *Drosophila*. The SOD1 *Drosophila* model created by Elia and colleagues was not particularly successful in investigating the biochemical mechanism by which mutations in *SOD* cause degeneration as high-level expression of the human FALS SOD in motor neurons of *Drosophila* does not cause or promote paralysis and premature death of adult *Drosophila* as reported in human and

transgenic mice. In contrast, the expression of FALS SOD extends lifespan, increases resistance to oxidative stress and partially rescues *SOD*-null mutants. The authors proposed that the degeneration of motor neurons in *Drosophila* could require the interaction of FALS SOD with other proteins that are either not present in *Drosophila* or that they do not interact with human SOD.

More recently, another *Drosophila* model of SOD1-induced ALS was published by Bonini and colleagues whereby wild type or mutant human SOD1 selectively expressed in motor neurons resulted in progressive climbing defects in adult flies. In addition, defective synaptic transmission of neural circuit, accumulations of SOD1 proteins in motor neurons and a chaperone stress response in the surrounding glia were observed. This fly model is at the moment the only *Drosophila* model that faithfully recapitulates characteristic hallmarks of sporadic ALS and SOD1-linked familial ALS disease. These hallmarks may present early changes in the disease pathogenesis as no gross motor neuron loss is observed. Moreover, the effects on glia suggest not only a cell autonomous damage to motor neurons, but also non cell-autonomous cellular interactions is conferred by SOD1. These findings provide a foundation to study the role of neuron-glial interactions in ALS pathogenesis (Watson *et al.*, 2008).

The discrepancies seen in both *Drosophila* models expressing mutant human SOD1 using the same motor neuron Gal4 driver could be due to the fact that different mutations of *SOD1* were used in the two studies. Elia and colleagues studied the G41S missense substitution while Watson and colleagues studied the A4V and G85R mutations linked to FALS. Moreover, the expression levels of the transgenes used by Elia and colleagues might not be sufficient to cause neurodegeneration.

1.7.9 Other mutations of ALS

Since the landmark discovery of mutations on the gene encoding SOD1, other even rarer familial cases of ALS with atypical disease features have been linked to

mutations in several other genes. Mutations in the Alsin gene encoding a putative guanine nucleotide exchange factor, have been identified in rare cases of autosomal recessive juvenile form of ALS (Hadano *et al.*, 2001; Yang *et al.*, 2001).

Alsin is enriched in nervous tissue, where it is peripherally bound to the cytoplasmic face of endosomal membranes, an association that requires the amino-terminal RCCI (regulator of chromatin condensation)-like GEF domain (Yamanaka *et al.*, 2003) and can act *in vitro* as an exchange factor for Rab5a , which functions in regulating endosomal trafficking and Rac1 activity (Kanekura *et al.*, 2004). Interestingly, mutant SOD1-mediated toxicity can be suppressed by alsin in motor neuron cell lines through binding of SOD1 via the RhoGEF domain (Kanekura te al., 2004). Loss of alsin however, does not cause motor neuron degeneration in mice, but does contribute to the predisposition to oxidative stress and causes age-dependent neurological defects and altered vesicle and endosome trafficking (Cai *et al.*, 2005; Hadano *et al.*, 2006).

Defects in Senataxin, a gene encoding a DNA/RNA helicase, has been shown to cause an autosomal dominant juvenile form of ALS (Chen *et al.*, 2004). Altered RNA processing has been implicated in two other inherited motor neuron diseases, spinal muscular atrophy (SMA) or severe infantile spinal muscular atrophy with respiratory distress (SMARD). Senataxin was recently identified as the mutated gene in an autosomal recessive ataxia-oculomotor apraxia 2 (AOA2) (Moreira *et al.*, 2004). Senataxin has been shown to be a nuclear protein and is involved in the response to oxidative stress (Suraweera *et al.*, 2007). Most recently, it was reported to be involved in transcriptional regulation and pre-mRNA processing in a cell culture model of AOA2 (Suraweera *et al.*, 2009).

1.7.10 ALS-FTD

The recent identification of 43kDa TAR DNA-binding protein (TARDBP or TDP-43) as a major component of ubiquinated protein aggregates found in patients with

sporadic ALS or frontotemporal lobar degeneration with ubiquinated inclusions (FTLD-U) (Arai *et al.*, 2006; Neumann *et al.*, 2006), have initiated a seismic shift in the understanding of ALS pathogenesis. TDP-43 is a widely expressed and predominantly nuclear, 414 amino acid long protein. It contains two RNA-recognition motifs and a C-terminal glycine-rich region that may mediate interactions with other proteins. TDP-43 immunoreactive inclusions are found in the cytoplasm and nucleus of neurons and glial cells in ALS and FTLD-U patients. Abnormal hyperphosphorylation and ubiquitination of TDP-43 with the production of ~25kDa C-terminal fragments that are missing their nuclear targeting domains are also present in the brains and spinal cords of patients with TDP-43 proteinopathy (Arai *et al.*, 2006; Neumann *et al.*, 2006). It has been proposed that ALS pathogenesis may be driven in part, by the loss of normal TDP-43 function in the nucleus. This is due to TDP-43 being partly cleared from the nuclei of neurons containing cytoplasmic aggregates (Neumann *et al.*, 2006; Van Deerlin *et al.*, 2008).

Dominant mutations at the C-terminal region in the TARDBP gene have since been reported to be the primary cause of ALS, with a total of 30 different mutations now known in 22 unrelated families and in 29 sporadic cases of ALS, proving that aberrant forms of TDP-43 can directly trigger neurodegeneration (Corrado *et al.*, 2009; Daoud *et al.*, 2009; Gitcho *et al.*, 2008; Kabashi *et al.*, 2008; Sreedharan *et al.*, 2008; Van Deerlin *et al.*, 2008). However, it is still not clear whether TDP-43 mutations lead to motor neuron degeneration through a gain of toxic function or a loss of function, which could arise from a sequestration of the protein in nuclear or cytoplasmic inclusions and the corresponding disruption of its interactions with protein partners or RNA targets.

Additional ALS mutations have been found in a gene encoding another DNA/RNA-binding protein called FUS (fused in sarcoma)/TLS (translocation in liposarcoma) causing both dominant (Kwiatkowski *et al.*, 2009) and autosomal recessive (Vance *et al.*, 2009) inheritance of ALS. FUS/TLS is a 526 amino acid long protein that is characterized by an N-terminal domain enriched in glutamine,

glycine, serine and tyrosine residues region, a glycine rich region, an RNA-recognition motif, multiple RGG repeats implicated in RNA binding, a C-terminal zinc finger motif and a highly conserved extreme C-terminal region. Most ALS-linked mutations lie in the extreme C-terminus (Kwiatkowski *et al.*, 2009; Vance *et al.*, 2009).

Similar to TDP-43, FUS/TLS is almost ubiquitously expressed and is predominantly localized in the nucleus, however, cytoplasmic accumulation has been detected in most cell types. Normal FUS/TLS staining in the nuclei of many neurons and glial cell was observed in brains and spinal cords of ALS patients with FUS/TLS mutations but aggregates of FUS/TLS are found in the cytoplasm of neurons. An increase in cytoplasmic accumulation of mutant FUS/TLS after expression of tagged wild type or mutant FUS/TLS was observed in cell fractionation experiments (Kwiatkowski *et al.*, 2009; Vance *et al.*, 2009).

Cytoplasmic FUS/TLS inclusions are absent in control individuals, in ALS patients with SOD1 mutations and in sporadic ALS patients who are presumably TDP-43 aggregates positive. Importantly, ALS patients with FUS/TLS mutations do not have TDP-43 inclusions, implying that mutant FUS/TLS-induced neurodegeneration is independent of TDP-43 aggregation (Vance *et al.*, 2009).

The precise roles of TDP-43 and FUS/TLS are not fully understood, but TDP-43 is able to bind DNA and RNA, which regulates transcription and splicing but may also be involved in microRNA biogenesis, apoptosis and cell division (Sreedharan *et al.*, 2008). FUS/TLS on the other hand, is known to be involved in DNA repair and the regulation of transcription, RNA splicing, and export to the cytoplasm. The RNA recognition motif (RRM), RGG repeat rich, and zinc finger domains are involved in RNA processing (Vance *et al.*, 2009). Mutations in motor proteins have been shown to elicit axonal transport defects and causing motor neuron degeneration (Puls *et al.*, 2003; Hafezparast *et al.*, 2003), interestingly, FUS/TLS also binds to the motor proteins (Yoshimura *et al.*, 2006). Furthermore, TDP-43 and FUS/TLS are found in

granules associated with RNA transport in neurons, with translocation to dendritic spines following neuronal stimuli. In addition, cultured neurons from FUS/TLS knockout mice exhibit aberrant dendritic spine morphology (Fujii *et al.*, 2005), suggesting both TDP-43 and FUS/TLS might play a role in neuronal plasticity by altering mRNA transport and local RNA translation.

The significance of the involvement of TDP-43 and FUS/TLS in neurodegeneration is not unique to ALS, as TDP-43 aggregates are found in most sporadic and familial FTLD-U patients while abnormal TDP-43 inclusions have been reported in Alzheimer's disease patients (Amador-Ortiz *et al.*, 2007). Furthermore, FUS/TLS has been reported to be a major component of aggregates in cellular models of Huntington's disease and SCA3. Intranuclear inclusions have also been identified in neurons of Huntington disease patients (Doi *et al.*, 2008). These results support a role for altered RNA processing in neurodegeneration. Indeed, altered RNA processing has already been implicated in other neurodegeneration such as SCA8 and Fragile X mental retardation (Mutsuddi *et al.*, 2004; Jin *et al.*, 2003). Hence, lessons learned from studying TDP-43 and FUS/TLS are likely to be insightful to neurodegenerative diseases that involve defects in RNA processing.

1.8 VAMP-associated proteins (VAPs)

1.8.1 VAP-induced ALS

In 2004, a genetic linkage study allowed the mapping of a locus responsible for a group of motor neuron diseases to chromosomal region 20q13.3. The disease, named ALS8, affects both sexes equally and the clinical onset occurs between the third and the fifth decade. Most patients have lower motor neuron symptoms but some show bulbar involvement (Nishimura *et al.*, 2004a). Mutation screening led to the identification of a Proline to Serine substitution (P56S) at codon 56 (Nishimura *et al.*, 2004b) in the VAPB (VAMP-associated protein B) protein. In a branch of the same large family the P56S mutation has been shown to cause a lower motor neuron

disorder accompanied by autonomic involvement and dyslipidemia (Marques *et al.*, 2006). The proline residue mutated in ALS8 patients is present in a stretch of amino acids that is very highly conserved from yeast to man in all VAP homologs.

1.8.2 Structure and characterization of VAPB

VAPs are type II integral membrane proteins of ~31 kDa that are highly conserved across species and were first identified in a yeast-two-hybrid screen of *Aplysia californica* (Skehel *et al*, 1995). Subsequently, two mammalian homologues of VAP, named VAPA and VAPB respectively, were identified in humans (Weir *et al*, 1998; Nishimura *et al*, 1999), rat (Nishimura *et al*, 1999) and mouse (Skehel *et al*, 2000). Other VAP homologues have also been found in yeast, known as SCS2 (supressor of choline sensitivity 2) (Kagiwada *et al*, 1998),and *Drosophila,* known as DVAP-33A (Pennetta *et al*, 2002). While VAPB shares 63% amino acid identity with VAPA, a splice variant of VAPB, known as VAPC, lacks both the coiled-coiled domain and the carboxyl terminal trans-membrane domain of VAPB (Nishimura *et al*, 1999).

VAPs have been implicated in diverse cellular functions such as regulation of neurotransmitter release, membrane trafficking, ER-Golgi and intra-Golgi transport, regulation of synaptic growth, lipid transport and metabolism, these wide range of functions have been reported in different cell types and species and mediated by different members of the same family (Soussan *et al.*, 1999; Skehel *et al.*, 1995; Lapierre *et al.*, 1999; Kagiwada *et al.*, 1998; Pennetta *et al.*, 2002; Foster *et al.*, 2000). Nevertheless, the overall structure of VAPs is similar.

Structurally, VAP consists of an N-terminal region facing the cytoplasm and a hydrophobic C-terminus that functions as a transmembrane domain. The trans-membrane domain contains a putative GxxxG motif that has been shown to participate in inner-membrane protein-protein interactions while a variable coiled-coiled domain near the C-terminus trans-membrane domain has been found in almost all t-SNAREs (and has been referred to as the t-SNARE homology domain)

(Nishimura *et al*, 1999; Weimbs *et al*, 1997). The cytoplasmic region contains a conserved N-terminal domain which shares a high degree of sequence and structural similarity with the *C. elegans* Major Sperm Proteins (MSP) (Kuwabara, 2003). MSPs are highly abundant proteins expressed in the amoeboid nematode sperm. The movement of these cells is driven by the assembly of MSP proteins into fibrous networks (Roberts and Stewart, 1995). MSP proteins have also been shown to function as signaling molecules as they antagonize ephrin/Eph receptor signaling in order to promote oocyte meiotic maturation and ovarian muscle contractions in *C. elegans* (Miller *et al.*, 2003).

Within the N-terminal, the MSP domain of VAP also contains a FFAT (diphenylalanine [FF] in an acidic tract) binding site that is highly conserved among VAPs from yeast to mammals but not in the related MSP protein (Loewen *et al.*, 2003; Kaiser *et al.*, 2005). The FFAT motif consists of a consensus amino acid sequence EFFDAxE and is a targeting signal responsible for localizing proteins to the cytosolic surface of the ER and nuclear membrane (Loewen *et al.*, 2003; Brickner and Walter, 2004). Proteins containing exposed FFAT motifs are targeted to the ER membranes by interaction with VAP proteins (Loewen *et al.*, 2003; Wyles *et al.*, 2002).

1.8.3 Cellular functions of VAP: Lipid metabolism and homeostasis

The interaction of VAP with FFAT motif containing proteins was first described between its yeast homologue SCS2p and Opi1p, a transcriptional regulator of phospholipid biosynthesis (Loewen *et al.*, 2003). Subsequently, VAP was found to interact with various lipid-binding and lipid-transport proteins that contain FFAT motifs, which include homologues of oxysterol-binding protein (OSBP) (Wyles *et al.*, 2002; Wyles and Ridgway, 2004), ceramide transport protein (CERT) (Kawano *et al.*, 2006) and phosphatidylinositol (PtdIns)/phosphatidylcholine (PtdCho)-transfer protein, Nir2 (Amarilio *et al.*, 2005).

In addition to the FFAT motif, OSBPs also have a highly conserved 350 amino acid C-terminal sterol or phospholipid binding domain and an N-terminal pleckstrin homology (PH) domain that mediate membrane association of proteins through phosphoinositide binding (Ridgway *et al.*, 1992; Xu *et al.*, 2001). OSBPs localize to the cytoplasm or with VAP in the ER (Wyles *et al.*, 2002), but translocate to the Golgi apparatus when cells are exposed to 25-hydroxycholesterol (25OH) or when subjected to conditions where cellular cholesterol is depleted and/or cholesterol synthesis is activated (Ridgway *et al.*, 1992; Ridgway *et al.*, 1998). This localization of OSBP to the Golgi involves phosphatidylinositol-4-phosphate (PtdIns-4-P) and the small GTPase, Arf1 (ADP-ribosylation factor 1) binding to the PH domain (Levine and Munro, 2002).

OSBPs were initially isolated as cytosolic receptors for oxysterols (Taylor and Kandutsch, 1985). Oxysterols, the product of cholesterol oxidation, are primarily involved in the transcriptional and post-transcriptional regulation of cholesterol metabolism (Venkateswaran *et al.*, 2000), degradation of 3-hydroxy-3-methylglutaryl coenzyme A (HMG-CoA) reductase, a rate limiting enzyme in the mevalonate pathway of cholesterol biosynthesis (Song and DeBose-Boyd, 2004) and the proteolytic activation of the sterol regulatory element binding transcription factors (Radhakrishnan *et al.*, 2004). Hence, OSBP has been thought as a mediator of the effects of oxysterols on the transcriptional regulation of cellular cholesterol homeostasis (Lehto and Olkkonen, 2003).

Additionally, OSBP has an oxysterol-sensing function and has also been shown to be involved in phospholipid and sphingomyelin metabolism (Legace *et al.*, 1999; Xu *et al.*, 2001). Exposure of Chinese hamster ovary (CHO)-K1 cells to 25OH stimulates sphingomyelin synthesis due to an increase in the transport of ceramide to the sphingomyelin synthase in the lumen of the Golgi (Ridgway, 1995; Huitema *et al.*, 2004). Sphingomyelin synthesis by 25OH stimulation can be increased by overexpression of OSBP and inhibited by expression of an OSBP PH domain mutant that constitutively localizes OSBP to the ER with VAP (Lagace *et al.*, 1999; Wyles *et*

al., 2002). This suggest that a ceramide transport pathway for sphingomyelin synthesis is activated by the translocation of OSBP to the Golgi-apparatus.

The mechanism of ER to Golgi transport of ceramide is in turn mediated by a 600 amino acid cytosolic protein called ceramide transfer protein (CERT) (Hanada *et al.*, 2003). In addition to a FFAT motif that binds VAP at the ER, CERT has a steroidogenic acute regulatory-related lipid transfer domain that binds ceramide at the C-terminus and a PH domain that binds PtdIns-4-P at the Golgi (Hanada *et al.*, 2003). It has been suggested that OSBP could regulate CERT activity by either directly or indirectly interacting with shared binding partners like VAP at the ER. Proof of this hypothesis comes from cell culture studies where 25OH was reported to enhance the interaction between VAP and CERT, moreover, CERT mediated ER to Golgi transport of ceramide is dependent on OSBP and VAP (Perry and Ridgway, 2006). Together with the fact that ER to Golgi transport of ceramide is impaired by mutations of the CERT FFAT motif implies that the CERT-VAP binding is important in ceramide transport at the ER-Golgi membrane contact site (Kawano *et al.*, 2006).

Ceramide is transferred from the ER to the Golgi where sphingomyelin is subsequently produced by sphingomyelin synthase on the lumen of the Golgi (Ridgway, 1995; Huitema *et al.*, 2004). VAP can thereby control sphingomyelin production at the Golgi by regulating lipid transfer and lipid binding proteins. Sphingolipids are important components of membranes where they associate with cholesterol to form lipid rafts. Lipid rafts on the other hand, are essential in the organization of synaptic domains, in signalling processes and in the structural remodelling underlying release of neurotransmitter and endocytosis of synaptic vesicles. Moreover, rafts localize and functionally modulate voltage-gated ion channels and metabotropic glutamate receptors (Suzuki *et al.*, 2001; Hering *et al.*, 2003). Given that sphingomyelin and cholesterol are metabolically co-regulated, VAP might play a regulatory role in the metabolic interface between sphingomyelin and cholesterol biosynthesis. However, the exact mechanism is not known (Ridgway, 2000).

1.8.4 Lipid sensing

The answer to how might the interaction of VAP and FFAT proteins regulate lipid biosynthesis comes from studies in yeast. It has been proposed that VAP and/or the FFAT proteins could 'sense' the change in their membrane environment through their lipid-binding or lipid-sensing activity (Loewen *et al.*, 2004). In yeast, Scs2p has been shown to bind phosphatidylinositol monophosphate (PI4P) and biphosphates ($PI4,5P_2$) *in vitro*. The phosphoinositide binding domain is within the MSP domain that partially overlaps with the FFAT binding domain. Therefore, the interaction of Scs2p with FFAT proteins has been proposed to be regulated by the availability of phosphoinositides (Kagiwada *et al.*, 2007). Remarkably, Sac1 (Suppressor of Actin) acts as a lipid phosphatase localized at the ER which primarily regulates the pool of PtdIns-4-P (Wei *et al.*, 2003) that is part of a Golgi membrane localization code of CERT and OSBP. Interestingly, in *Drosophila*, a genome-wide, yeast-two-hybrid screening identified Sac1 as another potential VAP interacting protein (http://www.thebiogrid.org).

Scs2 also plays a role in the transcriptional regulation of the INO1 gene, which is important in the synthesis of inositol (Kagiwada *et al.*, 1998). Opi1p has been shown to bind phosphatidic acid (PA), on the ER with Scs2p and is rapidly translocated to the nucleus in response to a decrease in PA levels. PA is a key player in the biosynthesis of PtdIns and PtdCho as PA is converted into diacylglycerol (DAG), a precursor of many lipid membranes. A decrease in levels of PA due to the production of PtdIns and PtdCho would facilitate the dissociation of Opi1p with Scs2p from the ER, resulting in the inhibition of transcription of INO1 in the nucleus and in turn, the production of inositol. Therefore, Scs2p and Opi1p are involved in 'sensing' the membrane environment and that their interaction is controlled by different phospholipids according to inositol availability (Loewen *et al.*, 2004).

It has previously been proposed that synapse formation in flies is dependent on DVAP-33A in a process similar to budding in yeast (Pennetta *et al.*, 2002; Zito *et*

al., 1999). DVAP-33A regulates synaptic bouton budding in a dosage-dependent manner as null mutants of DVAP-33A impair the ability to form new boutons while overexpression of DVAP-33A causes an increase in synaptic bouton formation (Pennetta *et al.*, 2002). Budding of boutons is therefore also likely to depend on DVAP-33A to 'sense' phospholipid and inositol available. Interestingly, it has been shown that MSP in *C. elegans* localizes to membranes and that it can generate the protrusive force necessary to induce vesicle budding from male germ cells (Kosinski *et al.*, 2005).

1.8.5 Microtubule dynamics

In *Drosophila*, DVAP-33A is enriched in neuromuscular junctions and binds to microtubule networks. DVAP-33A has been shown to regulate bouton budding at larval NMJs in a dosage-dependent manner. It is required for structural remodeling of synapses where it controls microtubule cytoskeleton dynamics. In *DVAP-33A* mutant flies, the presynaptic microtubule architecture is severely compromised, while overexpression of DVAP-33A causes denser organization of the microtubules with more loop like structures. DVAP-33A is therefore proposed to function as a bridge between microtubules and the presynaptic membrane (Pennetta *et al.*, 2002). The effect of VAPs on microtubules has also been observed in mammalian cells where co-expression of VAPB and its interacting protein Nir3 causes a gross remodelling of the ER, with bundling of thick microtubules along the altered ER membranes, suggesting that Nir3, a Nir/rdgB protein family member, either bridges VAPB to microtubules or increases the affinity of VAPB for microtubules (Amarilio *et al.*, 2005).

1.9 Rationale of project.

Although ALS was initially described more than 130 years ago, no effective remedy is yet available. With numerous experiments using mouse models of SOD1 mutations, however, the precise mechanism by which mutations in SOD cause

degeneration of motor neurons is not clear and how over 140 different mutations affecting more than 35 different residues of SOD protein can cause the same generic phenotype in patients. Various pathogenic mechanisms including oxidative damage, excitotoxicity, mitochondrial defects, and axonal transport that have been proposed to contribute to the disease, though symptomatic for the disease, these mechanisms may be secondary to the neurodegenerative process. Furthermore, compared to other neurodegenerative diseases such as Alzheimer's, Parkinson's and polyglutamine diseases, research on ALS has been lagging behind, perhaps due to the lack of a suitable animal model.

VAP at the moment, stands as an interesting candidate to study the pathogenesis of ALS. This is supported by several observations: Firstly, VAP expression in motor neurons from sporadic ALS patients and SOD1-ALS mice is reduced (Teuling *et al.*, 2007). In addition, VAPB is significantly reduced in spinal cords of patients with sporadic ALS and furthermore is selectively enriched in motor neurons at the mRNA and protein level (Anagnostou *et al.*, 2008). These studies strongly suggest that the decreased expression of VAPB might be a common feature associated with motor neuron degeneration.

The microtubule-binding protein tau has been implicated in the pathogenesis of Alzheimer's disease and related disorders such as fronto-temporal dementia (FTD) with Parkinsonism linked to chromosome 17 (FTDP-17), progressive supranuclear palsy and corticobasal degeneration, commonly referred to as tauopathies (Lee *et al.*, 2001). A significant link between ALS and other neurodegenerative diseases comes from overlapping symptoms of ALS and taupathies: A significant subset of patients affected by Frontotemporal Dementia (FTD) also present signs of motor neuron degeneration and other symptoms typical of ALS (Lomen-Hoerth, 2004).

On the other hand, Amyotrophic lateral sclerosis/parkinsonism–dementia complex have been linked to 17q21 and mutations have been identified in microtubule-associated protein tau (Hutton *et al.*, 1998) while many families with

dominant ALS have a phenotype that overlaps with FTD. A locus for ALS-FTD has also been reported in five families at 9q21 but no pathogenic mutation has been reported so far (Hosler, 2000). Karsten and colleagues reported that hVAPB expression is increased in a mouse model for FTD and that loss-of-function mutations in DVAP-33A suppress neuronal degeneration in a fly model for tauopathies. The authors propose that hVAPB could represent the molecular link between tauopathies and motor neuron diseases in FTD (Karsten *et al.*, 2006). Interestingly, while VAPB expression is upregulated in brain regions vulnerable to FTD, OSBP, a well- known interactor of VAP proteins, is strongly downregulated in brain regions that are relatively unaffected both in FTD and ALS (Karsten *et al.*, 2006). This strongly supports the notion that regulation of expression levels of VAP (and its interactors), might affect the selective susceptibility of some regions to neurodegeneration. Moreover, since TDP-43 inclusions are mostly found in tau-negative, ubiquitin positive cases of FTD while TDP-43 and FUS/TLS inclusions are absent in patients with familial SOD1 mutations (Kwiatkowski *et al.*, 2009; Vance *et al.*, 2009; Arai *et al.*, 2006; Neumann *et al.*, 2006; Van Deerlin *et al.*, 2008), this makes VAP an ideal focal point to study the molecular mechanisms of ALS pathogenesis and motor neuron disease in FTD.

The role of VAP in ALS pathogenesis is made even more significant due to the fact that VAP and its interactors are involved in lipid metabolism and homeostasis, and findings that increased energy expenditure is a typical feature of ALS. ALS patients are more likely to show evidence of hyperlipidemia compared to controls (Dupuis *et al.*, 2008) while reduced adiposity and hypermetabolism have also been reported in murine models of ALS. More importantly, these animals exhibit remarkable neuroprotection and extended survival when fed with a high fat diet (Dupuis *et al.*, 2004). Interestingly, patients carrying the pathogenic mutation in hVAPB also exhibit hyperlipidemia with a significant increase in cholesterol and triglyceride levels (Marques *et al.*, 2006). These data support the idea that hypermetabolism is a typical pathological trait of ALS and that defects in lipid metabolism may play a part in the neurodegenerative process.

Due to the role of VAP in the pathogenesis of ALS as supported by human genetics and biochemical studies in other animal models, and the possible implication of VAP in other neurodegenerative diseases syndromically-linked to ALS makes VAP an interesting linking molecule between ALS and these neurodegenerative diseases.

1.10 Aims of project.

To better understand the pathophysiology underlying VAP-induced ALS in humans, we aim to we decided to undertake a detailed functional characterization of VAP proteins in flies and to create a *Drosophila* model for ALS using VAPB to study the effects of pathogenic VAP at the neuromuscular junction. In particular, we plan to address the following:

1. To determine if human VAPB and its *Drosophila* counterpart, DVAP-33A are functionally interchangeable.
2. Investigate the nature of the pathogenic mutation that causes VAP-induced ALS.
3. What is the effect of the pathogenic mutation on synaptic morphology and function?
4. To recapitulate key aspects of ALS pathology in the fly model.

Lastly, we also aim to create a *Drosophila* model of ALS using the adult fly eye. With the creation of this fly model, we plan to harness the power of *Drosophila* genetics by conducting a pilot enhancer/suppressor screen to look genetic interactors of *DVAP-33A,* which would shed light on the molecular mechanisms of ALS pathogenesis

Chapter 2: Materials and Methods

2.1 Materials

2.1.1 Primary Antibodies

Antibody	Source
Mouse α--GluRIIA (8B4D2)	Developmental Studies Hybridoma Bank
Rabbit α-GluRIIB	Aaron DiAntonio
Rabbit α-GluRIII/C	Stephan Sigrist
Rabbit α-GluRIID	Stephan Sigrist
AffiniPure Rabbit α-HRP	Jackson ImmunoResearch
Guinea Pig α-DVAP (GP33)	G.Pennetta
Rabbit α-hVAPB	Sima Lev
Rabbit α-actin (A5060)	Sigma

Table 2.1 Primary Antibodies

2.1.2 Secondary Antibodies

Antibody	Source
Goat α-rabbit Biotinylated IgG	Vector Laboratories
Alexa Fluor® 488 goat α-rabbit IgG	Molecular Probes
Goat α-mouse Cy3 (Cyanine)	Jackson ImmunoResearch
Goat α-rabbit FITC (Fluorescein isothiocyanate)	Jackson ImmunoResearch
Goat α-rabbit Cy3	Jackson ImmunoResearch
Goat α-guinea pig Cy3	Jackson Immunoresearch
Goat α-rabbit HRP IgG	Jackson ImmunoResearch
Goat α-guinea pig HRP IgG	Jackson ImmunoResearch

Table 2.2 Secondary Antibodies

2.2 Fly stocks and genetics

2.2.1 Fly stocks

Strain	Source
Canton S	Bloomington *Drosophila* Stock Center
w⁻/Y; ey-Gal4/ey-Gal4; +/+ (5534)	Bloomington *Drosophila* Stock Center
w⁻/Y; ey-Gal4/CyO; +/+ (5535)	Bloomington *Drosophila* Stock Center
yw/Y; +/+; ey-Gal4/ey-Gal4 (8227)	Bloomington *Drosophila* Stock Center
yw/Y; ey-Gal4/CyO; +/+ (8228)	Bloomington *Drosophila* Stock Center
$elav^{C155}$*-Gal4/*$elav^{C155}$*-Gal4; +/+; +/+* (458)	Bloomington *Drosophila* Stock Center
yw/Y; C164-Gal4/C164-Gal4; +/+	Vivian Budnik
w⁻/Y; +/+; D42-Gal4/D42-Gal4 (8816)	Bloomington *Drosophila* Stock Center
w⁻/Y; +/+; UAS-DIAP1/UAS-DIAP1 (6657)	Bloomington *Drosophila* Stock Center
w⁻/Y; LPin/CyO-GFP; +/+	Andrew Jarman
yw/yw; UAS-DVAP/UAS-DVAP;+/+	G.Pennetta
yw/yw; UAS-DVAPP58S/UAS-DVAPP58S; +/+	G.Pennetta
yw/yw; +/+; UAS-hVAPB/UAS-hVAPB	G.Pennetta
yw/yw; UAS-hVAPP56S/UAS-hVAPP56S; +/+	G.Pennetta
DrosDel Deficiency Collection	Szeged European Stock Center
$DVAP\text{-}33A^{\Delta 20}$*/FM7; +/+; +/+*	G.Pennetta
$DVAP\text{-}33A^{\Delta 166}$*/FM7; +/+; +/+*	G.Pennetta
$DVAP\text{-}33A^{\Delta 448}$*/FM7; +/+; +/+*	G.Pennetta

Table 2.3 Fly Stocks
Numbers in brackets denote Bloomington stock number.

2.2.2 Rescue experiments

The ability of the hVAPB protein to rescue the lethality associated with *DVAP-33A*

mutations was tested by mating female flies of the genotype *DVAP-33A*$^{\Delta 448}$*/FM7; +/+; UAS-hVAPB/TM3*, to males contributing the *C164-Gal4* or *D42-Gal4* drivers. *DVAP-33A*$^{\Delta 448}$*/Y; C164-Gal4/+; UAS-hVAPB/+* adult, non-FM7, males were identified and counted. The specificity of the rescue was confirmed by the absence of *DVAP-33A*$^{\Delta 448}$*/Y; C164-Gal4/+; +/TM3* males. A similar genetic scheme was used to test the ability of *hVAPBP56S* and *DVAPP58S* to rescue the lethality associated with *DVAP-33A* mutations. In all cases, the rescue was confirmed by using all *DVAP-33A* mutant alleles in combination with several transgenic lines expressing *hVAPB*, *hVAPBP56S* or *DVAPP58S*.

2.2.3 Analysis of morphological and physiological rescue

The following crosses were performed:

yw/Y; C164-Gal4/C164-Gal4 males were crossed to *DVAP-33A*$^{\Delta 448}$*/FM7; +/+; UAS-hVAPB/UAS-hVAPB* females. *DVAP-33A*$^{\Delta 448}$*/Y; C164-Gal4/+; UAS-hVAPB/+* males were identified as y^+ third-instar larvae lacking the *FM7* chromosome. A similar genetic scheme was applied to test the ability of *Drosophila* and human mutant proteins to rescue the morphological and physiological phenotypes. To characterize the transgenic expression phenotype, the Gal4 drivers were crossed with transgenic lines. Embryos were collected for 20–24 hours and then transferred to a water-bath at 30°C.

2.2.4 Recombination to construct *ey-Gal4, UAS-DVAPP58S/CyO-GFP* fly stocks

ey-Gal4, UAS-DVAPP58S/CyO-GFP fly stocks were constructed as follow:

♀ *yw/yw; UAS-DVAPP58S/UAS-DVAPP58S; +/+*

X

♂ *w⁻/Y; ey-Gal4/CyO; +/+*

↓

yw/Y; UAS-DVAPP58S/CyO; +/+ *yw/Y; UAS-DVAPP58S/ey-Gal4; +/+*

yw/w⁻; UAS-DVAPP58S/CyO; +/+ ***yw/w⁻; UAS-DVAPP58S/ey-Gal4; +/+***

Each ♀ *yw/w⁻; UAS-DVAPP58S/ey-Gal4; +/+* from the above progenies were selected to cross with 5 males of the genotype *w⁻/Y; LPin/CyO-GFP; +/+*. 100 of these crosses were established:

♀ ***yw/w⁻; UAS-DVAPP58S/ey-Gal4; +/+*** X ♂ *w⁻/Y; LPin/CyO-GFP; +/+*

↓

yw/Y; UAS-DVAPP58S/CyO-GFP; +/+

yw/w⁻; UAS-DVAPP58S/CyO-GFP; +/+

w⁻/w⁻; UAS-DVAPP58S/CyO-GFP; +/+

w⁻/Y; UAS-DVAPP58S/CyO-GFP; +/+

yw/Y; ey-Gal4/CyO-GFP; +/+ *yw/w⁻; ey-Gal4/CyO-GFP; +/+*

w⁻/w⁻; ey-Gal4/CyO-GFP; +/+ ***w⁻/Y; ey-Gal4/CyO-GFP; +/+***

yw/Y; ey-Gal4/LPin; +/+

yw/w⁻; ey-Gal4/LPin; +/+

w⁻/w⁻; ey-Gal4/LPin; +/+

w⁻/Y; ey-Gal4/LPin; +/+

yw/Y; UAS-DVAPP58S/LPin; +/+

yw/w⁻; UAS-DVAPP58S/LPin; +/+

w⁻/w⁻; UAS-DVAPP58S/LPin; +/+

w⁻/Y; UAS-DVAPP58S/LPin; +/+

From the progeny of each individual cross, one male of either *w⁻/Y; UAS-DVAPP58S/CyO-GFP; +/+* or *w⁻/Y; ey-Gal4/CyO-GFP; +/+* genotypes were selected to cross with 5 virgin females of genotype *w⁻/w⁻; LPin/CyO-GFP; +/+*. From this point onwards, both *w⁻/Y; UAS-DVAPP58S/CyO-GFP; +/+* and *w⁻/Y; ey-Gal4/CyO-GFP; +/+* genotypes will be known as *w⁻/Y; ey-Gal4,UAS-DVAPP58S/CyO-GFP; +/+* for simplicity since recombination would have occurred in the germ cells of female progenies of genotype *yw/w⁻; UAS-DVAPP58S/ey-Gal4; +/+* from the first cross between *yw/yw; UAS-DVAPP58S/UAS-DVAPP58S; +/+* and *w⁻/Y; ey-Gal4/CyO; +/+*.

♂ ***w⁻/Y; ey-Gal4,UAS-DVAPP58S/CyO-GFP; +/+***

X

♀ *w⁻/w⁻; LPin/CyO-GFP; +/+*

↓

w⁻/w⁻; ey-Gal4,UAS-DVAPP58S/CyO-GFP; +/+

w⁻/Y; ey-Gal4,UAS-DVAPP58S/CyO-GFP; +/+

w⁻/Y; LPin/ ey-Gal4,UAS-DVAPP58S; +/+

w⁻/w⁻; LPin/ ey-Gal4,UAS-DVAPP58S; +/+

w⁻/w⁻; CyO-GFP/CyO-GFP; +/+

w⁻/Y; CyO-GFP/CyO-GFP; +/+

w⁻/Y; LPin/CyO-GFP; +/+

w⁻/w⁻; LPin/CyO-GFP; +/+

Stocks were established by selecting female virgins of genotype *w⁻/w⁻; ey-Gal4,UAS-DVAPP58S/CyO-GFP; +/+* and crossed to sibling males of genotype *w⁻/Y; ey-Gal4,UAS-DVAPP58S/CyO-GFP; +/+* from progenies of each individual cross in the above scheme.

♀ ***w⁻/w⁻; ey-Gal4,UAS-DVAPP58S/CyO-GFP; +/+***

X

♂ ***w⁻/Y; ey-Gal4,UAS-DVAPP58S/CyO-GFP; +/+***

↓

w⁻/Y; ey-Gal4,UAS-DVAPP58S/CyO-GFP; +/+

w⁻/w⁻; ey-Gal4,UAS-DVAPP58S/CyO-GFP; +/+

w⁻/Y; ey-Gal4,UAS-DVAPP58S/ey-Gal4,UAS-DVAPP58S; +/+

w⁻/w⁻; ey-Gal4,UAS-DVAPP58S/ey-Gal4,UAS-DVAPP58S; +/+

w⁻/Y; CyO-GFP/CyO-GFP; +/+

w⁻/w⁻; CyO-GFP/CyO-GFP; +/+

Only *ey-Gal4,UAS-DVAPP58S/CyO-GFP; +/+* would survive as *ey-Gal4,UAS-DVAPP58S/ey-Gal4,UAS-DVAPP58S; +/+* and *CyO-GFP/CyO-GFP; +/+* are lethal. Established stocks were then allowed a 24 hour period of egg-laying, the parents were transferred and the embryos were heat-shocked at a 30°C water bath. Recombination will have occurred in crosses that result in adult flies that exhibit a reduction in eye size and rough eye phenotype. The established original stocks were then kept for use.

2.2.5 Genetic Screen for dominant modifiers of DVAPP58S

To screen for dominant modifiers of ey-Gal4,UAS-DVAPP58S-induced eye phenotypes, single crosses between eight males coming from deficiency lines on the second or third chromosomes and eight virgins of the *ey-Gal4,UAS-DVAPP58S/CyO-GFP* recombinant line were set at 30°C. For deficiency lines on the X chromosome, eight virgins of each deficiency line were crossed with eight *ey-Gal4,UAS-DVAPP58S/CyO-GFP* males. The resulting progeny were raised at 30°C and screened for enhancement or suppression of eye defects.

The MATLAB software for eye quantification, allows a statistical representation of the range of eye phenotypes resulting from the expression of the UAS-DVAPP58S transgene. A deficiency line was selected as a suppressor of DVAPP58S if the majority of the experimental F1 progeny was centred above 2500 arbitrary units squared and the smallest eye size had a value above 50 arbitrary units squared when compared to 60% of *ey-Gal4,UAS-DVAPP58S/CyO-GFP* flies centred between 1500 and 2000 arbitrary units squared and 5% had eye sizes around 50 arbitrary units squared. Each deficiency line from the DrosDel collection are

molecularly mapped and information on the list of genes uncovered by each deficiency are available on Flybase (www.flybase.org).

2.3 Electrophysiology and Ultrastructural analysis

Electrophysiology and Transmission Electron Microscopy (TEM) for ultrastructural analysis were performed according to Chai *et al.*, 2008.

2.4 Immunohistochemistry

2.4.1 α-HRP stainings of third instar larval NMJs.

Third instar larvae were selected at the wandering stage after having left the food and dissected in PBS (Phosphate Buffered Solution). Larval NMJs were fixed in Bouin's fixative (15:5:1 mixture of saturated picric acid, 37% formaldehyde and glacial acetic acid) for 15 minutes, washed extensively in 0.1% PBT (PBS + 0.1% TritonX-100), blocked in 10% normal goat serum, NGS (Sigma) in 0.1% PBT for 30 minutes, and finally incubated with the primary antibody in the presence of 5% NGS overnight at 4°C. AffiniPure rabbit anti-HRP antibody (Jackson ImmunoResearch) was used at 1:200. Samples were washed in 0.1% PBT for 2 hours by changing solution every 15 minutes and then incubated with the secondary antibody (anti-rabbit Biothinylated IgG 1:400, Vector Laboratories) in presence of 5% NGS for 2 hrs at room temperature. Samples were then washed again in 0.1% PBT for 2 hours by changing solution every 15 minutes. Signal detection was carried out with a VectaStain ABC-HRP kit (Vector Laboratories). In short, samples were then incubated in the pre-incubated A+B mix with for at least 1 hour under constant agitation and washed for 1 hour with 0.1% PBT by changing solution every 15 minutes. The NMJs were transferred into a 24-well plastic plate in 1 ml of 0.1% PBT, 100 µl of DAB (3,3-diaminobenzidine tetrahydrochloride, Sigma) and 2-5 µl of 0.3% H_2O_2 (Hydrogen peroxidase) were added. The reaction was then observed under the dissection scope and stopped by washing the NMJs several times with 0.1% PBT. The NMJs were then be mounted in 90% glycerol (diluted with 1X PBS).

To quantify the phenotypes, at least 6 different synapses per genotype were counted on either muscles 6/7 or 12/13 at high magnification (60x) with Nomarski optics. The bouton numbers are corrected to a mean and ± 1 SD (standard deviation) for each transgenic phenotype.

2.4.2 Phalloidin stainings of NMJs.

Wandering third instar larvae were dissected in 1X PBS and fixed with 4% paraformaldehyde for 20 minutes. Samples were washed with 0.1% PBT and then blocked with 10% NGS for 1 hour on rotator. Samples were then incubated with AffiniPure rabbit anti-HRP (Horseradish peroxidase) (Jackson Immunoresearch) at a concentration of 1:200 with 5% NGS at 4°C overnight on rotator and washed with 0.1% PBT for 2 hours under rotation. After washing, samples were incubated with Alexa Fluor® 488 goat anti-rabbit IgG (Immunoglobulin G) (Molecular Probes) at a concentration of 1:400 with 5% NGS for 2 hours. After incubation, the samples were washed with PBT for 2 hours under rotation and then briefly with 1X PBS. Samples were then washed in 1X PBS for 5 minutes under rotation and then incubated in 1ml 1X PBS with the addition of Alexa Fluor® 568 Phalloidin (Molecular Probes) at a concentration of 1:40 for 20 minutes under rotation. Samples were washed twice for 5 minutes with PBS and mounted on slide in Vectashield (Vector Laboratories).

2.4.3 NMJ stainings of glutamate receptor subunits.

Larvae were dissected in 1xPBS. Larvae to be stained with GluRIIA and GluRIIB were fixed in Bouin's fixative for 5 minutes while larvae to be incubated with GluRII/IIC and GluRIID were fixed in 4% paraformaldehyde for 10 minutes. Fixatives were washed off with 0.1% PBT and blocked in 10% NGS for 30 minutes.

Antibody concentrations used were as follow:
α-GluRIIA 1:100

α-GluRIIB 1:1000

α-GluRIII 1:500

α-GluRIID 1:500

AffiniPure rabbit α-HRP 1:500

Primary antibodies were used with 5% NGS in 0.1%PBT. Samples were incubated overnight at 4°C on rotator and then washed with 0.1% PBT for 2 hours under rotation (i.e. 8 x 15 minutes).

Samples were incubated with their respective secondary antibodies with the following concentrations:

α mouse-Cy3 1:400 (For GluRIIA)

α rabbit-FITC 1:1000 (For AffiniPure rabbit α-HRP)

α rabbit-Cy3 1:1000 (For GluRIIB, GluRII/IIC and GluRIID)

Secondary antibodies were used with 5% NGS in 0.1% PBT on rotator for 2 hours at room temperature. Samples were then washed with 0.1% PBT for 2 hours under rotation and then mounted on slide with Vectashield (Vector Laboratories).

2.4.4 DVAP-33A stainings of third instar larval brains

Larvae were dissected in 1xPBS and then fixed brains and imaginal discs in Bouin's fixative for 5 minutes. Fixative was washed off with 0.1% PBT and the samples blocked with 10% NGS for 1 hour. Samples were incubated with AffiniPure rabbit α-HRP (1:500) and α-DVAP (GP33) (1:1000) in 5% NGS and 0.1% PBT overnight at 4°C on rotator. Samples were then washed with 0.1% PBT for 2 hours under rotation and incubated with secondary antibodies: α rabbit-FITC (1:100) and α GP-Cy3 (1:500) in 5% NGS and 0.1% PBT on rotator for 2 hours at room temperature. The samples were then washed with 0.1% PBT for 2 hours under rotation and mounted on slide with Vectashield (Vector Laboratories).

2.4.5 DVAP-33A stainings of third instar larval NMJs

Larvae with their respective genotypes were dissected in 1xPBS and then fixed in

Bouin's fixative for 5 minutes. The Bouin's fixative was washed off with 0.1% PBT and then transferred into 1.5ml microcentrifuge tubes to be further washed in 0.1% PBT. Larvae NMJs were then blocked with NGS for 30 minutes and incubated with AffiniPure rabbit α-HRP (1:500) and α-DVAP (GP33) (1:1000) in 5% NGS and 0.1% PBT overnight at 4°C on rotator. Samples were washed with 0.1% PBT for 2 hours under rotation and then incubated with secondary antibodies: α rabbit-FITC (1:1000) and α GP-Cy3 (1:500) in 5% NGS and 0.1% PBT on rotator for 2 hours at room temperature. The NMJ samples were then washed with 0.1% PBT for 2 hours under rotation and mounted on slide with Vectashield (Vector Laboratories).

2.5 Western Blot

Single, dissected brain and neuromuscular junction (NMJ) samples from *Drosophila* third instar larvae or optic lobes from adult flies of the respective genotypes were collected and kept at -20°C until homogenization. Samples were homogenized in Laemmli buffer (Biorad Laboratories) using strokes of a pellet pestle. After assembling the electrophoresis module (Biorad Laboratories), the protein extracts and molecular weight marker (Molecular Probes) were loaded to fill the corresponding wells of 8% SDS-PAGE gels. Electrophoresis was carried out at 100 Volts for 90 minutes. The gel was removed and proteins were transferred onto Hybond-P PVDF membranes (Amersham Biosciences) for 2 hours at 200mA. Then, the membranes were incubated overnight at 4°C under gentle agitation in blocking solution. The blocking solution consisted of 2% ECL Advance Blocking Agent (Amersham Biosciences) diluted in TBST(Tris Buffer Solution with Tween)-0/1% Tween 20 (Sigma) in TBS (Tris Buffer Solution) (8g NaCL, 20ml 1M Tris at pH7.6 brought up to a final volume of 1 litre). After the overnight blocking, briefly rinse the membrane with 2 washes in TBST before incubating the respective primary antibodies: α-DVAP (GP33) (made in guinea pig, diluted at 1:70000) or hVAPB (made in rabbit, diluted 1:7500) in blocking solution for 2 hours at room temperature with mild agitation. After primary antibody incubation, the membrane was rinsed briefly with 2 changes of TBST. The membrane was then submerged in 250ml of

TBST and placed on a shaker during washing for 2 hours, changing TBST solution every 15 minutes. The membranes were then incubated for 2 hours with mild agitation at room temperature with secondary antibody α-Guinea Pig HRP IgG, diluted at 1:60000 or α-Rabbit HRP IgG, diluted at 1:10000 in blocking solution. The rinse/wash cycles mentioned after primary antibody incubation were repeated. Signals on the membrane were detected using the ECL Advance Western Blotting Detection Kit (Amersham Biosciences). In brief, detection solutions A and B were mixed in a ratio of 1:1 and pipetted onto the membrane with the protein side facing upwards and left for 1 minute at room temperature. Excess detection reagent was drained before wrapping the blots with SaranWrap™. The wrapped membranes were placed quickly into an X-ray film cassette and exposed to autoradiography film (Hyperfilm™ECL) for 60 seconds. The film was removed and placed in developer for 30 seconds and then rinsed briefly before fixing. On the basis of the appearance of the first film, exposure times were varied for the subsequent films. The films were scanned onto a computer to obtain a digital image.

For actin-loading controls:

Membranes were kept in saran wrap at 4°C in a humid chamber until it was used in stripping protocol. The membrane was rewet for a few seconds with methanol and then washed in distilled water for 5 minutes. The membrane was then submerged in stripping buffer (100 mM mercaptoethanol, 2% (w/v) SDS, 62.5 mM Tris-HCl, pH 6.7) and incubated at 60°C for 30 minutes with occasional agitation. The membrane was subsequently washed twice for 10 minutes in TBST at room temperature using large volumes of wash buffer. The membrane was blocked overnight at 4°C with blocking solution and proceeded to the immunoblotting steps with primary and secondary antibodies as described above. The concentrations for antibodies are listed below:

Immunoblotting for actin loading control

Primary antibody concentration

Brains and NMJs

α-actin (Rabbit) A5060, Sigma 1:20000

Secondary antibody concentration

Brains and NMJs

α-rabbit HRP IgG (Jackson Immunoresearch) 1:20000

2.6 TUNEL staining for detection of apoptosis

Wandering third instar larval brains were dissected in 1X PBS and transferred in eppendorf tubes containing 1X PBS. Fixation was done by rapidly exchanging the dissecting buffer with 4% paraformaldehyde and fixed for 15 minutes at room temperature, on a rotator.

Larval brains were washed with 1X PBS quickly and then for 5 minutes at room temperature, under rotation. 1 µl of a 10mg/ml of Proteinase K (Promega) solution was diluted in 1 ml 1X PBS to give a final concentration of 10ug/ml Proteinase K. This solution was added to the brains and incubated for 10 minutes under rotation at room temperature. Samples were washed quickly with 1X PBS 3 times and then for 1 hour at room temperature, under rotation, exchanging PBS solution every 15 minutes. Larval brains were fixed again for 5 minutes at room temperature with 4% paraformaldehyde, washed quickly for 3 times with PBS and again for 3 times for 5 minutes. Samples were resuspended in 100 µl equilibration buffer for 5 minutes on the bench. Labelling reaction with TUNEL reaction mixture (Promega DeadEnd Fluorometric TUNEL System) were prepared as follow and kept on ice (90 µl Equilibration buffer, 10 µl Nucleotide mix and 2 µl rTdT Enzyme for each reaction). After incubation with equilibration buffer, the buffer was removed and the prepared reaction mix were added to to the brains and incubated for 2 hours at 37 °C in a water bath. The reaction mix was pipetted up and down carefully every 15 minutes. The reaction mixture was removed after incubation and 1 ml of 20 mM EDTA was added to terminate the reaction. Larval brains were washed with 1X PBS, thrice for 15

minutes, at room temperature under rotation. The excess liquid was drained out and larval brains were mounted on a slide in Vectashield (Vector Laboratories).

2.7 Scanning Electron Microscopy (SEM)

Analysis of adult eye phenotype by SEM was carried out by decapitating flies under carbon dioxide anaesthesia. Adult fly heads were fixed immediately with 3% Glutaraldehyde in 0.1M Sodium Cacodylate Buffer (pH7.4) for >3 hours, washed in 0.1M Sodium Cacodylate Buffer (pH7.4) for 3 x 20 minutes, incubated in 1% Osmium Tetroxide in 0.1M Sodium Cacodylate Buffer for 1-2 hours, washed for 30 minutes in distilled water, dehydrated in 50%, 70%, 90% and 100% acetone for 10 minutes each, and twice more in 100% acetone for 10 minutes each, dried with carbon dioxide in a Polaron E3000 SII CPD, sputter coated with 20nm Gold/Palladium (60/40) in an EMSCOPE SC500 Sputter Coater and viewed with Philips 505 scanning electron microscope.

2.8 Imaging and morphometric analysis

Larval NMJs were imaged using an Axiovert Zeiss Microscope. The same confocal gain settings were applied to control and mutant NMJs. A complete Z-stack was acquired for every NMJ and rendered on a 3D projection. For the morphometric analysis, images were initially trimmed using the Zeiss LSM Image Examiner 3.2.0.70 software (Carl Zeiss, 2002). Cluster counting and volume estimation were performed with the software package Imaris 4.7.2 (Bitplane AG, 2006). The minimum cluster radius was set to 0.4 μm and background object subtraction was used when applying the 'spot detection' function. The total cluster volume was found by fitting a 3D surface to the clusters with the iso-surface tool and no additional Gaussian smoothing or re-sampling steps were applied. The average volume of a single cluster was calculated by dividing the total cluster volume by the total number of clusters. Appropriate intensity thresholds were selected to properly identify clusters and ignore background intensities for both tools in the Imaris package.

Statistical analysis was performed using a two-tailed Student's *t*-test.

2.9 Larval locomotion behaviour

Wandering third instar larvae were collected from the vial and washed briefly in distilled water to remove traces of food. Each larva was transferred to the centre of a 9 cm Petri dish containing grape juice medium. The larva was then allowed to adjust to the Petri dish environment and the counting of the peristaltic waves was started only after observing the first wave of contractions. The contraction waves were counted for at least 2 min per larva and their number divided by the time in seconds to obtain the frequency of contractions expressed in Hertz (Hz). The Lillefors test was applied to check for normality in the distribution of the different datasets. Since the data concerning the elav; UAS-DVAPmt failed to pass the test for normality, the non-parametric Mann–Whitney U test was used to compare the datasets.

2.10 MATLAB software for eye quantification

Pictures of *Drosophila* eyes were taken on a camera attached to a light microscope with the same fixed magnification for all genotypes. The MATLAB software for eye quantification allows the user to trace the border of the eye at a zoomed-in level (see Figure 2.1 and Figure 2.2 below). The criterion used for selecting the border was that the border highlighting should run outside the eye, as close as possible to its boundary with the head. Errors in tracing the border can be corrected by deselecting the single pixels. The software has other features to check there are no gaps in the border traced and ensure that the border is one pixel wide. The software then calculates the circumference and area of the closed border surrounding the eye, which are then automatically transferred onto an Excel spreadsheet.

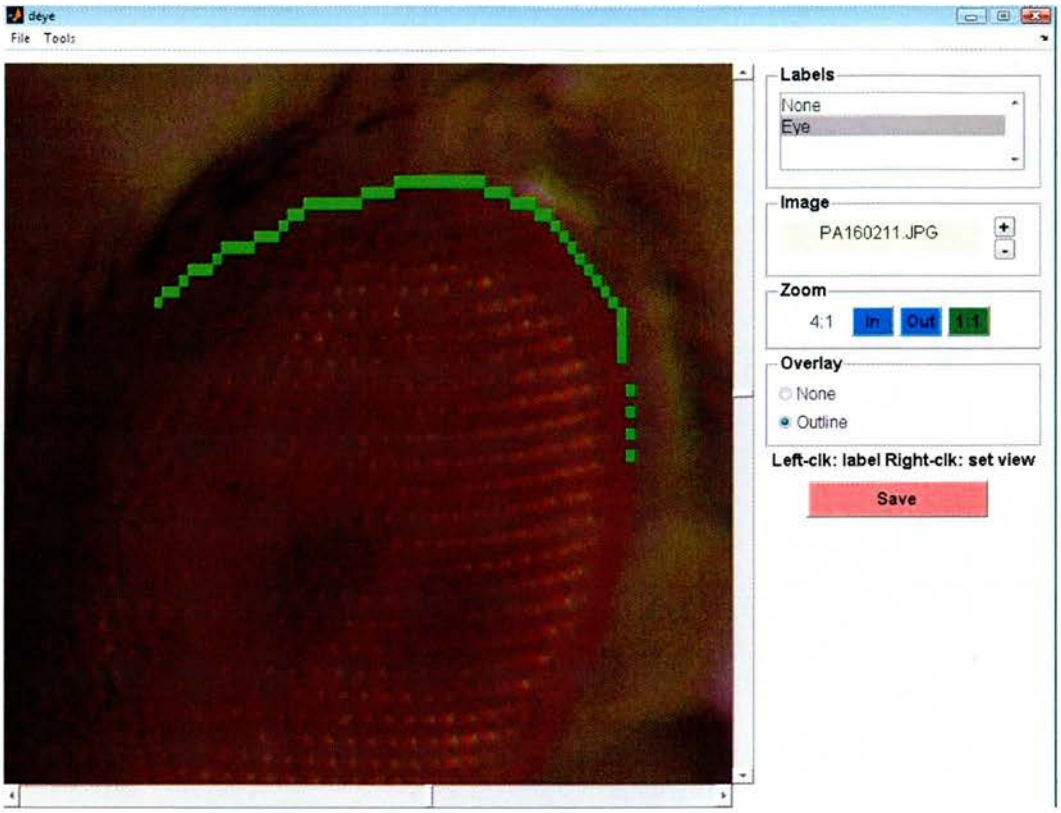

Figure 2.1. Zoomed-in picture displayed on the MATLAB eye quantification software.
Seen here is a picture of a wild-type eye with a partly traced border, highlighted in green.

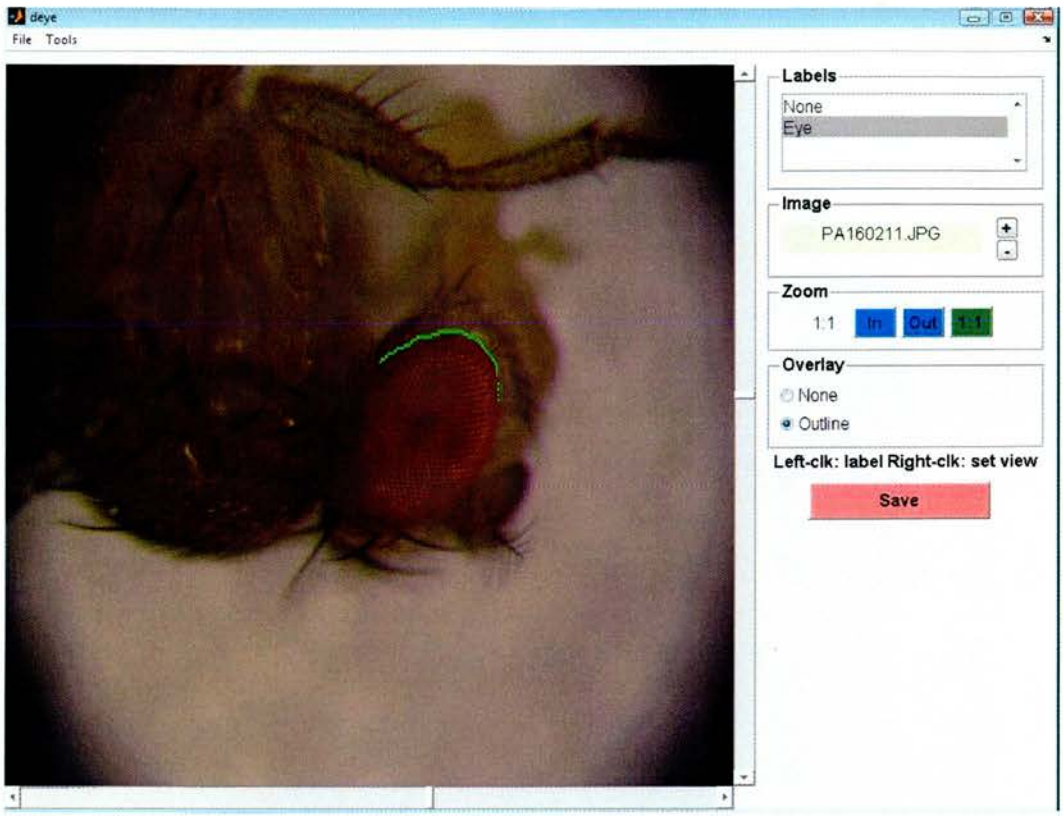

Figure 2.2. Zoomed-out picture on the MATLAB eye quantification software. Seen here is a picture of a wild-type eye with a partly traced border, highlighted in green. The traced border is extremely close to the edge of the eye, giving a more accurate quantification of eye size.

The Lillefors test was applied to check for normality in the distribution of the different datasets. Since all the datasets failed to pass the test for normality, with *ey-Gal4, UAS-DVAPP58S/CyO-GFP* flies and *ey-Gal4, UAS-DVAPP58S/Df(2L) ED695* flies bordering on normal (P=0.0153 and 0.0119 respectively), the non-parametric Mann–Whitney U test was used to compare the datasets. Since the distribution of *ey-Gal4, UAS-DVAPP58S/CyO-GFP* flies and *ey-Gal4, UAS-DVAPP58S/Df(2L) ED695* flies bordered on normal, the two-sampled student t-test was also used to test these two data sets and the difference in distribution was found to be highly significant ($P<0.005$).

Results

Chapter 3: DVAP-33A is the structural and functional homologue of hVAPB

3.1 DVAP-33A is the structural homologue of hVAPB

Human VAPB was found to be the causal agent of ALS8 and is a result of a missense mutation that causes the substitution of a serine for the conserved proline (P56S) at codon 56 (Nishimura *et al.*, 2004b). We decided to model ALS 8 in flies as it has been shown to be a very flexible and successful model system in studying neurodegenerative diseases (Warrick *et al.*, 1998, Jackson *et al.*, 1998, Struhl & Greenwald, 1999, Feany & Bender, 2000, Fernandez-Funez *et al.*, 2000). In order to model ALS8 in flies, we need to identify the structural homologue of hVAPB in *Drosophila*. Comparing structural similarities between proteins sequences of humans and *Drosophila* allows the identification of regions of similarity that may shed light on the function and evolutionary relationships of genes in both normal and disease states in these two organisms (Rubin *et al*, 2000, Fortini *et al*, 2000).

There are three proteins in *Drosophila* that show significant homology and structural similarity to hVAPB and they are CG33523, CG7919 (*Farinelli*) and CG5014 (*DVAP-33A*). Farinelli is specifically expressed in testes and larval fat body and is also required for male fertility (Pennetta *et al*, 2002). Both proteins encoded by CG33523 and *DVAP-33A* are ubiquitously expressed, however, global protein sequence alignment showed that protein encoded by CG33523 is only 34% similar while DVAP-33A is 62% similar to hVAPB.

CG33523 is 34% similar to hVAPB and encodes a VAP-like protein that spans a region of only 6kb on the *Drosophila* genome. Protein sequences corresponding to conceptual translation of CG33523 transcripts show that it contains a C-terminal region containing a putative transmembrane domain (TMD), a domain with strong homology to MSP and a putative Cellular retinaldehyde-binding/triple function (CRAL-TRIO) motif at the N-terminus that binds small lipophilic

molecules. This additional CRAL-TRIO domain found on CG33523 is unique and not found in classical VAPs, therefore, the only possible homologue of hVAPB in flies can only be DVAP-33A.

Using the ClustalW v1.82 alignment program available from EMBL-EBI, we showed that DVAP-33A and hVAPB exhibit 39.6% amino acids identity matches and 61.7% of amino acids were identity matches or conserved substitutions (Figure 3.1A). Structurally, DVAP-33A and hVAPB share a common tri-partite domain organization: an MSP homology domain at the N-terminal that contains a stretch of 16 amino acids that is perfectly conserved between DVAP-33A and hVAPB (Figure 3.1A and B), a coiled-coiled domain that may be involved in protein-protein interaction and a transmembrane domain at the C-terminal (Figure 3.1B; Amarilio *et al.*, 2005; Nishimura *et al.*, 1999). The higher degree of homology and higher degree of structural similarity suggest that DVAP-33A is most likely to be the *Drosophila* homologue of hVAPB.

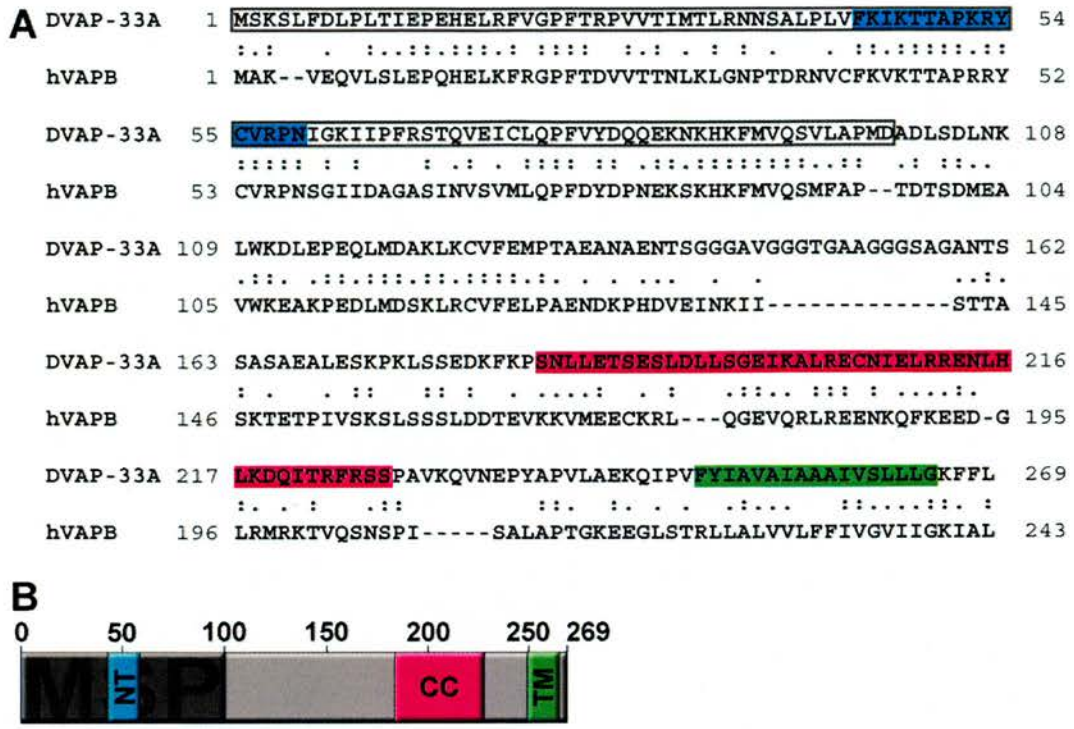

Figure 3.1. human VAPB (hVAPB) protein and its *Drosophila* homologue DVAP-33A are structurally similar.

(**A**) A global protein sequence alignment was performed using the ClustalW v1.82 alignment program available from EMBL-EBI. 39.6% amino acids were identity matches and 61.7% were identity matches or conserved substitutions. The sequence for DVAP-33A was taken from FlyBase (Flybase ID FBgn0029687) and the source for the hVAPB sequence was UniProt ID/accession code VAPB_HUMAN/O95292. In the rows between the aligned proteins, ":" represents an identity match, and "." is a conserved substitution according to the GONNET 250 matrix. (**B**) Structure analysis of VAP proteins predicts a transmembrane domain at the C-terminus (TM) and a coil-coiled domain (CC) in the middle. The grey boxed area corresponds to a domain of significant homology to the nematode Major Sperm Protein (MSP). This region includes the N-terminal (NT) sequence of 16 amino acids that is perfectly conserved between DVAP-33A and hVAPB.

3.2 Altered expression of DVAP-33A regulates the size and number of synaptic boutons at the larval NMJs

DVAP-33A has previously been characterized and shown to be involved in bouton budding at the *Drosophila* NMJ, control of microtubule cytoskeleton dynamics and is required for structural remodelling of synapses (Pennetta *et al.*, 2002). We found that hypomorphic and null mutations in *DVAP-33A* cause a severe decrease in bouton

number with a concomitant increase in bouton size. *DVAP-33A*$^{\Delta 166}$ mutants exhibit only 150 ± 7 boutons (Figure 3.2B and E), while controls contain 250 ± 8 boutons (Figure 3.2A and E).. Conversely, presynaptic overexpression of *DVAP-33A* induces a highly significant increase in the number of boutons with a concomitant decrease in their size (300 ± 7 versus 180 ± 8 in controls, Figure 3.2; Pennetta *et al.*, 2002). Despite the redistribution in sizes of boutons observed in these synapses, the total surface area does not significantly differ from wild type. In summary, loss of DVAP-33A causes a decrease in bouton number accompanied by an increase in their sizes while an increase in DVAP-33A dosage induce an increase in number of boutons with a decrease in their sizes.

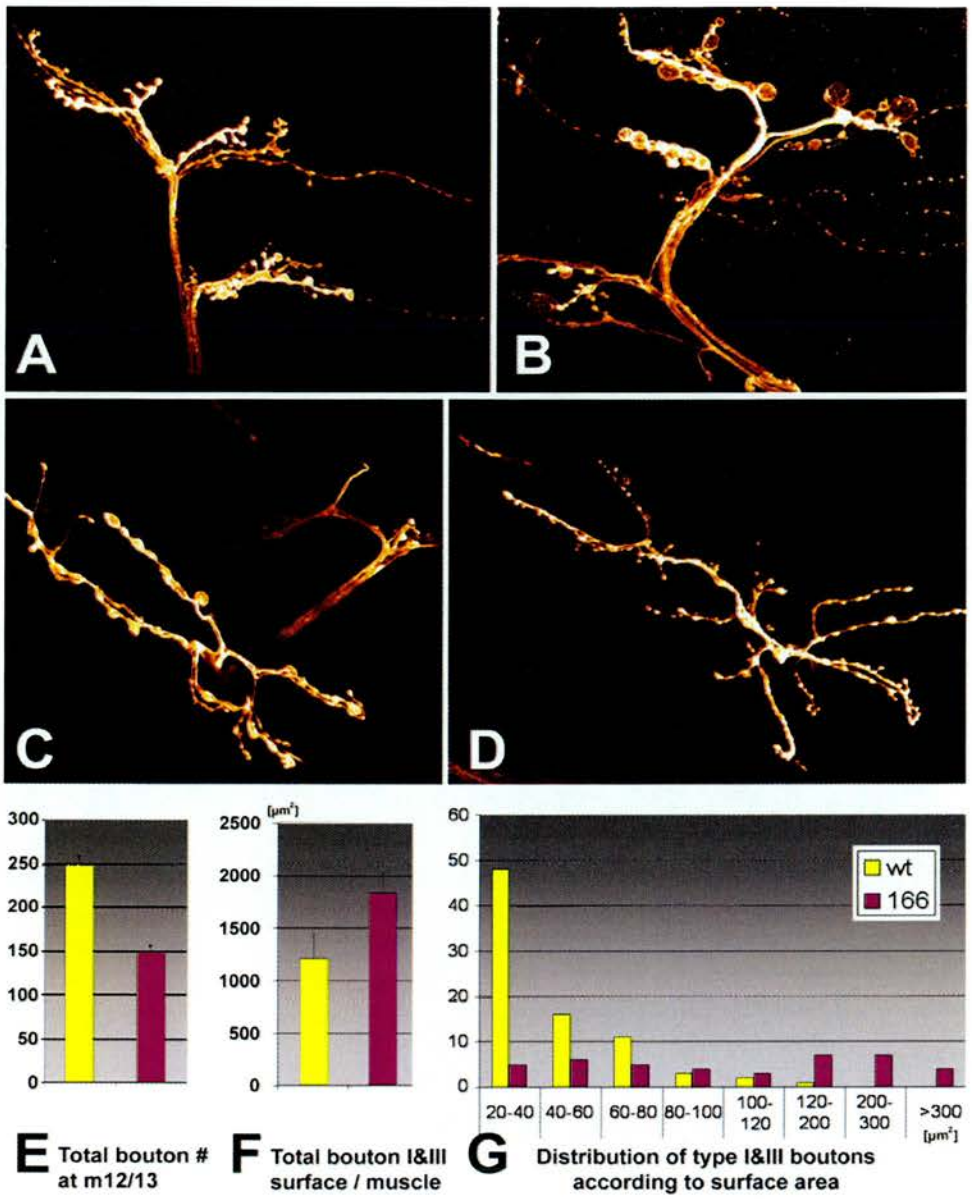

Figure 3.2. The dosage of DVAP-33A affects the number and size of boutons at the larval NMJs.

Anti-HRP staining of controls (A and C), *DVAP-33A*$^{\Delta 166}$ mutants (B) and UAS-DVAP-33A overexpressing NMJs (D). (E) Quantification of the total number of boutons in controls and Δ166 mutants. (F) Total surface area per muscle and calculation of the distribution in synaptic bouton area (G). A revertant line was used as a control in A, while in C the UAS-DVAP line was used as a control. The total number of boutons on muscles 12 and 13 was counted in the analysis of *DVAP-33A*$^{\Delta 166}$ mutants. The reduction in number of boutons is also accompanied by an increase in their size and surface area in null mutants (Figure 3.2F and G). Total number of boutons on muscles 6 and 7 was counted for the analysis of DVAP-33A overexpressing larvae.

3.3 Changes in DVAP-33A dosage does not affect normal synaptic transmission

Since the number and size of synaptic contacts between a neuron and its target may affect synaptic strength, we investigated whether the structural changes due to alterations in DVAP-33A dosage have any consequence on synaptic function. Electrophysiological analysis was focused on partial loss-of-function mutation *DVAP-33A*$^{\Delta 166}$ since many more mutants survive to the third instar larval stage than null mutants, while displaying very similar phenotypes to null mutants. As shown in Figures 3.3A and B, the amplitude of the evoked junctional potential (EJP) is not significantly different ($P > 0.05$) in synaptic terminals exhibiting fewer and larger boutons (36 ± 2 mV) relative to controls (37 ± 2 mV). To determine whether other aspects of synaptic transmission are altered in mutants, the properties of miniature excitatory junctional potentials (mEJPs) were also analyzed. We found an increase in the mean frequency of mEJPs in mutants when compared to controls (3.80 ± 0.24 Hz versus 2.00 ± 0.11 Hz, $P < 0.001$) (Figure 3.3E). In addition, as shown in Figure 3.3E and F, the mean amplitude of mEJPs is increased in partial loss-of-function mutants (1.30 ± 0.02 mV in *DVAP-33A*$^{\Delta 166}$ versus 0.80 ± 0.01 mV in controls). This difference in quantal size is significant ($P < 0.001$) and is also observed in null mutants (data not shown).

In synaptic terminals overexpressing *DVAP-33A (elav-GAL4; UAS-DVAP-33A)*, the EJP amplitude is not significantly changed compared to controls (32 ± 3 mV versus 33 ± 2 mV, $P > 0.05$) (Figure 3.3C and D). Conversely, in synaptic terminals overexpressing *DVAP-33A*, a significant decrease in quantal size was observed (0.59 ± 0.05 mV versus 0.90 ± 0.06 mV in the control, $P < 0.05$) (Figure 3.3G). Interestingly, cumulative amplitude histograms for both genotypes, indicate that the entire mEJP amplitude distribution is shifted towards larger values in mutants (Figure 3.3F) and towards smaller values in animals in which DVAP-33A is overexpressed (Figure 3.3G). Thus, changes in quantal size are, at least partially, responsible for maintaining normal synaptic transmission in loss-of-function and

overexpression paradigms.

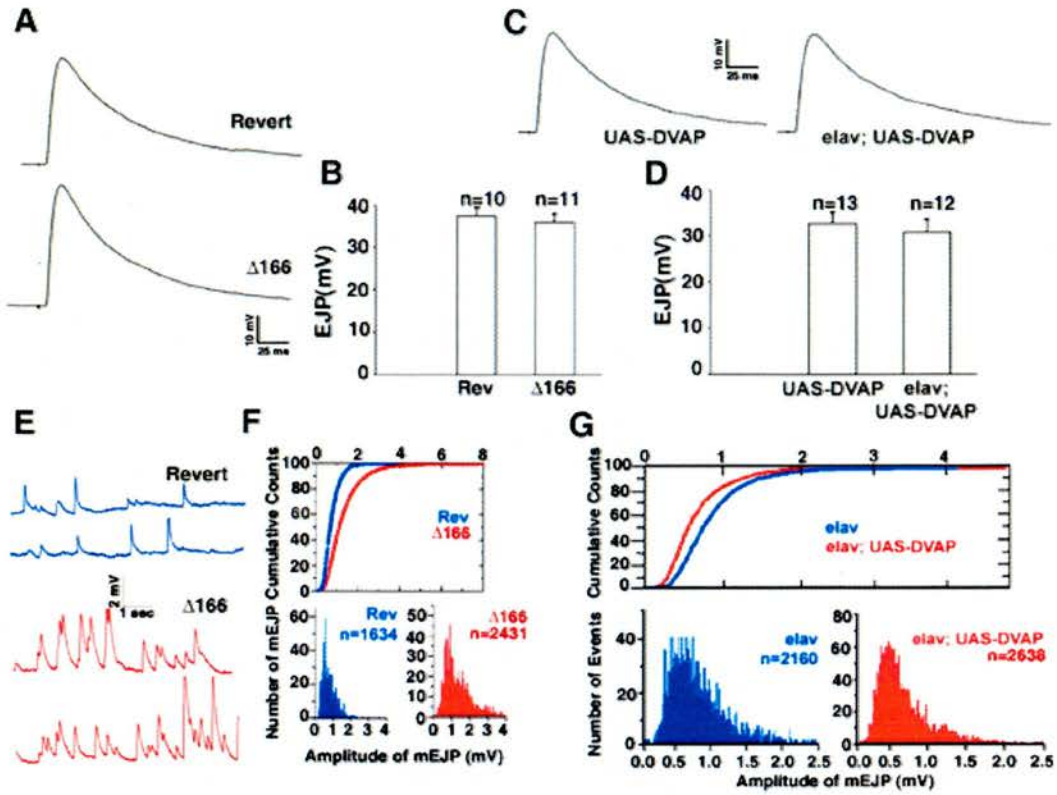

Figure 3.3. Normal synaptic transmission is maintained in animals lacking or overexpressing *DVAP-33A*.

(A-D) Evoked neurotransmitter release is normal in both *DVAP-33A* loss-of-function and overxpression mutants. (A) Examples of single traces showing EJPs in *DVAP-33A* mutants (Δ166) and controls (Revert). (B) Summary of EJP amplitudes for *DVAP-33A*$^{\Delta 166}$ mutants (Δ166, n=11) and controls (Rev. n=10). (C) Representative traces of EJPs in synaptic terminals overexpressing *DVAP-33A* (*elav*; *UAS-DVAP*) and controls (*UAS-DVAP*). (D) Summary of EJP amplitudes for overexpression mutants (n=12) and controls (n=13). (E-F) *DVAP-33A* mutations significantly increase the frequency and the amplitude of spontaneous miniature excitatory junctional potentials (mEJPs). (E) Representative traces of mEJPs for *DVAP-33A* mutants (Δ166) and controls (Revert). (F) Cumulative distribution of total mEJP amplitudes in *DVAP-33A* mutants (Δ166) and in controls (Rev.). Histograms of mEJPs for Rev. and Δ166 are shown. (G) Cumulative distribution of total mEJP amplitudes for terminals overexpressing *DVAP-33A* (*elav; UAS-DVAP)* and for the control (*elav*), and histograms of mEJPs for *elav; UAS-DVAP* and *elav.* The transgenic line used for overexpressing DVAP-33A was Drwt1. (Data and figure courtesy of Bing Zhang).

3.4 Ultrastructure remodeling of the synapse accompanies functional compensation at the NMJ

At the ultrastructural level, we investigated if changes within the synapse could account for the functional compensation in loss-of-function and overexpression of DVAP-33A. TEM analysis of terminals lacking and overexpressing DVAP-33A was performed and we found that there is an increase in number of active zones in boutons of DVAP-33A loss of function mutants (2.0 ± 0.2 active zones per bouton cross-sectional area versus 0.8 ± 0.3 in controls, Figure 3.4A-C and E) while in synapses overexpressing DVAP-33A the number of active zones per surface area is not affected. However, there are substantially more boutons which are significantly smaller in size when compared to wt boutons and we observed a decrease in density of vesicles per bouton (Figure 3.4D).

As reported in Figure 3.4F, in every small bouton resulting from DVAP-33A overexpression, more than 80% of the bouton cross-sectional area is empty, whereas in controls, numerous vesicles are packed in each bouton leaving only 40%-50% of the bouton area empty. No change in the size of synaptic vesicles was observed in any of the genotypes (not shown). The system seems to be able to concentrate the number of active zones in a reduced number of boutons in the loss of function mutants and on the other hand, dilute the density of vesicles in the overexpression of DVAP-33A that have an increased number of boutons. These data clearly indicate that synapses can undergo structural remodeling, whereby active zones can increase in a reduced number of boutons and the pool of vesicles can be diluted in an increased number of boutons to maintain functional and structural homoeostasis.

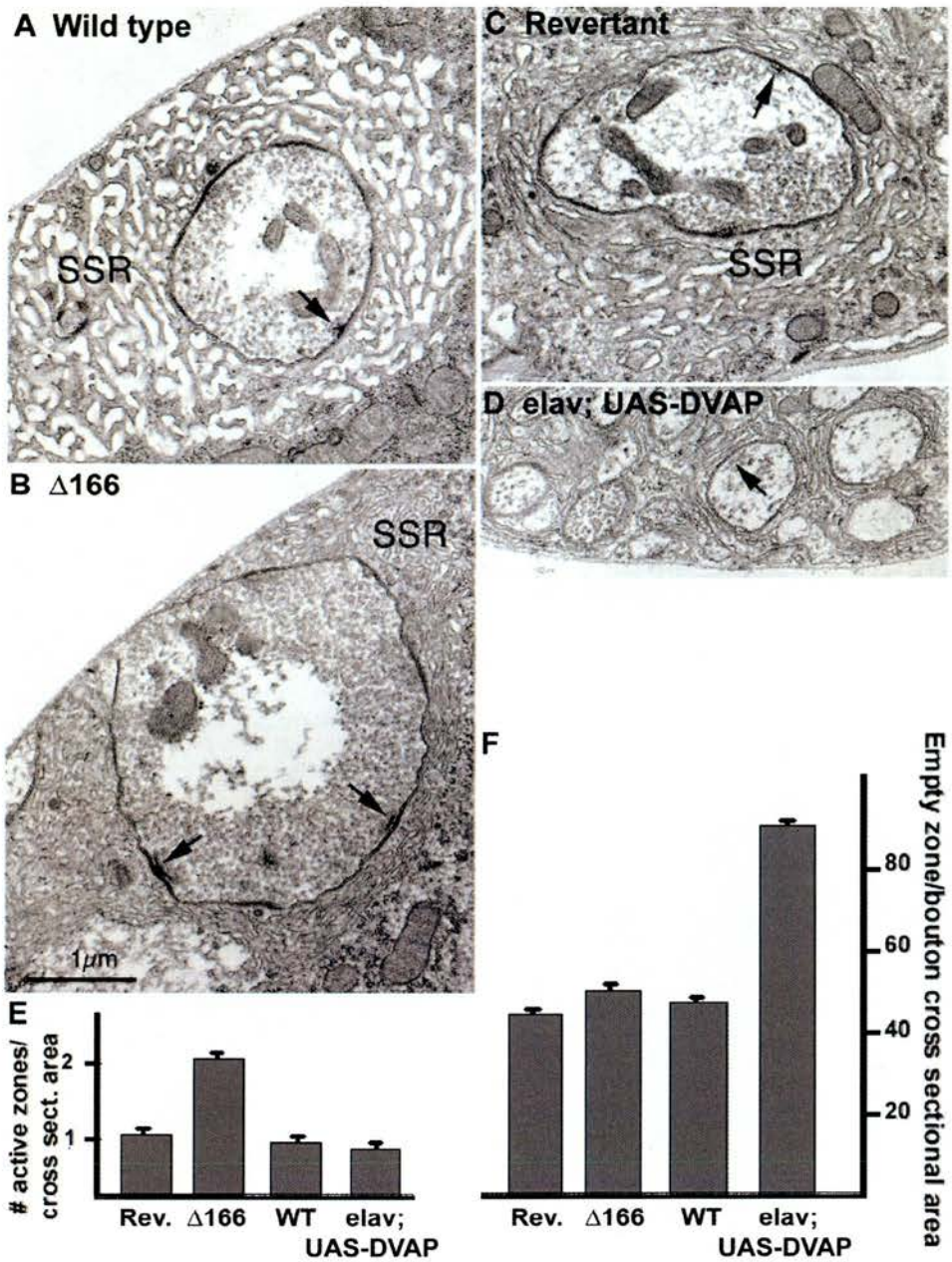

Figure 3.4. Loss of function and overexpression of DVAP-33A affects ultrastructural remodeling of the synapse.

Electron micrographs of NMJs from controls (A and C), *DVAP-33A*$^{\Delta 166}$ hypomorphic mutants (Δ166.) in B, and *DVAP-33A* (elav; UAS-DVAP*)* overexpressing larvae in D. Presynaptic active zones (arrows) and subsynaptic reticulum (SSR) are indicated. Arrows in D indicate synaptic vesicles. (E-F) Morphometric analysis of Δ166 mutants and *DVAP-33A* overexpressing terminals. Nerve terminals were sectioned and analyzed for the number of active zones per bouton cross sectional area (E) and for the bouton area devoid of synaptic vesicles (F). The transgenic line used for overexpressing DVAP-33A was Drwt1. (Figure and data courtesy of Vivian Budnik and Young Ho Koh)

3.5 hVAPB expression rescues the lethality, morphological and electrophysiological phenotype of DVAP-33A null mutants at the NMJ

Given the degree of homology and structural similarity between hVAPB and DVAP-33A, we want to test if hVAPB can functionally substitute for DVAP-33A in flies. It has been shown previously that the complete loss of DVAP-33A in DVAP-33A $^{\Delta 20}$ and DVAP-33A $^{\Delta 448}$ mutants cause lethality in second instar/early third instar larvae, and examination of NMJ morphology in the larvae showed an increase in size and decrease in number of boutons (Figure 3.2, this work; Pennetta *et al.*, 2002).

Transgenic flies carrying the UAS-hVAPB cDNAs were generated (Chai, A MSc Thesis, 2005) with the intention of rescuing the lethality and morphological phenotypes seen in DVAP-33A loss of function mutants. The *hVAPB* gene was expressed in null (*DVAP-33A* $^{\Delta 20}$ *and DVAP-33A* $^{\Delta 448}$) and hypomorphic (*DVAP-33A* $^{\Delta 166}$) mutant background using *C164-Gal4* (Torroja *et al*, 1999) and *D42-Gal4* (Elia *et al*, 1999) drivers. *C164-Gal4* has previously been used to rescue the lethality and morphological phenotypes seen in DVAP-33A loss of function mutants (Pennetta *et al.*, 2002). DVAP-33A is ubiquitously expressed and the zygotic loss results in lethality during second/early third instar larval stages with rare (~1%) adult escapers. The lethality associated with loss of DVAP-33A can be rescued by expressing hVAPB using both the *C164-Gal4* and *D42-Gal4* drivers in combination with several independent *UAS-hVAPB* transgenic lines with expected Mendelian ratios. Rescued flies were fertile and did not show any abnormal morphological and behavioural defects.

DVAP-33A loss of function mutants display an increase in bouton size and decrease in bouton number at the NMJ when compared to controls (150 ± 7 boutons versus 250 ± 8 in controls, $P<0.01$, Figure 3.2). This synaptic phenotype associated with DVAP-33A loss of function can also be rescued by the expression of hVAPB using *C164-Gal4* and *D42-Gal4* drivers. The number of synaptic boutons is similar

to controls (284 ± 11 boutons versus 278 ± 12 in controls, P>0.05, Figure 3.5A and B). Moreover, electrophysiological analysis of the same synapses shows that the EJP (36 ± 2 mV versus 37 ± 2 mV in controls; P>0.05) and mEJP (0.83 ± 0.02 mV versus 0.89 ± 0.03 mV in controls; P>0.05, Figure 3.5C and D) are both similar to controls. Hence, expression of hVAPB in neurons rescues the lethality, aberrant morphological phenotype and increase mEJP amplitude associated with loss of function of DVAP-33A mutations. These data show that hVAPB and DVAP-33A not only share structural similarities but hVAPB can also functionally substitute for DVAP-33A at the synapse.

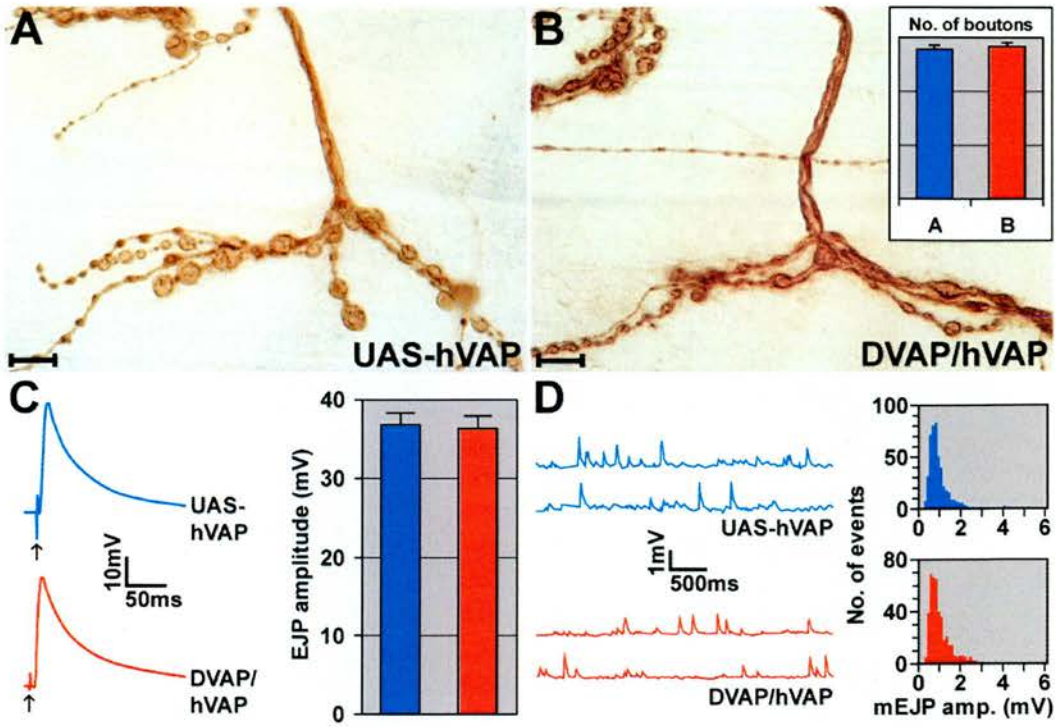

Figure 3.5. hVAPB rescues the lethality, morphological and electrophysiological phenotypes associated with DVAP-33A loss of function.
(A-D) Defects in synaptic function and morphology in *DVAP-33A* loss-of-function mutations are rescued by neuronal-specific expression of hVAPB. (A) Anti-HRP staining of controls NMJs (UAS-hVAP) and (B) NMJs expressing *hVAPB* in *DVAP-33A* mutant background (DVAP/hVAP). In the inset, total number of boutons on muscles 12 and 13 for controls (blue) and NMJs expressing hVAPB in *DVAP-33A* mutant background (red). (C) Examples of single traces showing EJPs in controls (UAS-hVAP) and NMJs expressing hVAPB in *DVAP-33A* mutant background (DVAP/hVAP). In the inset, summary of EJPs amplitudes for rescued and control animals. (D) Representative traces of mEJPs from controls (UAS-hVAP) and rescued animals (DVAP/hVAP). In the inset, histograms of mEJPs amplitudes for controls and rescued NMJs are shown. The neuronal-specific driver *P[Gal4w^{+}]C164* was used to drive the expression of hVAPB in a *DVAP-33A* mutant background (Torroja *et al.*, 1999). Transgenic lines HWT1 and HWT8 were used to rescue the mutant phenotype associated with *DVAP-33A* null mutations.

3.6 Transgenic expression of hVAPB phenocopies DVAP-33A overexpression.

To provide further support that hVAPB and DVAP-33A are functionally interchangeable, we investigated if the overexpression phenotype of hVAPB is similar to the overexpression phenotype of DVAP-33A. Neuronal overexpression of

DVAP-33A using the pan-neural driver *elav*-Gal4 results in a dramatic increase in bouton number and a concomitant decrease in bouton size (Figure 3.2). Despite severe changes to the synapse morphology, muscle EJPs are maintained within normal values (Figure 3.3) due to synaptic homeostatic mechanisms.

To further analyse the effect of hVAPB protein expression on synapse morphology and function we used the same *elav-Gal4* driver to overexpresss hVAPB in a DVAP-33A wt background. As shown in Figure 3.6A and B, we observed an increase ($P<0.001$) in bouton number (535 ± 16) accompanied by a decrease in the size of the boutons when compared to controls (297 ± 7). Similar to overexpression of DVAP-33A, expression of hVAPB in a wt background also causes a reduction in the average mEJP amplitude. In this instance, an almost 50% reduction in mEJP size (0.48 ± 0.01mV) compared to controls (0.82 ± 0.01mV; $P<0.001$, Figure 3.6D) compensates for the 10% reduction in EJP amplitude (35.0 ± 0.7mV versus 29.0 ± 0.8mV; $P<0.001$, Figure 3.6C), allowing a near normal postsynaptic response. Hence, the series of loss of function and gain of function experiments show that hVAPB and DVAP-33A are functionally interchangeable.

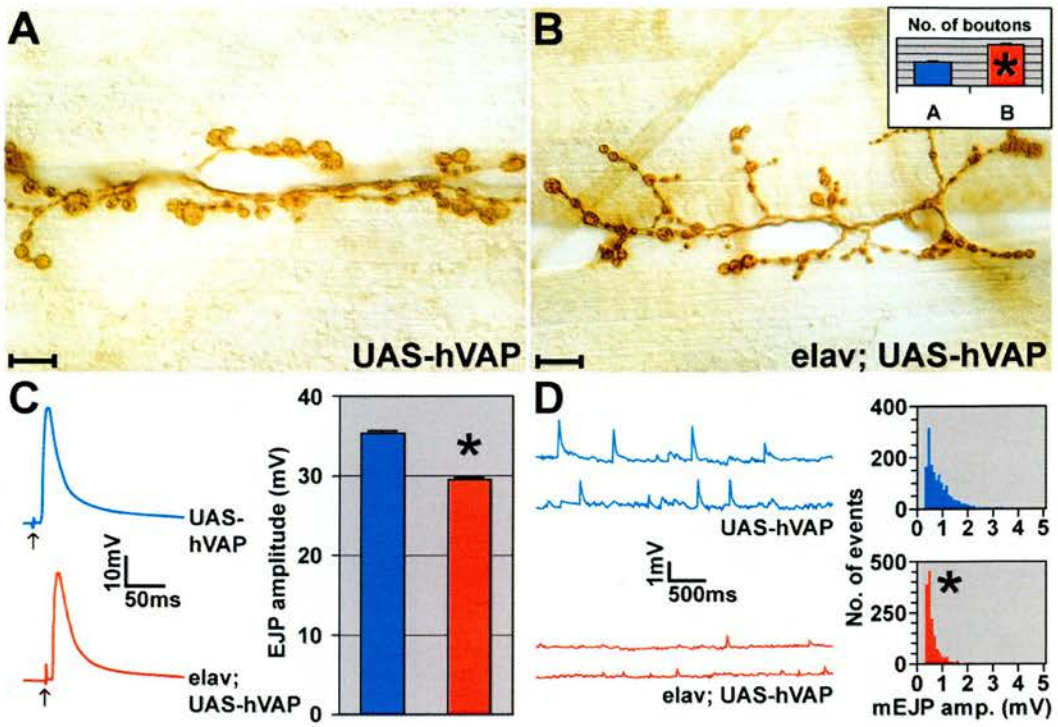

Figure 3.6. hVAPB overexpression phenocopies DVAP-33A overexpression and the morphological and electrophysiological level.

(A-D) Neuronal overexpression of the human protein induces an increase in the number of smaller boutons, a small but significant decrease in the evoked response and a decrease in mini amplitude. (A) Anti-HRP staining of controls (UAS-hVAP) and (B) NMJs overexpressing hVAPB in neurons (elav; UAS-hVAP). In the inset, the total number of boutons on muscles 12 and 13 is reported for controls (blue) and larvae overexpressing hVAPB (red). (C) Examples of traces of EJP amplitudes for controls (UAS-hVAP) and NMJs overexpressing hVAPB in a wt background for DVAP-33A (elav; UAS-hVAP). In the inset, a summary of EJP amplitudes for controls and NMJs overexpressing hVAPB in a wt background for DVAP-33A. (D) Representative traces of mEJP amplitudes for controls (UAS-hVAP) and synapses overexpressing hVAPB in a wt background for DVAP-33A (elav; UAS-hVAP). In the inset, histograms of mEJP amplitudes for controls and synapses overexpressing hVAPB are shown. "*" denotes statistically significant changes. Data reported in A-D were obtained using HWT4 and HWT5 transgenic lines. Scale bars = 10 μm.

3.7 hVAPBP56S expression also rescues the lethality, morphological and electrophysiological phenotype of DVAP-33A null mutants at the NMJ

The proline residue that is mutated in ALS8 patients is included in a stretch of 16 amino acids within the MSP homology domain at the N-terminal of VAP that is conserved in all VAP species (Nishimura *et al.*, 2004b, Figure 3.7, this work). The function of this domain is largely unknown but the high degree of conservation clearly suggests that it may be important for the function of the entire protein. Therefore, any mutation in this region would also very likely have similar consequences in all VAP homologues.

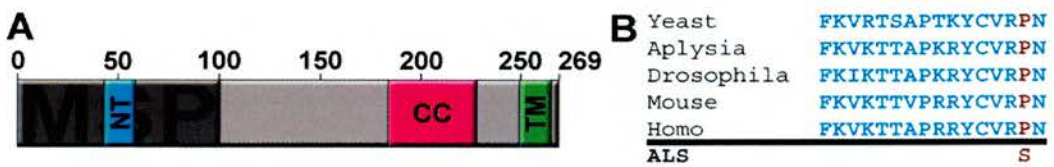

Figure 3.7. The Proline to Serine mutation in ALS8 patients is located at the MSP domain of VAP.
(A) The Proline to Serine mutation at codon 56 in ALS8 patients is situated in a stretch of highly conserved 16 amino acid within the MSP domain of VAP. (B) The stretch of 16 amino acids containing the ALS8 mutation changing the Proline 58 into a Serine in DVAP-33A. The alignment shows that this domain is highly conserved in VAP proteins from different species.

The P56S mutation in ALS8 is inherited in a dominant manner, dominantly inherited mutations can be caused by loss of function, which can be due to a dominant negative or a haploinsufficiency, or caused by a gain of function which can be due to hypermorphic or neomorphic mutations (Greenspan, R.J., 2004). To help define the nature of the ALS8 mutation, we expressed mutant VAP proteins in a null background for DVAP-33A. Flies carrying the human VAP mutant transgene (UAS-hVAPBP56S) and the *Drosophila* mutant VAP transgene (UAS-DVAPP58S) were previously generated (Chai, A, MSc Thesis, 2005) to test the ability of these transgene to rescue the lethality and morphological phenotypes associated with loss

of DVAP-33A. Lethality was rescued when UAS-hVAPBP56S transgene was driven by *D42-Gal4* and *C164-Gal4* drivers in a null background for DVAP-33A (*DVAP-33A*$^{\Delta 20}$ *and DVAP-33A*$^{\Delta 448}$). Moreover, as shown in Figure 3.8A and B, the number of boutons in flies expressing the human mutant protein (C164-Gal4; UAS-hVAPmt, bouton number: 290 ± 11) is not significantly different from control flies (UAS-hVAPmt, bouton number: 304 ± 11; P>0.05).

In addition, no significant difference in EJPs and quantal sizes were observed in flies expressing hVAPBP56S (36 ± 2 mV) compared with controls (34 ± 2 mV, $P >$ 0.05, Figure 3.8C). Finally, flies expressing hVAPBP56S exhibit quantal sizes (0.89 ± 0.02 mV) similar to those of control animals (0.83 ± 0.03 mV, $P > 0.05$, Figure 3.7D). Similar data in viability, morphological and electrophysiological properties were also observed when the UAS-DVAPP58S transgene was expressed in a null background for DVAP-33A using the *C164-Gal4* driver (data not shown). The fact that both the human and *Drosophila* VAP mutant protein can functionally substitute for DVAP-33A indicates that the pathogenic allele of VAP in ALS8 is not a loss of function.

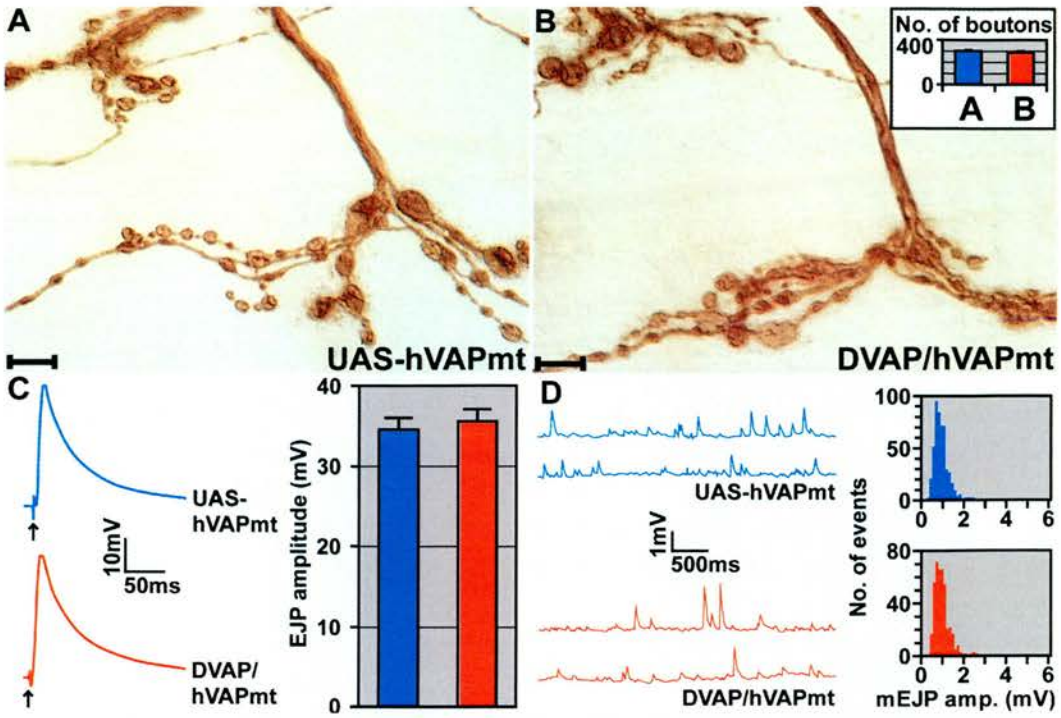

Figure 3.8. hVAPP56S rescues the mutant phenotypes associated with *DVAP-33A* mutations.

(A-D) Defects in synaptic function and morphology in *DVAP-33A* loss-of-function mutations are rescued by neuronal-specific expression of *hVAPB* carrying the pathogenic mutation. (A) anti-HRP staining of control NMJs (UAS-hVAPmt) and NMJs expressing mutant hVAPB in *DVAP-33*A mutant background (DVAP/hVAPmt) in B. In the inset the total number of boutons on muscles 12 and 13 for the same genotypes is reported. (C) EJP traces are reported for controls (UAS-hVAPmt) and the DVAP/hVAPmt NMJs. In the inset a summary of EJPs amplitudes is reported for the respective genotypes. (D) Representative traces of mEJPs amplitudes for controls (UAS-hVAPmt) and DVAP/hVAPmt NMJs. In the inset histograms of mEJPs amplitudes are shown for the corresponding genotypes. The data reported in A-D were collected using the HMT2 transgenic line.

3.8 Overexpression of hVAPBP56S results in drastic oversprouting of boutons at the NMJ

We next examine the phenotype associated with the robust overexpression of hVAPP56S throughout the nervous system. Neuronal overexpression of hVAPB and DVAP-33A induces an oversprouting of small boutons (522 ± 16 in hVAPB compared to 535 ± 7 in DVAP-33A). When the human mutant protein (UAS-hVAPBP56S) was overexpressed using the same *elav-Gal4* driver, we observed a drastic increase in bouton number (656 ± 15 compared to 322 ± 9 in controls, $P<0.001$ in Figure 3.9A and B) with a remarkable decrease in bouton size. This increase in bouton number is significantly more elevated than overexpression of hVAPB and DVAP-33A. In addition, unlike the EJPs associated with overexpression of DVAP-33A or hVAPB, there was a reduction of more than 50% in the EJP amplitude (14.0 ± 0.9 mV versus 34.0 ± 0.5mV in controls, $P<0.001$, Figure 3.8C). As shown in Figure 3.9D, the mean quantal size (mEJP amplitude) is only 0.37 ± 0.05mV, less than half the corresponding control (0.90 ± 0.02 mV). The cumulative distribution shows a redistribution of the mEJP values towards smaller values for all mEJPs.

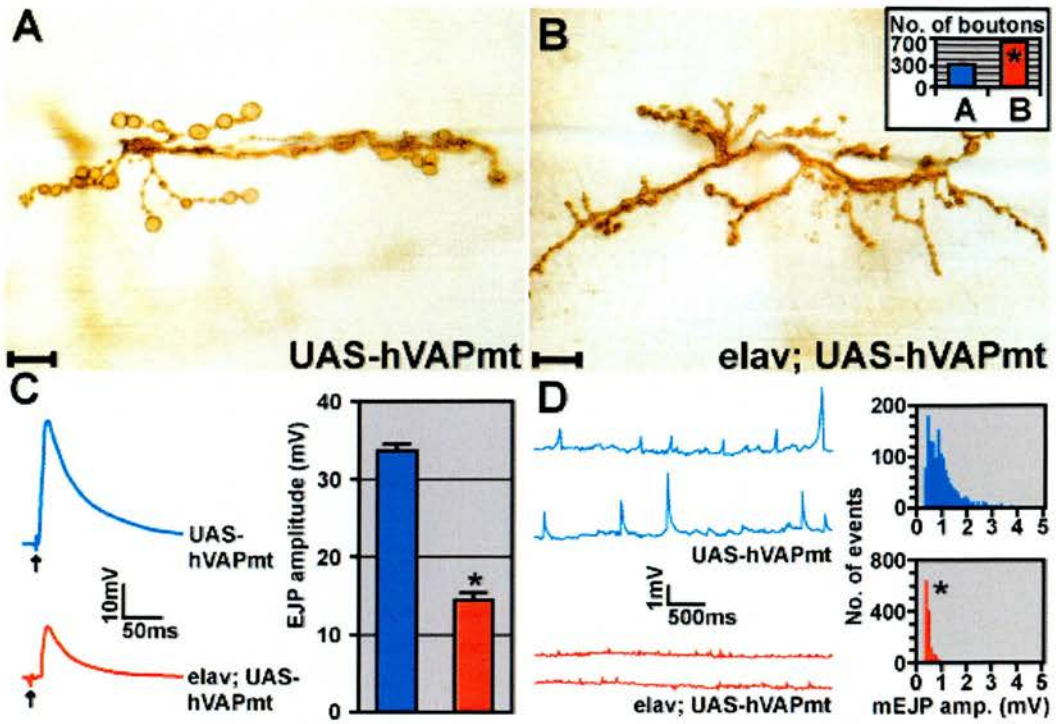

Figure 3.9. Neuronal overexpression of mutant hVAPBP56S reduces transmitter release and quantal size.

(A) Anti-HRP immunohistochemistry of NMJs overexpressing mutant hVAPB in a wt background for DVAP-33A (elav; UAS-hVAPmt) (B) , and of UAS-hVAPmt NMJs as a control in (A). Total number of boutons for the respective genotypes is reported in the inset in (B). Representative traces of EJP amplitudes for the same genotypes in (C) with the corresponding histograms for EJP amplitudes in the inset. (D) Representative traces of mEJP amplitudes for the same genotypes and histograms in the inset showing the distribution of mEJP amplitudes for the same genotypes as in (A) and (B). For the neuronal overexpression of the human mutant protein the HMT11 transgenic line was used. "*" denotes statistically significant changes. Scale bars equal 10 μm.

The effect of hVAPB and hVAPP56S overexpression on synaptic morphology and electrophysiology is observed in transgenic lines of hVAPB and hVAPP56S expressing comparable amounts of proteins as assessed by densitometric analysis of Western blots (Figure 3.10). In Figure 3.10B , OE HWT4 and OE HMT11 have comparable levels of protein as measured by a densitometer. However, the morphological and electrophysiological phenotypes at the synapse seen in transgenic expression of hVAPP56S (OE HMT11) is much more exacerbated than the phenotypes seen in transgenic expression of hVAPB (OE HWT4) (Compare Figure

3.6 with Figure 3.9). In addition, transgenic expression of hVAPP56S has more severe electrophysiological and morphological phenotypes at the synapse compared to transgenic expression of hVAPB (OEHWT3) that has roughly 10 times more protein expressed (data not shown).

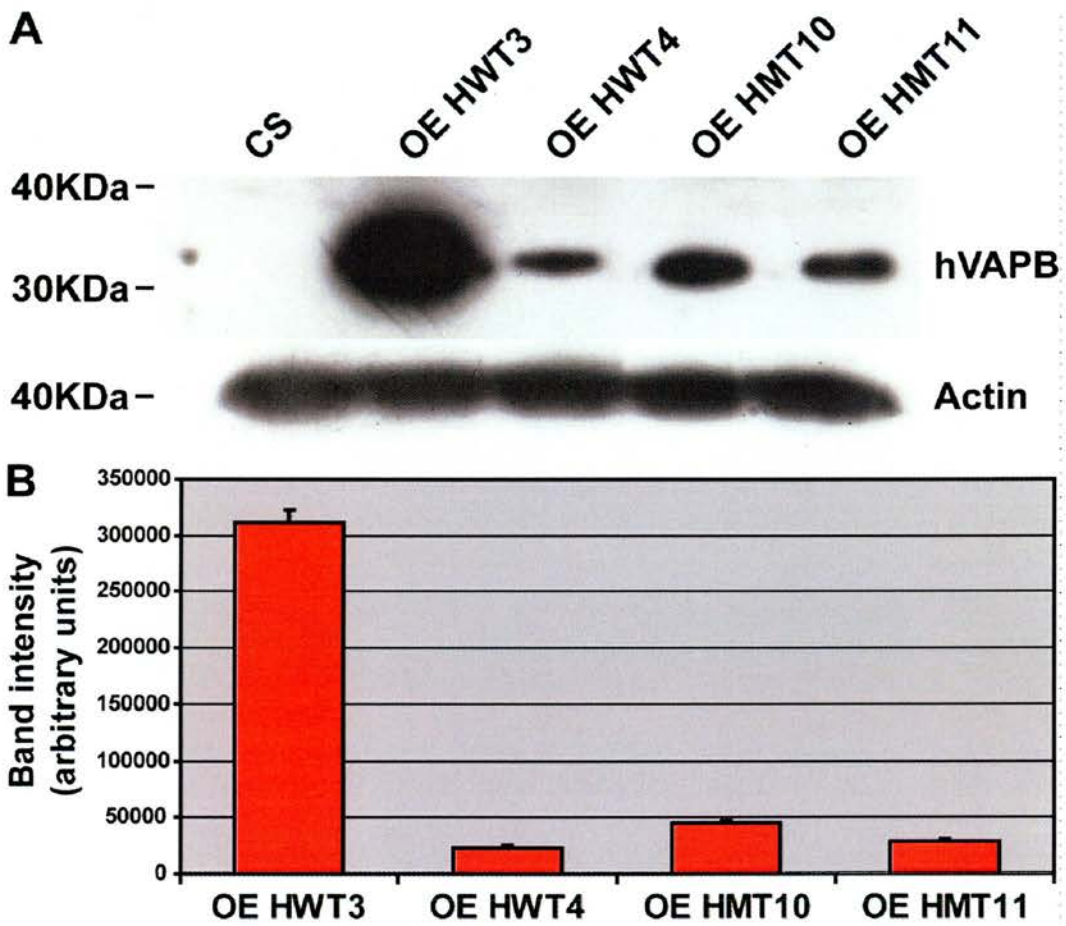

Figure 3.10. Western Blot Analysis of Transgenic Lines Expressing hVAPB and mutant hVAPB.

(A) Representative Western Blot of protein extracts from several transgenic NMJs expressing hVAPB (HWT) and hVAPBP56S (HMT) probed with an antibody specific for the human protein. An anti-Actin antibody was used as loading control. The slot labeled "CS" are Canton S (wt) NMJs. No signal is detected in wt NMJs, showing that the antibody is specific for the human protein. (B) Densitometric analysis of band intensity corresponding to transgenic NMJs expressing hVAPB (HWT) and hVAPBP56S (HMT) in (A).

Chapter 4: Expression levels of VAP affect the abundance and volume of post-synaptic glutamate receptor (GluR) subunits

In DVAP-33A loss-of-function mutations, an increase in quantal size ensures functional homeostasis despite a significant decrease in the number of boutons and an increase in their sizes (Figures 3.2C and 3.3). On the other hand, neuronal overexpression of DVAP-33A and hVAPB result in a decrease in quantal sizes (Figures 3.3 and 3.6D) in spite of an increase in bouton numbers and a decrease in bouton sizes (Figures 3.2D and 3.6B). This change in postsynaptic response to spontaneous release in neurotransmitter release is usually due to a number of factors.

Quantal size is defined as the synaptic response to the release of neurotransmitter from a single vesicle during exocytosis (Fatt and Katz, 1952). Quantal size can be affected by the size of the vesicle and also the sensitivity, number or distribution of postsynaptic glutamate receptors. Neurotransmitter is released from presynaptic specializations called active zones. In wild type animals, glutamate receptors are clustered in puncta that lie opposite the presynaptic active zones, placing them in an ideal position to detect neurotransmitter released (DiAntonio, A., 2006).

Since no change in the size of synaptic vesicles was observed in loss-of -function and overexpression of DVAP-33A NMJs (Vivian Budnik, personal communication) it is most likely that changes in glutamate receptor subunit composition and/or abundance can account for the change in quantal sizes in the overexpression of hVAPB, hVAPBP56S and DVAP-33A loss of function mutants.

To date, five iGluRs have been identified in *Drosophila*: GluRIIA, GluRIIB (Petersen *et al.*, 1997; Schuster *et al.*, 1991), GluRIII (Marrus *et al.*, 2004; Qin *et al.*, 2005), GluRIID and GluRIIE (Qin *et al.*, 2005; Featherstone *et al.*, 2005). The iGluRs are heterotetrameric and are made up of four distinct subunits: GluRIII,

GluRIID, GluRIIE and either GluRIIA or GluRIIB (Qin *et al.*, 2005). It has been shown that the removal of GluRIIA decreases quantal size while an overexpression of GluRIIA increases quantal size. GluRIIA has been shown to be important in channel open time (DiAntonio *et al.*, 1999, Petersen *et al.*, 1997), therefore, suggests that the density of GluRIIA may be a crucial determinant of quantal size. In this series of experiments, we set out to investigate if a change in the composition of glutamate receptors could account for the change in quantal sizes seen in different expression levels of VAP.

4.1 DVAP-33A loss-of-function mutations affect abundance and cluster size of post-synaptic glutamate receptors

In order to assess whether the change in quantal sizes are due to changes in the structure or composition of glutamate receptors, NMJs of VAP loss of function and overexpression larvae were stained with antibodies specific for every glutamate receptor subunit. An extensive morphometric analysis of glutamate receptors with high resolution confocal data were applied to these NMJs to assess glutamate abundance and distribution in these synapses.

DVAP-33A loss of function mutants exhibit an increase in mEJP (quantal size) (Figure 3.3 and Tsuda *et al.*, 2008). This increase in quantal size ensures functional homeostasis of the synapse despite an increase in bouton size and a decrease in bouton number (Figure 3.2). In the synapse of these mutants, a significant increase in cluster count ($P<0.05$) and a marked increase in average cluster volume for GluRIIA were observed ($P<0.01$, Figure 4.1A-C). For all other subunits, a small but statistically significant decrease in cluster count was found ($P<0.05$, Figure 4.1C). GluRIIB and GluRIII also exhibit a marked reduction in the average cluster volume (30% reduction for GluRIIB, Figure 4.1C; 46% for GluRIII, Figure 4.1C-E, $P<0.001$) while cluster size for GluRIID is similar to controls (Figure 4.1C). The staining intensity of every subunit does not differ significantly between controls and mutants (data not shown).

In synapses lacking DVAP-33A, the increase in quantal size is accompanied by an increase in mean volume of GluRIIA clusters and an increase in the average volume per cluster and a slight increase in cluster count. This data show that a change in glutamate receptor volume could account for the increase in quantal size in DVAP-33A mutants.

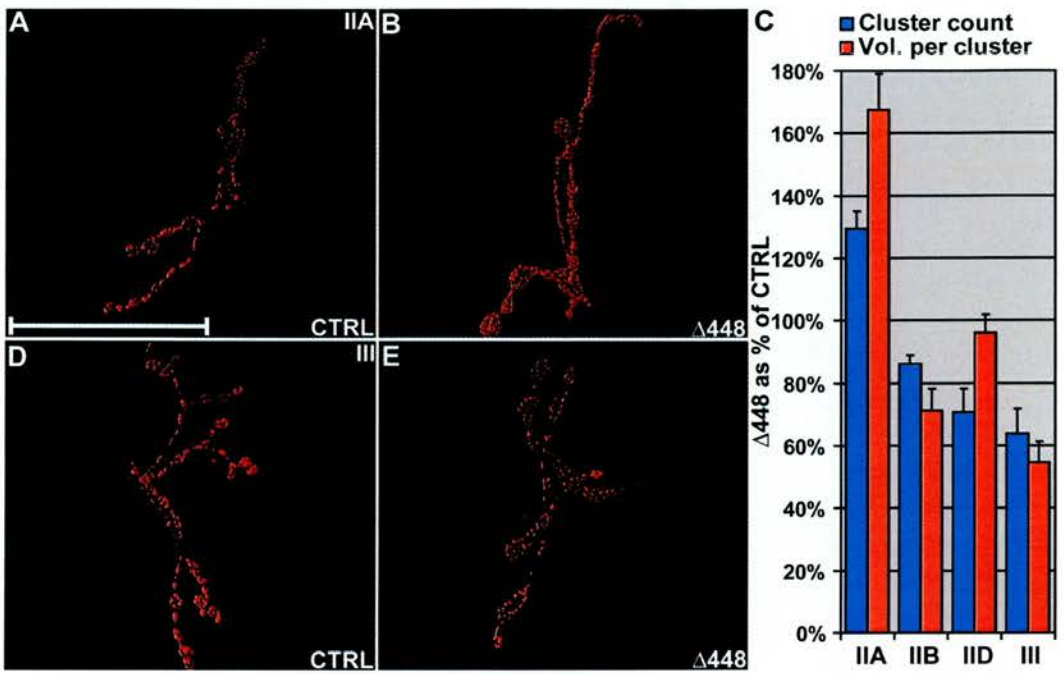

Figure 4.1. DVAP-33A loss-of-function mutations affect subunit abundance and cluster size of post-synaptic glutamate receptors.
(A) Volume renderings of controls stained with anti-GluRIIA antibodies. (B) Mutant synapses for *DVAP-33A* (Δ448) stained with the same antibodies as in (A). (D) Control synapses stained with anti-GluRIII antibodies. (E) Δ448 synapses stained with the same antibodies as in (D). (C) Morphometric analysis of Δ448 NMJs reporting cluster count and mean cluster volume for every GluR subunit as percentages of control values. A striking increase in the average cluster volume for GluRIIA subunit is observed in *DVAP-33A* mutants. The revertant line generated by precise excision of the original P-element was used as a control in this experiment (Pennetta *et al.*, 2002). Data in (C) are shown as mean ± s.e.m and N= 5 larvae for every analyzed genotype. Scale bar = 50 μm.

4.2 Neuronal expression of hVAPB affects post-synaptic glutamate receptor composition

A striking physiological feature of transgenic expression of VAP proteins in neurons is a significant decrease in quantal size (Figures 3.3G and 3.6D). We investigated if

the reduction in quantal size is also associated with a change in postsynaptic glutamate receptor composition and/or abundance. The focus of our analysis was directed at synapses expressing transgenic hVAPB in neurons as these synapses exhibit a greater decrease in quantal size when compared to DVAP-33A transgenic expression in neurons (0.48 ± 0.01mV versus 0.59 ± 0.05mV in DVAP-33A overexpression, Figures 3.6D and 3.3G).

This decrease in quantal size seen in animals overexpressing hVAPB is accompanied by a marked decrease in GluRIIA abundance ($P<0.001$) when compared to controls (Figure 4.2A-G). This decrease was specific for GluRIIA as no difference in expression levels between controls and mutants was observed for any other subunits (data not shown). Synapses expressing transgenic hVAPB also exhibit a decrease in average cluster volume for subunit GluRIIA ($P<0.001$ Figure 4.2H-J), GluRIIB and GluRIII ($P<0.05$ for both subunits, Figure 4.2J). Cluster count does not change significantly ($P>0.05$) except for GluRIII where a small but statistically significant increase is observed ($P<0.05$, Figure 4.2J) while no significant changes ($P>0.05$, Figure 4.2J) were observed in cluster count and average volume cluster for GluRIID. This data agrees with the fact that the decrease in quantal size in the transgenic expression of hVAPB is accompanied by a decrease in glutamate receptor fields of GluRIIA, GluRIIB and GluRIII subunits.

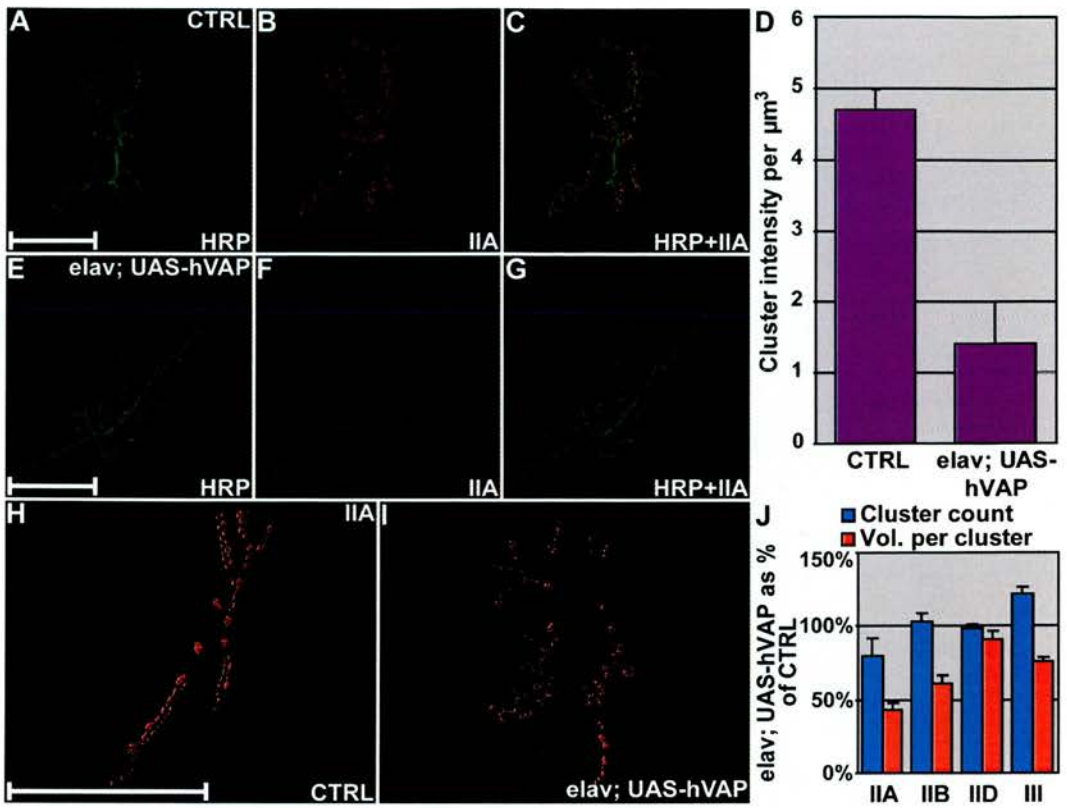

Figure 4.2. Neuronal expression of VAP proteins affects post-synaptic glutamate receptor composition.

(A–C) GluRIIA subunit localization (red) at control NMJs visualized by using the neuronal cell surface marker anti-HRP (green). (E–G) Synapses expressing transgenic hVAPB (elav; UAS-hVAP) stained using the same antibodies as in (A–C). (D) Quantification of the fluorescence intensity per volume unit of GluRIIA clusters in controls and in elav; UAS-hVAP synapses. (H and I) Synapses of relevant genotypes stained with anti-GluRIIA antibodies are shown as an example. Volume renderings of clusters immunoreactive to GluRIIA are presented irrespective of their signal intensity. (J) Morphometric analysis of cluster count and mean cluster volume for every GluR subunit in elav; UAS-hVAP synapses are presented as percentages of control values. Neuronal expression of VAP proteins induces a decrease in the expression levels of GluRIIA and a reduction in the receptor field size. NMJ of Canton S larvae were used as controls. Data in (D) and (J) are shown as mean ± s.e.m and in (D) the intensity is presented in arbitrary units. $N = 5$ larvae for every analyzed genotype. Scale bars = 50 µm.

4.3 Presynaptic overexpression of hVAPBP56S affects the abundance of GluRIIA subunit and the volume of postsynaptic receptor clusters

Presynaptic overexpression of hVAPBP56S causes a drastic increase in bouton number and a decrease in their size compared to the overexpression of the human

and *Drosophila* wild type VAP protein. In addition, unlike the EJPs associated with the overexpression of DVAP-33A and hVAPB, there was a reduction of more than 50% in the EJP amplitude (Figure 3.9C and D). The mean quantal size (mEJP amplitude) is less than half the value of the corresponding control. We also extended our morphometric analysis to synapses overexpressing hVAPBP56S.

We found that subunit GluRIIA was downregulated to about 33% of the wt value ($P<0.001$) when assessed by measuring the intensity of the flurorescent signal per volume unit on synapses stained with antibody specific for this subunit (Figure 4.3A-G). Using the same measurements, there was no significant difference between wt and mutants for the other subunits. However, a decrease in cluster volume to 50%-60% of the wt value for every other subunit was observed. There was also a small but not statistically significant decrease in number of clusters in all the subunits (Figure 4.3H-J). Consistent with the downregulation of quantal size, presynaptic overexpression of hVAPBP56S decreases the abundance of GluRIIA subunit and the average cluster size of postsynaptic glutamate receptors.

Taken together, data from this series of experiments indicate that changes in quantal sizes in different expression levels of VAP proteins are paralled by postsynaptic remodeling of glutamate receptors. Consistent with our data, the size of receptor field and the amount of GluR IIA subunits have also been shown to be the most important parameters in affecting synaptic strength (Davis *et al.*, 1998, DiAntonio *et al.*, 1999, Petersen *et al.*, 1997, Marrus *et al.*, 2004). Most significantly, our data also suggest that VAP proteins are components of a trans-synaptic signal as presynaptic expression of VAP affects the postsynaptic sensitivity to neurotransmitters.

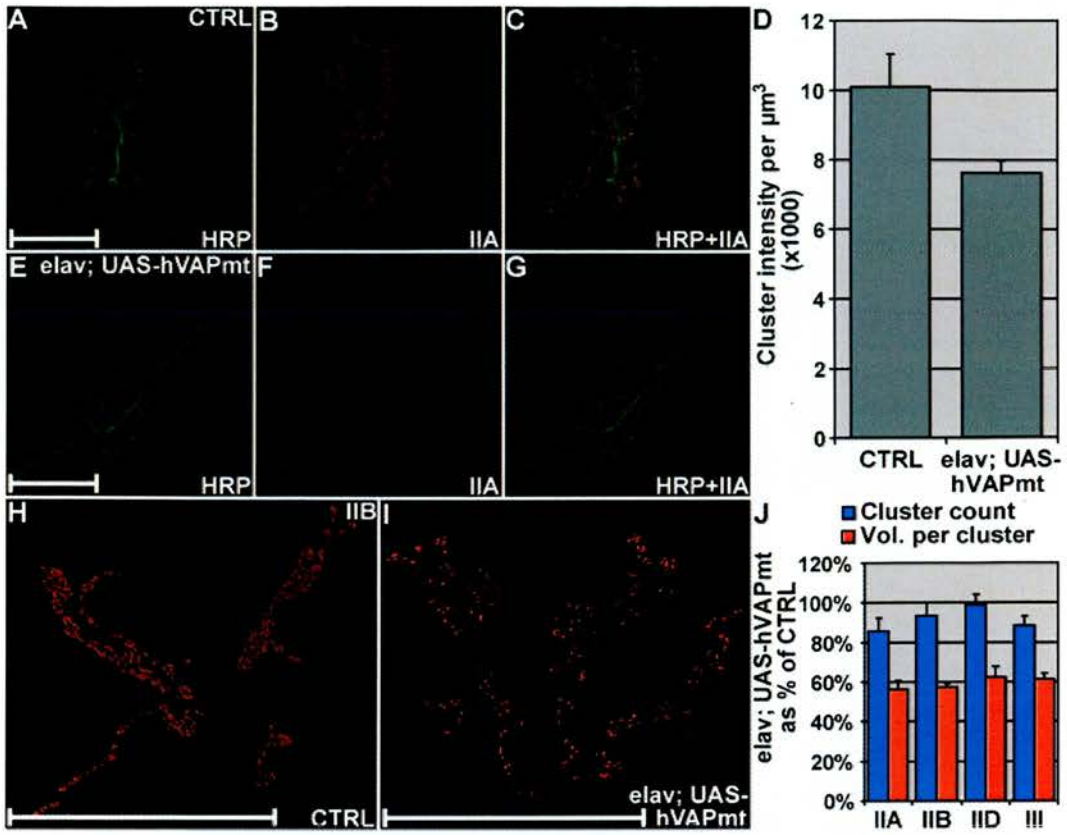

Figure 4.3. Expression Levels of VAP Proteins Affect Subunit Abundance and Cluster Size of Post-Synaptic Glutamate Receptors.

(A-G) Representative images of GluRIIA subunit localization (red) at NMJs visualized by using the neuronal membrane marker, HRP, (green) in controls (A-C) and in synapses overexpressing mutant hVAPB (E-G). Quantification of the fluorescence intensity per volume unit of GluRIIA clusters in controls and synapses overexpressing hVAPBP56S (elav; UAS hVAPmt) in (D). Morphometric analysis of number of clusters and mean volume per cluster for every subunit in synapses overexpressing hVAPBP56S are presented as percentages of the control values. Synapses stained with an antibody specific for GluRIIB is shown as an example (H-J). For the analysis of the NMJs overexpressing hVAPBP56S the transgenic line HMT10 was used. This line expresses the highest level of transgenic protein (see Figure 3.10). Similar phenotypes were observed in other transgenic lines (data not shown). Data in (D) and (J) are shown as mean ± s.e.m while in (D) the intensity is presented in arbitrary units. $N = 5$ larvae for each analyzed genotype. Scale bars: 50 µm.

Chapter 5: Transgenic expression of DVAPP58S recapitulates hallmarks of ALS disease symptoms

Expression of hVAPB and hVAPBP56S in neurons rescues the lethality, morphological and electrophysiological phenotypes associated with DVAP-33A loss-of -function mutations. This indicates that hVAPB and DVAP-33A are orthologues and that the pathogenic allele partly retains some wild-type properties of VAP. It has been shown that human VAP-B not only binds to human VAP-A, but also dimerizes in vitro (Nishimura *et al.*, 1999). This ability to self-oligomerize is a common feature in VAP homologues (Soussan *et al.*, 1999; Kanekura *et al.*, 2006; Weir *et al.*, 2001).

We tested if the human and *Drosophila* VAPs also exhibit this ability using a yeast-two-hybrid screen. We found that DVAP-33A and hVAPB can form homodimers, supporting the data that DVAP-33A and hVAPB are functionally interchangeable. DVAPP58S and hVAPBP56S were also able to homodimerize and form heterodimers with their respective wild type protein, demonstrating that the mutant proteins retain part of its wild type properties. However, wild type and mutant VAP-33 were not able to undergo cross-species interaction (ie. human mutant and wild type proteins do not interact with *Drosophila* mutant and wild type proteins) (K. Parry and G. Pennetta). This observation suggest that the best way to model the dominantly inherited ALS8 in flies is to utilise the *Drosophila* proteins. The major features of ALS in patients include degeneration of motor neurons, paralysis, muscle atrophy and cell death. In this chapter, we show that transgenic expression of DVAPP58S in neurons recapitulates hallmarks of ALS disease.

5.1 Transgenic expression of DVAPP58S in neurons induces nerve fragmentation and muscle wasting

The neuropathology of ALS is primary degeneration of upper and lower motor neurons. Neurogenic atrophy of affected muscle groups, and hardening of the lateral white matter funiculus in spinal cord (corresponding to degeneration of the corticospinal tract) are common pathological features of ALS patients (Mulder, D.W.,

1986; Talbot, K., 2002). We decided to model this aspect of the disease in flies and found that transgenic expression of DVAPP58S in neurons causes degeneration of nerves and muscles atrophy.

In wt larvae, the motor axon entering the neuromuscular junction is thick and terminal branches contact and sprout on muscle fibers to form a stereotypic arbor (Figure 5.1A). Transgenic DVAPP58S expressing synapses exhibit a high range of abnormal morphologies: nerves at the point where they branch onto the muscle fibers are fragmented and the corresponding synapses are not connected to the nerve (compare arrows in Figure 5.1C and 5.1D). In other cases, the branching nerve is not visible (compare arrows in Figure 5.1B and 5.1A) and synapses become a highly disorganized, degenerating structure (compare arrowheads in Figure 5.1B and 5.1A). These synapses contact muscles that exhibit an aberrant morphology when observed by Nomarski optics.

Fluorescence-conjugated phalloidin staining was used to assess the integrity of the muscles at the NMJs of DVAPP58S synapses. Approximately half of the muscles exhibit an aberrant morphology in 84% of DVAPP58S transgenic larvae when compared to controls. Muscles are also deformed, slender and exhibit an altered striated pattern (Figure 5.1D versus 5.1C). In addition, a localized region of severe muscle disruption was observed: muscles become detached from the body wall insertion sites, and muscle loss is accompanied with some remnants of muscle fibers (Figure 5.1E). In the remaining 16% of the larvae, sporadic disorganized muscles were observed (Figure 5.1F and data not shown). We have hence shown that pan-neural expression of the pathogenic form of *Drosophila* VAP can induce fragmentation of nerves and muscle degeneration that is observed in ALS patients.

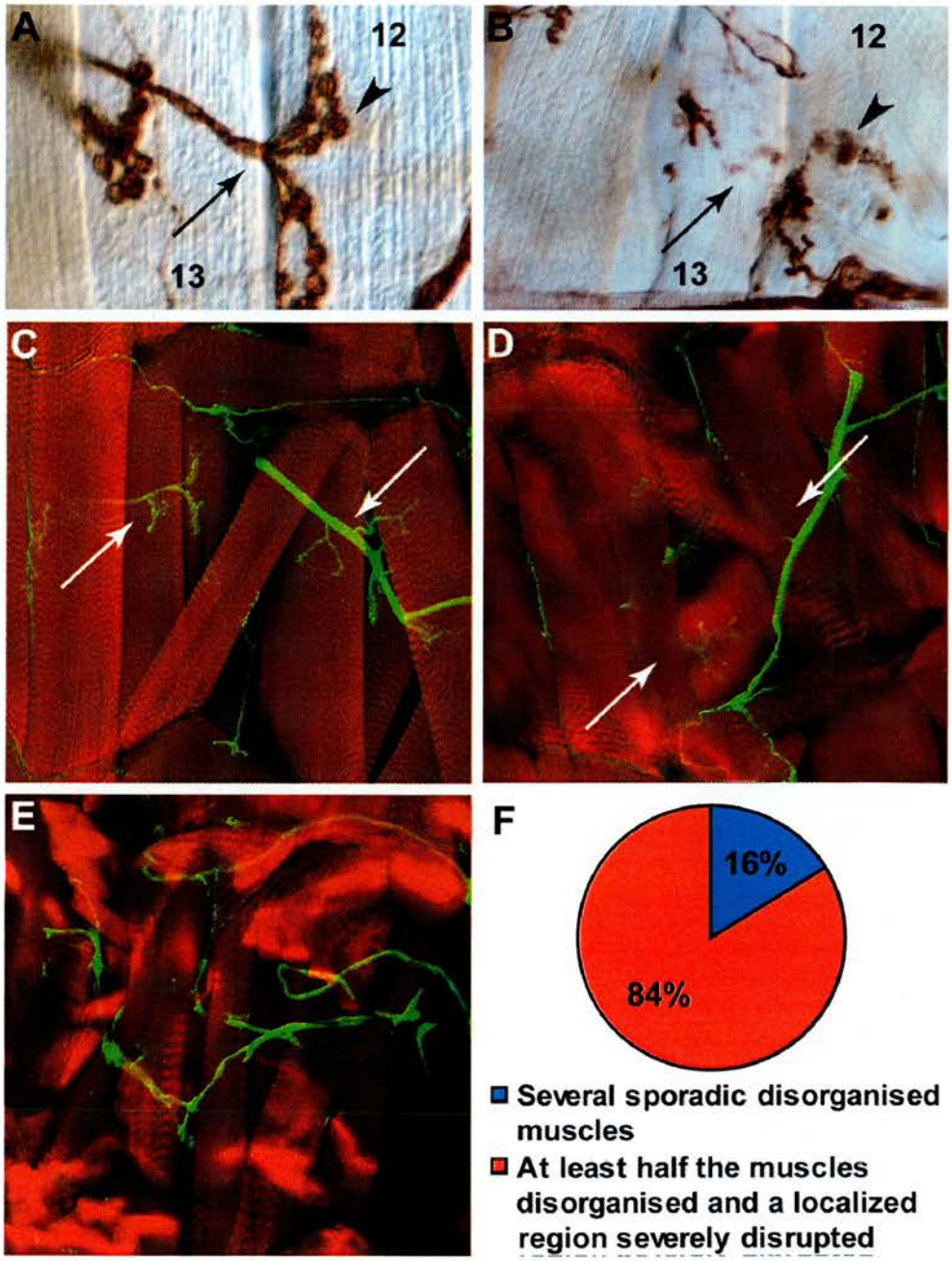

Figure 5.1. Transgenic expression of DVAPP58S in neurons induces nerve fragmentation and muscle wasting.

(A) Anti-HRP immunohistochemistry of control NMJs. (B) NMJs expressing transgenic DVAPP58S stained with the same antibodies as in (A). (C) Anti-HRP immunohistochemistry and phalloidin staining in control synapses. (D and E) Transgenic DVAPP58S expressing synapses subjected to anti-HRP and phalloidin stainings. (F) Quantification of the mutant phenotype. Canton S larvae were used as control in all the experiments reported in this figure. At least 10 larvae per experiment were analyzed.

5.2 Transgenic expression of DVAPP58S in neurons induces larval locomotion defects and apoptosis

One of the earliest and most common signs of ALS in humans are impaired movement and paralysis (Mulder, D.W., 1982; Talbot, K., 2002). Similarly, transgenic larvae expressing DVAPP58S in neurons were found to be sluggish and uncoordinated. A quantitative analysis was hence performed on the crawling behaviour of these larvae. Wild type larvae have very stereotypic crawling behaviour; forward locomotion in larvae consists of contractions of the posterior end alternating with extension of the anterior body regions (Fox *et al.*, 2006; Wang *et al.*, 2002). Third instar larvae expressing transgenic DVAPP58S and control larvae reared in the same environmental conditions were observed on an agarose substrate for a period of at least 2 minutes. The frequency of strides in Hz (number of events per second) was calculated by dividing the number of strides by their duration.

Unexpectedly, transgenic larvae expressing DVAPP58S revealed significant heterogeneity in the mobility phenotype compared with controls. As shown in Figure 5.2A, 34% of the larvae are completely paralyzed or exhibit very few peristaltic contractions while the majority has a frequency of strides that is only 30% of the wt value. In controls, the frequency of strides is homogeneous (0.85 ± 0.01 Hz) (Figure 5.2A). The difference in frequency distribution between mutants and controls is statistically significant ($P < 0.001$, non-parametric Mann–Whitney U test)

Motor neuron death is one of the hallmarks of ALS in patients and SOD1 mouse models (Li *et al.*, 2000, Bruijn *et al.*, 2004). It has been shown that increasing the expression of the anti-apoptotic factor Bcl-2 slowed disease onset and improved the survival of $SOD1^{G93A}$ mice (Kostic *et al.*, 1997) and that Bcl-2 binds and aggregates with mutant SOD1 in spinal cord mitochondria of mouse models and patients (Pasinelli *et al.*, 2004). Several groups have also observed the activation of caspase 3 during cell death of motor neurons and astrocytes in mouse models

expressing mutant SOD1 (Vukosavic *et al.*, 2000, Li *et al.*, 2000, Pasinelli *et al.*, 2000).

TUNEL analysis was therefore performed on brains of transgenic larvae expressing DVAPP58S to determine the presence of neuronal cell death. Significantly enhanced neuronal death was observed in the central neurons of larvae expressing transgenic DVAPP58S when compared with controls (Figure 5.2B). This observed neuronal cell death is similar to those reported in mouse models of SOD1 mutations and ALS patients, showing that DVAPP58S-induced ALS is also able to reproduce this aspect of the disease (Li *et al.*, 2000, Bruijn *et al.*, 2004).

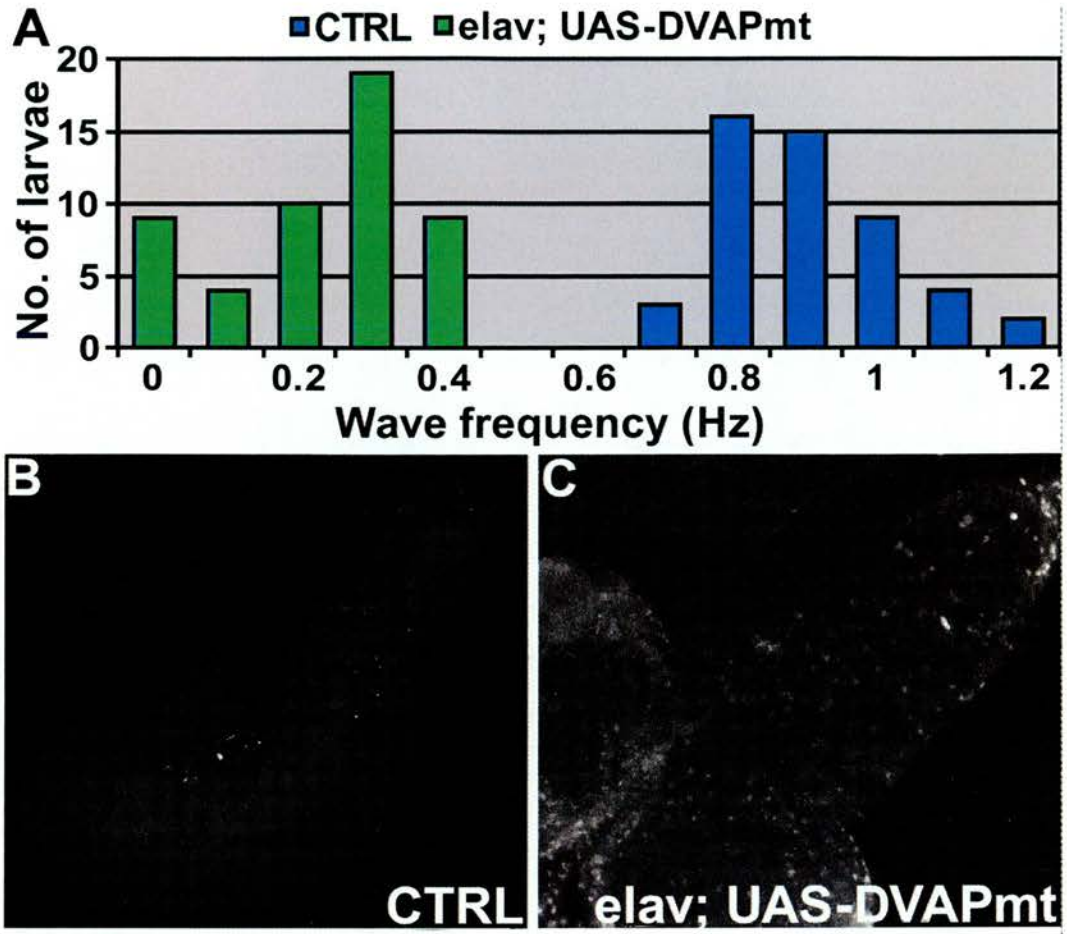

Figure 5.2. Transgenic expression of DVAPP58S in neurons induces locomotion defects and neuronal cell death.
(A) Summary of the frequency of peristaltic waves for *elav; UAS-DVAPmt* larvae (green) and for controls (blue). $n = 49$ for controls and $n = 51$ for *elav; UAS-DVAPmt*. Differences between genotypes were highly significant ($P < 0.001$, accordingly to the non-parametric Mann–Whitney U test when the data sets relative to elav; UAS-DVAPmt were compared with controls. In this experiment, the *UAS-DVAPP58S* transgenic line without the driver was used as a control. (B) Neuronal cell death in *UAS-DVAPP58S/+* control brains. (C) Neuronal cell death within larval brains expressing transgenic DVAPP58S.

5.3. Aggregates formed in 3rd instar larva nerves and brains are strongly immuno-reactive to DVAP-33A antibodies

Formation of aggregates that are strongly immunoreactive to SOD1 antibodies accompanies the paralytic phenotype and neuronal cell death in many mouse models of ALS expressing pathogenic SOD1 (Hart, P.J., 2006). Similarly, aggregates containing pathogenic SOD1 have been reported in sporadic and familial cases of

ALS in humans (Bruijn *et al.*, 1998). Parkinson's and polyQ disease models have showed that there is a correlation between aggregates and toxicity (Chan *et al.*, 2002; Periquet *et al.*, 2007). Similarly, several SOD1 mouse models exhibit misfolded SOD1 aggregates (Bruijn *et al.*, 1998; Johnston *et al.*, 2000; Pasinelli *et al.*, 2004). To assess if formation aggregates is also common to VAP-induced ALS and to identify the location of these DVAPP58S induced aggregates, confocal analysis was performed on brains and nerve fibres of third instar larvae expressing transgenic DVAPP58S. These third instar larval tissues were stained with antibodies specific for DVAP-33A.

In control nerves, faint but uniform DVAP-33A staining were observed while aggregates of variable sizes that are intensively stained with DVAP-33A antibodies are found in nerve fibres of DVAPP58S mutant larvae (Figure 5.3A and B). Accumulation of large aggregates was observed in the region of the nerves close to the brain and in their terminal tracts just before motor nerves sprout on the muscles to form the synaptic arbor (Figure 5.3B). In between these regions, the deposition of aggregates was less prominent (Figure 5.3C). DVAP-33A associates mainly with the plasma membrane of neuronal cell bodies (Figure 5.3D). However, in neuronal cell bodies of DVAPP58S larval brains, aggregate formation was observed. The DVAP-33A immunoreactivity is associated with intracellular aggregates of variable sizes (Figure 5.3E) while the wt protein associated with the plasma membrane decreased to nearly undetectable levels (compare Figures 5.3E with 5.3D).

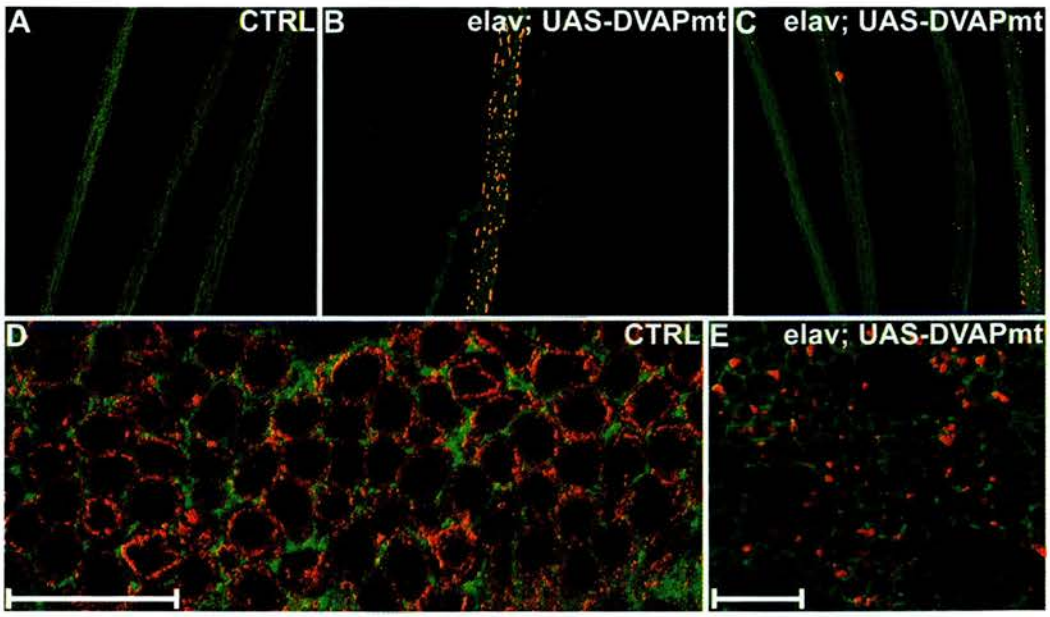

Figure 5.3. Transgenic expression of DVAPP58S induces aggregate formation in nerve fibres and neuronal cell bodies of third instar larvae.
Nerve fibers and brains of third instar larvae were stained with antibodies for DVAP-33A (red) and with antibodies for the neuronal cell surface marker anti-HRP (green). (**A**) Nerve fibers of control larvae. (**B** and **C**) Nerve fibers of larvae expressing transgenic DVAPP58S (elav; UAS-DVAPmt). (**D**) Brains of control larvae stained with anti-HRP (green) and anti DVAP-33A antibodies (red). (**E**) Brains of larvae expressing transgenic DVAPP58S (elav; UAS-DVAPmt) using the same antibodies. The anti DVAP-33A antibodies used in this report do not discriminate between the wt and the mutant protein. By western analysis, these antibodies recognize a band of similar size to the wt protein in protein extracts from NMJs expressing DVAPP58S in a null background for the endogenous protein (Figure 5.6). In (D) and (E), single sections of confocal images are shown. Canton S larvae were used as controls in the experiments reported in this figure. Scale bars = 20 μm.

5.4 Transgenic expression of DVAPP58S depletes endogenous DVAP-33A from its normal localization

Confocal analysis was also extended to neuromuscular synapses of third instar larvae expressing transgenic DVAPP58S to determine whether aggregate formation has any effect on regional differences of the endogenous DVAP-33A protein. In neuromuscular synapses of DVAPP58S transgenic larvae, DVAP-33A positive immuno-reactivity was undetectable. The DVAP-33A immuno-fluorescence signal was quantified and was found to be less than 8% of wt levels (Figure 5.4A-C and G-J). This observation was consistent in five other DVAPP58S transgenic lines that

were examined. On the contrary, when DVAP-33A was overexpressed in neurons, the protein is correctly targeted to the NMJ even when fluorescence intensity levels were four times the wt level (Figure 5.4A-F and J). Furthermore, no aggregates were formed in nerve fibres and neuronal cell bodies of these DVAP-33A overexpressing lines (data not shown, compare arrows in Figure s 5.4E and 5.4F). In *DVAPP58S* transgenic lines, aggregates are evident in the terminal part of the nerve (arrow in 5.4H) and the endogenous protein at the synapse is nearly undetectable (Figure 5.4H and J). These data indicate that transgenic expression of DVAPP58S induced the formation of DVAP-33A immuno-reactive aggregates and that overexpression of DVAPP58S depletes wt DVAP-33A (the endogenous protein) from its normal localization.

At the *Drosophila* NMJ, decreasing the amount of DVAP-33A causes a decrease in the number of boutons and an increase in the size of the boutons (Figure 3.2). Similarly, the depletion of endogenous DVAP-33A at the NMJ by transgenic expression of DVAPP58S causes a decrease in bouton number that is only 40% of wt levels (122 ± 3 as compared 283 ± 12 in controls, $P>0.001$, data not shown, compare Figures 5.4A with 5.4G). Although not quantified, we also observed an increase in the size of the boutons in DVAPP58S transgenic larvae (compare Figures 5.4A with 5.4G again).

Taken together, the data presented here indicate that neuronal expression of DVAPP58S in the presence of the wt protein recapitulates major hallmarks of the disease including locomotion defects, neuronal apoptosis and aggregate formation. The formation of aggregates is accompanied by the depletion of endogenous protein from its normal localization and consequently resulting in a decrease in protein function at the NMJ.

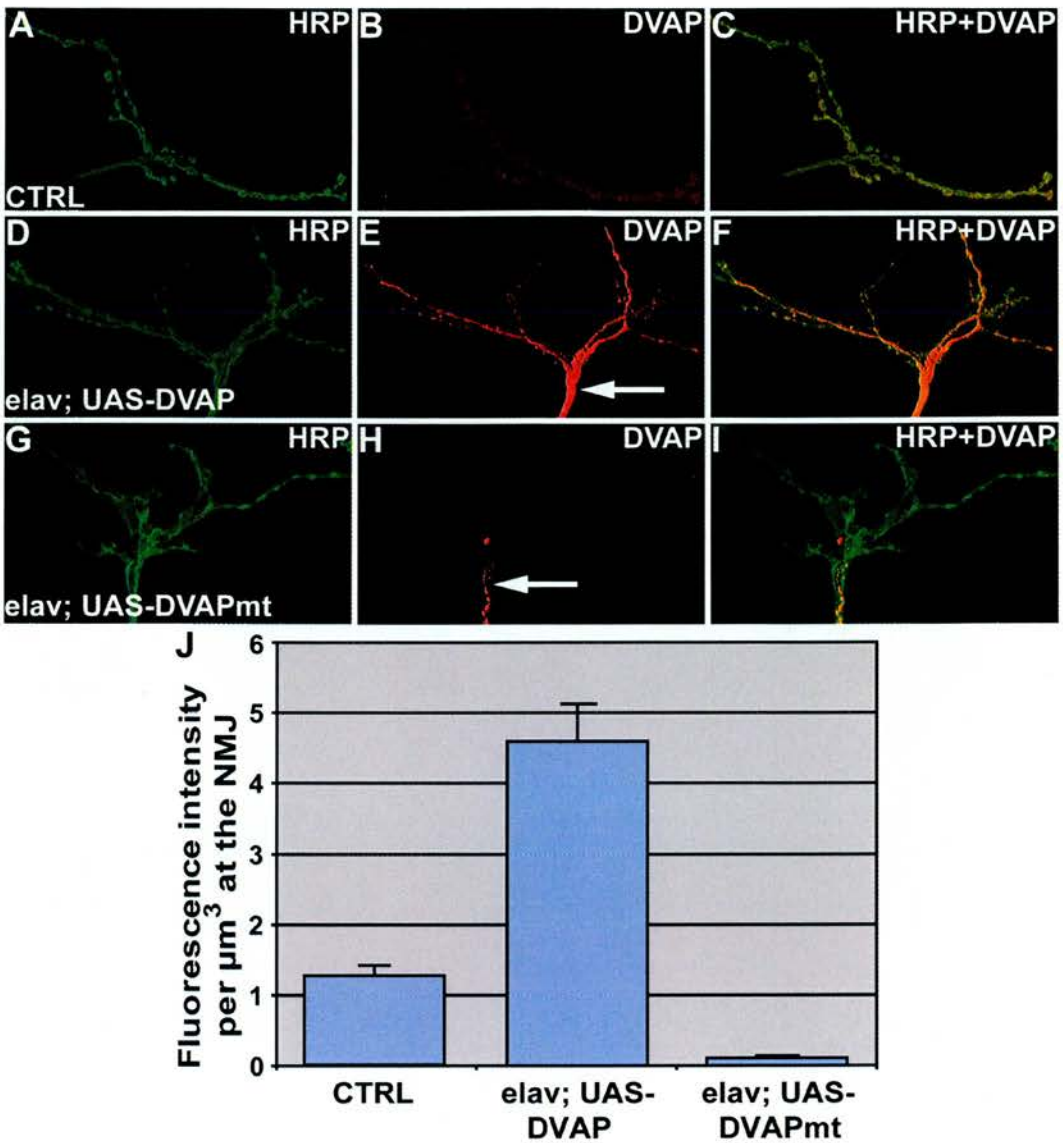

Figure 5.4. Transgenic expression of DVAPP58S depletes the endogenous protein from its normal localization.

NMJs were stained with antibodies specific for DVAP-33A (red, DVAP) and for anti-HRP (green) to visualize the synapses. (**A–C**) Control NMJs. (**D–F**) NMJs overexpressing DVAP-33A (elav; UAS-DVAP). (**G–I**) NMJs expressing transgenic DVAPP58S (elav; UAS-DVAPmt). (**J**) Quantification of synaptic DVAP-33A fluorescence intensity for the reported genotypes. Canton S larvae were used as controls in the experiment reported in this figure. In (J) fluorescence intensity is presented in arbitrary units. Scale bar = 10 µm.

Chapter 6: Finding interactors of VAP: Modelling VAP-induced ALS in the Drosophila eye

Since the patho-mechanism of ALS has not yet been elucidated, it is imperative to identify genes that interact with VAP-33. Building on the success of modifier screens carried out in neurodegenerative diseases such as Spinocerebellar Ataxia-1 (SCA-1), Huntington disease and tauopathies, I attempted a dominant enhancers/suppressors screen utilizing the DrosDel isogenic deficiency kit (Ryder *et al*, 2004) available from the Szeged European Stock Center by using the *Drosophila* model for ALS that has been created.

We tested the possibility of modelling the disease in the *Drosophila* adult eye as it an experimentally-tractable structure in which to model human neurodegenerative diseases in flies. The majority of modifier screens for neurodegenerative diseases utilized the eye-specific driver, GMR-Gal4 to express the protein of interest in the developing fly eye (Fernandez-Funez *et al*, 2000; Wittmann *et al*., 2001; Kazemi-Esfarjani and Benzer, 2002; Guo *et al*., 2003; Mutsuddi *et al*., 2004; Shulman and Feany, 2003). One caveat is that *GMR-Gal4* driver produces a background rough eye in flies and has been shown to have deleterious eye effects on eye architecture. *GMR-Gal4* homozygous flies alone (i.e. without any UAS transgene) have a highly disorganized eye morphology (Kramer and Staveley, 2003). In addition, *GMR-Gal4* homozygotes and heterozygotes have higher number of apoptotic cells in third instar larval imaginal discs than wild type controls (Kramer and Staveley, 2003).

We decided against using the *GMR-Gal4* driver for the expression of VAP proteins in the eye as it has been shown that *GMR-Gal4* driver alone exhibit a rough eye phenotype (Fernandez-Funez *et al*., 2000, Cukier *et al*., 2008). Using the commonly employed *GMR-Gal4* driver might impede our study as enhancers or suppressors of GMR-induced rough eye phenotype might be picked up from our genetic screen instead of VAP-33 interactors. To circumvent this problem, we investigated the possibility of using an alternative eye driver in which the Gal4

protein is under the control of *Eyeless*, a gene specifically and strongly expressed in the *Drosophila* eye.

6.1 Eye-specific expression of DVAPP58S using ey-Gal4 induces degeneration in the adult eye

The expression of eyeless starts in the eye-antennal disc precursor cell at stage 15 of embryonic development (Hauck *et al.*, 1999) and in third instar larval development, eyeless expression is found at high levels in cells posterior to the morphogenetic furrow and in a faint and fading pattern anterior to the furrow (Halder *et al.*, 1995; Hauck *et al.*, 1999). To this end, the expression of *Drosophila* pathogenic VAP (DVAPP56S) was targeted to the adult *Drosophila* eye using the *UAS-Gal4* system and *eyeless-Gal4* as a driver (Brand and Perrimon, 1993). We directed the overexpression of DVAPP58S in the developing fly eye by crossing with several ey-Gal4 driver lines. To increase the dosage of DVAPP56S, embryos from the resulting crosses were heat-shocked at 30°C till eclosion. We found that flies of both driver lines *ey-Gal4* (8227) and *ey-Gal4* (8228) have deformed eyes, and we had to abandon the crosses as they would not be ideal drivers for the modifier screen.

Remarkably, overexpression of DVAPP58S in the developing eye using *ey-Gal4/CyO* (5535) and *ey-Gal4* (5534) results in flies exhibiting a rough eye phenotype (Figure 6.1B and C) at 30°C as compared to wild type eyes (Figure 6.1A). SEM analysis revealed a reduction in size, extra bristles and fused ommatidia (Figures 6.1E) when compared to wild type flies (Figure 6.1D). *CyO/UAS-DVAPP58S* internal controls from the cross between *ey-Gal4* (5535) and *UAS-DVAPP58S* transgenic flies did not exhibit any rough eye phenotype or obvious reduction in eye size.

As additional controls, we heat-shocked both driver lines *ey-Gal4* (5534), *ey-Gal4/CyO* (5535) and the UAS-DVAPP58S transgene independently to confirm that the reduction in eye-size, rough eye and missing inter-ommatidial bristles seen in *ey-*

Gal4/UAS-DVAPP58S flies were not due to the effect of either the driver lines or UAS-DVAPP58S line alone. We found that heat-shocked *ey-Gal4/CyO* (5535) and UAS-DVAPP58S had no eye abnormalities as well as one copy of *ey-Gal4* (5534).

The activity of Gal4 is temperature dependent (Duffy, J.B., 2002), allowing one to express different levels of protein by altering the temperature. We decided to investigate how lower levels of DVAPP58S can affect the reduction in eye sizes, the frequently missing inter-ommatidial bristles and a rough eye phenotype seen in the overexpression of DVAPP58S in the eye. We raised *ey-Gal4/UAS-DVAPP58S* embryos at 28°C till eclosion and found that flies have a less severe reduction in eye size and roughness (Figure 6.1B).

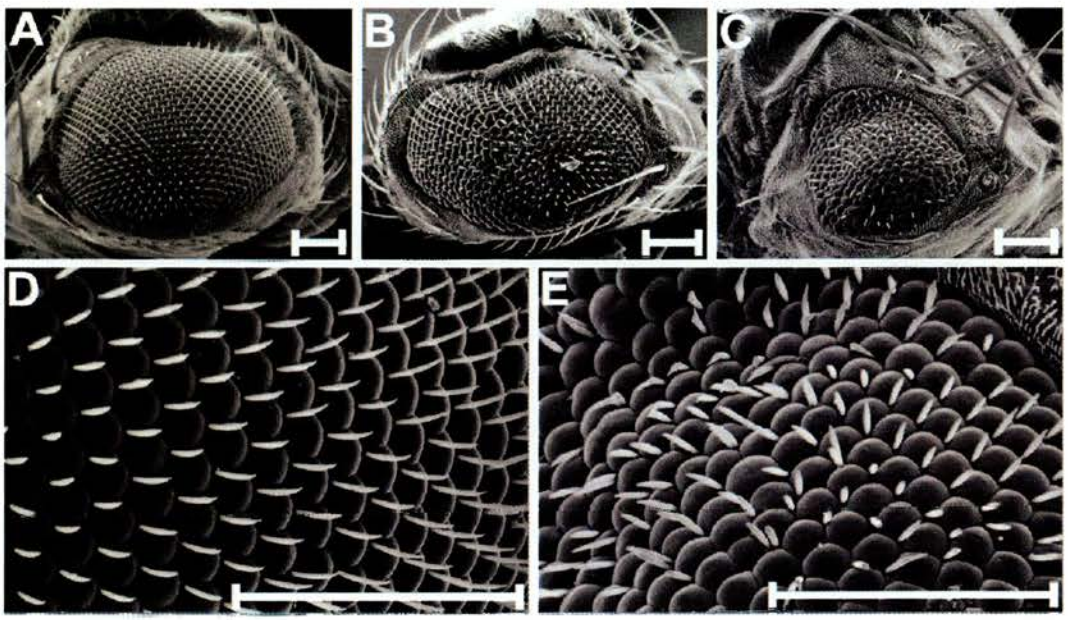

Figure 6.1. Eye-specific transgenic expression of DVAPP58S induces a degenerative eye phenotype in the adult fly.
SEM images of wild type (Canton S) (A) and transgenic eyes overexpressing DVAPP58S at 28°C (B) and at 30°C (C). The expression of *UAS-DVAPP58S* transgene was targeted to the eye by using *ey-Gal4* driver (5535). *Ey-Gal4/CyO* males were crossed with *UAS-DVAPP58S/UAS-DVAPP58S* females and *Ey-Gal4/UAS-DVAPP58S* flies were identified and subjected to phenotypic analysis. No obvious phenotype was observed in *CyO/UAS-DVAPP58S* controls. (D) and (E) are higher magnifications of the eyes in (A) and (C) respectively. The severity of the phenotype was dependent on the strength of the transgene. Scale bars: 100 μm.

6.2 Generating *ey-Gal4, DVAPP58S/CyO-GFP* flies by meiotic recombination

We have found that transgenic expression of DVAPP58S induces a degenerative eye phenotype when expressed specifically in the eye using the *ey-Gal4* (5535) driver. The *UAS-DVAPP58S* insertion situated on chromosome 2 was recombined with the *ey-Gal4* (5535) insertion also situated on chromosome 2, to generate a recombinant chromosome 2 bearing both of these insertions. The resulting *ey-Gal4,UAS-DVAPP58S* chromosome was balanced over *CyO-GFP* and several *ey-Gal4,UAS-DVAPP58S/CyO-GFP* recombined lines were recovered. The detailed genetic scheme of meiotic recombination is described in section 2.2.4 of Material and Methods.

The resultant *ey-Gal4,UAS-DVAPP58S/CyO-GFP* fly stocks all exhibit rough eye phenotypes with reduced eye size, missing bristles and fused ommatidia when raised at 30°C. Milder rough eye phenotype and less severe reduction in eye size was also observed in *ey-Gal4,UAS-DVAPP58S/CyO-GFP* flies raised at a lower temperature of 28°C and 29°C respectively.

Chapter 7: DVAPP58S induced eye degeneration recapitulates major hallmarks of the disease model

The aim of creating a *Drosophila* model of ALS in the adult fly eye is to facilitate the convenience of conducting a genetic screen as this is now the standard structure of modelling neurodegenerative diseases in *Drosophila*. Moreover, the adult fly eye offers many advantages such as the possibility to observe the degeneration in a temporal manner while overcoming possible lethality and fertility problems. Modifiers of the degenerative eye phenotype would be tested for their modifying effects on the larval neuromuscular phenotypes to be confirmed as true interactors of DVAP-33A. To ensure that the *Drosophila* eye model is a faithful model of ALS, we sought to recapitulate several key aspects of the disease hallmarks.

7.1 DVAPP58S induced eye degeneration is dosage dependent

VAP-induced ALS8 is dominantly inherited and transgenic expression of DVAPP58S in the presence of endogenous DVAP-33A induces a degenerative eye phenotype. DVAP-33A has also been shown to affect synaptic sprouting in a dosage-dependent manner (Pennetta *et al.*, 2002) To ensure that the degenerative eye phenotype is due to the dosage dependent effects and the expression of DVAPP58S, two copies of the UAS-DVAPP58S transgene were targeted to the eye by crossing virgin females of *w⁻/w⁻; ey-Gal4, UAS-DVAPP58S/CyO-GFP; +/+* genotype with males of *yw/y; UAS-DVAPP58S/UAS-DVAPP58S; +/+* genotype.

The embryos were raised at a lower temperature of 25°C and the resultant non-CyO progeny exhibit a degenerative phenotype with reduced eye size, missing bristles and fused ommatidia that is similar to *ey-Gal4/UAS-DVAPP58S* flies raised at 30°C (compare Figures 6.1C with 7.1B). This demonstrates that transgenic eye-specific expression of DVAPP58S induces a degenerative eye phenotype in a dosage dependent manner. *ey-Gal4, UAS-DVAPP58S/UAS-DVAPP58S* embryos raised at 30°C were lethal as they failed to eclose after pupal stages. This pupal lethality could

possibly be a consequence of the leaky expression of the *UAS-DVAP58S* transgene or *ey-Gal4* driver into other tissues. Leaky expression of Gal4 drivers is not uncommon, leaky expression of the *GMR-Gal4* driver has been attributed to cause lethality in methyl-CpG–binding protein 2 (MeCP2) overexpression in the fly eye at higher temperatures. MeCP2 is a transcriptional regulator involved in chromatin remodelling and loss of *MeCP2* causes classic Rett syndrome (Cukier *et al.*, 2008).

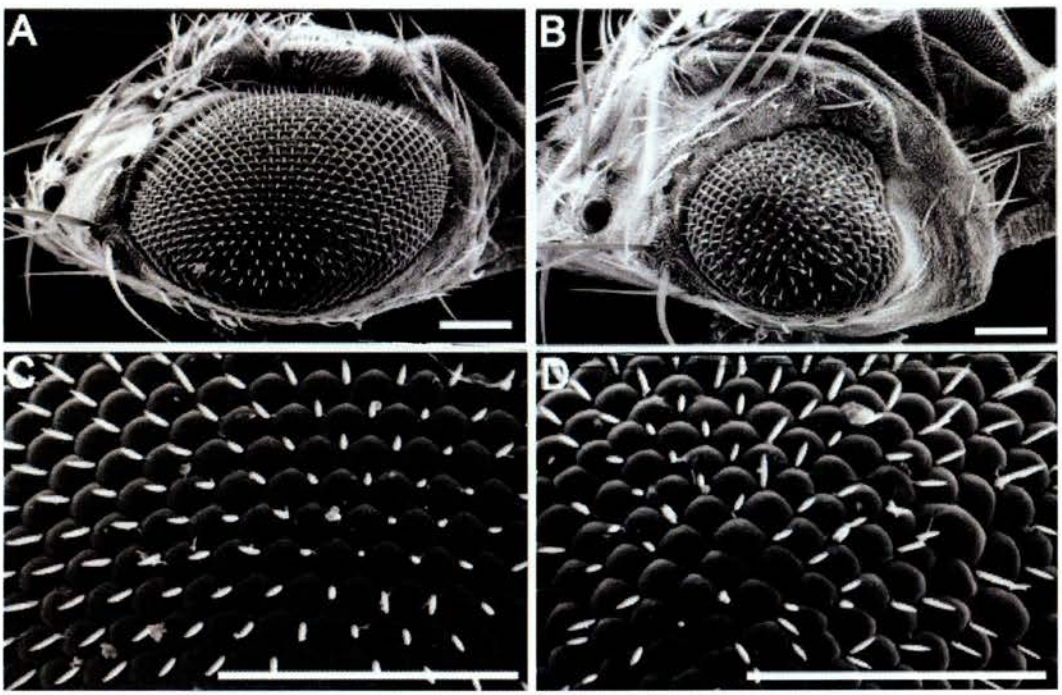

Figure 7.1. DVAPP58S induced eye degeneration is dosage dependent.
SEM images of (A) Control and (B) flies expressing double copy of the UAS-DVAPP58S transgene raised at 25°C. *ey-Gal4, UAS-DVAPP58S/CyO-GFP* females were crossed to *UAS-DVAPP58S/UAS-DVAPP58S* males. Progeny of *ey-Gal4, UAS-DVAPP58S/UAS-DVAPP58S* genotype exhibit a degenerative phenotype with reduced eye size, missing bristles and fused ommatidia. (C) and (D) are higher magnifications of (A) and (B) respectively. Scale bars: 100 μm.

7.2 DVAPP58S induced eye degeneration is partly due to apoptosis

Another hallmark of ALS is motor neuron death in both patients and mouse models (Li *et al.*, 2000, Bruijn *et al.*, 2004). By TUNEL staining, we also observed significantly enhanced apoptosis in cell bodies of larva brains expressing transgenic

DVAPP58S in our ALS model when compared to controls (Figure 5.2B). Members of the *Drosophila* Inhibitor of Apoptosis Protein (DIAP) family block the intrinsic machinery of the canonical cell death pathway by binding to and neutralizing the pro-apoptotic caspases. The activity of DIAPs is in turn antagonized upon binding with pro-apoptosis proteins such as Rpr, Grim and Hid, thereby liberating caspases (Wang *et al.*, 1999).

We found that the co-expression of DIAP1 with the eye-specific expression of DVAPP58S partially suppresses the degenerative eye phenotype induced by transgenic expression of DVAPP58S alone (Compare Figures 7.2A and 7.2B). SEM analysis shows that the eye sizes are brought towards control eye sizes (Figure 7.2C) while the fused ommatidia and missing bristles were also less pronounced in flies that suppress the degenerative eye phenotype (Figures 7.2B and 7.2E). This demonstrates that the degenerative eye phenotype induced by the transgenic expression of DVAPP58S is partly due to cell death occurring in the eye.

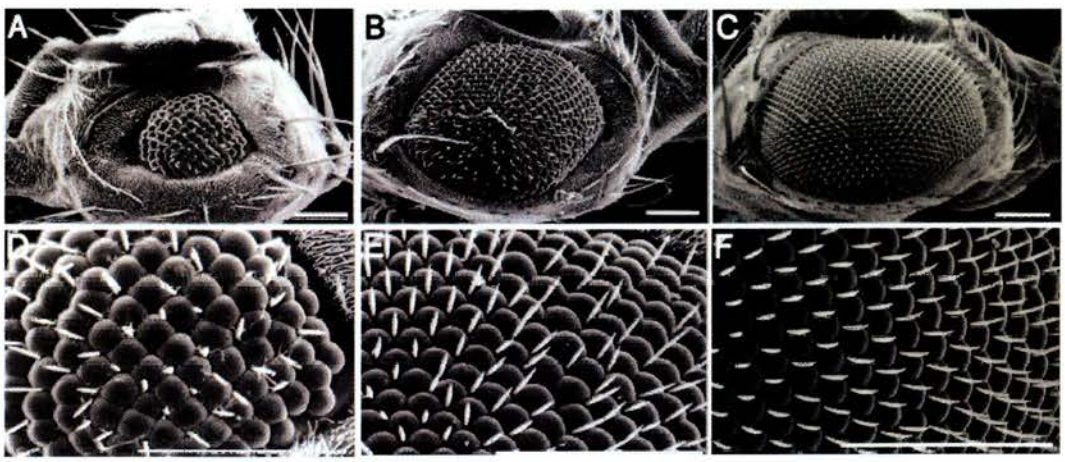

Figure 7.2. Co-expression of DIAP1 partially suppresses the DVAPP58S-induced degenerative eye phenotype.
SEM images of (A) ey-Gal4, UAS-DVAPP58S/CyO-GFP flies , (B) co-expression of DIAP1 with ey-Gal4, UAS-DVAPP58S, (C) control flies. (D),(E) and (F) are higher magnifications of (A), (B) and (C) respectively. Flies were raised at
30°C and scale bars: 100 μm.

7.3 Recombined *ey-Gal4, UAS-DVAPP58S/CyO-GFP* flies exhibit dosage-dependent eye degeneration and aggregate formation in the optic lobes of adult flies

A prominent feature of all neurodegenerative diseases is the characteristic deposits of protein inclusions or aggregates that are either cytoplasmic, nuclear or extracellular (Taylor *et al.*, 2002). In our ALS fly model, we have also observed the deposition of aggregates immunoreactive to DVAP-33A antibodies in larval brains of flies expressing transgenic DVAPP58S. Similarly, DVAP-33A immunoreactive aggregates were also found in the optic lobes of adult flies transgenically expressing DVAPP58S (data not shown).

To confirm that the recombined *ey-Gal4, UAS-DVAPP58S/CyO-GFP* flies exhibits the same phenotypes as *ey-Gal4/UAS-DVAPP58S* flies, we raised several lines of the recombined flies at 28°C and 30°C. We found that eyes of these recombined flies all exhibit the dosage dependent effect of DVAPP58S induced eye degeneration phenotype with reduction in eye size, fused ommatidia and missing bristles (data not shown). The recombined *ey-Gal4, UAS-DVAPP58S/CyO-GFP* flies therefore, also exhibit the same dosage dependent degenerative phenotype as *ey-Gal4/UAS-DVAPP58S* flies

These results, together with the fact that apoptosis contributes to the degenerative eye phenotype when expressing DVAPP58S in the eye, shows that both the eye model and the NMJ model of ALS8 can be used interchangeably. This in turn, allows modifiers of DVAPP58S-induced degenerative eye phenotype to be used in the NMJ model for detailed analysis and to confirm the interactions with DVAP-33A.

Chapter 8: Using the DVAPP58S induced eye degeneration in a deficiency screen

Sensitized screens are commonly employed as a means of uncovering novel regulators of gene function. Loss-of-function mutations in almost all genes are recessive, which indicates that 50% of the wild-type level of a protein is sufficient for normal development. When a particular process is already partially disrupted by another mutation, however, this amount might no longer suffice, and mutations in the genes that are involved in the pathway can therefore be identified as dominant enhancers or suppressors in this sensitized genetic background (St. Johnston, D., 2002).

A single Proline to Serine substitution at codon 56 in human VAPB causes ALS8 in patients. We have created a fly model of ALS at the larval NMJ by mutating the DVAP-33A at codon 58 from Proline to Serine (DVAPP58S). The expression of UAS-DVAP58S transgene in the developing eye using an *ey-Gal4* driver, induces a degenerative eye phenotype in flies with rough and reduced eyes (Figure 6.1). Mutations that enhance or suppress this phenotype resulting from the transgenic expression of DVAPP58S are likely to define genes that are involved in the same biological process or pathway as *DVAP-33A*.

To facilitate systemic dominant-modifier screens in *Drosophila*, the DrosDel collection of 209 deficiency lines has been generated which covers 60% of the euchromatic genome. This deficiency collection is composed of molecularly-mapped deletions with single-based-pair resolution in an isogenic background. Each deletion uncovers an average of 44 genes or 368kb and genes uncovered by the interacting deficiency lines can be easily identified by their annotations on Flybase (www.flybase.org) (Ryder *et al.*, 2004, Ryder *et al.*, 2007). Therefore, we embarked on a deficiency screen using this DrosDel collection because of the potential for a 'low-resolution' genome scan. Specific area of interests highlighted in this DrosDel collection screen can then be honed in at higher resolution using the Exelixis

collection as it has an average deletion size of 140kb and a coverage of ~56% of the genome (Parks *et al.*, 2004).

8.1 Interacting deficiencies from the DrosDel collection affects the severity of DVAPP58S-induced degenerative eye phenotype

The F1 progeny of crosses between males bearing the deletions and females of the sensitized recombinant line expressing DVAPP58S under the control of the *ey-Gal4* driver were screened for enhancers and suppressors of DVAP58S eye defects (Figure 6.1 in Chapter 6). Figure 8.1 shows an outline of the F1 eye-based screen for dominant modifiers of the eye phenotype using the DrosDel deficiency collection.

Figure 8.1. Outline of the F1 eye-based screen for dominant modifiers of *ey-Gal4, UAS-DVAPP58S/CyO-GFP* by deficiency on the second, third and X chromosomes.

Deficiencies on the 3rd chromosome, *w^{1118}/Y; +/+; Df(3)/TM3, Sb*

(P) ♀ *w^-/w^-; ey-Gal4, UAS-DVAPP58S/CyO-GFP; +/+*

X

♂ *w^{1118}/Y; +/+; Df(3)/TM3, Sb*

↓

(F1) Experimental class:

♂ *w^-/Y; ey-Gal4, UAS-DVAPP58S/+; Df(3)/+*

♀ *w^{1118}/w^-; ey-Gal4, UAS-DVAPP58S/+; Df(3)/+*

Select non-CyO, non-Sb

Internal control class:

♂ *w^-/Y; ey-Gal4, UAS-DVAPP58S/+;+/TM3, Sb*

♀ *w^{1118}/w$^-$; ey-Gal4, UAS-DVAPP58S/+;+/TM3, Sb*

Select non-CyO, Sb

Other genotypes:

♂ *w$^-$/Y; +/CyO-GFP; +/TM3, Sb*

♀ *w^{1118}/w$^-$; +/CyO-GFP; +/TM3, Sb*

♂ *w$^-$/Y; +/CyO-GFP; Df(3)/+*

♀ *w^{1118}/w$^-$; +/CyO-GFP; Df(3)/+*

Deficiencies on the 2nd chromosome, *w^{1118}/Y; Df(2)/CyO; +/+*

(P) ♀ *w$^-$/w$^-$; ey-Gal4, UAS-DVAPP58S/CyO-GFP; +/+*

X

♂ *w^{1118}/Y; Df(2)/CyO; +/+*

↓

(F1) Experimental class:

♂ *w$^-$/Y; ey-Gal4, UAS-DVAPP58S/Df(2); +/+*

♀ *w^{1118}/w$^-$; ey-Gal4, UAS-DVAPP58S/Df(2); +/+*

Select non-CyO

Internal control class:

♂ *w$^-$/Y; ey-Gal4, UAS-DVAPP58S/CyO; +/+*

♀ *w^{1118}/w$^-$; ey-Gal4, UAS-DVAPP58S/CyO; +/+*

Select CyO and small, rough eye phenotype

Other genotypes:

♂ *w⁻/Y; Df(2)/CyO-GFP; +/+*

♀ *w^{1118}/w⁻; Df(2)/CyO-GFP; +/+*

♂ *w⁻/Y; CyO/CyO-GFP; +/+*

♀ *w^{1118}/w⁻; CyO/CyO-GFP; +/+*

Deficiencies on the X chromosome, *Df(X)/FM7; +/+; +/+*

(P) ♂ *w⁻/Y; ey-Gal4, UAS-DVAPP58S/CyO-GFP; +/+*

X

♀ *Df(X)/FM7; +/+; +/+*

↓

(F1) Experimental class:

♀ *Df(X)/w⁻; ey-Gal4, UAS-DVAPP58S/+; +/+*

♂ *Df(X)/Y; ey-Gal4, UAS-DVAPP58S/+; +/+*

Select non-CyO, dark eye colour

Other genotypes:

♀ *Df(X)/w⁻; CyO-GFP/+; +/+*

♂ *Df(X)/Y; CyO-GFP/+; +/+*

♂ FM7/*Y; ; ey-Gal4, UAS-DVAPP58S/+; +/+*

♀ *w⁻/FM7; ey-Gal4, UAS-DVAPP58S/+; +/+*

♂ FM7/*Y; ; CyO-GFP/+; +/+*

♀ *w⁻/FM7; CyO-GFP/+; +/+*

8.1.1 Df(2L)ED700, a small deletion that suppresses DVAPP58S-induced eye phenotype

We isolated several interacting deficiency lines that uncover genes that suppress *ey-Gal4, UAS-DVAPP58S* induced eye defects. One example is a small deficiency known as Df(2L)ED700 which lies on the second left hand chromosome of the *Drosophila* genome. *ey-Gal4, UAS-DVAPP58S/Df(2L)ED700* flies have eye sizes larger than internal control (*ey-Gal4, UAS-DVAPP58S/CyO*) and *ey-Gal4, UAS-DVAPP58S/CyO-GFP* flies. SEM analysis also show that the fused ommatidia, missing bristles and rough eye phenotype seen in internal controls and ey-Gal4, UAS-DVAPP58S/CyO-GFP flies are less pronounced in *ey-Gal4, UAS-DVAPP58S/Df(2L)ED700* flies. The external appearance of the eye has been brought towards the smooth external appearance seen in wild-type (Figure 8.2). *ey-Gal4, UAS-DVAPP58S/CyO* internal control class also did not show any reduction in eye sizes and rough eye defects (data not shown).

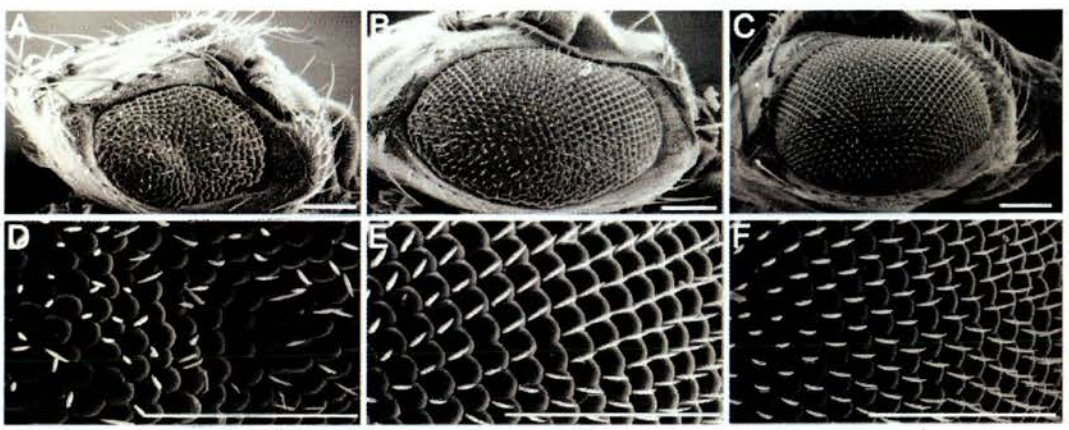

Figure 8.2. Df(2L)ED700 suppresses DVAPP58S-induced eye phenotype.
SEM images of (A) *ey-Gal4, UAS-DVAPP58S/CyO-GFP* adult eye, (B) *ey-Gal4, UAS-DVAPP58S/Df(2L)ED700* adult eye, (C) wild-type flies. (D), (E) and (F) are higher magnifications of (A), (B) and (C) respectively. Flies were raised at 30°C and scale bars: 100 μm.

Df(2L)ED700 deletes 6 genes (CG33300, CG13124, CG5899, CG4602, CG4600, CG5885) and partially deletes one gene (CG5920) (Figure 8.3B). Df(2L)ED700 lies within another larger deficiency line, Df(2L) ED695, that deletes

49 genes and partially deletes 1 gene (Figure 8.3A). *ey-Gal4, UAS-DVAPP58S/Df(2L) ED695* flies also suppresses the *ey-Gal4, UAS-DVAPP58S* induced eye defects, bringing the normally reduced eye size and rough eye phenotype towards wild type phenotype (data not shown). These data show that the effect of this region to suppress the degenerative eye phenotype is specific. We attempted to narrow down to the gene responsible for the suppression and obtained five P-element insertions that could disrupt five of the genes uncovered in this small deficiency. However, P-element insertions of CG13124, sop (CG5920), Srp54 (CG4602), CG5885 and yip2(CG4600) tested so far did not show any suppression (data not shown).

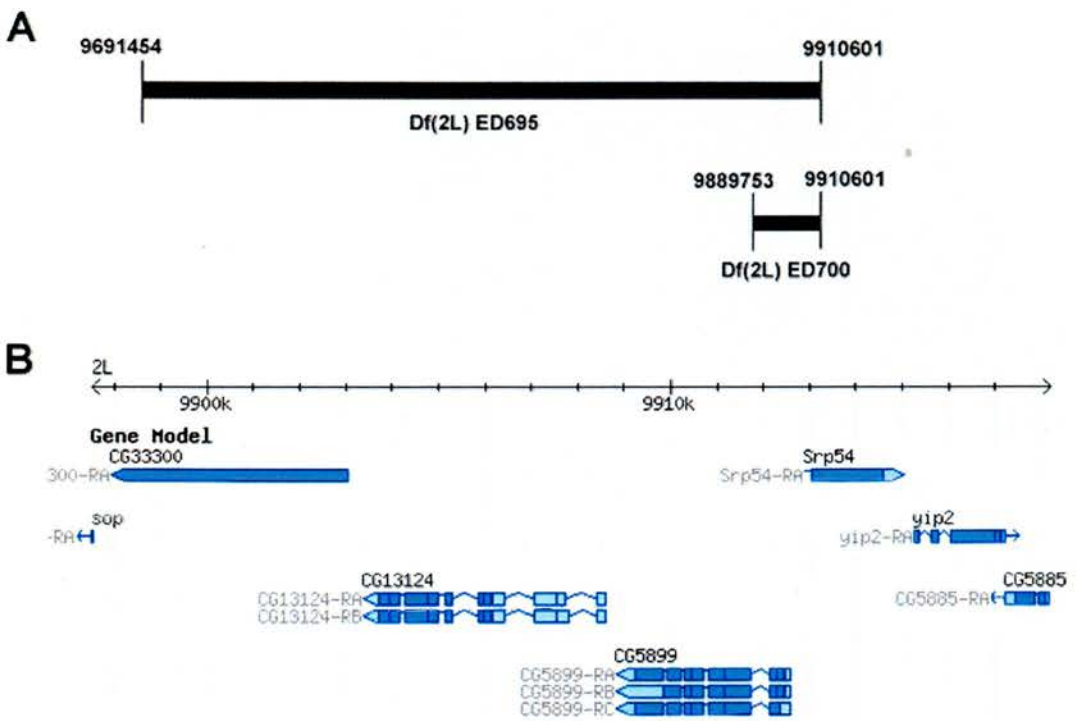

Figure 8.3. Two overlapping deficiencies that suppress DVAPP58S-induced eye phenotype.
(A) Size and coordinates of Df(2L) ED700 and Df(2L) ED695. Df(2L) ED700 lies within the genomic region of Df(2L) ED695. (B) Genes deleted by Df(2L) ED700.

8.1.2 Df(X)ED7424, a suppressor of DVAPP58S on the X chromosome

Another deficiency line that exhibits suppressing effects on the ey-Gal4, UAS-DVAPP58S induced degenerative eye phenotype is located on the X chromosome of the *Drosophila* genome. *Df(X)ED7424/+; ey-Gal4, UAS-DVAPP58S/+* flies have increased eye size that is similar to wild type sizes when compared to *ey-Gal4, UAS-DVAPP58S/CyO-GFP* flies (compare Figure 8.4A with Figure 8.4B and 8.4C). SEM analysis also shows that the rough eye phenotype with fused ommatidia and missing bristles are also suppressed in *Df(X)ED7424/+; ey-Gal4, UAS-DVAPP58S/+* flies (compare Figure 8.4D with Figure 8.4E and 8.4F).

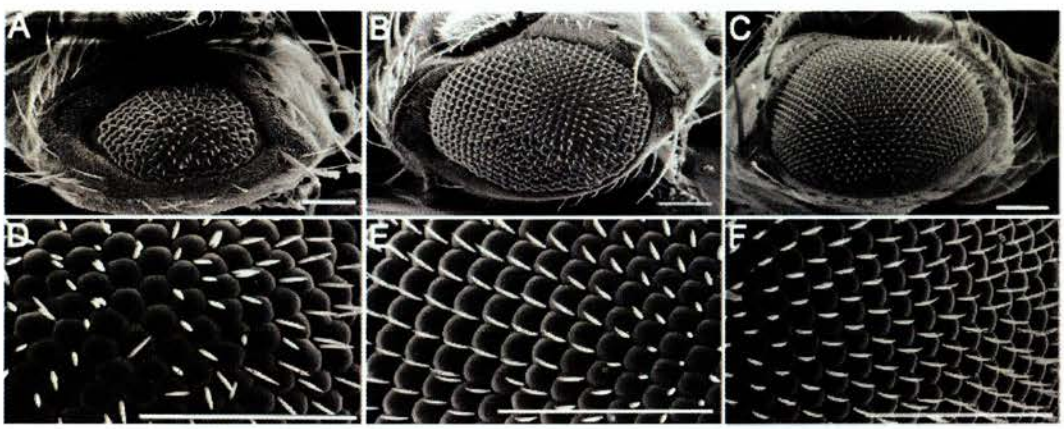

Figure 8.4. Df(X)ED7424 suppresses DVAPP58S-induced eye phenotype.
SEM images of (A) *ey-Gal4, UAS-DVAPP58S/CyO-GFP* adult eye, (B) *Df(X)ED7424/+; ey-Gal4, UAS-DVAPP58S/+* adult eye, (C) wild-type flies. (D), (E) and (F) are higher magnifications of (A), (B) and (C) respectively. Flies were raised at 30°C and scale bars: 100 μm.

Df(X)ED7424 deletes 72 genes and partially deletes 1 gene. This deficiency overlaps with two other deficiencies, Df(X)ED447 and Df(X)ED7413 (Figure 8.5) that also exhibit suppressing effects on ey-Gal4, UAS-DVAPP58S induced degenerative eye phenotype (data not shown). Out of the three deficiency lines that suppresses ey-Gal4, UAS-DVAPP58S induced degenerative eye phenotype, Df(X)ED7413 uncovers the smallest region, deleting 28 genes and partially deleting one gene (Table 8.1). We obtained P-element insertion lines that could disrupt the 29

genes uncovered by this smallest overlapping deletion to try and narrow down to the gene responsible for the suppression of the eye phenotype, however, *Pk17E* (CG7001), CG7101, CG6695, CG6961, Pvf1 (CG7103), CG7326 and CG6891 with P-element insertions tested so far did not show any suppression (data not shown). 13 other genes that do not have any P-element insertion however, do have RNAi constructs. Four remaining genes have neither P-element insertions nor RNAi constructs.

Of the 29 genes deleted, *bnb* (bangles and beads, CG7088), presents the most interest as it has also been identified as a direct interactor of DVAP-33A in a yeast-two-hybrid screen carried out in our laboratory (K. Parry and G.Pennetta, unpublished data). Bnb is closely related to mammalian GAP-43 protein with consensus sequences that could potentially serve as phosphorylation sites and for calmodulin binding (Ng *et al.*, 1989, Eberl *et al.*, 1992).

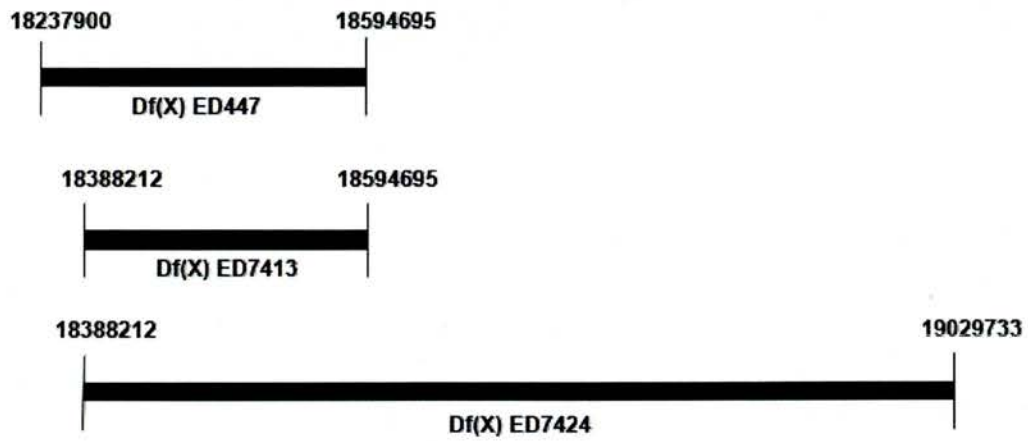

Figure 8.5. Three overlapping deficiencies on the X chromosome that suppress DVAPP58S-induced eye phenotype.
Shown here are the size and coordinates of Df(X) ED447, Df(X) ED7413 and Df(X) ED 7424. Df(X) ED 7413 is the smallest deficiency that deletes 28 genes and partially deletes one gene.

CG6551	CG7088
CG6816	CG32543
CG6873	CG7274
CG6891	CG7322
CG6900	CG7326
CG7053	CG6578
CG7095	CG6585
CG7103	CG32540
CG7282	CG7001
CG32544	CG7058
CG6696	CG7101
CG6857	CG7280
CG12609	CG7288
CG18259	CG6659
CG6961	

Table 8.1. List of genes that are deleted by the smallest overlapping deficiency, Df(X) ED7413.

8.1.3 Other interacting deficiencies

Table 8.2 shows a number of other deficiencies that either suppress or enhance the ey-Gal4, UAS-DVAPP58S induced degenerative eye phenotype.

Supressors	Enhancers
Df(2L)ED1165	Df(X)ED411
Df(2L)ED1455	Df(X)ED6474
Df(2R)ED1673	Df(2L)ED1186
Df(2R)ED1715	Df(3L)ED4341
Df(2R)ED2436	
Df(3L)ED231	
Df(3L)ED224	
Df(3L)ED225	
Df(3L)ED4710	

Table 8.2. List of other deficiencies that enhanced or suppressed the ey-Gal4,

UAS-DVAPP58S induced degenerative eye phenotype.

8.2 MATLAB software for quantification of eye phenotype

The majority of modifier screens demonstrate qualitatively the extent of enhancement or suppression of various eye phenotypes. Efforts have been made to quantify the enhancement or suppression of modifiers in genetic screens and studies of gene activity utilizing the *Drosophila* adult eye. For instance, calculating the average number of unfused ommatidia (Mutsuddi *et al.*, 2004), the average number of photoreceptor cells per ommatidium (St. Pierre *et al.*, 2002), the percentage of correctly orientated bristles (Paricio *et al.*, 1999) and the number of ommatidia (Jones *et al.*, 2006, Protzer *et al.*, 2008). Other less direct quantification include assigning individual eyes a numerical score based on the severity of the defects (Corona *et al.*, 2004, Armstrong *et al.*, 2005) and scoring retinal phenotypes according to objective criteria (Pandey *et al.*, 2007).

Several groups have also performed quantification of eye sizes by area measurement (Vidal *et al.*, 2007, Protzer *et al.*, 2008,), circumference measurement (Hyun *et al.*, 2005) or calculating the longest distance of a side view of the eye from dorsal to ventral plus anterior to posterior (Oldham *et al.*, 2002), when the resulting eye phenotype involves a change in eye sizes.

The quantification of eye sizes by area measurement has traditionally been done using the NIH ImageJ software that calculates statistics of user-defined regions. For any manually-driven selection then differences in operator bias and skill can lead to variation in the location of the border surrounding the eye, and in ImageJ this operation involves tracing the area using a free-hand selection tool. To mitigate the differences occurring due to the operator's skill with the selection tool, the border should be traced using as many control points as possible.

In collaboration with James Withers at the Neuroinformatics department, we

have produced similar software in MATLAB which streamlines the border tracing and analysis. Light micrographs of eyes are taken with a camera mounted on a dissection microscope and using this software (see section 2.10 of Materials and Methods for details), we attempt to quantify the suppressing effects of some of the interacting deficiencies that mitigates the ey-Gal4, UAS-DVAPP58S induced degenerative eye phenotype reported in Table 8.1 by crossing *ey-Gal4, UAS-DVAPP58S/CyO-GFP* flies with flies carrying the different deficiencies.

The ey-Gal4, UAS-DVAPP58S induced degenerative eye phenotype seen in adult flies have a heterogeneity in the severity of the phenotype as assessed by the size of the eyes. The distribution of the eye sizes seen in a cohort of 61 flies carrying the *ey-Gal4, UAS-DVAPP58S* genotype showed that 5% of flies have an eye area of around 50 arbitrary square units while the majority (60%) of flies have eye sizes centred between 1500 and 2000 arbitrary square units. Wild type flies on the other hand have 60% of eye sizes centred at 4500 arbitrary square units and 20% at 4000 and 4750 arbitrary square units each.

8.2.1 Df(2L)ED695 strongly suppresses DVAPP58S-induced eye phenotype

Df(2L)ED695 is a deficiency line that also uncovers the region on the *Drosophila* second chromosome that is deleted by Df(2L)ED700. Both deficiencies have been found to suppress the ey-Gal4, UAS-DVAPP58S-induced degenerative eye phenotype (see 8.1.1). Quantification of *ey-Gal4, UAS-DVAPP58S/Df(2L) ED695* flies showed that 46% of eye sizes centred on 3500 arbitrary square units compared to 60% centred between 1500 and 2500 arbitrary square units in *ey-Gal4, UAS-DVAPP58S/CyO-GFP* flies. Only 4% of *ey-Gal4, UAS-DVAPP58S/Df(2L) ED695* flies had an eye area of 1500 arbitrary square units while 5% of *ey-Gal4, UAS-DVAPP58S/CyO-GFP* flies have an eye area of 50 arbitrary square units (Figure 8.6). The difference in frequency distribution between *ey-Gal4, UAS-DVAPP58S/Df(2L) ED695* flies and *ey-Gal4, UAS-DVAPP58S/CyO-GFP* flies is statistically significant ($P<0.001$, Mann-Whitney U test and Two Sampled Student t-test. See Legend and

Materials and Methods for details). The area of eye sizes seen in ey-*Gal4, UAS-DVAPP58S/Df(2L) ED695* flies has been brought towards wild type eye sizes with 15% of ey-*Gal4, UAS-DVAPP58S/Df(2L) ED695* flies even reaching the normal wild type eye sizes (4000 arbitrary square units, Figure 8.6).

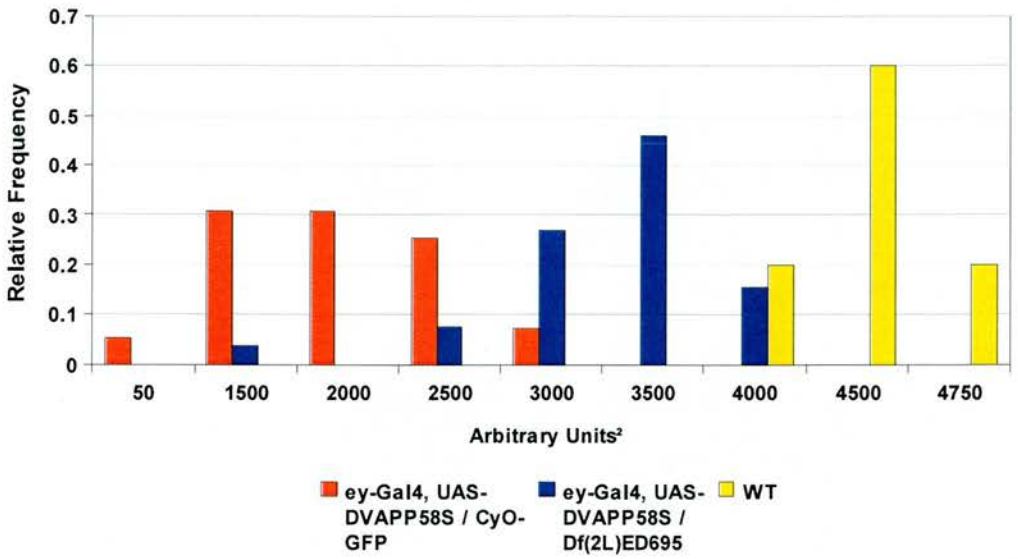

Figure 8.6. Df(2L)ED695 dramatically increases the eye area of *ey-Gal4, UAS-DVAPP58S/Df(2L) ED695* flies.
ey-Gal4, UAS-DVAPP58S/CyO-GFP flies (red) have eye size areas centred between 1500 and 2500 arbitrary square units (N=61, S.D=654) compared to 46% of *ey-Gal4, UAS-DVAPP58S/Df(2L) ED695* flies (blue, N=31, S.D=547) centred on 3500 arbitrary square units that is slightly below wild type values (WT, yellow, 4000-4750 arbitrary units squared, N=20, S.D=261). Differences between eye sizes of *ey-Gal4, UAS-DVAPP58S/CyO-GFP* flies and ey-Gal4, UAS-DVAPP58S/Df(2L) ED695 flies were highly significant ($P<0.001$, according to the non-parametric Mann-Whitney U test and the Two Sampled Student t-test when comparing the two data sets). Flies were raised at 30°C.

8.2.2 Df(2R)ED1673 and Df(2R)ED1715 are two overlapping deficiencies showing moderate suppressor effects

Two overlapping deficiencies that also mitigates the ey-Gal4, UAS-DVAPP58S induced degenerative eye phenotype are Df(2R)ED1673 and Df(2R)ED1715 located on the second right hand chromosome of the *Drosophila* genome. Quantification of *ey-Gal4, UAS-DVAPP58S/Df(2R) ED1673* showed that 35% of eye sizes centred on 3000 arbitrary square units and 29% at 3500 arbitrary square units (Figure 8.7, blue) while e*y-Gal4, UAS-DVAPP58S/Df(2R) ED1715* flies had 80% of eyes centred on 3500 arbitrary square units (not shown) compared to 60% centred between 1500 and 2000 arbitrary square units in *ey-Gal4, UAS-DVAPP58S/CyO-GFP* flies. The difference in frequency distribution between *ey-Gal4, UAS-DVAPP58S/Df(2R) ED1673* flies and *ey-Gal4, UAS-DVAPP58S/CyO-GFP* flies is statistically significant ($P<0.001$, Mann-Whitney U test. See Legend and Materials and Methods for details). Difference in frequency distribution between and *ey-Gal4, UAS-DVAPP58S/Df(2R) ED1715* flies and *ey-Gal4, UAS-DVAPP58S/CyO-GFP* flies is also statistically significant ($P<0.001$, Mann-Whitney U test). The area of eye sizes seen in *ey-Gal4, UAS-DVAPP58S/Df(2R) ED1673* and *ey-Gal4, UAS-DVAPP58S/Df(2R) ED1715* flies have been brought towards wild type eye sizes as 8% of *ey-Gal4, UAS-DVAPP58S/Df(2R) ED1673* flies are 4000 arbitrary units squared (Figure 8.7). Df(2R)ED1673 deletes 82 genes and partially deletes one gene while Df(2R)1715 deletes 90 genes and partially deletes two genes. The overlapping region uncovered by these two deficiencies consists of 34 genes.

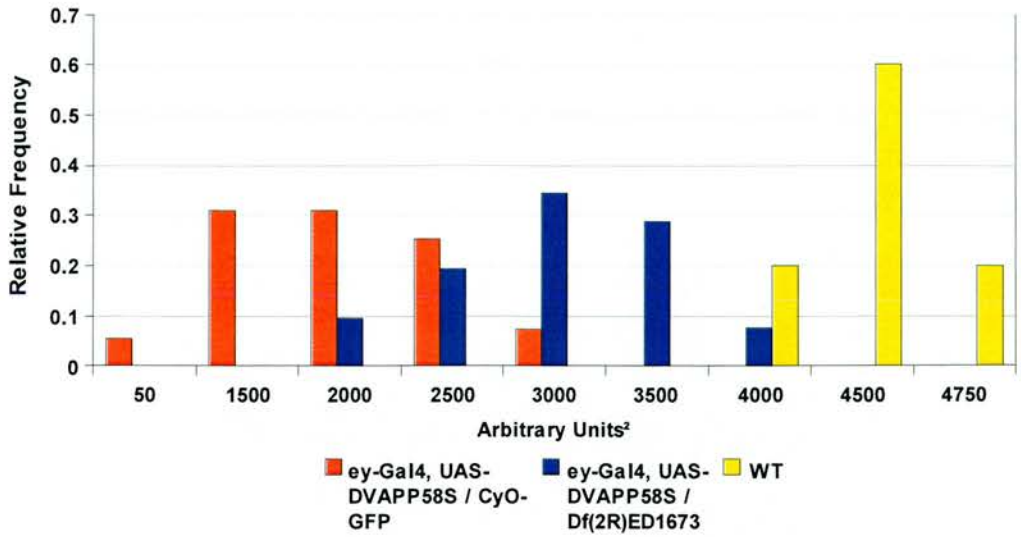

Figure 8.7. Df(2R)ED1673 moderately suppresses DVAPP58S-induced eye phenotype.

ey-Gal4, UAS-DVAPP58S/CyO-GFP flies (red) have eye size areas centred between 1500 and 2500 arbitrary square units (N=61, S.D=654) compared to *ey-Gal4, UAS-DVAPP58S/Df(2R) ED1673* flies (blue) which have 35% of eye sizes centred on 3000 arbitrary square units and 29% at 3500 arbitrary square units (N=52, S.D=520). Differences between eye sizes of *ey-Gal4, UAS-DVAPP58S/CyO-GFP* flies and *ey-Gal4, UAS-DVAPP58S/Df(2R) ED1673* flies were highly significant ($P<0.001$, according to the non-parametric Mann-Whitney U test when comparing the two data sets). Flies were raised at 30°C.

8.2.3 Df(2L)ED1165 is a weak supressor

Df(2L)ED1165 is a deficiency line that deletes 23 genes and partially deletes one gene on the *Drosophila* second chromosome. Quantification of *ey-Gal4, UAS-DVAPP58S/Df(2L) ED1165* flies showed that 37% of eye sizes centred on 3000 arbitrary square units compared to 60% centred between 1500 and 2000 arbitrary square units in *ey-Gal4, UAS-DVAPP58S/CyO-GFP* flies. The 19% of eye sizes fall between 3500 and 4000 arbitrary units squared (Figure 8.8). The difference in frequency distribution between *ey-Gal4, UAS-DVAPP58S/Df(2L)ED1165* flies and *ey-Gal4, UAS-DVAPP58S/CyO-GFP* controls is statistically significant ($P<0.001$, Mann-Whitney U test. See Legend and Materials and Methods for details).

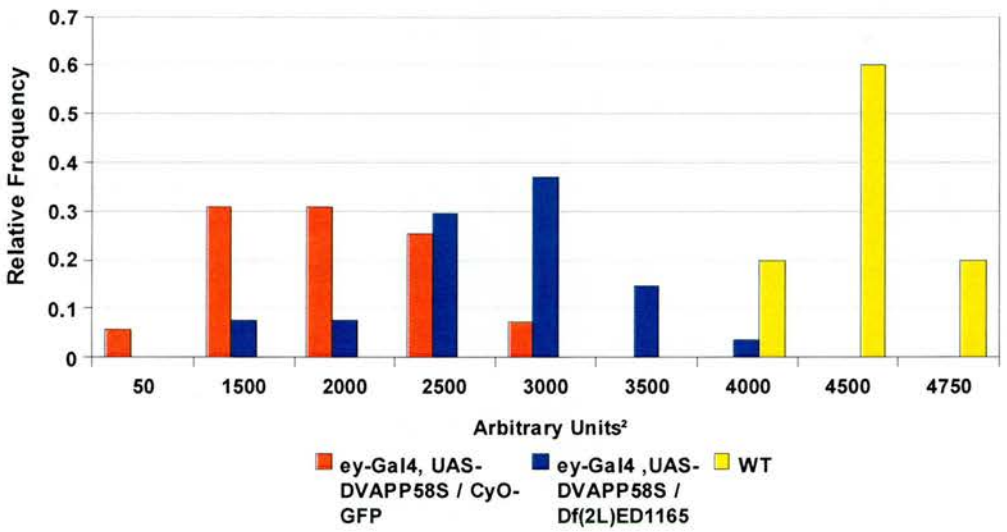

Figure 8.8. Df(2L)ED1165 slightly increases the area of *ey-Gal4, UAS-DVAPP58S/Df(2L) ED1165* flies.

ey-Gal4, UAS-DVAPP58S/CyO-GFP flies (red) have eye size centred between 1500 and 2000 arbitrary square units (N=61, S.D=654)compared to 37% of *ey-Gal4, UAS-DVAPP58S/Df(2L) ED1165* flies (blue) centred at 3000 arbitrary square units. 19% of flies have eye sizes between 3500 and 4000 arbitrary square units (blue, N=27, S.D=589) that is towards wild type values (yellow, N=20, S.D=261). Differences between eye sizes of *ey-Gal4, UAS-DVAPP58S/CyO-GFP* flies and *ey-Gal4, UAS-DVAPP58S/Df(2L) ED1165* flies were highly significant ($P<0.001$, according to the non-parametric Mann-Whitney U test when comparing the 2 data sets). Flies were raised at 30°C.

8.2.4 Df(2L)ED1455 is a weak suppressor of DVAPP58S-induced eye phenotype

Another deficiency that qualitatively suppresses the ey-Gal4, UAS-DVAPP58S-induced degenerative eye phenotype is Df(2L)ED1455 that deletes a region that uncovers 193 genes (data not shown). Quantification of eye sizes showed that *ey-Gal4, UAS-DVAPP58S/Df(2L) ED1455* flies also have increased towards higher values (39% centred on 2500 aribitrary units squared) compared to *ey-Gal4, UAS-DVAPP58S/CyO-GFP* flies (60% centred between 1500 and 2000 arbitrary square units) (Figure 8.9). 29% of *ey-Gal4, UAS-DVAPP58S/Df(2L) ED1455* flies have eye sizes of 3000 arbitrary square units while 9% have between 3500 and 4000 arbitrary square units. The difference in frequency distribution between *ey-Gal4, UAS-DVAPP58S/Df(2L)ED1455* flies and *ey-Gal4, UAS-DVAPP58S/CyO-GFP* flies is statistically significant ($P<0.001$, Mann-Whitney U test).

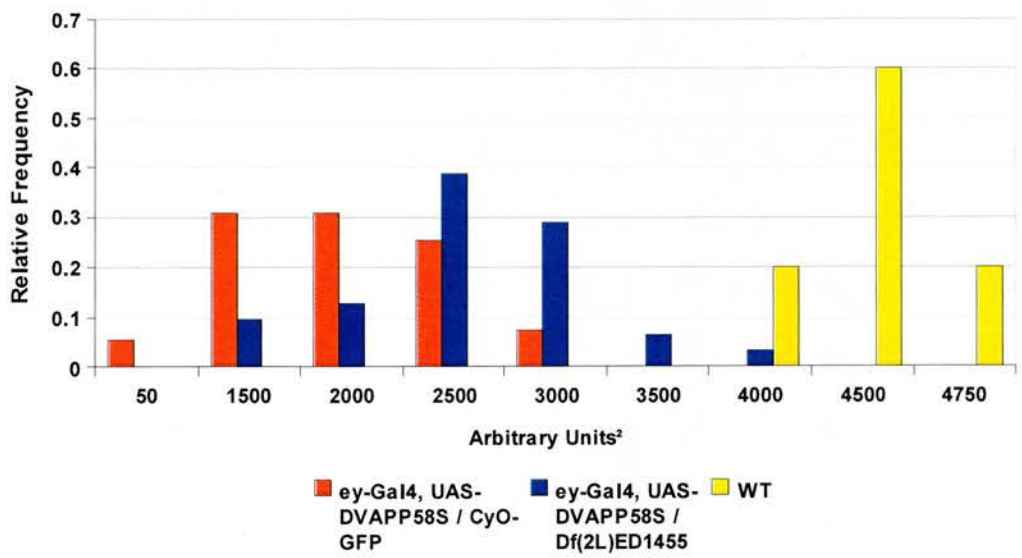

Figure 8.9. Df(2L)ED1455 weakly suppresses the DVAPP58S-induced eye phenotype.
ey-Gal4, UAS-DVAPP58S/CyO-GFP flies (red) have eye size areas centred between 1500 and 2000 arbitrary square units (N=61, S.D=654) compared to 39% of *ey-Gal4, UAS-DVAPP58S/Df(2L) ED1455* flies (blue) that is centred on 2500 arbitrary square units and 9% that are between 3500 and 4000 arbitrary square units (N=37, S.D=607) Differences between eye sizes of *ey-Gal4, UAS-DVAPP58S/CyO-GFP* flies and *ey-Gal4, UAS-DVAPP58S/Df(2L) ED1455* flies were highly significant ($P<0.001$, according to the non-parametric Mann-Whitney U test when comparing the two data sets). Flies were raised at 30°C.

8.2.5 Df(3L)ED4710, Df(3L)ED224 and Df(3L)ED225 suppress the reduction of the eye size phenotype due to DVAPP58S overexpression

The ey-Gal4, UAS-DVAPP58S-induced degenerative eye phenotype is also suppressed by three overlapping deficiencies located on the third chromosome, namely Df(3L)ED4710, Df(3L)ED224 and Df(3L)ED225 (Figure 8.10, red rectangle). These three deficiency lines delete 63, 19 and 24 genes respectively and partially one gene each. Df(3L)ED4710 and Df(3L)ED224 have 18 overlapping genes, Df(3L)ED224 and Df(3L)ED225 have 12 overlapping genes while Df(3L)ED4710 and Df(3L)ED225 have no overlapping regions at all (www.DrosDel.org.uk). Figure 8.11 shows the quantification of the suppressing effects of Df(3L)ED225. 74% of *ey-Gal4, UAS-DVAPP58S/+; Df(3L)ED225/+* flies (blue, Figure 8.11) have an eye area centred on between 3000 and 3500 arbitrary square units compared to 60% centred between 1500 and 2000 arbitrary square units seen in *ey-Gal4, UAS-DVAPP58S/CyO-GFP* flies (red, Figure 8.11). 10% of flies have eyes that are 4000 arbitrary units squared, which is wild type eye size (yellow, Figure 8.11).

The difference in frequency distribution between *ey-Gal4, UAS-DVAPP58S/ +; Df(3L)ED225/+* flies and *ey-Gal4, UAS-DVAPP58S/CyO-GFP* flies is statistically significant ($P<0.001$, Mann-Whitney U test). *ey-Gal4, UAS-DVAPP58S/+; Df(3L)ED4710/+* flies have the majority (84%) of eye size ranging between 3000 and 3500 arbitrary units squared that are of much higher values compared to *ey-Gal4, UAS-DVAPP58S/CyO-GFP* flies. The difference in distribution frequency is also statistically significant when comparing these two data sets (Mann-Whitney U test, data not shown). Hence, we can conclude from these data that the gene/genes responsible for the suppressing effects must lie in the overlapping region between Df(3L)ED4710 and Df(3L)ED224 and the overlapping region between Df(3L)ED224 and Df(3L)ED225.

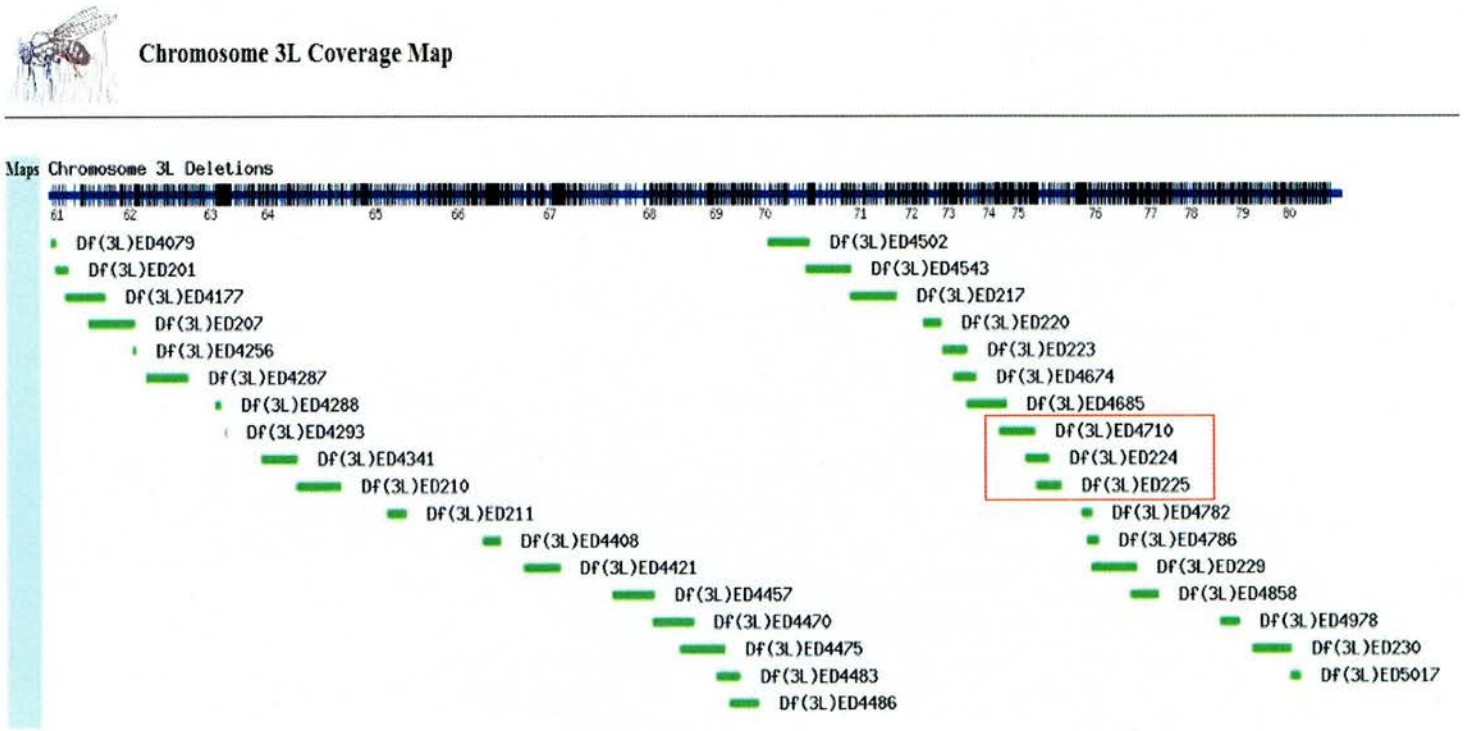

Figure 8.10. DrosDel deficiency kit coverage of the 3rd left hand chromosome of the *Drosophila* genome.
Red rectangular box highlights the three overlaping deficiency lines, Df(3L)ED4710, Df(3L)ED224 and Df(3L)ED225, that supresses the ey-gal4; UAS-DVAPP58S-induced degenerative eye phenotype.

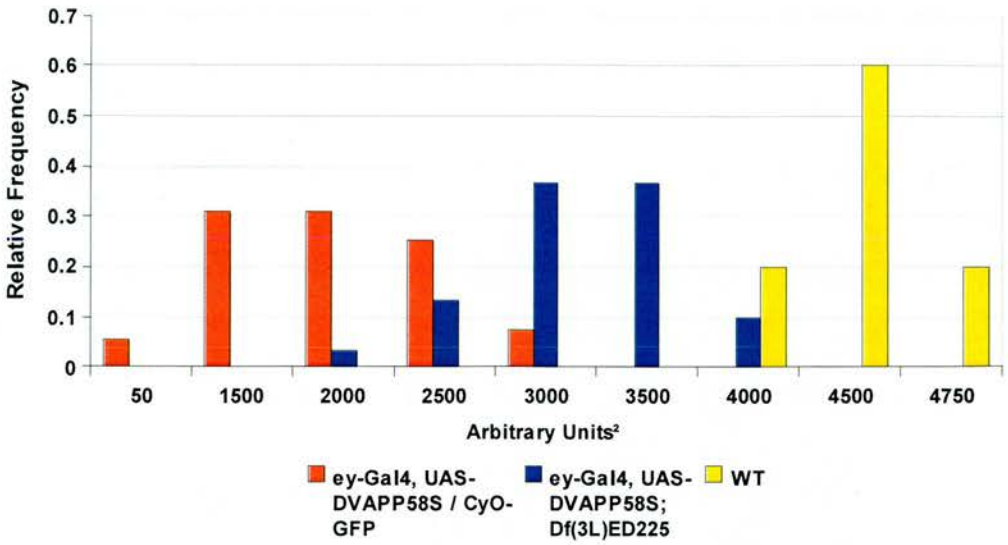

Figure 8.11. Df(3L)ED225 suppresses DVAPP58S-induced eye phenotype.
60% of *ey-Gal4, UAS-DVAPP58S/CyO-GFP* flies (red) have eye size areas centred between 1500 and 2000 arbitrary square units (N=61, S.D=654) compared to 74% of *ey-Gal4, UAS-DVAPP58S/+; Df(3L)ED225/+* flies (blue) that are centred between 3000 and 3500 arbitrary square units and 10% at 4000 arbitrary square units (N=36, S.D=378) that is towards wild type values (yellow, N=20, S.D=261). Differences between eye sizes of *ey-Gal4, UAS-DVAPP58S/CyO-GFP* flies and *ey-Gal4, UAS-DVAPP58S/+; Df(3L)ED225/+* flies were highly significant ($P<0.001$, according to the non-parametric Mann-Whitney U test when comparing the 2 data sets). Flies were raised at 30°C.

8.2.6. Mean area of eye sizes is also increased by suppressing deficiencies

As shown in the frequency distributions in Figures 8.6-8.9 and Figure 8.11, the respective deficiencies suppressed the DVAPP58S-induced eye phenotype by bringing the eye sizes towards wild-type values. Using the two sampled (unequal variances), two-tailed Student t-Test, statistics showed that the differences between the eye sizes in *ey-Gal4, UAS-DVAPP58S/CyO-GFP* flies and deficiencies-suppressed flies were significant. We also quantified the mean eye area and Figure 8.12 clearly shows that not only is the mean eye area of wild-type flies (WT, in grey) significantly higher than *ey-Gal4, UAS-DVAPP58S/CyO-GFP* flies (dark green), the mean eye areas of deficiency-suppressed flies (various colours, see legend) have significantly increased as compared to *ey-Gal4, UAS-DVAPP58S/CyO-GFP* flies.

This result supports the data reported in the frequency distributions and confirms that the deficiencies that has been uncovered in this screen truly exhibit modifying abilities.

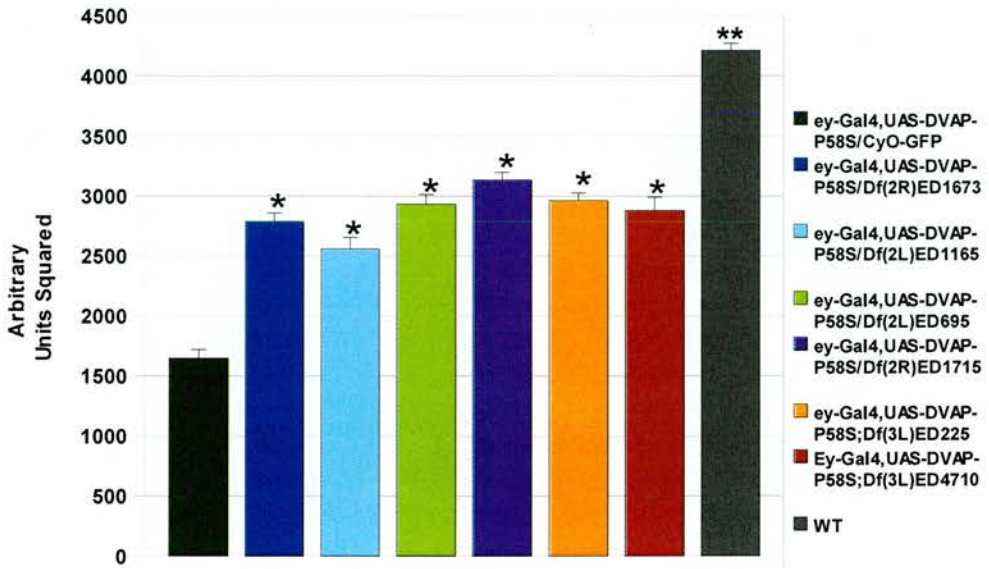

Figure 8.12. Suppressing deficiencies statistically increase average eye sizes compared to controls.

The average eye sizes seen in the suppression of the DVAPP58S-induced eye phenotype has increased compared to *ey-Gal4, UAS-DVAPP58S/CyO-GFP* control flies (dark green) when measured using the quantification software. The difference in average eye sizes is highly significant when comparing wild type flies (WT, grey) with *ey-Gal4, UAS-DVAPP58S/CyO-GFP* flies (dark green). Deficiencies that modify the degenerative eye phenotype is listed in the legend. '*' and '**' denote statistically significant changes when compared to *ey-Gal4, UAS-DVAPP58S/CyO-GFP* flies.

Chapter 9: Discussion

9.1 Levels of VAP proteins play an important role in synaptic homeostasis and in shaping postsynaptic glutamate receptor fields

VAPs are integral endoplasmic reticulum membrane proteins that are highly conserved and ubiquitously expressed in all eukaryotic organisms (Kagiwada *et al.*, 1998, Skehel *et al.*, 2000, Skehel *et al.*, 1995, Nishimura *et al.*, 1999). VAPs interact with a large number of intracellular proteins and have been implicated in the regulation of a variety of cellular functions such as membrane trafficking (Skehel *et al.* 1995, Soussan *et al.*, 1999), microtubule organization (Skehel *et al.*, 2000, Pennetta *et al.*, 2002), unfolded protein response (UPR) (Brickner and Walter, 2004, Kanekura *et al.*, 2006), lipid transport and metabolism (Kagiwada and Zen, 2003, Kawano *et al.*, 2006).

Although the most established function of VAPs is the regulation of lipid transport and metabolism, The role of VAPs in vesicular trafficking (Foster *et al.*, 2000; Skehel *et al.*, 1995) has been the most debated. In *Aplysia*, VAP-33 is a cell membrane protein that interacts with the vesicle-associated protein VAMP/synaptobrevin and is required for the exocytosis of neurotransmitter at the synapse (Skehel *et al.*, 1995). However, conflicting reports by others suggest a somewhat different role for VAP-33 at the synapse. Firstly, in *Drosophila,* mutations in proteins controlling neurotransmitter release such as synaptotagmin, cysteine string protein, synaptobrevin and syntaxin1A drastically affect evoked muscle depolarization (Littleton *et al.*, 1993; Schulze *et al.*, 1995; Zinsmaier *et al.*, 1994; Deitcher *et al.*, 1998). By contrast, our electrophysiological analysis shows that the complete removal of DVAP-33A has no effect on calcium-evoked release of neurotransmitter. Secondly, the interaction between VAP-33 and the v-SNARE protein VAMP has not been reported in any other system including yeast (Gavin *et al.*, 2002), *Drosophila* (Giot *et al.*, 2003), rat (Soussan *et al.*, 1999) and humans (Wyles *et al.*, 2002). Thirdly, VAP-33 has been shown to "promiscuously" interact *in vitro* with both v- and t-SNAREs (Weir *et al.*, 2001) clearly questioning the *in vivo* relevance of these data. Fourthly, at the *Drosophila* NMJs VAP-33 localizes to the

periactive zones where proteins required for synaptic growth are clustered. Conversely, proteins involved in the release of neurotransmitter are expected to segregate at the active zones (Pennetta *et al.*, 2002).

In *Drosophila*, *DVAP-33A, Farinelli* and CG33523 have significant homology with *VAPB.* One of the three genes encoding VAP, DVAP-33A has been found to be the only homologue of hVAPB because DVAP-33A has the highest similarity to VAPB. Farinelli is exclusively expressed in the testes and fat body while CG33523 has a CRAL-Trio domain that is not found in classical VAPs. DVAP-33A has been shown to regulate the budding of synaptic boutons at the larval neuromuscular junction in a dosage dependent manner and is required for structural remodelling of synapses where it controls microtubule cytoskeleton dynamics. The DVAP-33A dependent process of synapse formation has been proposed to be similar to the budding of yeast (Pennetta *et al.*, 2002).

hVAPB has been shown to be the causative gene of late-onset autosomal dominant forms of motor neuron disorders, including typical and atypical ALS and late-onset spinal muscular atrophy (Nishimura *et al.*, 2004a, Nishimura *et al.*, 2004b). The pathogenic mutation predicts a substitution of a Serine for a conserved Proline (P56S). We decided to use *Drosophila* as a model system to study the role of hVAPB in ALS.

One of the hallmarks associated with the loss-of-function and neuronal overexpression of *DVAP*-33A is decreased and increased bouton formation at the NMJ, respectively. Despite this structural alteration, synaptic transmission is maintained within a wt range. At the mechanistic level, muscles respond to a decreased number of boutons and quantal content by upregulating quantal size; conversely muscles compensate an increase in number of boutons and quantal content by downregulating quantal size. Quantal size is the response of a muscle to the spontaneous release of a single synaptic vesicle and it is thought to be determined, in large part, by the properties of transmitter receptors. At the

Drosophila NMJ, there are two classes of glutamate receptors: 1) receptors containing the subunit IIA together with IID, III and IIE subunits; 2) receptors containing the subunits IID, III and IIE associated with the subunit IIB (Schuster *et al.*, 1991; Petersen *et al.*, 1997; DiAntonio *et al.*, 1999; Marrus *et al.*, 2004; Qin *et al.*, 2005; Featherstone *et al.*, 2005)

We found that the increase in quantal size in DVAP-33A loss-of-function mutations is associated with an increase in the number and cluster volume for the subunit IIA, while cluster size for subunits III and IIB is decreased. No significant changes in cluster size for subunit IID were found. Interestingly, it has been reported that subtype IIB and subtype IIA receptors have different functional properties: IIB channels desensitize almost ten times faster than IIA channels and the time constant for the decay of the synaptic event is much faster (DiAntonio *et al.*, 1999; Davis *et al.*, 1998; Pawlu *et al.*, 2004). In agreement with our data, overexpression of the IIA subunit has been shown to induce an increase in both quantal size and receptor channel open times (Petersen *et al.*, 1997, Marrus *et al.*, 2004).

Conversely, neuronal overexpression of VAP proteins causes a decrease in quantal size that is accompanied by a decrease in the postsynaptic level of the receptor subunit IIA and a reduction in the mean volume of the receptor field. Interestingly, mutants in the receptor subunit IIA display a reduced receptor channel open time and a smaller quantal size (DiAntonio *et al.*, 1999; Petersen *et al.*, 1997). These data indicate that VAP proteins may be part of a trans- synaptic mechanism that ensures synaptic efficacy by coordinating structural remodelling of the synapse and postsynaptic sensitivity to neurotransmitter.

From the genetic point of view, opposite phenotypes in the loss of function and overexpression implies regulatory function of the gene in the process it controls (Greenspan, R.J., 2004). On the other hand, since it has been shown that there is a dosage dependent effect of DVAP-33A on synaptic sprouting (Pennetta *et al.*, 2002), and the fact that synaptic homeostasis still occurs in DVAP-33A loss of function

mutants, indicates that DVAP-33A is not required for homeostasis. Our best working hypothesis is that DVAP-33A dosage could function as a sensor of synaptic surface area that could trigger homeostatic regulation of synaptic efficacy.

Previous work has shown that in mild glutamate receptor mutants, a homeostatic increase in neurotransmitter release compensate for the reduction in quantal size and the evoked response is maintained within normal values. (DiAntonio *et al.*, 1999; Petersen *et al.*, 1997). However, in conditions when receptors become limited such as in the case of mutants for subunit III, it has been proposed that homeostatic mechanisms are insufficient to normalize evoked release and a marked deficit in synaptic function is observed (DiAntonio, 2006). The reduction in quantal size observed in larvae overexpressing hVAPB and mutants overexpressing hVAPBP56S is similar to that reported in strong mutations for the subunit III (Marrus and DiAntonio, 2004). As predicted, we also observe a breakdown of the homeostatic mechanism when overexpressing hVAPP56S, the evoked response exhibit a 50% decrease while in the case of hVAPB, a near normal postsynaptic response was observed. Interestingly, decrease in quantal size has also been reported in muscle biopsies of ALS patients (Maselli *et al.*, 1993).

While these data clearly indicate that changes in the expression levels of VAP proteins have a critical role in shaping the post-synaptic glutamate receptor field and the abundance of specific subunits, the mechanism by which this phenomenon occurs remains elusive. However, studies on MSP have provided intriguing insights into how this trans-synaptic mechanism might occur. MSP, also found to have high homology to the N-terminal domain of VAP, has been shown to control ephrin/Eph receptor pathway in *C. elegans* (Miller *et al.*, 2003). MSP is a 14kD protein that is highly abundant in nematode sperm and controls the movement of the sperm by regulating the assembly and disassembly of filaments composed of MSP (Roberts and Stewart, 1995).

MSP is also a signalling molecule for oocyte maturation and ovarian sheath

cell contractions in *C.elegans* by its secretion into the reproductive tract from the sperm cytosol and binds to Eph receptors on oocyte and sheath cell surfaces (Miller *et al.*, 2003). Eph receptors and ephrins have been implicated in multiple aspects of synaptic function, including clustering and modulation of glutamate receptors (Yamaguchi and Pasquale, 2004). In addition, Ephrin/Eph receptors are also involved in synaptic plasticity, cytoskeletal remodelling and axonal pathfinding (Birgbauer *et al.*, 2001, Henderson *et al.*, 2001, Shamah *et al.*, 2001). Interestingly, Tsuda and colleagues reported that the MSP domain of DVAP-33A is cleaved and secreted. More significantly, both the MSP domain of hVAPB and DVAP-33A genetically interacts with Eph receptors in *C.elegans.* The pathogenic protein on the other hand, is not cleaved or secreted and is trapped in ER aggregates, suggesting a disruption of the potential activity of the secreted fragment by the pathogenic mutation. However, the cleavage and secretion of VAPB might be tissue specific as not all cell types in *Drosophila* are capable of secreting cleaved VAPB, moreover, the cleavage and secretion of VAPB was tested only in cell culture system and the wing imaginal discs. The authors extrapolated this data and proposed that both defects may contribute to produce features of ALS8 pathology (Tsuda *et al.*, 2008). Nonetheless, the authors failed to show that such a mechanism actually operates in the NMJ or nervous system, the tissues that are mostly affected by ALS.

9.2 hVAPB and DVAP-33A are functionally interchangeable at the NMJ

We showed that hVAPB and DVAP-33A are not just structural homologues but they are in fact functional homologues as the expression of hVAPB in neurons rescues the lethality, morphological and electrophysiological phenotypes associated with *DVAP-33A* loss of function mutations. Moreover, the overexpression of hVAPB phenocopies the phenotype of DVAP-33A overexpression at the morphological and electrophysiological level: overexpression of hVAPB and DVAP-33A causes an increase in the number of synaptic boutons and a consequential decrease in bouton sizes when compared to controls while accompanied by a decrease in quantal sizes in

these synapses. These results show that hVAPB and DVAP-33A perform homologous functions at the synapse and as a consequence, information gained from the study of DVAP-33A will also be relevant to the function of hVAPB.

In order to gain insight into the mechanism of the human disease, we asked whether the pathogenic mutation is a gain- or a loss-of-function mutation. The data presented here show that the pathogenic protein carrying the P56S mutation and the corresponding *Drosophila* P58S mutant protein were able to rescue the lethality, morphological and electrophysiological phenotypes associated with *DVAP-33A* loss of function mutations. This points toward two possibilities: the mutation is irrelevant to the pathogenesis of ALS8 or the mutant allele has a pathogenic effect while retaining certain functional properties of the wild type protein.

The second hypothesis is very much plausible for several reasons. Firstly, the P56S mutation has been reported to be causative for an inherited form of MNDs in humans. This mutation affects nine related families totalling 1500 individuals of which 200 suffer from motor neuron disorders (Nishimura *et al.*, 2005; also refer to appendix). Second, many of the phenotypes associated with the overexpression of human or *Drosophila* wild type protein are similar to those due to the overexpression of the pathogenic proteins. The main difference is that the pathogenic mutation causes a more severe phenotype than the one generated by the overexpression of the corresponding wt protein, when transgenic lines expressing comparable amounts of protein were compared. Third, a genetic model for ALS has been generated where the expression of the mutant VAP recapitulates major hallmarks of the human disease such as locomotion defect, neuronal cell death and aggregate formation, clearly indicating that the mutation has a pathogenic effect. Fourth, both the *Drosophila* and the human mutant proteins retain some functional wild type properties such as the ability to self-oligomerize (K. Parry and G. Pennetta; Kanekura *et al.*, 2006). However, neuronal expression of the pathogenic protein in the presence of wt DVAP-33A depletes the wild type protein from its normal localization at the NMJ and induces aggregate formation. These effects are not observed when the wild type

protein is overexpressed. Moreover, this depletion of the endogenous DVAP-33A in transgenic expression of pathogenic DVAP-33A produces a morphological phenotype that is similar to the loss of function morphological phenotype of DVAP-33A at the NMJ, suggesting a dominant negative effect. Indeed, several other groups have proposed a dominant negative effect for the Proline to Serine substitution in VAP (Kanekura *et al.*, 2006; Teuling *et al.*, 2007; Ratnaparkhi *et al.*, 2008). Despite this, the depletion of endogenous DVAP-33A from its normal localization cannot be the principal mechanism of the disease as DVAP-33A loss of function mutants do not develop ALS suggesting that the mutant protein has acquired an abnormal, new toxic property.

9.3 A genetic model for ALS in *Drosophila* that recapitulates major hallmarks of the disease

One of the most common features of ALS and nearly all neurodegenerative diseases is the accumulation of aggregates that are intensively immunoreactive to disease-related proteins (Bruijn *et al.*, 2004). Each disease, however, differs with respect to the anatomical location and morphology of the aggregates. The major component of the aggregates is usually the protein encoded by the gene mutated in the familial forms, which is also unique to each disease. Despite this diversity, a bulk of circumstantial evidence support the hypothesis that aggregates are typical hallmarks of neurodegenerative diseases and have a toxic effect on neurons (Caughey and Lansbury, 2003). While no autopsy material is available for familial cases with the P56S mutation, SOD1-positive inclusions have been reported in human sporadic and familial ALS cases as well as in SOD1 mouse models (Bruijn *et al.*, 1998, Shaw *et al.*, 2008). We found the presence of aggregates that are intensively immuno-reactive for DVAP-33A both in neuronal cell bodies and in nerve fibers of our ALS model. Interestingly, human and *Drosophila* VAPB carrying the pathogenic mutation have also been shown to undergo intracellular aggregation when expressed in cell culture systems (Kanekura *et al.*, 2006, Teuling *et al.*, 2007) and in fly models (Tsuda *et al.*, 2008; Ratnaparkhi *et al.*, 2008). However, similarities between human disease and

our fly model are not limited to aggregate formation as flies expressing transgenic VAP proteins carrying the ALS8 mutation, exhibit other hallmarks of the human disease such as neuronal cell death, muscle wasting and defective locomotion behaviour (Mulder *et al.*, 1986).

It remains to be established whether the VAP protein in the aggregates in our fly model of ALS represents the mutant protein, the endogenous protein or a mixture of both, however, we observe a regional decrease in the level of the endogenous DVAP protein. The DVAP-33A protein that is normally associated with the plasma membrane in neuronal cell bodies and at the neuromuscular synapses is nearly undetectable in *DVAPP58S* transgenic animals. As a result of this decrease in synaptic levels of the endogenous protein, a decrease in the number of boutons is observed (Chai *et al.*, 2008; Ratnaparkhi *et al.*, 2008; Tsuda *et al.*, 2008). It was previously shown that DVAP-33A regulates bouton formation at the synapse in a dosage-dependent manner (Pennetta *et al.*, 2002). Despite these structural alterations, a homeostatic mechanism is established to maintain synaptic efficacy within functional boundaries. We speculate that the depletion of the endogenous protein from its normal localization and the formation of aggregates would affect the homeostatic mechanism linking structural remodelling and synaptic efficacy controlled by DVAP-33A. Although not directly tested in our model, experiments in cell culture and yeast studies show that overexpression of mutant VAPB induces formation of aggregates in which the endogenous wild type protein is recruited (Kanekura *et al.*, 2006; Teuling *et al.*, 2007; Suzuki *et al.*, 2009). This would suggest that the pathogenic allele functions as a dominant negative. Indeed, other groups have also proposed that the P56S mutation causes ALS8 through a dominant-negative mechanism (Kanekura *et al.*, 2006; Teuling *et al.*, 2007; Tsuda *et al.*, 2008; Ratnaparkhi *et al.*, 2008).

Similar to what has been proposed for other neurodegenerative diseases, the formation of aggregates may directly interfere with critical cellular processes and /or compromise the ability of the system to keep up with the degradation of aggregated

proteins (Petrucelli *et al.*, 2004; Zeng *et al.*, 2004; Venkatraman *et al.*, 2004; Bence *et al.*, 2001). We have also observed that Hsp70, a major stress-induced molecular chaperone in flies, is upregulated and closely associated with aggregates in larval brains transgenic for the P58S protein while in controls, a faint and diffuse cytoplasmic staining is observed (data not shown). Aggregates associated with neurodegenerative diseases are immunoreactive for various molecular chaperones and for components of the protein quality control machinery, including the ubiquitin/proteosome complex and the lysosome-mediated autophagy system. These data have suggested that cells recognize aggregated disease proteins as abnormal and that recruitment of chaperones and components of protein clearance systems to inclusions, may serve to refold, disaggregate and/or degrade the mutant proteins (Chan *et al.*, 2002; Taylor *et al.*, 2002). On the other hand, it has also been suggested that aggregates might be harmful to cells by sequestering away proteosomes, molecular chaperones and transcription factors that are normally essential for cell viability (Taylor *et al.*, 2003; Zhou *et al.*, 2003).

Despite major efforts in research, is still not clear what contributes to the degeneration of synapses in neurodegenerative diseases. However, studies in animal models have supported the role of synaptic dysfunction in nerodegenerative disease pathogenesis. In several animal models for motor neuron diseases (Frey *et al.*, 2000; Pinter *et al.*, 1997) as well as in patients affected by ALS (Maselli *et al.*, 1993), synaptic deficits are detected since the very early stages of the disease and exacerbation of these lesions correlates with time and speed of disease progression (Dengler *et al.*, 1990). Maintaining synaptic function is dependent on the precise regulation of neural excitability and neurons have the capacity to respond to perturbations such as inappropriate synaptic function or altered innervation to maintain their function within a normal physiological range. (Davis and Goodman, 1998). The significance of synaptic homeostasis to appropriate neural function suggests that there are links to neural disease. Strikingly, mutant proteins that are implicated in causing neurodegenerative disorders impair the integrity or function of presynaptic terminals and postsynaptic specializations (Walsh and Selkoe, 2004;

Palop *et al.*, 2006). For instance, disruption of synaptic transmission (Chee *et al.*, 2005), synaptic toxicity (Yoshiyama *et al.*, 2007) and delocalization of PSD-95 (postsynaptic density-95), a key postsynaptic scaffolding protein (Almeida *et al.*, 2005; Gylys *et al.*, 2004; Roselli *et al.*, 2005; Zhang *et al.*, 2007) are reported in AD mouse model and patients, and an animal model of tauopathy. In addition, α-synuclein genetically interacts with cysteine-string protein-α (CSPα), a protein important in facilitating the folding and refolding of synaptic SNARE proteins critical for neurotransmitter release, vesicle-recycling and synaptic integrity (Chandra *et al.*, 2005).

Defects in retrograde signalling can also contribute to a breakdown of synaptic homeostasis and function. Bone morphogenetic protein (BMP) signalling has been implicated in the potential mechanism of pathogenesis of hereditary spastic paraplegia (Wang *et al.*, 2007). BMP signalling regulates synaptic growth, function and stabilization at the *Drosophila larval* NMJ by postsynaptic retrograde signalling (McCabe *et al.*, 2004), and is involved in the maintenance of microtubules and axonal transport (Wang *et al.*, 2007). Interestingly, pathogenic DVAP-33A has been reported to interfere with BMP signalling pathways at the NMJ (Ratnaparkhi *et al.*, 2008). These observations demonstrate that proteins normally required for synaptic function and signalling mutated in neurodegenerative diseases could play a major part in the degenerative process.

9.4 Modelling VAP-induced ALS in the *Drosophila* adult eye facilitates enhancer/suppressor screens

The molecular mediators and cellular events that contribute to the pathogenesis of most human neurodegenerative diseases are still poorly understood. Studying these diseases in model organisms enables one to exploit powerful genetic analysis to dissect such disease processes. Genome wide screens that have been performed in recent years looking at interactors of a pathological phenotype have successfully

identified genes that are involved in RNA processing, transcriptional regulation, phosphorylation, molecular chaperones and components of protein clearance system as potent suppressors of neurotoxicity in several fly models of neurodegenerative diseases (Fernandez-Funez, 2000; Kazemi-Esfarjani and Benzer, 2000, Shulman and Feany, 2003; Mutsuddi *et al.*, 2004). These enhancer/suppressor screens have been conducted exclusively using the adult *Drosophila* eye as a read-out as it is an experimentally-tractable structure in which to model human neurodegenerative diseases in flies.

Since the patho-mechanism of ALS has not yet been established, we tested the possibility of modelling ALS8 in the adult fly eye with the intention of conducting a genome-wide screen for interactors of DVAP-33A. In order to carry out the modifier screen, we first searched for a suitable eye-specific driver that does not exhibit non-specific eye defects on its own as *GMR-Gal4* does. Although *GMR-Gal4* has been extensively used in disease models and modifier screens, we believe that finding a more suitable eye-specific driver to substitute *GMR-Gal4* would avoid the problem of identifying enhancer or suppressors of *GMR-Gal4* instead of true interactors of DVAP-33A.

By exploring the usage of other eye-specific drivers, we were able to show that the expression of the DVAPP58S transgene in the adult eye using the *eyeless-Gal4* driver exhibit a rough phenotype with a reduction in size, extra bristles and fused ommatidia. As observed in the larval NMJ, we also found that cell degeneration in the eye is due to apoptosis: overexpression of DIAP-1, a gene inhibiting apoptosis in flies partially suppresses the mutant eye phenotype. This partial rescue could be explained by the short in vivo half-life (about 30 minutes) of DIAP1 protein (Kuranaga *et al.*, 2006) while another explanation would be that other mechanisms such as necrosis or autophagy could play a part in the degenerative phenotype. These data are consistent with the conclusion that a degree of cell death is occurring in the eye expressing the pathogenic protein. As previously described for the nervous system of third instar larvae, we also observe in the eye the formation of

microscopically visible aggregates.

The similarity between the phenotypes in the adult *Drosophila* eye and in the larval NMJ indicate that these two systems can be used interchangeably to model key aspects of VAP-induced ALS in *Drosophila*. Although eye phenotypes are useful tools to rapidly identify genetic modifiers of a particular gene, retinal degeneration is not a characteristic feature of ALS. A more effective strategy is to first identify genes that modulate VAP-induced toxicity in the adult eye and, subsequently, validate the modifying activity of these interactors in other tissues that are more characteristically affected in ALS patients such as the larval NMJ and motor systems including locomotion behaviour.

Our model of ALS is highly and potentially more powerful than other models for neurodegenerative diseases in flies. This is strengthened by the fact that human VAPB rescues the phenotype associated with the loss of function of the *Drosophila* protein. This means that whatever that is learnt about the wt protein in flies can be related to the human protein. Most of the other neurodegenerative disease models rely on the strong overexpression of a heterologous human protein (Fernandez-Funez *et al.*, 2000; Warrick *et al.*, 1998; Jackson *et al*; 1998; Feany and Bender; 2000; Wittmann *et al.*, 2001; Jackson *et al.*, 2002). Especially in the case of the Parkinson's disease model where α-synuclein has no real homologue in flies (Feany and Bender, 2000), the neurotoxicity phenotypes observed in these fly models might result from the heterologous expression of human diseased proteins. Despite this, it has been shown that toxicity of SCA3 (caused by expanded polyglutamine repeats of Ataxin 3) can be modulated by normal activity of Ataxin 2, whose expanded polyglutamine repeats causes SCA2 (Lessing *et al.*, 2008). Al-Ramahi and colleagues have also shown previously that wild type *Drosophila* Ataxin 2 modifies human expanded Ataxin 1-induced degeneration. These two studies utilizing the human pathogenic protein of Ataxin 1 and Ataxin 3 showed a functional link and revealed commonalities between neurodegenerative disorders with common clinical features but different etiology. We are therefore even more confident that using our model of

VAP-induced ALS in the eye would potentially uncover novel and interesting genes that are involved in ALS pathogenesis.

9.5 A genome-wide deficiency screen to search for genetic interactors of *DVAP-33A*

In *Drosophila*, genetic screens have been particularly invaluable in identifying the missing components of a pathway. Loss of function mutations in most genes are recessive, which indicates that 50% of the protein is sufficient to ensure an almost normal function. When a particular pathway is partially disrupted by an existing mutation, this amount might no longer suffice and mutations in the genes that are involved in the pathway can therefore be identified as dominant enhancers or suppressor in a sensitized genetic background (St. Johnston, D., 2002).

We carried out a small pilot screen to test whether our *Drosophila* eye model is sensitive enough to detect modifiers. As deficiencies are equivalent to null mutations in the genes that are deleted, a rapid way to scan the genome for potential target genes in enhancer and suppressor screens is to look for dominant effects in heterozygote deficiencies. We embarked on a quick survey of the genome using deficiencies and information gained from any interacting regions in this pilot screen would be used as a starting point for a high resolution misexpression screen. Flies that carry both the *eyeless-Gal4* driver and the UAS-DVAPP58S transgene in the presence of the wild-type protein were generated by meiotic recombination. This *ey-Gal4/UAS-DVAPP58S* fly stock was used in a F1 screen deficiency screen to look for genetic modifiers of DVAP-33A.

The DrosDel Collection was used to identify enhancers and suppressors of the eye degenerative phenotype. Out of deficiencies screened so far, we identified 14 suppressors and 3 enhancers of the DVAPP58S induced degenerative eye phenotype and the remaining deficiencies on the third chromosome are subjected to ongoing analysis. Three overlapping deletions on the X chromosome are strong suppressors of the degenerative eye phenotype. This suggests that the same gene is removed by

the three deficiencies and that the gene responsible for the suppression should be found in the overlapping region between the three deficiencies. This smallest overlapping deletion also contains the *bangles and beads* gene. *Bangles and beads (Bnb)* represents, at the moment, our best suppressor candidate gene, as it has been shown to be a physical interactor of DVAP-33A by a yeast two hybrid screen (K. Parry and G. Pennetta). Bnb is closely related to mammalian GAP-43 protein (Ng *et al.*, 1989), a neuronal growth associated protein that affects filopodial extension and branching, axonal pathfinding, and synaptic plasticity (Benowitz and Routtenberg, 1997). GAP-43 is enriched in the membranes of growth cones during development and axonal regeneration. It is phosphorylated after long-term potentiation, implicating GAP-43 in learning and memory and a loss of GAP-43 results in axonal pathfinding defects (Benowitz & Routtenberg, 1997, Strittmatter *et al.*, 1995). This proves extremely interesting as the loss of DVAP-33A also affects synaptic branching at the larval NMJ (Pennetta *et al.*, 2002) and axonal pathfinding defects at the adult mushroom bodies (data not shown and Tsuda *et al.*, 2008).

We have also found seven deficiencies on the second chromosome and four deficiencies on the first half of the left third chromosome acting as suppressors of the VAP-induced neurotoxicity in the eye. Df(2L)ED700 the smallest deficiency that suppresses the eye phenotype has six genes deleted and one gene deleted partially. This finding is rather significant as three out of the seven genes uncovered by this deletion, together with *DVAP-33A*, code for proteins found in lipid droplet fractions of *Drosophila* embryos. Lipid droplets are ubiquitous organelles that are storage sites for energy, sterols, and precursors of membrane phospholipids with central roles in cholesterol homeostasis and lipid metabolism. It has been shown by mass spectrometry of purified lipid droplets of *Drosophila* embryos that DVAP-33A (CG5014), sop (CG5920) and CG5885 proteins are represented significantly in lipid-droplet fractions while yip2 (CG4600) is represented abundantly (Cermelli *et al.*, 2006). It is appealing to hypothesize about the connection between VAP, lipid metabolism and cholesterol homeostasis, considering the fact that VAP and its interactors such as CERT and OSBP have been implicated in regulating lipid

metabolism and homeostasis. Recent studies in the field of ALS have revealed that dyslipidemia extends survival of ALS patients (Depuis *et al.*, 2008). Consistently, increasing the lipid content in the diet of ALS animal models that exhibit reduced adiposity and increased rates of energy expenditure offers neuroprotection and extends survival in these animals (Depuis *et al.*, 2004).

Transgenic expression of DVAPP58S using the *ey-Gal4* driver induces a heterogeneous rough eye phenotype and reduction in eye sizes. Such variability in eye phenotypes is not uncommon as *GMR-Gal4* driven expression of human SCA8 protein also causes variability in rough eye phenotypes (Mutsuddi *et al.*, 2004). Due to the heterogeneous nature of the eye sizes seen in DVAPP58S-induced eye phenotype, software for quantifying the area and circumference of the region of the image occupied by the eye was also developed with the help of an informatics collaborator to better quantify the suppressing or enhancing effects of modifiers on the degenerative eye phenotype. This software, developed by James Withers was written using MATLAB (Mathworks Inc.) allows tracing of the eye border with calculation of its area and circumference. It allows a more flexible and accurate way of tracing the eye than the commonly used ImageJ software because it eliminates operator error as tracing the border of the eye depends very much on the skill of the operator using free-hand tool in ImageJ. Operator bias is also reduced with our quantification software because it has the ability to segment the tracing of eye boundaries by introducing more control points (in this case, pixel by pixel). The operator in this case decides at every control point where the border of the eye and head is. We were able to use this software to quantify some of the deficiencies that showed suppressing effects on the degenerative eye phenotype and confirmed our initial findings using a purely qualitative method of screening. Of all the deficiencies that showed modifying activity, we were able to confirm that the increase in eye sizes were statistically significant and are in the midst of identifying the gene responsible for the suppression.

Although deficiency screens provide a quick and easy means of screening the

genome for interacting regions, it is however, difficult to pinpoint the actual modifying gene using P-element insertions because many of these insertions are not associated with a phenotype and does not disrupt the gene it is associated with. In many cases, imprecise P-element excision is needed to generate new mutant alleles (Venken and Bellen, 2005). We attempted to identify the genes responsible for the suppression effect by crossing the transgenic line expressing the pathogenic protein with P-element insertion lines for the genes deleted in the deficiency and as expected, found that the P-element insertion lines used did not suppress the degenerative eye phenotype. This could also be due to several other factors: firstly, the suppression could be allele specific; secondly, there might be a need to remove two or more genes to be able to observe a suppression, especially in the case of large deletions; thirdly, the P-element insertions that were tested either do not disrupt the genes they are associated with or possibly the position of the P-element insertions may not have caused a sufficient reduction in the amount of proteins to cause a suppression. Of all the P-element insertions tested thus far, only two were lethal insertions. This suggest that although the P-element is present, the insertion might not be affecting the gene it is associated with.

One way to overcome these problems is to utilise more specific alleles if available or overexpressing the candidate genes to observe an opposite phenotype (an enhancement in these cases). We also plan to hone in on the gene responsible for the suppression or enhancement by utilizing the Exelixis Collection where the average deletion is 140kb. The Exelixis Collection can also be used to fill up the gaps in the DrosDel Collection with deletions present in the Exelixis Collections. In this first screen, because we chose the most severe eye degenerative phenotype, we may have selected for particularly strong suppressors. A milder phenotype can be selected as the phenotype is dependent on the expression levels of the mutant transgene.

Despite the problem of identifying the gene responsible for the modifying effects of the degenerative eye phenotype, the deficiency screen is progressing by searching for interacting deficiencies on the third chromosome. This is because the

deficiency screen has proven that the degenerative eye phenotype is modifiable and we have so far identified 14 suppressors and 3 enhancers with this approach. This provides a crucial proof of principal for a broader misexpresssion screen of single gene mutations and that interacting deficiencies uncovered by this current screen will be used as early candidates for a high resolution misexpression screen that is being planned in the lab.

Perspectives

Following the publication of our fly model of VAP-induced ALS, two other groups subsequently published their fly models of ALS8 (Chai *et al.*, 2008; Ratnaparkhi *et al.*, 2008; Tsuda *et al.*, 2008). Both groups have independently suggest that pathogenic VAPB functions as a dominant negative brought about by aggregation of VAP and recruitment of wild type VAP. Tsuda and colleagues also showed that the MSP domain of VAP is cleaved and secreted and further proposed that the trapping of wild type VAP by pathogenic protein aggregates and the initiation of the UPR cause a reduced secretion of cleaved VAPB may contribute to produce features of ALS8 pathology. These reports reinforce the idea that *Drosophila* models of ALS are crucial in dissecting the molecular mechanisms of ALS pathogenesis.

The value of *Drosophila* as a model of neurodegenerative disorders is its capacity to provide a platform for unbiased genetic screens aimed at identifying molecular components of a pathological pathway. The generation of *Drosophila* models of ALS has taken some time compared to other neurodegenerative disease models such as polyglutamine diseases, Parkinson's, Alzheimer's and tauopathies (Warrick *et al.*, 1998; Jackson *et al.*, 1998; Struhl & Greenwald, 1999; Feany & Bender, 2000; Fernandez-Funez *et al.*, 2000; Wittmann *et al.*, 2001; Jackson *et al.*, 2002; Guo *et al.*, 2003; Iijima *et al.*, 2004; Mutsuddi *et al.*, 2004). This disadvantage of generating an ALS fly model only recently means that our understanding of molecular mechanisms involved in ALS pathogenesis is still in its "infancy" compared to other neurodegenerative diseases. On the other hand, genome-wide screens looking at interactors of a pathological phenotype have identified, among others, molecular chaperones and components of the protein clearance systems as potent suppressors of neurotoxicity in several fly models of neurodegenerative diseases (Kazemi-Esfarjani and Benzer, 2000; Auluck *et al.*, 2002; Auluck and Bonini, 2002; Chan *et al.*, 2000; Warrick *et al.*, 1999) suggesting commonalities between what have been traditionally thought as distinct diseases based on syndromic classifications of neurodegenerative disorders. Since a role for these

pathways in mitigating neurotoxicity in VAP-induced ALS is largely unexplored, we can exploit the genetic and pharmacological tools that have been generated from these previous modifier screens.

Even though the genome-wide F1 deficiency screen identified several interacting regions, narrowing down to the modifying gene proves to be extremely challenging. This is because the genes uncovered by the deficiencies might not be disrupted by P-element insertions and therefore generation of new mutant alleles due to imprecise excision of the P-elements might be necessary to create a real mutation. A more direct approach would be conducting a misexpression screen that is designed to select modifiers that affect toxicity upon upregulation. A P-element based misexpression screen would be a better means for screening due to the fact that the modifier gene can be directly identified as information on the P-element insertions and which gene it affects is readily available on Flybase. This approach has been very successfully applied to *Drosophila* models of polyglutamine-repeat disorders (Fernandez-Funez *et al.*, 2000; Bilen and Bonini, 2007; Kazemi-Esfarjani and Benzer, 2000) and tauopathies (Shulman and Feany, 2003; Blard *et al.*, 2007) where a large number of interesting genes have been identified.

Genetic screens carried out in *Drosophila* models of neurodegenerative diseases have so far been using a collection of 2,276 p(EP) lines and have mainly identified chaperones and components of the protein clearance systems as major determinants in the pathogenesis (Fernandez-Funez *et al.*, 2000; Bilen and Bonini, 2007; Kazemi-Esfarjani and Benzer, 2000; Shulman and Feany, 2003; Blard *et al.*, 2007). These findings clearly suggest that commonalities exist among different neurodegenerative diseases. However, one caveat of using the EP collection is the screen can never be saturated because of hotspots for P-element insertions and it is also possible that the 2,276 p(EP) lines contain a high degree of redundancy. Thus, it is very likely that screening the same collection with another disease model will continue to "spot" the same genes.

We plan to utilize a set of 5,183 lines with the potential of misexpressing a neighbouring gene that has been assembled by the Bloomington Stock Centre. This collection comprises insertions of transposable elements with little redundancy among mutant lines and the possibility to screen 40% of the total 13,366 *Drosophila* genes. These genes are very likely to be different ones as, in assembling this collection; particular care was taken to avoid redundancy in the mutant lines. Only lines whose insertion points could be uniquely and unambiguously localized by sequence comparison to the genomic sequence, were maintained and new lines that mutate genes already disrupted by other transposable elements, were discarded (Bellen *et al.*, 2004). This makes our approach more powerful than other modifier screens relying on the p(EP) collection and also increases our chances of identifying additional and different classes of modifiers of VAP-induced neurotoxicity.

In particular, an F1 screen of the established collection of 5,183 transposable elements will be carried out by crossing flies expressing the pathogenic VAP in the eye, to individual transposable element-insertion lines and examine the progeny for dominant enhancement or suppression of the VAP-induced rough eye phenotype. When one of these transposable elements is inserted proximal to a gene and in the same orientation, it allows the specific misexpression of the gene under the control of Gal4. Alternatively, when inserted in the reverse orientation, the transposable element often inactivates the expression of the gene. Thus this screen has the potential to identify both loss-of-function and gain-of-function modifiers of VAP-induced toxicity and the identification of these interacting genes will shed new light on the molecular mechanisms underlying VAP-induced ALS.

To facilitate an enhancer/suppressor screen using our *Drosophila* eye model, software to quantify the effects of modifiers by measurement of eye sizes was developed. The software is also being further improved to allow semi-automated tracing of the fly eye, decreasing the time spent tracing the eye area. This allows a

larger sample size of eyes to be traced in a minimum amount of time, thus increasing statistical power and improving our statistical analysis of the data. Furthermore, by increasing the sample size of eyes traced, it allows for a clearer definition of which eye size has the highest frequency, thus better enabling us to categorise enhancers and suppressors as strong, medium or weak. Also included in the pipeline is a function that could quantify the extent of the rough eye phenotype by measuring the degree of "entropy" of the structure of ommatidia and orientation of bristles. In most of the methods used in quantifying the rough eye phenotype, a particular area was chosen to perform the quantification manually, be it calculating the average number of unfused ommatidia (Mutsuddi *et al.*, 2004), photoreceptor cells per ommatidium (St. Pierre *et al.*, 2002) or the percentage of correctly orientated bristles (Paricio *et al.*, 1999). This would certainly introduce an operator bias in the phenotype description as some areas of the eyes could be more affected then others. Conversely in our software, quantification is performed by looking at the entire surface of the eye, hence ensuring a real average situation can be described.

This high resolution misexpression screen for modifiers of VAP-induced ALS has never been attempted before and it is crucial that a fast, accurate and efficient system of screening is put in place. We are confident that this approach, coupled with the enhanced software in quantifying the enhancing and suppressing effects of modifiers, will provide modifier genes that can be quickly subjected to functional analysis to further address their role in ALS pathogenesis.

Bibliography

Afifi, A.K., Aleu, F.P., Goodgold, J. and MacKay, B. (1966) Ultrastructure of atrophic muscle in amyotrophic lateral sclerosis. *Neurology*, **16**, 475–481.

Agapite, J. and Steller, S. (1997) Neuronal cell death. In Molecular and Cellular Approaches to Neuronal Development, W.M. Cowan, T.M. Jessell, and S.L. Zipursky, eds. (New York: Oxford University Press), pp. 264–289.

Al-Ramahi, I., Pérez, A.M., Lim, J., Zhang, M., Sorensen, R., de Haro, M., Branco, J., Pulst, S.M., Zoghbi, H.Y., Botas, J. (2007) dAtaxin-2 mediates expanded ataxin-1-induced neurodegeneration in a *Drosophila* model of SCA1. *PLoS Genet.* **3**, 2551-2564.

Amador-Ortiz, C., Lin, W.L., Ahmed, Z., Personett, D., Davies, P., Duara, R., Graff-Radford, N.R., Hutton, M.L. and Dickson, D.W. (2007) TDP-43 immunoreactivity in hippocampal sclerosis and Alzheimer's disease. *Ann Neurol.*, **61**, 435-445

Amarilio, R., Ramachandran, S., Sabanay, H. and Lev, S. (2005) Differential regulation of endoplasmic reticulum structure through VAP-Nir protein interaction. *J. Biol. Chem.*, **280**, 5934-5944.

Anagnostou, G., Akbar, M.T., Paul, P., Angelinetta, C., Steiner, T.J. and de Belleroche, J. (2008) Vesicle associated membrane protein B (VAPB) is decreased in ALS spinal cord. *Neurobiol. Aging,* Article in press.

Andersen, P.M. (2000) Genetic factors in the early diagnosis of ALS. *Amyotroph. Lateral Scler. Other Motor Neuron Disord.* **1**, S31-42.

Arai, T., Hasegawa, M., Akiyama, H., Ikeda, K., Nonaka, T., Mori, H., Mann, D., Tsuchiya, K., Yoshida, M., Hashizume, Y. *et al.* (2006) TDP-43 is a component of ubiquitin-positive tau-negative inclusions in frontotemporal lobar degeneration and amyotrophic lateral sclerosis. *Biochem. Biophys. Res. Commun.,* **351**, 602-611.

Armstrong, J.A., Sperling, A.S., Deuring, R., Manning, L., Moseley, S.L., Papoulas, O., Piatek, C.I., Doe, C.Q., Tamkun, J.W. (2005) Genetic screens for enhancers of brahma reveal functional interactions between the BRM chromatin-remodeling complex and the Delta-Notch signal transduction pathway in *Drosophila*. *Genetics*, **170**,1761-1774.

Atsumi, T. (1981) The ultrastructure of intramuscular nerves in amyotrophic lateral sclerosis. *Acta Neuropathol. (Berl.)*, **55**, 193-198.

Auluck, P.K., Chan, H.Y., Trojanowski, J.Q., Lee, V.M. and Bonini, N.M. (2002) Chaperone suppression of alpha-synuclein toxicity in a *Drosophila* model for Parkinson's disease. *Science,* **295**, 865-868.

Auluck, P.K. and Bonini, N.M. (2002) Pharmacological prevention of Parkinson disease in *Drosophila*. *Nat. Med.*, **8**, 1185-1186.

Beal, M.F., Ferrante, R.J., Browne, S.E., Matthews, R.T., Kowall, N.W., Brown Jr, R.H. (1997) Increased 3-nitrotyrosine in both sporadic and familial amyotrophic lateral sclerosis. *Ann Neurol.*, **42**, 644-654.

Beckman, J.S., Carson, M., Smith, C.D. and Koppenol, W.H. (1993) ALS, SOD and peroxinitrate. *Nature*, **364**, 584.

Bellen, H. J., Levis, R. W., Liao, G., He, Y., Carlson, J. W., Tsang, G., Evans-Holm, M., Hiesinger, P. R., Schulze, K. L., Rubin, G. M. *et al.* (2004) The BDGP gene disruption project: single transposon insertions associated with 40% of *Drosophila* genes. *Genetics,* **167**, 761-781.

Benowitz, L.I. and Routtenberg, A. (1997) GAP-43: an intrinsic determinant of neuronal development and plasticity. *Trends Neurosci.*, **20**, 84-91.

Bergemalm, D., Jonsson, P.A., Graffmo, K.S., Andersen, P.M., Brannstrom, T., Rehnmark, A. and Marklund, S.L. (2006) Overloading of stable and exclusion of unstable human superoxide dismutase-1 variants inmitochondria of murine amyotrophic lateral sclerosis
models. *J. Neurosci.*, **26**, 4147-4154.

Bilen, J. and Bonini, N.M. (2007) Genome-wide screen for modifiers of ataxin-3 neurodegeneration in *Drosophila*. *PLoS Genet.*, **3**, 1950-1964.

Birgbauer, E., Oster, S.F., Severin, C.G. and Sretavan, D.W. (2001) Retinal axon growth cones respond to EphB extracellular domains as inhibitory axon guidance cues. *Development*, **128**, 3041-3048.

Blard, O., Feuillette, S., Bou, J., Chaumette, B., Frebourg, T., Campion, D. and Lecourtois, M. (2007) Cytoskeleton proteins are modulators of mutant tau-induced neurodegeneration in *Drosophila*. *Hum. Mol. Genet.*, **16**, 555-566.

Boillée, S., Yamanaka, K., Lobsiger, C.S., Copeland, N.G., Jenkins, N.A., Kassiotis, G., Kollias, G. and Cleveland, D.W. (2006) Onset and progression in inherited ALS determined by motor neurons and microglia. *Science*, **312**, 1389-1392.

Boston-Howes, W., Gibb, S.L., Williams, E.O., Pasinelli, P., Brown, R.H., Jr. and Trotti, D. (2006) Caspase-3 cleaves and inactivates the glutamate transporter EAAT2. *J. Biol. Chem.*, **281**, 14076-14084.

Borchelt, D.R., Lee, M.K., Slunt, H.S., Guarnieri, M., Xu, Z.S., Wong, P.C., Brown Jr, R.H., Price, D.L., Sisodia, S.S. and Cleveland, D.W. (1994) Superoxide dismutase 1 with mutations linked to familial amyotrophic lateral sclerosis possesses significant

activity. *Proc. Natl. Acad. Sci. USA.*, **91**, 8292-8296.

Bowling, A.C., Barkowski, E.E., McKenna-Yasek, D., Sapp, P., Horvitz, H.R., Beal, M.F., and Brown Jr, R.H. (1995) Superoxide dismutase concentration and activity in familial amyotrophic lateral sclerosis. *J. Neurochem.*, **64**, 2366-2369.

Brand, A.H. and Perrimon, N. (1993) Targeted gene expression as a means of altering cell fates and generating dominant phenotypes. *Development,* **118**, 401-415.

Brickner, J.H. and P. Walter (2004) Gene recruitment of the activated INO1 locus to the nuclear membrane. *PLoS Biol.,* **2**, 1843-1853.

Bruijn, L.I., Becher, M.W., Lee, M.K., Anderson, K.L., Jenkins, N.A., Copeland, N.G., Sisodia, S.S., Rothstein, J.D., Borchelt, D.R., Price, D.L. and Cleveland, D.W. (1997) ALS-linked SOD1 mutant G85R mediates damage to astrocytes and promotes rapidly progressive disease with SOD1-containing inclusions. *Neuron*, **18,** 327-338.

Bruijn, L.I., Houseweart, M.K., Kato, S., Anderson, K.L., Anderson, S.D., Ohama, E., Reaume, A.G., Scott, R.W. and Cleveland, D.W. (1998) Aggregation and motor neuron toxicity of an ALS-linked SOD1 mutant independent from wild-type SOD1. *Science,* **281**, 1851-1854

Bruijn, L.I., Miller, T.M. and Cleveland, D.W. (2004) Unraveling the mechanisms involved in motor neuron degeneration in ALS. *Annu. Rev. Neurosci.*, **27**, 723-749.

Bukau, B. and Horwich, A.L. (1998) The Hsp70 and Hsp60 chaperone machines. *Cell*, **92**, 351-366.

Cai, H., Lin, X., Xie, C., Laird, F.M., Lai, C., Wen, H., Chiang, H.C., Shim, H., Farah, M.H., Hoke, A., Price, D.L., Wong, P.C. (2005) Loss of ALS2 function is insufficient to trigger motor neuron degeneration in knock-out mice but predisposes neurons to oxidative stress. *J. Neurosci.*, **25**, 7567-7574.

Caughey, B. and Lansbury, P.T. (2003) Protofibrils, pores, fibrils, and neurodegeneration: separating the responsible protein aggregates from the innocent bystanders. *Annu. Rev. Neurosci.*, **26**, 267-298.

Cermelli, S., Guo, Y., Gross, S.P. and Welte, M.A. (2006) The lipid-droplet proteome reveals that droplets are a protein-storage depot. *Curr. Biol.*, **16**, 1783-1795.

Chai, A. (2005) *Drosophila* as a model system of Amytotrophic Lateral Sclerosis (ALS). Msc Thesis

Chai, A., Withers, J., Koh, Y.H., Parry, K., Bao, H., Zhang, B., Budnik, V. and Pennetta, G. (2008) hVAPB, the causative gene of a heterogeneous group of motor neuron diseases in humans, is functionally interchangeable with its *Drosophila*

homologue DVAP-33A at the neuromuscular junction. *Hum. Mol. Genet.*, **17**, 266-280.

Chan, H.Y., Warrick, J.M., Andriola, I., Merry, D. and Bonini, N.M. (2002) Genetic modulation of polyglutamine toxicity by protein conjugation pathways in *Drosophila*. *Hum. Mol. Genet.*, **11**, 2895–2904.

Chandra, S., Gallardo, G., Fernández-Chacón, R., Schlüter, O.M., Südhof, T.C (2005) Alpha-synuclein cooperates with CSPalpha in preventing neurodegeneration. *Cell*, **123**,383-396.

Chee, F., Mudher, A., Newman, T.A., Cuttle, M., Lovestone, S. and Shepherd, D. (2005) Over-expression of tau results in defective synaptic transmission in *Drosophila* neuromuscular junctions. *Neurobiol. Dis.*, **20**, 918-928.

Chen, H.K., Fernandez-Funez, P., Acevedo, S.F., Lam, Y.C., Kaytor, M.D., Fernandez, M.H., Aitken, A., Skoulakis, E.M., Orr, H.T., Botas, J. *et al.* (2003) Interaction of Akt-phosphorylated ataxin-1 with 14-3-3 mediates neurodegeneration in spinocerebellar ataxia type 1. *Cell,* **113**, 457-468.

Chen, Y.Z., Bennett, C.L., Huynh, H.M., Blair, I.P., Puls, I., Irobi, J., Dierick, I., Abel, A., Kennerson, M.L., Rabin, B.A., *et al.* (2004) DNA/RNA helicase gene mutations in a form of juvenile amyotrophic lateral sclerosis (ALS4). *Am. J. Hum. Genet.*, **74**, 1128-1135.

Clark, I.E., Dodson, M.W., Jiang, C., Cao, J.H., Huh, J.R., Seol, J.H., Yoo, S.J., Hay, B.A. and Guo, M. (2006) *Drosophila* pink1 is required for mitochondrial function and interacts genetically with parkin. *Nature*, **441**, 1162-1166.

Clement, A.M., Nguyen,M.D., Roberts, E.A., Garcia, M.L., Boillée, S., Rule, M., McMahon, A.P., Doucette, W., Siwek, D., Ferrante, R.J., *et al.* (2003) Wild-type nonneuronal cells extend survival of SOD1 mutant motor neurons in ALS mice. *Science*, **302**, 113-117.

Cleveland, D. W. and Rothstein, J. D. (2001) From Charcot to Lou Gehrig: deciphering selective motor neuron death in ALS. *Nature Rev. Neurosci.*, **2**, 806-819.

Corona, D.F., Armstrong, J.A. and Tamkun, J.W. (2004) Genetic and cytological analysis of *Drosophila* chromatin-remodeling factors. *Methods Enzymol.*, **377**, 70-85.

Corrado, L., Ratti, A., Gellera, C., Buratti, E., Castellotti, B., Carlomagno, Y., Ticozzi, N., Mazzini, L., Testa, L., Taroni, F., *et al.* (2009) High frequency of TARDBP gene mutations in Italian patients with amyotrophic lateral sclerosis. *Hum. Mutat.*, **30**, 688-94.

Couillard-Després, J.-S., Zhu, Q., Wong, P.C., Price, D.L., Cleveland, D.W. and

Julien, J.-P. (1998) Protective effect of neurofilament NF-H overexpression in motor neuron disease induced by mutant superoxide dismutase. *Proc. Natl. Acad. Sci. USA.*, **95**, 9626-9630.

Cukier, H.N., Perez, A.M., Collins, A.L., Zhou, Z., Zoghbi, H.Y. and Botas, J. (2008) Genetic Modifiers of MeCP2 Function in *Drosophila*. *PLoS Genet.*, **4**, 1-12.

Dal Canto, M.C. and Gurney, M.E. (1995) Neuropathological changes in two lines of mice carrying a transgene for mutant human Cu,Zn SOD, and in mice overexpressing wild type human SOD: a model of familial amyotrophic lateral sclerosis (FALS). *Brain Res.*, **676**, 25-40.

Daoud, H., Valdmanis, P.N., Kabashi, E., Dion, P., Dupre, N., Camu, W., Meininger, V. and Rouleau, G.A. (2008) Contribution of TARDBP mutations to sporadic amyotrophic lateral sclerosis. *J. Med. Genet.*, **46**, 112-114.

Davis, G.W. and Goodman, C.S. (1998) Genetic analysis of synaptic development and plasticity: homeostatic regulation of synaptic efficacy. *Curr. Opin. Neurobiol.*, **8**, 149-156.

Deitcher, D.L., Ueda, A., Stewart, B.A., Burgess, R.W., Kidokoro, Y. and Schwarz, T.L. (1998) Distinct requirements for evoked and spontaneous release of neurotransmitter are revealed by mutations in the *Drosophila* gene neuronal synaptobrevin. *J. Neurosci.*, **18**, 2028-2039.

Dengler, R., Konstanzer, A., Ku ther, G., Hesse, S., Wolf, W. and Struppler, A. (1990) Amyotrophic lateral sclerosis: macro-EMG and twitch forces of single motor units. *Muscle Nerve,* **13**, *545-550.*

De Strooper, B. (2003) Aph-1, Pen-2, and Nicastrin with Presenilin generate an active g-secretase complex. *Neuron*, **38**, 9–12.

DiAntonio, A., Petersen, S.A., Heckmann, M. and Goodman, C.S. (1999) Glutamate receptor expression regulates quantal size and quantal content at the *Drosophila* neuromuscular junction. *J. Neurosci.*, **19**, 3023-3032.

DiAntonio, A. (2006) Glutamate receptors at the *Drosophila* neuromuscular junction. *Int. Rev. Neurobiol.*, **75**, 165-179.

Doi, H., Okamura, K., Bauer, P.O., Furukawa, Y., Shimizu, H., Kurosawa, M., Machida, Y., Miyazaki, H., Mitsui, K., Kuroiwa, Y., *et al.* (2008) RNAbinding protein TLS is a major nuclear aggregate-interacting protein in huntingtin exon 1 with expanded polyglutamine-expressing cells. *J. Biol. Chem.*, **283**, 6489-6500.

Drewes, G., Ebneth, A., Preuss, U., Mandelkow, E.M. and Mandelkow, E. (1997) MARK, a novel family of protein kinases that phosphorylate microtubuleassociated

proteins and trigger microtubule disruption. *Cell,* **89**, 297-308.

Duffy, J.B. (2002) GAL4 system in *Drosophila*: a fly geneticist's Swiss army knife. *Genesis*, **34**, 1-15.

Dupuis, L., Oudart, H., Rene, F., Gonzalez de Aguilar, J.L. and Loeffler, J.P. (2004) Evidence for defective energy homeostasis in amyotrophic lateral sclerosis: benefit of a high-energy diet in a transgenic mouse model. *Proc. Natl. Acad. Sci. USA.*, **101**, 11159-11164.

Dupuis, L., Corcia, P., Fergani, A., Gonzalez de Aguilar, J.L, Bonnefont-Rousselot, D., Bittar, R., *et al.* (2008) Dyslipidemia is a protective factor in amyotrophic lateral sclerosis. *Neurology,* **70**, 1004-1009.

Eberl, D.F., Perkins, L.A., Engelstein, M., Hilliker, A.J. and Perrimon, N. (1992) Genetic and developmental analysis of polytene section 17 of the X chromosome of *Drosophila* melanogaster. *Genetics*, **130**, 569-583.

Eisen, A. 2000 Amyotrophic Lateral Sclerosis (ALS): The Diagnosis and Treatment of this Debilitating Disease. *Geriatrics and Aging*, **3**, 26-27

Elia, A.J., Parkes, T.L., Kirby, K., St George-Hyslop, P., Boulianne, G.L., Phillips J.P. and Hilliker, A.J. (1999) Expression of human FALS SOD in motorneurons of *Drosophila. Free. Radic. Biol. Med.,* **26**, 1332-1338.

Emamian, E.S., Kaytor, M.D., Duvick, L.A., Zu, T., Tousey, S.K., Clark, H.B., Zoghbi, H.Y. and Orr, H.T. (2003) Serine 776 of ataxin-1 is critical for polyglutamineinduced disease in SCA1 transgenic mice. *Neuron,* **38**, 375–387.

Eyer, J., Cleveland, D.W., Wong, P.C. and Peterson, A.C. (1998) Pathogenesis of two axonopathies does not require axonal neurofilaments. *Nature*, **391**, 584-587.

Fairman, W. A., Vandenberg, R. J., Arriza, J. L., Kavanaugh, M. P. and Amara, S. G. (1995) An excitatory aminoacid transporter with properties of a ligand-gated chloride channel. *Nature,* **375**, 599-603.

Farah, C. A., Nguyen, M. D., Julien, J. P. and Leclerc, N. (2003) Altered levels and distribution of microtubule-associated proteins before disease onset in a mouse model of amyotrophic lateral sclerosis. *J. Neurochem.*, **84**, 77-86.

Fatt, P. and Katz, B. (1952) Spontaneous subthreshold activity at motor nerve endings. *J Physiol.,* **117,** 109-128.

Feany, M.B. and Bender, W.W. (2000) A *Drosophila* model of Parkinson's disease. *Nature*, 404, 394-398.

Featherstone, D.E., Rushton, E., Rohrbough, J., Liebl, F., Karr, J., Sheng, Q.,

Rodesch, C.K. and Broadie, K. (2005) An essential *Drosophila* glutamate receptor subunit that functions in both central neuropil and neuromuscular junction. *J. Neurosci.*, **25**, 3199-3208.

Fernandez-Funez, P., Nino-Rosales, M.L., de Gouyon, B., She, W.C., Luchak, J.M., Martinez, P., Turiegano, E., Benito, J., Capovilla, M., Skinner, P.J. *et al.* (2000) Identification of genes that modify ataxin-1-induced neurodegeneration. *Nature*. 408, 101-106.

Finelli, A., Kelkar, A., Song, H.J., Yang, H. and Konsolaki, M. (2004) A model for studying Alzheimer's A_42-induced toxicity in *Drosophila* melanogaster. *Mol. Cell. Neurosci.* **26**, 365–375.

Fortini, M.E., Skupski, M.P., Boguski, M.S. and Hariharan, I.K. (2000) A survey of human disease gene counterparts in the *Drosophila* genome. *J. Cell Biol.* 150, F23-30

Foster, L.J., Weir, M.L., Lim, D.Y., Liu, Z., Trimble, W.S. and Klip, A. (2000) A functional role for VAP-33 in insulin-stimulated GLUT4 traffic. *Traffic*, **1**, 512-521.

Fox, L.E., Soll, D.R. and Wu, C.F. (2006) Coordination and modulation of locomotion pattern generators in *Drosophila* larvae: effects of altered biogenic amine levels by the tyramine beta hydroxlyase mutation. *J. Neurosci.*, **26**, 1486-1498.

Frey, D., Schneider, C., Xu, L., Borg, J., Spooren, W. and Caroni, P. (2000) Early and selective loss of neuromuscular synapse subtypes with low sprouting competence in motoneuron diseases. *J. Neurosci.*, **20**, 2534-2542.

Fujii, R., Okabe, S., Urushido, T., Inoue, K., Yoshimura, A., Tachibana, T., Nishikawa, T., Hicks, G.G. and Takumi, T. (2005) The RNA binding protein TLS is translocated to dendritic spines by mGluR5 activation and regulates spine morphology. *Curr. Biol.*, **15**, 587-593.

Gaudette, M., Hirano, M. and Siddique, T. (2000) Current status of SOD1 mutations in familial amyotrophic lateral sclerosis. *Amyotroph. Lateral Scler. Other Motor Neuron Disord.* 1, 83-89.

Gavin, A.C., Bosche, M., Krause, R., Grandi, P., Marzioch, M., Bauer, A., Schultz, J., Rick, J.M., Michon, A.M., Cruciat, C.M., *et al.* (2002) Functional organization of the yeast proteome by systematic analy-sis of protein complexes. *Nature*, **415**, 123-124.

Giot, L., Bader, J.S., Brouwer, C., Chaudhari, A., Kuang, B., Li, Y., Hao, L., Ooi, C.E., Godwin, B., Vitols, E., *et al.* (2003) A protein interaction map of *Drosophila* melanogaster. *Science*, **302**, 1727-1736.

Gitcho, M.A., Baloh, R.H., Chakraverty, S., Mayo, K., Norton, J.B., Levitch, D., Hatanpaa, K.J., White, C.L., III, Bigio, E.H., Caselli, R., *et al.*, (2008) TDP-43

A315T mutation in familial motor neuron disease. *Ann. Neurol.*, **63**, 535-538.

Glover, J. R., and Lindquist, S. (1998) Hsp104, Hsp70, and Hsp40: a novel chaperone system that rescues previously aggregated proteins. *Cell*, **94**, 73-82.

Goedert, M., Jakes, R., Qi, Z., Wang, J.H. and Cohen, P. (1995) Protein phosphatase 2A is the major enzyme in brain that dephosphorylates tau protein phosphorylated by proline directed protein kinases or cyclic AMP-dependent protein kinase. *J. Neurochem.*, **65**, 2804–2807.

Gong, Y.H., Parsadanian, A.S., Andreeva, A., Snider, W.D. and Elliott, J.L. (2000) Restricted expression of G86R Cu/Zn superoxide dismutase in astrocytes results in astrocytosis but does not cause motoneuron degeneration. *J. Neurosci.*, **20**, 660-665.

Greene, J. C., Whitworth, A. J., Kuo, I., Andrews, L. A., Feany, M. B. and Pallanck, L. J. (2003) Mitochondrial pathology and apoptotic muscle degeneration in *Drosophila* parkin mutants. *Proc. Natl. Acad. Sci. USA.*, **100**, 4078-4083.

Greenspan, R.J. (2004) Fly Pushing: Theory and Practice of *Drosophila* Genetics. 2nd Edition. Cold Spring Harbor Press.

Guo, H., Lai, L., Butchbach, M.E., Stockinger, M.P., Shan, X., Bishop, G.A. and Lin, C.L. (2003) Increased expression of the glial glutamate transporter EAAT2 modulates excitotoxicity and delays the onset but not the outcome of ALS in mice. *Hum. Mol. Genet.*, **12**, 2519-2532.

Gurney, M.E., Pu, H., Chiu, A.Y., Dal Canto, M.C., Polchow, C.Y., Alexander, D.D., Caliendo, J., Hentati, A., Kwon, Y.W., Deng, H.X. (1994) Motor neuron degeneration in mice that express a human Cu/Zn superoxide dismutase mutation. *Science,* **264**, 1772-1775.

Gylys, K.H., Fein, J.A., Yang, F., Wiley, D.J., Miller, C.A. and Cole, G.M. (2004) Synaptic changes in Alzheimer's disease: increased amyloid- and gliosis in surviving terminals is accompanied by decreased PSD-95 fluorescence. *Am. J. Pathol.*, **165**, 1809 -1817.

Hadano, S., Hand, C.K., Osuga, H., Yanagisawa, Y., Otomo, A., Devon, R.S., Miyamoto, N., Showguchi-Miyata, J., Okada, Y., Singaraja, R., *et al.* (2001) A gene encoding a putative GTPase regulator is mutated in familial amyotrophic lateral sclerosis 2. *Nat. Genet.*, **29**, 166-173.

Halder, G., Callaerts, P. and Gehring, W.J. (1995) Induction of ectopic eyes by targeted expression of the eyeless gene in *Drosophila. Science,* **267**, 1788-1792.
Hauck, B., Gehring, W.J. and Walldorf, U. (1999) Functional analysis of an eye specific enhancer of the eyeless gene in *Drosophila. Proc. Natl. Acad. Sci. USA.*, **96**, 564-569.

Hafezparast, M., Klocke, R., Ruhrberg, C., Marquardt, A., Ahmad-Annuar, A., Bowen, S., Lalli, G., Witherden, A.S., Hummerich, H., Nicholson, S., *et al.* (2003) Mutations in dynein link motor neuron degeneration to defects in retrograde transport. *Science*, **300**, 808-812.

Hart, P.J. (2006) Pathogenic superoxide dismutase structure, folding, aggregation and turnover. *Curr. Opin. Chem. Biol.*, **10**, 131-138.

Henderson, J.T., Georgiou, J., Jia, Z.P., Robertson, J., Elowe, S., Roder, J.C. And Pawson, T. (2001) The receptor tyrosine kinase EphB2 regulates NMDA-dependent synaptic function. *Neuron*, **32**, 1041-1056.

Hering, H., Lin, C.C. and Sheng, M. (2003) Lipid rafts in the maintenance of synapses, dendritic spines, and surface AMPA receptorstability. *J. Neurosci.*, **23**, 3262-3271.

Higgins, C.M., Jung, C. and Xu, Z. (2003) ALS-associated mutant SOD1G93A causes mitochondrial vacuolation by expansion of the intermembrane space and by involvement of SOD1 aggregation and peroxisomes. *BCM Neurosci.*, **4**, 16.

Hockly, E., Richon, V.M., Woodman, B., Smith, D.L., Zhou, X., Rosa, E., Sathasivam, K., Ghazi-Noori, S., Mahal, A., Lowden, P.A. *et al.* (2003) Suberoylanilide hydroxamic acid, a histone deacetylase inhibitor, ameliorates motor deficits in a mouse model of Huntington's disease. *Proc. Natl. Acad. Sci. USA.*, **100,** 2041-2046.

Hadano, S., Benn, S.C., Kakuta, S., Otomo, A., Sudo, K., Kunita, R., Suzuki-Utsunomiya, K., Mizumura, H., Shefner, J.M., Cox, G.A., *et al.* (2006) Mice deficient in the Rab5 guanine nucleotide exchange factor ALS2/alsin exhibit age-dependent neurological deficits and altered endosome trafficking. *Hum. Mol. Genet.*, **15**, 233-250.

Hanada, K., Kumagai, K., Yasuda, S., Miura, Y., Kawano, M., Fukasawa, M. and Nishijima, M. (2003) Molecular machinery for non-vesicular trafficking of ceramide. *Nature*, **426**, 803-809.

Hosler, B.A. Siddique, T., Sapp, P.C., Sailor, W., Huang, M.C., Hossain, A., Daube, J.R., Nance, M., Fan,C., Kaplan, J. *et al.* (2000) Linkage of familial amyotrophic lateral sclerosis with frontotemporal dementia to chromosome 9q21-q22. *JAMA*, **284**, 1664-1669.

Howland, D.S., Liu, J., She, Y., Goad, B., Maragakis, N.J., Kim, B., Erickson, J., Kulik, J., DeVito, L., Psaltis, G., *et al.* (2002) Focal loss of the glutamate transporter EAAT2 in a transgenic rat model of SOD1 mutant-mediated amyotrophic lateral sclerosis (ALS). *Proc. Natl. Acad. Sci. USA.*, **99**, 1604-1609.

Huitema, K., van den Dikkenberg, J., Brouwers, J.F., and Holthuis, J.C. (2004) Identification of a family of animal sphingomyelin synthases. *EMBO J.*, **23**, 33-44.

Hutton, M., Lendon, C.L., Rizzu, P., Baker, M., Froelich, S., Houlden, H., Pickering-Brown, S., Chakraverty, S., Isaacs, A., Grover, A. *et al.* (1998) Association of missense and 5Y-splice-site mutations in tau with the inherited dementia FTDP-17. *Nature*, **393**, 702-705.

Hyun, J., Jasper, H. and Bohmann, D. (2005) DREF is required for efficient growth and cell cycle progression in *Drosophila* imaginal discs. *Mol. Cell Biol.* **25**, 5590-5598.

Iijima, K., Liu, H.P., Chiang, A.S., Hearn, S.A., Konsolaki, M. and Zhong, Y. (2004) Dissecting the pathological effects of human AK40 and AK42 in *Drosophila*: a potential model for Alzheimer's disease. *Proc Natl Acad Sci USA.*, **101**, 6623-6628.

Iwata, N., Tsubuki, S., Takaki, Y., Shirotani, K., Lu, B., Gerard, N .P., Gerard, C., Hama, E., Lee, H. J. and Saido, T. C. (2001) Metabolic regulation of brain Abeta by neprilysin. *Science*, **292**, 1550-1552.

Jaarsma, D., Haasdijk, E.D., Grashorn, .JA., Hawkins, R., van Duijn, W., Verspaget, H.W., London, J., Holstege, .JC. (2000) Human Cu/Zn superoxide dismutase (SOD1) overexpression in mice causes mitochondrial vacuolization, axonal degeneration, and premature motoneuron death and accelerates motoneuron disease in mice expressing a familial amyotrophic lateral sclerosis mutant SOD1. *Neurobiol. Dis.*, **7**, 623–643.

Jackson, G.R., Salecker, I., Dong, X., Yao, X., Arnheim, N., Faber, P.W., MacDonald, M.E. and Zipursky, S.L. (1998) Polyglutamine-expanded human huntingtin transgenes induce degeneration of *Drosophila* photoreceptor neurons. *Neuron*, **21**, 633-642.

Jackson, G.R., Wiedau-Pazos, M., Sang, T.K., Wagle, N., Brown, C.A., Massachi, S. and Geschwind, D.H. (2002) Human wild-type tau interacts with wingless pathway components and produces neurofibrillary pathology in *Drosophila*. *Neuron*, **34**, 509-519.

Jin, P., Zarnescu, D.C., Zhang, F., Pearson, C.E., Lucchesi, J.C., Moses, K. and Warren, S.T. (2003) RNA-mediated neurodegeneration caused by the fragile X premutation rCGG repeats in *Drosophila*. *Neuron,* **39,** 739-747.

Johnston, J.A., Dalton, M.J., Gurney, M.E. and Kopito, R. R. (2000) Formation of high molecular weight complexes of mutant Cu,Zn-superoxide dismutase in a mouse model for familial amyotrophic lateral sclerosis. *Proc. Natl Acad. Sci. USA.*, **97**, 12571-12576.

Jones, C., Reifegerste, R. and Moses, K. (2006) Characterization of *Drosophila mini-*

me, a Gene Required for Cell Proliferation and Survival. *Genetics*, **173**, 793-808.

Kabashi, E., Valdmanis, P.N., Dion, P., Spiegelman, D., McConkey, B.J., Vande Velde, C., Bouchard, J.P., Lacomblez, L., Pochigaeva, K., Salachas, F., *et al.* (2008) TARDBP mutations in individuals with sporadic and familial amyotrophic lateral sclerosis. *Nat. Genet.*, **40,** 572-574.

Kagiwada, S., Hosaka, K., Murata, M., Nikawa, J. and Takatsuki, A. (1998) The *Saccharomyces cerevisiae* SCS2 gene product, a homolog of a synaptobrevin-associated protein, is an integral membrane protein of the endoplasmic reticulum and is required for inositol metabolism. *J. Bacteriol.*, **180**, 1700-1708.

Kagiwada, S. and Zen, R. (2003) Role of the Yeast VAP Homolog, Scs2p, in INO1 Expression and Phospholipid Metabolism. *J. Biochem.*, **133**, 515-522.

Kagiwada, S. and Hashimoto, M. (2007) The yeast VAP homolog Scs2p has a phosphoinositide-binding ability that is correlated with its activity. *Biochem. Biophys. Res. Commun.*, **364**, 870-876.

Kaiser, S.E., Brickner, J.H., Reilein, A.R., Fenn, T.D., Walter, P. and Brunger, A.T. (2005) Structural basis of FFAT motif-mediated ER targeting. *Structure*, **13**, 1035-1045.

Kanekura, K., Hashimoto, Y., Niikura, T., Aiso, S., Matsuoka, M. and Nishimoto, I. (2004) Alsin, the Product of ALS2 Gene, Suppresses SOD1 Mutant Neurotoxicity through RhoGEF Domain by Interacting with SOD1 Mutants. *J. Biol. Chem.*, **279**, 19247-19256.

Kanekura, K., Nishimoto, I., Aiso, S. and Matsuoka, M. (2006) Characterization of amyotrophic lateral sclerosis-linked P56S mutation of vesicle-associated membrane protein-associated protein B (VAPB/ALS8). *J. Biol. Chem.*, **281**, 30223-30233.

Karsten, S. L., Sang, T. K., Gehman, L. T., Chatterjee, S., Liu, J., Lawless, G. M., Sengupta, S., Berry, R. W., Pomakian, J., Oh, H. S., *et al.* (2006) A genomic screen for modifiers of tauopathy identifies puromycin-sensitive aminopeptidase as an inhibitor of tau-induced neurodegeneration. *Neuron*, **51**, 549-560.

Kawano, M., Kumagai, K., Nishijima, M. and Hanada, K. (2006) Efficient trafficking of ceramide from the endoplasmic reticulum to the Golgi apparatus requires a VAMP-associated protein-interacting FFAT motif of CERT. *J. Biol. Chem.*, 281, 30279-30288.

Kazemi-Esfarjani, P. and Benzer, S. (2000) Genetic suppression of polyglutamine toxicity in *Drosophila*. *Science*, **287**, 1837-1840.

Kitada, T., Asakawa, S., Hattori, N., Matsumine, H., Yamamura, Y., Minoshima, S.,

Yokochi, M., Mizuno, Y. and Shimizu, N. (1998) Mutations in the parkin gene cause autosomal recessive juvenile parkinsonism. *Nature*, **392**, 605-608.

Kong, J. and Xu, Z. (1998) Massive mitochondrial degeneration in motor neurons triggers the onset of amyotrophic lateral sclerosis in mice expressing mutant SOD1. *J. Neurosci.*, **18**, 3241-3250.

Kong, J. and Xu, Z. (2000) Overexpression of neurofilament subunit NF-L and NF-H extends survival of a mouse model for amyotrophic lateral sclerosis. *Neurosci. Lett.*, **281**, 72-74.

Kosinski, M., McDonald, K., Schwartz, J., Yamamoto, I. and Greenstein, D. (2005) C. elegans sperm bud vesicles to deliver a meiotic maturation signal to distant oocytes. *Development*, **132**, 3357-3369.

Kostic, V., Jackson-Lewis, V., De Bilbao, F., Dubois-Dauphin, M. and Przedborski, S. (1997) Bcl-2: prolonging life in a transgenic mouse model of familial amyotrophic lateral sclerosis. *Science*, **277**, 559-562.

Kramer, J.M. and Staveley, B.E. (2003) GAL4 causes developmental defects and apoptosis when expressed in the developing eye of *Drosophila* melanogaster. *Genet. Mol. Res.* **2**, 43-47.

Kruger, R., Kuhn, W., Muller, T., Woitalla, D., Graeber, M., Kosel, S.,Pzuntek, H., Epplen, J.T., Schols, L. and Riess, O. (1998) Ala30Promutation in the gene encoding alpha-synuclein in Parkinson's disease. *Nat. Genet.*, **18**, 107-108.

Kumagai, K., Yasuda, S., Okemoto, K., Nishijima, M., Kobayashi, S. and Hanada, K. (2005) CERT mediates intermembrane transfer of various molecular species of ceramides. *J. Biol. Chem.*, **280**, 6488-6495.

Kuranaga, E., Kanuka, H., Tonoki, A., Takemoto, K., Tomioka, T., Kobayashi, M., Hayashi, S. and Miura, M. (2006) *Drosophila* IKKrelated kinase regulates nonapoptotic function of caspases via degradation of IAPs. *Cell*, **126**, 583-596.

Kuwabara, P.E. (2003) The multifaceted C. elegans major sperm protein: an ephrin signaling antagonist in oocyte maturation. *Genes Dev.*, **17**, 155-161.

Kwiatkowski, T.J. Jr, Bosco, D.A., LeClerc, A.L., Tamrazian, E., Vanderburg, C.R., Russ, C., Davis, A., Gilchrist, J., Kasarskis, E.J., Munsat, T., *et al.* (2009) Mutations in the FUS/TLS gene on chromosome 16 cause familial amyotrophic lateral sclerosis. *Science*, **323**,1205-1208.

Lagace, T.A., Byers, D.M., Cook, H.W. and Ridgway, N.D. (1999) Chinese hamster ovary cells overexpressing the oxysterol binding protein (OSBP) display enhanced synthesis of sphingomyelin in response to 25-hydroxycholesterol. *J. Lipid Res.*, **40**, 109-116.

LaMonte, B., Wallace, K.E., Holloway, B.A., Shelly, S.S., Ascano, J., Tokito, M., Van Winkle, T., Howland, D.S. and Holzbaur, E.L.F. (2002) Disruption of dynein/dynactin inhibits axonal transport in motor neurons causing late-onset progressive deterioration. *Neuron*, **34**, 715-727.

Lang, A.E. and Lozano, A.M. (1998) Parkinson's disease. (Part 1). *N. Engl. J. Med.*, **339**, 1044-1053

Lapierre, L.A., Tuma, P.L., Navarre, J., Goldenring, J.R. and Anderson, J.M. (1999) VAP-33 localizes to both an intracellular vesicle population and with occludin at the tight junction. *J. Cell Sci.*, **112**, 3723-3732.

Lee, M.K., Marszalek, J.R. and Cleveland, D.W. (1994) A mutant neurofilament subunit causes massive, selective motor neuron death: Implications for the pathogenesis of human motor neuron disease. *Neuron*, **13**, 975-988.

Lee, V.M., Goedert, M. and Trojanowski, J.Q. (2001) Neurodegenerative tauopathies. *Annu. Rev. Neurosci.*, 24, 1121-1159.

Lehto, M. and Olkkonen, V. M. (2003) The OSBP-related proteins: a novel protein family involved in vesicle transport, cellular lipid metabolism and cell signalling. *Biochim. Biophys. Acta,* **1631**, 1-11.

Leigh, P.N., Whitwell, H., Garofalo, O., Buller, J., Swash, M., Martin, J.E., Gallo, J.M., Weller, R.O. and Anderton, B.H. (1991) Ubiquitin-immunoreactive intraneuronal inclusions in amyotrophic lateral sclerosis. Morphology, distribution, and specificity. *Brain,* **114**, 775-788.

Leigh, P.N. and Ogarofolo, O. (1995) The molecular pathology of motor neurone disease. In Motor neurone disease. M. Swash and P.N. Leigh, editors. *Springer Verlag, London,* 139-161.

Lessing, D. and Bonini, N.M. (2008) Polyglutamine genes interact to modulate the severity and progression of neurodegeneration in *Drosophila.* PLoS Biol., **6**, 0266-0274.

Levine, T.P. and Munro, S. (2002) Targeting of Golgi-specific pleckstrin homology domains involves both PtdIns 4-kinase-dependent and -independent components. *Curr. Biol.*, **12**, 695-704.

Li, M., Ona, V.O., Guegan, C., Chen, M., Jackson-Lewis, V., Andrews, L.J., Olszewski, A.J., Stieg, P.E., Lee, J.P., Przedborski, S., *et al.* (2000) Functional role of caspase-1 and caspase-3 in an ALS transgenic mouse model. *Science,* **288**, 335-339.

Liao, H., Li, Y., Brautigan, D. L. and Gundersen, G.G. (1998) Protein phosphatase 1 is targeted to microtubules by the microtubule-associated protein tau. *J. Biol. Chem.,*

273, 21901-21908.

Lino, M.M., Schneider, C. and Caroni, P. (2002) Accumulation of SOD1 mutants in postnatal motoneurons does not cause motoneuron pathology or motoneuron disease. J. *Neurosci*., **22**, 4825-4832.

Littleton, J.T., Stern, M., Schulze, K., Perin, M. and Bellen, H.J. (1993) Mutational analysis of *Drosophila* synaptotagmin demonstrates its essential role in Ca(21)-activated neurotransmitter release. *Cell,* **74**, 1125-1134.

Loewen, C.J., Roy, A. and Levine, .TP. (2003) A conserved ER targeting motif in three families of lipid binding proteins and in Opi1p binds VAP. *EMBO J.,* **22**, 2025-2035.

Loewen, C.J., Gaspar, M.L., Jesch, S.A., Delon, C., Ktistakis, N.T., Henry, S.A. and Levine, T.P. (2004) Phospholipid metabolism regulated by a transcription factor sensing phosphatidic acid. *Science*, **304,** 1644-1647.

Lomen-Hoerth, C. (2004) Characterization of amyotrophic lateral sclerosis and frontotemporal dementia. *Dement. Geriatr. Cogn. Disord.* **17**, 337-341.

Lucas, J.J., Hernandez, F., Gomez-Ramos, P., Moran, M.A., Hen, R. and Avila, J. (2001) Decreased nuclear beta-catenin, tau hyperphosphorylation and neurodegeneration in GSK-3beta conditional transgenic mice, *EMBO J.*, **20**, 27-39.

McCabe, B.D., Hom, S., Aberle, H., Fetter, R.D., Marques, G., Haerry, T.E., Wan, H., O'Connor, M.B., Goodman, C.S. and Haghighi, A.P. (2004) Highwire regulates presynaptic BMP signaling essential for synaptic growth. *Neuron*, **41**, 891-905.

Marques, V.D., Barreira, A.A., Davis, M.B., Abou-Sleiman, P.M., Silva, W.A., Jr, Zago, M.A., Sobreira, C., Fazan, V. and Marques, W., Jr (2006) Expanding the phenotypes of the Pro56Ser VAPB mutation: proximal SMA with dysautonomia. *Muscle Nerve*, **34**, 731-739.

Marrus, S.B. and DiAntonio, A. (2004) Preferential localization of glutamate receptors opposite sites of high presynaptic release. *Curr. Biol.*, **14**, 924-931.

Marrus, S.B., Portman, S.L., Allen, M.J., Moffat, K.G. and DiAntonio, A. (2004) Differential localization of glutamate receptor subunits at the *Drosophila* neuromuscular junction. *J. Neurosci.*, **24**, 1406-1415.

Maselli, R. A., Wollman, R. L., Leung, C., Distad, B., Palombi, S., Richman, D. P., Salazar-Grueso, E. F. and Roos, R. P. (1993) Neuromuscular transmission in amyotrophic lateral sclerosis. *Muscle Nerve*, **16**, 1193-1203.

McCampbell, A., Taye, A.A., Whitty, L., Penney, E., Steffan, J.S. and Fischbeck,

K.H. (2001) Histone deacetylase inhibitors reduce polyglutamine toxicity. *Proc. Natl. Acad. Sci. USA.*, **98**, 15179–15184.

Miller, M.A., Ruest, P., Kosinski, M., Hanks, S., and Greenstein,D. (2003) An Eph receptor sperm-sensing control mechanismfor oocyte meiotic maturation in *Caenorhabditis elegans*. *Genes Dev.*, **17**, 187-200.

Moreira, M.C., Klur, S., Watanabe, M., Németh, A.H., Le Ber, I., Moniz, J.C., Tranchant, C., Aubourg, P., Tazir, M., Schöls, L., *et al.* (2004) Senataxin, the ortholog of a yeast RNA helicase, is mutant in ataxia-ocular apraxia. *Nat. Genet.*, **36**, 225-227.

Mulder, D. W., Kurland, L. T., Offord, K. P. and Beard, C. M. (1986) Familial adult motor neuron disease: amyotrophic lateral sclerosis. *Neurology,* **36**, 511-517.

Mutsuddi, M., Marshall, C.M,, Benzow, K.A., Koob, M.D. and Rebay, I. (2004) The spinocerebellar ataxia 8 noncoding RNA causes neurodegeneration and associates with staufen in *Drosophila*. *Curr. Biol.*, **14**, 302–308.

Neumann, M., Sampathu, D.M., Kwong, L.K., Truax, A.C., Micsenyi, M.C., Chou, T.T., Bruce, J., Schuck, T., Grossman, M., Clark, C.M., *et al.* (2006) Ubiquitinated TDP-43 in frontotemporal lobar degeneration and amyotrophic lateral sclerosis. *Science*, **314**, 130-133.

Ng, S.C., Perkins, L.A., Conboy, G., Perrimon, N. and Fishman, M.C. (1989) A *Drosophila* gene expressed in the embryonic CNS shares one conserved domain with the mammalian GAP-43. *Development*, **105**, 629-638.

Nishimura, Y., Hayashi, M., Inada, H. and Tanaka, T. (1999) Molecular cloning and characterization of mammalian homologues of vesicle-associated membrane protein-associated (VAMP-associated) proteins. *Biochem. Biophys. Res. Commun.*, **254**, 21-26.

Nishimura, I., Yang, Y. and Lu, B. (2004) PAR-1 kinase plays an initiator role in a temporally ordered phosphorylation process that confers tau toxicity in *Drosophila*. *Cell,* **116**, 671-682.

Nishimura, A.L., Mitne-Neto, M., Silva, H.C., Oliveira, J.R., Vainzof, M. and Zatz, M (2004a) A novel locus for late onset amyotrophic lateral sclerosis/motor neurone disease variant at 20q13. *J. Med. Genet.*, **41**, 315-320.

Nishimura, A.L., Mitne-Neto, M., Silva, H.C., Richieri-Costa, A., Middleton, S., Cascio, D., Kok, F., Oliveira, J.R., Gillingwater, T., Webb, J. *et al.* (2004) A mutation in the vesicle-trafficking protein VAPB causes late-onset spinal muscular atrophy and amyotrophic lateral
sclerosis. *Am. J. Hum. Genet.*, **75**, 822-831.

Niwa, J., Ishigaki, S., Hishikawa, N., Yamamoto, M., Doyu, M., Murata, S., Tanaka, K., Taniguchi, N. and Sobue, G. (2002) Dorfin ubiquitylates mutant SOD1 and prevents mutant SOD1-mediated neurotoxicity. *J. Biol. Chem.*, **277**, 36793–36798.

Noble, W., Olm, V., Takata, K., Casey, E., Mary, O., Meyerson, J., Gaynor, K., LaFrancois, J., Wang, J., Kondo, T., *et al.* (2003) Cdk5 is a key factor in tau aggregation and tangle formation *in vivo*. *Neuron*, **38**, 555–556.

Oldham, S., Stocker, H., Laffargue, M., Wittwer, F., Wymann, M. and Hafen, E. (2002) The *Drosophila* insulin/IGF receptor controls growth and size by modulating PtdInsP(3) levels. *Development,* **129**, 4103-4109.

Palop, J. J., Chin, J. and Mucke, L. (2006) A network dysfunction perspective on neurodegenerative diseases. *Nature*, **443**, 768-773.

Pandey, U.B., Nie, Z., Batlevi, Y., McCray, B.A., Ritson, G.P., Nedelsky, N.B., Schwartz, S.L., DiProspero, N.A., Knight, M.A., Schuldiner, O., *et al.* (2007) HDAC6 rescues neurodegeneration and provides an essential link between autophagy and the UPS. *Nature,* **447**, 859-863.

Paricio, N., Feiguin, F., Boutros, M., Eaton, S. and Mlodzik, M. (1999) The *Drosophila* STE20-like kinase misshapen is required downstream of the frizzled receptor in planar polarity signaling. *EMBO J.*, **18**, 4669-4678.

Park, J., Lee, S.B., Lee, S., Kim, Y., Song, S., Kim, S., Bae, E., Kim, J., Shong, M., Kim, J.M. *et al.* (2006) Mitochondrial dysfunction in *Drosophila* PINK1 mutants is complemented by parkin. *Nature*, **441**, 1157-1161.

Parks, A.L., Cook, K.R., Belvin, M., Dompe, N.A., Fawcett, R., Huppert, K., Tan, L.R. and Winter, C.G. (2004) Systematic generation of high-resolution deletion coverage of the *Drosophila* melanogaster genome. *Nat Genet.*, **36**, 288-292.

Pasinelli, P., Houseweart, M. K., Brown Jr, R. H. and Cleveland, D. W. (2000) Caspase-1 and -3 are sequentially activated in motor neuron death in Cu,Zn superoxide dismutase-mediated familial amyotrophic lateral sclerosis. *Proc. Natl Acad. Sci. USA.*, **97**, 13901-13906.

Pasinelli, P., Belford, M.E., Lennon, N., Bacskai, B.J., Hyman, B.T., Trotti, D. and Brown Jr., R.H. (2004) Amyotrophic lateral sclerosis-associated SOD1 mutant proteins bind and aggregate with Bcl-2 in spinal cord mitochondria. *Neuron*, **43**, 19-30.

Pawlu, C., DiAntonio, A. and Heckmann, M. (2004) Postfusional control of quantal current shape. *Neuron,* **42**, 607-618.

Pennetta, G., Hiesinger, P.R., Fabian-Fine, R., Meinertzhagen, I.A. and Bellen, H.J. (2002) *Drosophila* VAP-33A directs bouton formation at neuromuscular junctions in

a dosage-dependent manner. *Neuron*, **35**, 291-306.

Periquet, M., Fulga, T., Myllykangas, L., Schlossmacher, M.G. And Feany, M.B. (2007) Aggregated alpha-synuclein mediates dopaminergic neurotoxicity in vivo. *J. Neurosci.*, **27**, 3338-3346.

Perry, R. J. and Ridgway, N. D. (2006) Oxysterol-binding protein and vesicleassociated membrane protein-associated protein are required for sterol-dependent activation of the ceramide transport protein. *Mol. Biol. Cell*, **17**, 2604-2616.

Pesah, Y., Burgess, H., Middlebrooks, B., Ronningen, K., Prosser, J., Tirunagaru, V., Zysk, J. and Mardon, G. (2005) Whole-mount analysis reveals normal numbers of dopaminergic neurons following misexpression of α-Synuclein in *Drosophila*. *Genesis*, **41**, 154-159.

Pesah, Y., Pham, T., Burgess, H., Middlebrooks, B., Verstreken, P., Zhou, Y., Harding, M., Bellen, H. and Mardon, G. (2004) *Drosophila parkin* mutants have decreased mass and cell size and increased sensitivity to oxygen radical stress. *Development*, **131**, 2183-2194.

Petersen, S. A., Fetter, R. D., Noordermeer, J. N., Goodman, C. S. and DiAntonio, A. (1997) Genetic analysis of glutamate receptors in *Drosophila* reveals a retrograde signal regulating presynaptic transmitter release. *Neuron*, **19**, 1237-1248.

Pinter, M. J., Waldeck, R. F., Cope, T. C. and Cork, L. C. (1997) Effects of 4-aminopyridine on muscle and motor unit force in canine motor neuron disease. *J. Neurosci.*, ***17***, 4500-4507.

Polymeropoulos, M.H., Lavedan, C., Leroy, E., Ide, S.E., Dehejia, A., Dutra, A., Pike, B., Root, H., Rubenstein, J., Boyer, R. *et al.* (1997) Mutation in the alpha-synuclein gene identified in families with Parkinson's disease. *Science*, ***276***, 2045–2047.

Protzer, C.E., Wech, I., Nagel, A.C, (2008) Hairless induces cell death by downregulation of EGFR signalling activity. *J. Cell Sci.*, **121**, 3167-3176.

Puls, I., Jonnakuty, C., LaMonte, B.H., Holzbaur, E.L., Tokito, M., Mann, E., Floeter, M.K., Bidus, K., Drayna, D., Oh, S.J., *et al.* (2003) Mutant dynactin in motor neuron disease. *Nat. Genet.*, **33**, 455-456.

Qin, G., Schwarz, T., Kittel, R.J., Schmid, A., Rasse, T.M., Kappei, D., Ponimaskin, E., Heckmann, M. and Sigrist, S.J. (2005) Four different subunits are essential for expressing the synaptic glutamate receptor at neuromuscular junctions of *Drosophila*. *J. Neurosci.*, **25**, 3209-3218.

Radhakrishnan, A., Sun, L.P., Kwon, H.J., Brown, M.S. and Goldstein, J.L. (2004) Direct Binding of Cholesterol to the Purified Membrane Region of SCAP; Mechanism for a Sterol-Sensing Domain. *Mol. Cell*, **15**, 259-268.

Ratnaparkhi, A., Lawless, G., Schweizer, F., Golshani, P. and Jackson, G. (2008) A *Drosophila* model of ALS: Human ALS-associated mutation in VAP33A suggests a dominant negative mechanism. *PLoS ONE,* **3**, 1-14.

Reaume, A.G., Elliott, J.L., Hoffman, E.K., Kowall, N.W., Ferrante, R.J., Siwek, D.F., Wilcox, H.M., Flood, D.G., Beal, M.F., Brown Jr, R.H., *et al.* (1996) Motor neurons in Cu/Zn superoxide dismutase-deficient mice develop normally but exhibit enhanced cell death after axonal injury. *Nat Genet.*, **13**, 43-47

Reiter, L.T., Potocki, L., Chien, S., Gribskov, M. and Bier, E. (2001). A systematic analysis of human disease-associated gene sequences in *Drosophila* melanogaster. Genome Res. 11:1114–25.

Ridgway, N.D., Dawson, P.A., Ho, Y.K., Brown, M.S. and Goldstein, J.L. (1992) Translocation of oxysterol binding protein to Golgi apparatus triggered by ligand binding. *J. Cell Biol.*, **116**, 307-319.

Ridgway, N.D. (1995) 25-Hydroxycholesterol stimulates sphingomyelin synthesis in Chinese hamster ovary cells. *J. Lipid Res.*, **36**, 1345-1358.

Ridgway, N.D., Lagace, T.A., Cook, H.W. and Byers, D.M. (1998) Differential effects of sphingomyelin hydrolysis and cholesterol transport on oxysterol-binding protein phosphorylation and Golgi localization. *J. Biol. Chem.*, **273**, 31621-31628.

Ridgway, N.D. (2000). Interactions between metabolism and intracellular distribution of cholesterol and sphingomyelin. *Biochim. Biophys. Acta*, ***1484,*** 129-141.

Roberts, T.M. and Stewart, M. (1995) Nematode sperm locomotion. *Curr. Opin. Cell Biol.*, **7**, 13-17.

Rosen, D.R., Siddique, T., Patterson, D., Figlewicz, D.A., Sapp, P., Hentati, A., Donaldson, D., Goto, J., O'Regan, J.P., Deng, H.X. *et al.* (1993) Mutations in Cu/Zn superoxide dismutase gene are associated with familial amyotrophic lateral sclerosis. *Nature*, **362**, 59–62.

Roselli, F., Tirard, M., Lu, J., Hutzler, P., Lamberti, P., Livrea, P., Morabito, M. and Almeida, O.F. (2005) Soluble beta-amyloid1-40 induces NMDA-dependent degradation of postsynaptic density-95 at glutamatergic synapses. *J. Neurosci.*, **25**, 11061-11070.

Rothstein, J. D. Tsai, G., Kuncl, R.W., Clawson, L., Cornblath, D.R., Drachman,

D.B., Pestronk, A., Stauch, B.L. and Coyle, J.T. (1990) Abnormal excitatory amino acid metabolism in amyotrophic lateral sclerosis. *Ann. Neurol.*, **28**, 18-25.

Rothstein, J.D., Dykes-Hoberg, M., Pardo, C.A., Bristol, L.A., Jin, L., Kuncl, R.W., Kanai, Y., Hediger, M.A., Wang, Y., Schielke, J.P., *et al.* (1996) Knockout of glutamate transporters reveals a major role for astroglial transport in excitotoxicity and clearance of glutamate. *Neuron*, **16**, 675-686.

Rubin,G.M., Yandell,M.D., Wortman,J.R., Gabor Miklos,G.L., Nelson,C.R., Hariharan,I.K., Fortini,M.E., Li,P.W., Apweiler,R., Fleischmann,W. *et al.* (2000) Comparative genomics of the eukaryotes. *Science*, **287**, 2204–2215.

Ryder, E., Blows, F., Ashburner, M., Bautista-Llacer, R., Coulson, D., Drummond, J., Webster, J., Gubb, D., Gunton, N., Johnson, G., *et al.* (2004) The DrosDel collection: a set of P-element insertions for generating custom chromosomal aberrations in *Drosophila* melanogaster. *Genetics,* **167**, 797-813.

Ryder, E., Ashburner, M., Bautista-Llacer, R., Drummond, J., Webster, J., Johnson, G., Morley, T., Chan, Y.S., Blows, F., Coulson, D., *et al.* (2007) The DrosDel deletion collection: a *Drosophila* genomewide chromosomal deficiency resource. *Genetics*, **177**, 615-629.

Sang, T.K., Li, C., Liu, W., Rodriguez, A., Abrams, J.M., Zipursky, S.L. and Jackson, G.R. (2005) Inactivation of *Drosophila* Apaf-1 related killer suppresses formation of polyglutamine aggregates and blocks polyglutamine pathogenesis. *Hum. Mol. Genet.*, **14**, 357-372.

Sasaki, S., Warita, H., Murakami, T., Abe, K., and Iwata, M. (2004). Ultrastructural study of mitochondria in the spinal cord of transgenic mice with a G93A mutant SOD1 gene. *Acta Neuropathol. (Berl.)*, **107**, 461-474.

Sasaki, S., Warita, H., Abe, K. and Iwata, M. (2005) Impairment of axonal transport in the axon hillock and the initial segment of anterior horn neurons in transgenic mice with a G93A mutant SOD1 gene. *Acta Neuropathol. (Berl.),* **100**, 48-56.

Schulze, K., Broadie, K., Perin, M. and Bellen, H.J. (1995) Genetic and electrophysiological studies of *Drosophila* syntaxin-1A demonstrate its role in nonneuronal secretion and neurotransmission. *Cell,* **80**, 311-320.

Schuster, C. M., Ultsch, A., Schloss, P., Cox, J. A., Schmitt, B. and Betz, H. (1991) Molecular cloning of an invertebrate glutamate receptor subunit expressed in *Drosophila* muscle. *Science*, **254**, 112-114.

Shamah, S.M., Lin, M.Z., Goldberg, J.L., Estrach, S., Sahin, M., Hu, L., Bazalakova, M., Neve, R.L., Corfas, G., Debant, A. and Greenberg, M.E. (2001) EphA receptors regulate growth cone dynamics through the novel guanine nucleotide exchange

factor Ephexin. *Cell*, **105**, 233-244.

Shaw, B. F., Lelie, H. L., Durazo, A., Nersissian, A. M., Xu, G., Chan, P. K., Gralla, E. B., Tiwari, A. J., Hayward, L. J., Borchelt, D. R., *et al.* (2008) Detergent-insoluble aggregates associated with amyotrophic lateral sclerosis in transgenic mice contain primarily full-length, unmodified superoxide dismutase-1. *J. Biol. Chem.*, **283**, 8340-8350.

Shinder, G.A., Lacourse, M.C., Minotti, S. and Durham, H.D. (2001) Mutant Cu/Znsuperoxide dismutase proteins have altered solubility and interact with heat shock/stress proteins in models of amyotrophic lateral sclerosis. *J. Biol. Chem.*, **276**, 12791-12796.

Shulman, J.M. and Feany, M.B. (2003) Genetic modifiers of tauopathy in *Drosophila. Genetics*, **165,** 1233-1242.

Siklos, L., Engelhardt, J., Harati, Y., Smith, R.G., Joo, F. and Appel, S.H. (1996) Ultrastructural evidence for altered calcium in motor nerve terminals in amyotrophic lateral sclerosis. *Ann. Neurol.*, **39**, 203-216.

Singleton, A.B., Farrer, M., Johnson, J., Singleton, A., Hague, S., Kachergus, J., Hulihan, M., Peuralinna, T., Dutra, A., Nussbaum, R. *et al.* (2003) Alpha-synuclein locus triplication causes Parkinson's disease. *Science*, **302**, 841.

Skehel, P.A., Martin, K.C., Kandel, E.R. and Bartsch, D. (1995) A VAMP-binding protein from Aplysia required for neurotransmitter release. *Science*, **269**, 1580-1583.

Skehel, P.A., Fabian-Fine, R. and Kandel, E.R. (2000) Mouse VAP33 is associated with the endoplasmic reticulum and microtubules. *Proc. Natl. Acad. Sci. USA.*, **97**, 1101-1106.

Sobue, G., Hashizume, Y., Yasuda, T., Mukai, E., Kumagai, T., Mitsuma, T. and Trojanowski, J.Q.(1990) Phosphorylated high molecular weight neurofilament protein in lower motor neurons in amyotrophic lateral sclerosis and other neurodegenerative diseases involving ventral horn cells. *Acta Neuropathol.*, **79**, 402-408.

Song, B.L. and DeBose-Boyd, R.A. (2004) Ubiquitination of 3-hydroxy-3-methylglutaryl-CoA reductase in permeabilized cells mediated by cytosolic E1 and a putative membrane-bound ubiquitin ligase. *J. Biol. Chem.*, **279**, 28798-28806.

Sontag, E., Nunbhakdi-Craig ,V., Lee, G., Brandt, R., Kamibayashi, C., Kuret, J., White III, C.L., Mumby, M.C. And Bloom, G.S. (1999) Molecular interactions among protein phosphatase 2A, tau, and microtubules. Implications for the regulation of tau phosphorylation and the development of tauopathies. *J Biol Chem.*, **274**, 25490-25498.

Soussan, L., Burakov, D., Daniels, M.P., Toister-Achituv, M., Porat, A., Yarden, Y. and Elazar, Z. (1999) ERG30, a VAP-33-related protein, functions in protein transport mediated by COPI vesicles. *J. Cell. Biol.*, **146**, 301-311.

Spillantini, M.G., Crowther, R.A., Jakes, R., Hasegawa, M., and Goedert, M. (1998) α-synuclein in filamentous inclusions of Lewy bodies from Parkinson's disease and dementia with Lewy bodies. *Proc. Natl. Acad. Sci. USA.*, **95**, 6469–6473.

Spreux-Varoquaux, O., Bensimon, G., Lacomblez, L., Salachas, F., Pradat, P.F., Le Forestier, N., Marouan, A., Dib, M. and Meininger, V. (2002) Glutamate levels in cerebrospinal fluid in amyotrophic lateral sclerosis: a reappraisal using a new HPLC method with coulometric detection in a large cohort of patients. J. *Neurol. Sci.*, **193**, 73-78.

Sreedharan, J., Blair, I.P., Tripathi, V.B., Hu, X., Vance, C., Rogelj, B., Ackerley, S., Durnall, J.C., Williams, K.L., Buratti, E., *et al.* (2008) TDP-43 mutations in familial and sporadic amyotrophic lateral sclerosis. *Science*, *319*, 1668-1672.

Steffan, J.S., Bodai, L., Pallos, J., Poelman, M., McCampbell, A., Apostol, B.L., Kazantsev, A., Schmidt, E., Zhu, Y.Z., Greenwald, M. *et al.* (2001) Histone deacetylase inhibitors arrest polyglutamine-dependent neurodegeneration in *Drosophila*. *Nature*, **413**, 739-743.

St Johnston, D. (2002) The Art and Design of Genetic Screens: *Drosophila Melanogaster*. *Nat. Rev. Gen.*, **3**, 176-188.

St Pierre, S.E., Galindo, M.I., Couso, J.P. and Thor, S. (2002) Control of *Drosophila* imaginal disc development by rotund and roughened eye: differentially expressed transcripts of the same gene encoding functionally distinct zinc finger proteins. *Development*, **129**, 1273-1281.

Strittmatter, S.M., Fankhauser, C., Huang, P.L., Mashimo, H. and Fishman, M.C. (1995) Neuronal pathfinding is abnormal in mice lacking the neuronal growth cone protein GAP-43. *Cell*, **80**, 445-452.

Strong, M.J., Sopper, M.M., Crow, J.P., Strong, W.L. and Beckman, J.S. (1998) Nitration of the low molecular weight neurofilament is equivalent in sporadic amyotrophic lateral sclerosis and control cervical spinal cord. *Biochem. Biophys. Res. Commun.*, **248,**157-164.

Struhl, G. and Greenwald, I. (1999) Presenilin is required for activity and nuclear access of Notch in *Drosophila*. *Nature*, **398**, 522-525.

Subramaniam, J.R., Lyons, W.E., Liu, J., Bartnikas, T.B., Rothstein, J., Price, D.L., Cleveland, D.W., Gitlin, J.D. and Wong, P.C. (2002) Mutant SOD1 causes motor neuron disease independent of copper chaperone-mediated copper loading. *Nat.*

Neurosci., **5,** 301-307

Suraweera, A., Becherel, O.J., Chen, P., Rundle, N., Woods, R., Nakamura, J., Gatei, M., Criscuolo, C., Filla, A., Chessa, L., *et al.* (2007) Senataxin defective in ataxia oculomotor apraxia type 2, is involved in the defense against oxidative DNA damage. *J. Cell Biol.*, 177, 969-979.

Suraweera, A., Lim, Y.C., Woods, R., Birrell, G.W., Nasim, T., Becherel, O.J. and Lavin, M.F. (2009) Functional role for senataxin, defective in ataxia oculomotor apraxia type 2, in transcriptional regulation. *Hum. Mol. Genet.*, Advance Access Online Publication.

Suzuki, T., Ito, J., Takagi, H., Saitoh, F., Nawa, H. and Shimizu, H. (2001) Biochemical evidence for localization of AMPA-type glutamate receptor subunits in the dendritic raft. *Brain Res. Mol. Brain Res.*, **89**, 20-28.

Suzuki, H., Kanekura, K., Levine, T.P., Kohno, K., Olkkonen, V.M., Aiso, S. and Matsuoka, M. (2009) ALS-linked P56S-VAPB, an aggregated loss-of-function mutant of VAPB, predisposes motor neurons to ER stress-related death by inducing aggregation of co-expressed wild-type VAPB. *J. Neurochem.*, **108**, 973-985.

Takeyama K, Ito S, Yamamoto A, Tanimoto H, Furutani T, Kanuka, H., Miura, M., Tabata, T. and Kato, S. (2002) Androgen-dependent neurodegeneration by polyglutamine-expanded human androgen receptor in *Drosophila*. *Neuron*, **35**, 855–864.

Talbot, K. (2002) Motor neurone disease. *Postgrad. Med. J.*, **78**, 513–519.

Tanenbaum, S.B., Gorski, S.M., Rusconi, J.C. and Cagan, R.L. (2000) A screen for dominant modifiers of the irreC-rst cell death phenotype in the developing *Drosophila* retina. *Genetics*, **156**, 205-217.

Tanzi, R.E. and Bertram, L. (2005) Twenty years of the Alzheimer's disease amyloid hypothesis: a genetic perspective. *Cell*, **120**, 545–555.

Taylor, F.R. and Kandutsch, A.A. (1985) Oxysterol binding protein. *Chem. Phys. Lipids.*, **38**, 187-194.

Taylor, J.P., Hardy, J. and Fischbeck, K.H. (2002) Toxic proteins in neurodegenerative disease. *Science*, **296**, 1991-1995.

Taylor, J.P., Tanaka, F., Robitschek, J., Sandoval, C.M., Taye, A., Markovic-Plese, S. and Fischbeck, K.H. (2003) Aggresomes protect cells by enhancing the degradation of toxic polyglutamine-containing protein. *Hum. Mol. Genet.*, **12**, 749-757.

Teuchert, M., Fischer, D., Schwalenstoecker, B., Habisch, H.J., Bockers, T.M. and Ludolph, A.C. (2006) A dynein mutation attenuates motor neuron degeneration in

SOD1(G93A) mice. *Exp. Neurol.*, **198**, 271-274.

Teuling, E., Ahmed, S., Haasdijk, E., Demmers, J., Steinmetz, M.O., Akhmanova, A., Jaarsma, D. and Hoogenraad, C.C. (2007) Motor neuron diseaseassociated mutant vesicle-associated membrane protein-associated protein (VAP) B recruits wild-type VAPs into endoplasmic reticulum-derived tubular aggregates. *J. Neurosci.*, *27*, 9801-9815.

Torroja, L., Packard, M., Gorczyca, M., White, K. and Budnik, V. (1999) The *Drosophila* beta-amyloid precursor protein homolog promotes synapse differentiation at the neuromuscular junction. *J. Neurosci.*, **19**, 7793-7803.

Tsuda, H., Han, S.M., Yang, Y., Tong, C., Lin, Y.Q., Mohan, K., Haueter, C., Zoghbi, A., Harati, Y., Kwan, J., *et al.* (2008) The Amyotrophic Lateral Sclerosis 8 protein VAPB is cleaved, secreted, and acts as a ligand for Eph receptors. *Cell*, **133**, 963-977.

Valente, E.M., Abou-Sleiman, P.M., Caputo, V., Muqit, M.M., Harvey, K., Gispert, S., Ali, Z., Del Turco, D., Bentivoglio, A. R., Healy, D. G., *et al.* (2004) Hereditary early-onset Parkinson's disease caused by mutations in PINK1. *Science*, **304**, 1158-1160.

Vance, C., Rogelj, B., Hortobágyi, T., De Vos, K.J., Nishimura, A.G., Sreedharan, J., Hu, J., Smith, B., Ruddy, D., Wright, P., *et al.* (2009) Mutations in FUS, an RNA processing protein, cause familial amyotrophic lateral sclerosis type 6. *Science*, **323**, 1208-1211.

Van Deerlin, V.M., Leverenz, J.B., Bekris. L.M., Bird, T.D., Yuan, W., Elman. L.B., Clay, D., Wood, E.M., Chen-Plotkin, A.S., Martinez-Lage, M., *et al.* (2008) TARDBP mutations in amyotrophic lateral sclerosis with TDP-43 neuropathology: a genetic and histopathological analysis. *Lancet Neurol.* 7, 409-416.

Venkateswaran, A., Laffitte, B.A., Joseph, S.B., Mak, P.A., Wilpitz, D.C., Edwards, P.A. and Tontonoz, P. (2000) Control of cellular cholesterol efflux by the nuclear oxysterol receptor LXR alpha. *Proc. Natl. Acad. Sci. USA.*, **97**, 12097-12102.

Venken, K.J. and Bellen, H.J. (2005) Emerging technologies for gene manipulation in *Drosophila melanogaster*, *Nat. Rev. Genet.*, **6**, 167-178.

Vidal, M., Warner, S., Read, R.D. and Cagan, R. (2007) Differing Src signaling levels have distinct outcomes in *Drosophila*. *Cancer Res.*, **67**, 10278-10285.
Vukosavic, S., Stefanis, L., Jackson-Lewis, V., Guegan, C., Romero, N., Chen, C., Dubois-Dauphin, M. and Przedborski, S. (2000) Delaying caspase activation by Bcl-2: a clue to disease retardation in a transgenic mouse model of amyotrophic lateral sclerosis. *J. Neurosci.*, **20,** 9119–9125.

Walsh, D. M. and Selkoe, D. J. (2004) Deciphering the molecular basis of memory

failure in Alzheimer's disease. *Neuron*, **44**, 181-193.

Wang, S.L., Hawkins, C.J., Yoo, S.J., Muller, H.A. and Hay, B.A. (1999) The *Drosophila* caspase inhibitor DIAP1 is essential for cell survival and is negatively regulated by HID. *Cell*, **98**, 453-463.

Wang, J.W., Soll, D.R. and Wu, C.F. (2002) Morphometric description of the wandering behavior in *Drosophila* larvae: a phenotypic analysis of K+ channel mutants. *J. Neurogenet.*, **16**, 45-63.

Wang, D., Qian, L., Xiong, H., Liu, J., Neckameyer, W.S., Oldham, S., Xia, K., Wang, J., Bodmer, R. and Zhang, Z. (2006) Antioxidants protect PINK1-dependent dopaminergic neurons in *Drosophila*. *Proc. Natl Acad. Sci. USA.*, **103**, 13520-13525.

Wang, X., Shaw, W.R., Tsang, H.T.H., Reid, E., O'Kane, C.J. (2007) *Drosophila* spichthyin inhibits BMP signaling and regulates synaptic growth and axonal microtubules. *Nat. Neurosci.*, **10**, 177-185.

Warrick, J.M. Chan, H.Y., Gray-Board, G.L., Chai, Y., Paulson, H.L. and Bonini, N.M. (1999) Suppression of polyglutamine-mediated neurodegeneration in *Drosophila* by the molecular chaperone HSP70. *Nat. Genet.*, **23**, 425-428

Warrick, J.M., Paulson, H.L., Gray-Board, G.L., Bui, Q.T., Fischbeck, K.H., Pittman, R.N. and Bonini, N.M. (1998) Expanded polyglutamine protein forms nuclear inclusions and causes neural degeneration in *Drosophila*. *Cell*, **93**, 939-949.

Watson, M.R., Lagow, R.D., Xu, K., Zhang, B. and Bonini, N.M. (2008) A *Drosophila* model for amyotrophic lateral sclerosis reveals motor neuron damage by human SOD1. *J. Biol. Chem.*, **283**, 24972-24981.

Wei, H. C., Sanny, J., Shu, H., Baillie, D. L., Brill, J. A., Price, J. V. and Harden, N. (2003) The Sac1 lipid phosphatase regulates cell shape change and the JNK cascade during dorsal closure in *Drosophila*. *Curr. Biol.*, **13**, 1882-1887.

Weir, M.L., Klip, A. and Trimble, W.S. (1998) Identification of a human homologue of the vesicle-associated membrane protein (VAMP)-associated protein of 33 kDa (VAP-33): a broadly expressed protein that binds to VAMP. *Biochem. J.*, **333**, 247-251.

Weir, M.L., Xie,H., Klip,A. and Trimble,W.S. (2001) VAP-A binds promiscuously to both v- and tSNAREs. *Biochem. Biophys. Res. Commun.*, **286**, 616-621.

Weidemann, F.R., Winker, D., Kuznetsov, A.V., Bartels, C., Vielhaber, S., Feistner, H. and Kunz, H. (1998) Impairment of mitochondrial function in skeletal muscle of patients with amyotrophic lateral sclerosis. *J. Neurol. Sci.*, **156**, 65–72.

Weimbs, T., Low, S.H., Chapin, S.J., Mostov, K.E., Bucher, P. and Hofmann, K. (1997) A conserved domain is present in different families of vesicular fusion proteins: a new superfamily. *Proc Natl Acad Sci USA.*, **94**, 3046-3051.

Wiedau-Pazos, M., Goto, J.J., Rabizadeh, S., Gralla, E.B., Roe, J.A., Lee, M.K., Valentine, J.S. and Bredesen, D.E. (1996) Altered reactivity of superoxide dismutase in familial amyotrophic lateral sclerosis. *Science*, **271**, 515-518.

Williamson, T.L. and Cleveland, D.W. (1999) Slowing of axonal transport is a very early event in the toxicity of ALS-linked SOD1 mutants to motor neurons. *Nat. Neurosci.*, **2**, 50-56.

Williams, D.W., Tyrer, M. and Shepherd, D. (2000) Tau and tau reporters disrupt central projections of sensory neurons in *Drosophila. J. Comp. Neuro*l., **428**, 630-640.

Williamson, T.L., Bruijn, L.I., Zhu, Q., Anderson, K.L., Anderson, S.D., Julien, J.P. and Cleveland, D.W. (1998) Absence of neurofilaments reduces the selective vulnerability of motor neurons and slows disease caused by a amyotrophic lateral sclerosis-linked superoxide dismutase 1 mutant. *Proc. Natl. Acad. Sci. USA* ., **95**, 9631-9636.

Wittmann, C.W., Wszolek, M.F., Shulman, J.M., Salvaterra, P.M., Lewis, J., Huttôn, M. and Feany, M.B. (2001) Tauopathy in *Drosophila:* neurodegeneration without neurofibrillary tangles. *Science*, **293**, 711–714.

Wolff, T., Martin, K.A., Rubin, G.M. and Zipursky, S.L. (1997) The development of the *Drosophila* visual system. In Molecular and Cellular Approaches to Neuronal Development, W.M. Cowan, T.M. Jessell, and S.L. Zipursky, eds. (New York: Oxford University Press), pp. 474–508.

Wong, P.C., Pardo, C.A., Borchelt, D.R., Lee, M.K., Copeland, N.G., Jenkins, N.A., Sisodia, S.S., Cleveland, D.W., Price, D.L. (1995) An adverse property of a familial ALS-linked SOD1 mutation causes motor neuron disease characterized by vacuolar degeneration of mitochondria. *Neuron*, **14**, 1105-1116.

Wyles, J.P., McMaster, C.R. and Ridgway, N.D. (2002) VAMP-associated protein-A (VAP-A) interacts with the oxysterol binding protein (OSBP) to modify export from the endoplasmic reticulum. *J. Biol. Chem.*, **277**, 29908-29918.

Wyles, J.P. and Ridgway, N.D. (2004) VAMP-associated protein-A regulates partitioning of oxysterol-binding protein-related protein-9 between the endoplasmic reticulum and Golgi apparatus. *Exp. Cell. Res.*, **297**, 533-547.

Xu, Z., Cork, L.C., Griffin, J.W. and Cleveland, D.W. (1993) Increased expression of neurofilament subunit NF-L produces morphological alterations that resemble the

pathology of human motor neuron disease. *Cell*, **73**, 23-33.

Xu, Y., Liu, Y., Ridgway, N.D. and McMaster, C.R. (2001) Novel members of the human oxysterol-binding protein family bind phospholipids and regulate vesicle transport. *J. Biol. Chem.*, **276**, 18407-18414.

Yamaguchi, Y. and Pasquale. E.B. (2004) Eph receptors in the adult brain. *Curr. Opin. Neurobiol.*, **14**, 288-296.

Yamanaka, K., Vande Velde. C., Bertini, E., Boespflug-Tanguy, O. and Cleveland, D.W. (2003) Unstable mutants in the peripheral endosomal membrane component ALS2 cause early onset motor neuron disease. *Proc. Natl. Acad. Sci. USA.*, **100**, 16041-16046.

Yang, Y., Hentati, A., Deng, H.X., Dabbagh, O., Sasaki, T., Hirano, M., Hung, W.Y., Ouahchi, K., Yan, J., Azim, A.C., *et al.* (2001) The gene encoding alsin, a protein with three guanine-nucleotide exchange factor domains, is mutated in a form of recessive amyotrophic lateral sclerosis. *Nat. Genet.*, **29**, 160-165.

Yang, Y., Gehrke, S., Imai, Y., Huang, Z., Ouyang, Y., Wang, J.W., Yang, L., Beal, M.F., Vogel, H. and Lu, B. (2006) Mitochondrial pathology and muscle and dopaminergic neuron degeneration caused by inactivation of *Drosophila* Pink1 is rescued by Parkin. *Proc. Natl Acad. Sci. USA.*, **103**, 10793-10798.

Yoshimura, A., Fujii, R., Watanabe, Y., Okabe, S., Fukui, K. and Takumi, T. (2006) Myosin-Va facilitates the accumulation of mRNA/protein complex in dendritic spines. *Curr. Biol.*, **16**, 2345-2351.

Yoshiyama, Y., Higuchi, M., Zhang, B., Huang, S.M., Iwata, N., Saido, T.C., Maeda, J., Suhara, T., Trojanowski, J.Q. and Lee, V.M. (2007) Synapse loss and microglial activation precede tangles in a P301S tauopathy mouse model. *Neuron*, **53**, 337-351.

Zhang, S., Xu, L., Lee, J., and Xu, T. (2002) *Drosophila* atrophin homolog functions as a transcriptional corepressor in multiple developmental processes. *Cell*, 108, 45-56.

Zhang, Y., Guo, H., Kwan, H., Wang, J.W., Kosek, J. and Lu, B. (2007) PAR-1 kinase phosphorylates Dlg and regulates its postsynaptic targeting at the *Drosophila* neuromuscular junction. *Neuron*, **53**, 201-215.

Zhou, H., Cao, F., Wang, Z., Yu, Z.X., Nguyen, H.P., Evans, J., Li, S.H. and Li, X.J. (2003) Huntingtin forms toxic NH2-terminal fragment complexes that are promoted by the age-dependent decrease in proteasome activity. *J. Cell Biol.*, **163**, 109-118.

Zinsmaier, K.E., Eberle, K.K., Buchner, E., Walter, N. and Benzer, S. (1994) Paralysis and early death in cysteine string protein mutants of *Drosophila*. *Science*,

263, 977-980.

Zito, K., Parnas, D., Fetter, R.D., Isacoff, E.Y. and Goodman, C.S. (1999) Watching a synapse grow: noninvasive confocal imaging of synaptic growth in *Drosophila*. *Neuron,* **22**, 719-729.

Appendix

This appendix includes data from two projects currently ongoing in the lab that I am involved in. Also included is a published paper which contains data discussed in the main text of this thesis.

Appendix 1

The role of Sac1 in the pathogenesis of ALS

hVAPB (human VAMP-associated protein B) is the causative gene of a late onset autosomal dominant form of ALS in humans (ALS8, Nishimura *et al.*, 2004). We have generated a *Drosophila* model for ALS in which the neuronal overexpression of the mutant VAP protein recapitulates major hallmarks of the human disease including locomotion defects, neuronal death and aggregate formation. However, the molecular mechanism of ALS pathogenesis has not been defined. Here we show that *Sac1* is an interactor of *DVAP-33A*. Sac1 is a lipid phosphatase that is involved in a wide range of cellular processes such as regulating actin cytoskeleton organization, cell morphology and growth. Similar to DVAP-33A, the dosage of Sac1 also induces a change in number and size of boutons at the NMJ. Decrease in the levels of Sac1 induced the formation of large boutons and a decrease in their number while overexpression of Sac1 induces an increase in bouton number and a decrease in their sizes. Targeted knockdown of Sac1 in the eye by RNAi was shown to effectively induce rough eye phenotype and neuronal degeneration. Our results suggest that VAP and Sac1 are in the same molecular pathway and further studies into the role of Sac1 at the synapse and nervous system should shed new light on the molecular pathogenesis of ALS and should assist in the development of rational therapies for this progressive fatal disorder.

Human VAMP-associated protein B (*hVAPB*) is the causative gene of a late onset, autosomal dominant form of motor neuron disorders, including typical and atypical ALS and late-onset spinal muscular atrophy (Nishimura *et al.*, 2004). The pathogenic mutation causes a substitution of a Serine for a Proline at codon 56 (P56S) in a stretch of 16 amino acids that is very highly conserved from yeast to man in all VAP homologs.

Drosophila VAP-33 (DVAP-33A), the structural homologue of hVAPB in flies, regulates synaptic remodelling by affecting the size and the number of boutons at Neuromuscular Junctions (NMJs) (Pennetta *et al.*, 2002). We and others have produced a VAP-induced *Drosophila* model of ALS that recapitulates major hallmarks of the disease including locomotion defects, neuronal apoptosis, aggregate deposition and ultra-structural synaptic abnormalities (Chai *et al.*, 2008, Tsuda *et al.*, 2008, Ratnaparkhi *et al.*, 2008). However, the underlying molecular mechanism of ALS pathogenesis remains unknown.

A genome-wide yeast-two-hybrid screening in *Drosophila* identified Sac1 (Suppressor of Actin) as a potential VAP interacting protein (Giot *et al.*, 2003) and an independent yeast two hybrid study has confirmed that Sac1 is a protein interacting with DVAP-33A as well as with its human homologue hVAPB (K. Parry and G. Pennetta). Sac1 dephosphorylates several phosphatidylinositol (PtdIns) phosphates and acts as a lipid phosphatase localized at the ER which primarily regulates the synthesis and the turnover of PtdIns phosphates. PtdIns phosphates are important regulators of a wide range of cellular processes including cytoskeletal organization, vesicular trafficking, apoptosis, proliferation and differentiation (Hughes *et al.*, 2000).

In *Drosophila*, Sac1 is involved in cell-shape changes during gastrulation by acting on the Jun N-terminal kinase (JNK) MAPK signalling (Wei *et al.*, 2003). Loss of Sac1 function results in embryonic lethality due to the fact that Sac1 directs morphogenetic movements controlling dorsal closure during embryonic development (Wei *et al.* 2003a). The function of Sac1 in the nervous system, however, has not been previously addressed nor has the role of this protein in human neurodegeneration. Because Sac1 mutants die well before the development of the nervous system, it is imperative to circumvent the early lethality of null mutations. Hypomorphic allele of Sac1 has previously been generated (Wei *et al.*, 2003b), unfortunately this allele is lost and no longer available. We therefore decided to overcome the early lethality of null mutations by generating hypomorphic mutations

and dominant negative alleles. Hypomorphic mutations were generated by expressing the UAS-Sac1 transgene in a null background for the same gene. UAS transgenic lines have been reported to induce leaky expression of a gene even in the absence of Gal4 (Marrus and DiAntonio, 2004), hence the hypormorphic mutations may allow bypassing of the first developmental requirement for Sac1.

Studies performed in yeast indicate that the highly conserved -RXNCLDCLDRTN- motif represents the catalytic core of the Sac1 phosphatase (Hughes *et al.*, 2000 and references therein). The Sac1 dominant negative alleles was produced by generating transgenes containing either a deletion of this catalytic domain or an amino acid substitution where the first Aspartate (D) residue is changed to an Asparagine (N) at the catalytic domain of Sac1. The deletion and the amino acid substitution should disrupt the catalytic activity whilst maintaining the normal folding such that it successfully competes with the wild type protein. The expression of the dominant alleles will be driven in a temporal- and tissue-specific manner by using the UAS-Gal4 system (Brand and Perrimon, 1993) in a wild-type background. The effect of the dominant negative allele will be confirmed by observing similar phenotypes with a loss of function mutation by Sac1 RNAi.

Here we show that alterations in the dosage of Sac1 affects synaptic bouton number and size while decreasing the level of Sac1 in neurons also causes degeneration in the adult eye. Our yeast-two-hybrid studies confirmed that Sac1 is a protein interacting with DVAP-33A as well as with its human homologue hVAPB (data not shown). We found that decreasing the level of Sac1 in neurons caused an increase of the size of boutons at the synapse when compared to the wild-type synapses. The effect of Sac1 loss of function on synapses have also been confirmed using RNAi (Figure 1B). Conversely, overexpression of Sac1 led to a formation of filliform synapses and smaller bouton sizes. We also observed a change in number of bouton at these synapses that warrants detailed quantification (Figure 1). This effect on synaptic bouton size and numbers at the NMJ is similar to the effect of altering DVAP-33A dosage: *DVAP-33A* loss of function mutants caused an increase in bouton

size and a decrease in their numbers while overexpression of DVAP-33A caused filliform synapses and decrease in bouton size (Chai *et al.*, 2008). Thus the effect of Sac1 manipulation mirrors that of DVAP-33A. It has been proposed that DVAP-33A affects bouton budding at the NMJ by controlling membrane remodelling (Pennetta *et al.*, 2002). Interestingly, Sac1 was also shown to affect membrane remodelling during morphogenic movements of cells during dorsal closure (Wei *et al.* 2003a). These observations strongly suggest that Sac1 is not only a biochemical interactor of VAPB, but also control the same molecular pathways.

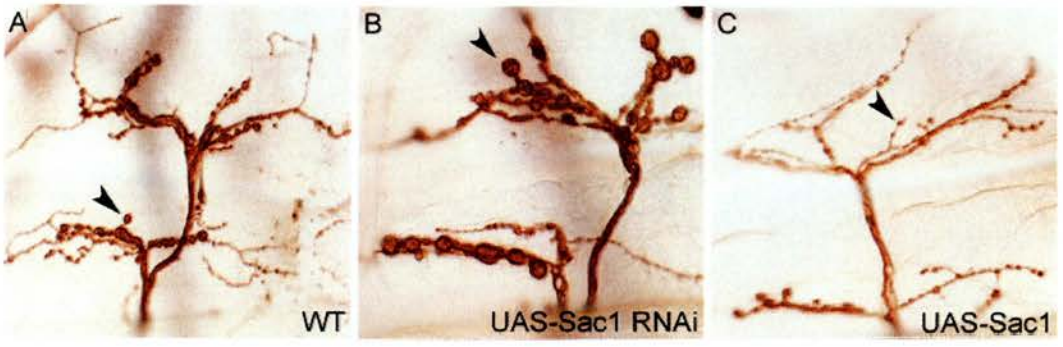

Figure 2. Changes in Sac1 levels cause morphological phenotype at the NMJ. Anti-HRP stainings of (A) WT larva NMJ (B) UAS-Sac1 RNAi line showing increased bouton size (arrowhead) and decreased bouton number. (C) Overexpression of Sac1 in NMJs caused formation of filliform synapses, small size (arrowhead) and large number of boutons. All pictures were taken at the same magnification. Muscles 12 and 13 were examined in this instance and *elav-Gal4* was used to drive both transgenes.

We next examined the effect of reducing Sac1 levels in the *Drosophila* adult eye and expression in the nervous system of an RNAi transgene specific for Sac1 shows a very dramatic phenotype. A decrease in the expression levels of Sac1 in the eye causes morphological defects, loss of pigmentation and extensive black, necrotic patches covering the majority of the eye surface (Figure 2). The severity of the phenotype depends on the strength of the transgene and it was consistently more severe in males than in females. This is due to the fact that the transgene is inserted on the X chromosome and therefore dosage-compensation will lead to a ~2 fold higher levels of transgene expression in males than in females.

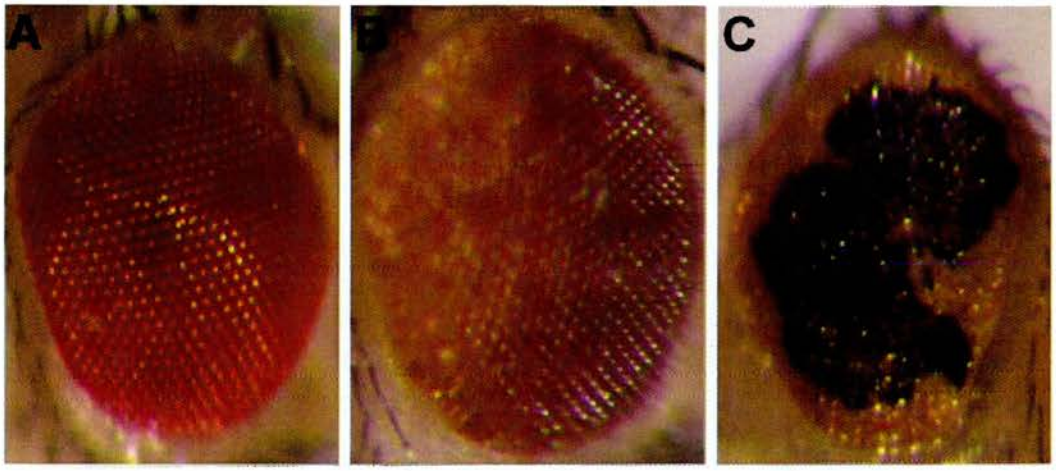

Figure 2. Decrease in Sac1 levels in the adult eye causes extensive neurodegeneration. Expression of an RNAi transgene specific for Sac1 driven by a pan-neural driver (*elav-Gal4*) in females (B) and males (C). In (A) the adult eye of a control fly is shown.

SEM (scanning electron microscope) analysis of male adult eyes shows that the whole eye of the male flies was affected by neurodegeneration (Figure 3A and B). Although the size of the eye stayed roughly the same, the neurodegeneration was represented by loss of photoreceptors, missing bristles and fused ommatidia (Figure 3C and D, arrowheads). This observed eye phenotype is specific and it is unlikely to be due to an effect on off-target genes as an independently generated, hypomorphic allele of Sac1 shows the same phenotype (Wei *et al.*, 2003b). However, this allele is lost and unavailable. Transgenic expression of Sac1 in the nervous system also induces progressive locomotion defects. Adult flies with an increased Sac1 expression in neurons exhibit fairly normal locomotion behaviour upon hatching but within a few days, they display a progressive reduction in motor activity, becoming sluggish and uncoordinated (data not shown).

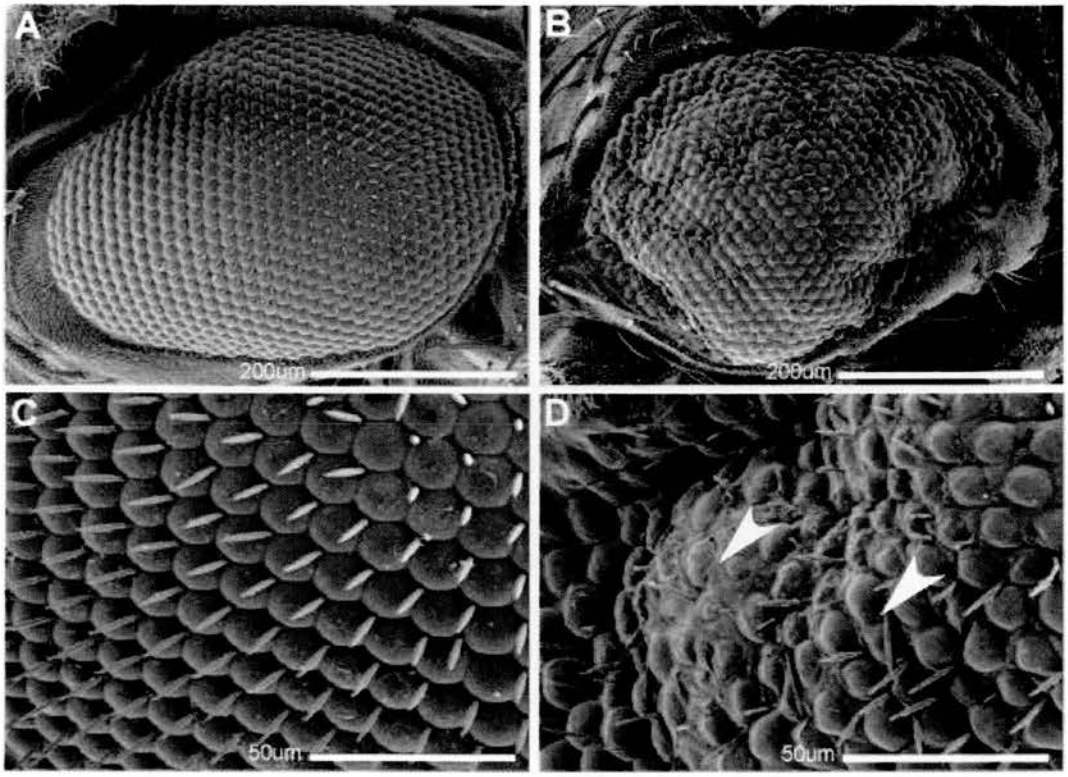

Figure 3. Decreasing the dosage of Sac1 causes necrotic patches in the *Drosophila* eye. (A) Wild type male fly showing normal eye composition, compared with (B) male fly eye expressing Sac1 RNAi with rough eye phenotype. (C) Pattern of ommatidia and hair bristles as seen in the wild-type as compared to (D) showing fused ommatidia and loss of bristles (arrowheads) as representation of necrotic patches. *elav-Gal4* was used to drive the RNAi transgene.

Finally, the reported biochemical interaction between DVAP-33A and Sac1 is likely to be functionally relevant as decreasing the dosage of Sac1 in a mutant background for DVAP-33A exacerbates the DVAP33A-induced morphological phenotype at the *Drosophila* NMJ (data not shown). We have shown that interactors of VAP that affects lipid metabolism such as Sac1 have similar phenotypes at the larval NMJ, strongly suggesting that VAP and Sac1 are in the same molecular pathway.

In yeast and cell culture systems, hVAPB has been reported to interact with several proteins affecting lipid metabolism including OSBP and CERT (Wyles *et al.*, 2002; Loewen and Levine, 2005; Loewen *et al.*, 2003; Kawano *et al.*, 2006). These

interactions are a conserved feature of many VAP proteins, supporting the idea that they can be functionally relevant. CERT is required for the transport of ceramide from the ER to the Golgi complex, a process critical for the synthesis and maintenance of normal sphingolipid levels (Acharya and Acharya, 2005, Yan and Olkkonen, 2008). OSBPs affect membrane dynamics and act as sterol sensors controlling local lipid composition (Legace *et al.*, 1999; Xu *et al.*, 2001). CERT and OSBPs are both lipid transfer proteins that share a common basic structure: they both localize to the ER by the binding of their FFAT (two phenylalanines in an acidic tract) motif with VAP proteins and to the Golgi apparatus through their pleckstrin homology (PH) domain which binds Phosphotidylinositol-4-phosphate (PtdIns(4)P) (Yan and Olkkonen, 2008). In particular, they both use PtdIns(4)P as part of a Golgi membrane localization code which also includes the PH domain and a small GTPase. (Acharya and Acharya, 2005, Yan and Olkkonen, 2008; Legace *et al.*, 1999; Xu *et al.*, 2001). Remarkably, Sac1 that is localized at the ER primarily regulates the pool of PtdIns(4)P (Wei *et al.*, 2003a).

These and other data reported above lead us to propose that VAPs function as scaffolding proteins that recruit to specific subcellular compartments several lipid regulators such as Sac1, CERT and OSPB to adjust local lipid composition and thereby to influence membrane remodelling, signal transduction and cytoskeletal dynamics. Interestingly, correlative evidence have indicated that disruption in lipid metabolism is a common trait of ALS pathogenesis (Dupuis *et al.*, 2008; Dupuis *et al.*, 2004; Marques *et al.*, 2006). Further experiments will also be done to address the biochemical interaction of Sac1 with pathogenic VAP and the ability of Sac1 to affect pathogenic VAP-induced hallmarks of ALS in the nervous system. These approaches will provide insight on the functional importance of the Sac1-VAP interaction, the effect of this interaction on the ability of the pathogenic VAP to induce a disease-related phenotype and the role of lipid metabolism in ALS pathogenesis.

Materials and Methods

Fly stocks, genetics and molecular techniques

UAS-Sac1 RNAi flies were obtained from Vienna *Drosophila* RNAi Center (VDRC), *elav-Gal4* was obtained from Bloomington *Drosophila* Stock Center.

The full length transcript for Sac1 was retrieved from the GH08349 clone obtained from BDGP (http://flybase.bio.indiana.edu/) and cloned into pUAST vector using BglII – Kpn1 linkers. The Aspartate to Asparagine amino acid change (D→N) and deletion of the -RXNCLDCLDRTN- catalytic motif was introduced into Sac1 cDNA cloned in pBluescript (G. Pennetta) by site-directed mutagenesis using QuickChange II XL Site Directed Mutagenesis Kit (Stratagene) and following manufacturer's instructions. The introduction of the D→N amino acid change and -RXNCLDCLDRTN- deletion were each verified by direct sequencing of the corresponding clone. The Sac1 cDNA carrying the amino acid change and -RXNCLDCLDRTN-motif deletion were each isolated by PCR amplification and cloned into independent pUAST vectors using BamHI - KpnI linkers.

All transgenic lines were established by following standard protocols (Spradling and Rubin, 1982). Basic molecular biology techniques were performed according to (Ausubel *et al.*, 1998).

Immunohistochemistry and confocal immunofluorescence

Stainings of third instar larval NMJs and analysis of the morphological phenotype was performed as described in (Pennetta *et al.*, 2002).

Scanning Electron Microscopy (SEM)

SEM was done according to methods described in the main text of the thesis.

References

Ausubel F.M., Brent R., Kingston R.E., Moore D.D., Seidman J.G., Smith A.J., Struhl K. Current Protocols in Molecular Biology (1998) New York: John Wiley & Son.

Brand, A.H., and Perrimon, N. (1993). Development *118*, 401-415.
Chai, A., Withers, J.P.J., Koh, Y.H., Parry, K., Zhang, B., Budnik, V., Pennetta, G. (2008). *Hum. Mol. Genet.* **17:** 266-280.
Dupuis, L., Oudart, H., René, F., Gonzalez de Aguilar, J.L., Loeffler, J.P. (2004). *Proc Natl Acad Sci U S A.* **101:** 11159-11164.
Dupuis, L., Corcia, P., Fergani, A., Gonzalez de Aguilar, J.L, Bonnefont-Rousselot, D., Bittar, R., *et al.* (2008). *Neurology.* **70:** 1004-1009.
Giot, L., Bader, J.S., Brouwer, C., Chaudhuri, A., Kuang, B., Li, Y., *et al.* (2003) *Science.* **302:** 1727-1736.
Hughes,W.E., Cooke, F.T., and Parker, P.J. (2000). *Biochem. J.* **350:** 337–352.
Kawano, M., Kumagai, K., Nishijima, M., Hanada, K. (2006). *J Biol Chem.* **281:** 30279-30288.
Lagace, T.A., Byers, D.M., Cook, H.W. and Ridgway, N.D. (1999). J. Lipid Res. **40:** 109–116.
Loewen, C.J., Roy, A., Levine, T.P. (2003). *EMBO J.* **22:** 2025-2035.
Loewen, C.J., Levine T.P. (2005). *J Biol Chem.* **280:** 14097-14104.
Marques, V.D., Barreira, A.A., Davis, M.B., Abou-Sleiman, P.M., Silva, W.A. Jr, Zago, M.A., *et al.* (2006). *Muscle Nerve.* **34:** 731-739.
Marrus, S.B. and DiAntonio, A. (2004). *Curr. Biol.* **14:** 924-931.
Nishimura, A.L., Mitne-Neto, M., Silva, H.C., Richieri-Costa, A., Middleton, S., Cascio, D., *et al.* (2004). *Am. J. Hum. Genet.* **75:** 822-831.
Pennetta, G., Hiesinger, P.R., Fabian-Fine, R., Meinertzhagen, I.A., Bellen, H.J. (2002). *Neuron.* **35:** 291-306.
Ratnaparkhi, A., Lawless, G.M., Schweizer, F.E., Golshani, P., Jackson, G.R. (2008). *PLoS ONE.* **3:** e2334.
Spradling A.C., Rubin G.M. (1982) **218:**341–347.
Tsuda, H., Han, S.M., Yang, Y., Tong, C., Lin, Y.Q., Mohan, K., *et al.* (2008). *Cell.* **133:** 963-977.
Wei, H.C., Sanny, J., Shu, H., Baillie, D.L., Brill, J.A., Price, J.V., Harden, (2003a). *Curr Biol.* **13:** 1882-1887.
Wei, H.C., Shu, H., Price, J.V. (2003b). *Genome.* **46:** 1049-1058.
Wyles, J.P., McMaster, C.R., Ridgway, N.D. (2002). *J Biol Chem.* **277**: 29908-29918.
Xu, Y., Liu, Y., Ridgway, N.D., and McMaster, C.R. (2001). *J. Biol. Chem.* ***276:*** 18407-18414.
Yan, D., Olkkonen, V.M. (2008). *Int Rev Cytol.* **265:** 253-285.

Acknowledgements

I thank G. Pennetta and K. Parry for designing the cloning strategy, performing the molecular cloning of pUAST-Sac1, pUAST-Sac1 -RXNCLDCLDRTN-deletion and pUAST-Sac1 D→N constructs and providing the yeast two hybrid data..

Appendix 2

The role of VAP and lipid binding proteins in ALS pathogenesis.

hVAPB (human VAMP-associated protein B) was shown to be the causative gene of a late onset, autosomal dominant form of motor neuron disorders, including typical and atypical ALS and late-onset spinal muscular atrophy in a large Brazilian kindred. The mutation was identified as a Proline to Serine substitution at position 56 (P56S) on the N-terminal domain of hVAPB that is very well conserved across species from yeast to man, suggesting an important functional role for this residue. VAP has been shown to interact with various lipid-binding, and lipid-transport proteins that contain FFAT motifs, such as oxysterol-binding protein (OSBP) and ceramide transport protein (CERT) which affect lipid metabolism. Correlative evidence have indicated that disruption in lipid metabolism is a common trait of ALS pathogenesis. However, the underlying molecular mechanism remains obscure. Here we report another mutation on hVAPB that causes typical ALS in an unrelated family. This new mutation causes a Threonine to Isoluecine at residue 46 at the N-terminal of the protein. Interestingly, T46 is part of a conserved core domain of VAP responsible for binding proteins containing FFAT motifs that are involved in lipid metabolism. We also show that transgenic expression of corresponding *Drosophila* pathogenic protein (DVAPT48I) induces aggregate formation, fragmentation of the ER and upregulation of Hsp70. Transgenic expression of DVAPT48I specifically in the eye also induces a degenerative eye phenotype. We also observe the colocalization of DVAP-33A with dCERT (*Drosophila* CERT) in larval tissues and in a cell culture system. We demonstrate hVAPB is indeed a causative gene of ALS and major hallmarks of ALS are recapitulated by transgenic expression of DVAPT48I. Moreover, our colocalization studies strongly suggest a physical interaction between VAP and dCERT and we are currently confirming these interactions for the fly proteins by using coimmunoprecipitation experiments and yeast-two hybrid assay. We are

confident that studying VAP interactors such as CERT and the Threonine to Isoleucine mutation of VAP will help us understand the role of lipid metabolism in the function of the nervous system and how lipid dysfunction can lead to motor neuron degeneration.

A mutation in human VAMP-associated protein B (hVAPB) in a large Brazilian family was found to be the causative gene for a late onset autosomal dominant form of ALS in humans (ALS8, Nishimura *et al.*, 2004). This mutation affects nine related families totalling 1500 individuals of which 200 suffer from motor neuron disorders including typical and atypical ALS and late-onset spinal muscular atrophy (Nishimura *et al.*, 2005). The mutation was identified as a Proline to Serine substitution at position 56 (P56S) in a stretch of highly conserved 16 amino acids on the N-terminal domain of the protein (Nishimura *et al.*, 2004).

Recently, another mutation in hVAPB was identified in an unrelated family affected by typical ALS. The mutation changes the Threonine at position 46 (T46) into an Isoleucine (Prof. Jacqueline de Belleroche, Imperial College London, personal communication). This amino acid also resides in the same stretch of 16 amino acids that is very well conserved in all VAP homologues including the fly homologue DVAP-33A (refer to the main body of the thesis). More interestingly, an extensive site-directed mutagenesis on Scs2, the homologue of VAP in yeast, showed that T46 is part of a conserved core domain of VAP responsible for binding proteins involved in lipid metabolism (Loewen and Levine, 2005). This finding is also supported by the analysis of the crystal structure of the N-terminal portion of VAP showing that this residue is indeed localized in the pocket of VAP responsible for interacting with the FFAT motif of lipid binding proteins (Kaiser *et al.*, 2005).

In yeast and cell culture experiments VAPs have been shown to interact with OSBPs and CERT, lipid binding proteins that contain a FFAT motif that associates with the ER via interaction with VAPs and a PH domain that targets both proteins to the Golgi (Wyles *et al.*, 2002, Loewen and Levine, 2005, Loewen *et al.*, 2003,

Kawano *et al.*, 2006). CERT is required for the transport of ceramide from the ER to the Golgi complex, a process critical for the synthesis and maintenance of normal sphingolipid levels (Acharya and Acharya, 2005, Yan and Olkkonen, 2008). OSBPs affect membrane dynamics and act as sterol sensors controlling local lipid composition. Sterols and sphingolipids are the major components of the lipid rafts and, in *Drosophila*, lipid rafts are positive regulators of metabotropic glutamate receptors at the synapse. They also regulate voltage-gated ion channel signalling and the synaptic vesicle cycling underlying neurotransmission (Rohrbough and Broadie, 2005).

Interestingly, it has been reported that the P56S substitution in hVAPB responsible for ALS in humans impairs the binding with FFAT motif (Teuling *et al.*, 2007). In addition, patients carrying the P56S pathogenic mutation in hVAPB also showed hyperlipidemia with a significant increase in cholesterol and triglyceride levels (Marques *et al.*, 2006). Studies have also revealed increased energy expenditure as a typical feature of ALS pathogenesis and that ALS patients were more likely to show evidence of hyperlipidemia relative to controls (Dupuis *et al.*, 2008). Reduced adiposity and hypermetabolism have also been reported in murine models of ALS and, more importantly, these animals exhibit remarkable neuroprotection and extended survival when fed with a high fat regimen (Dupuis *et al.*, 2004). Taken together, these data suggest dysfunction in lipid metabolism could play a part in motor neuron disease pathogenesis.

In an effort to assess the functional significance of the T46I amino acid change, we have generated transgenic flies expressing the pathogenic mutation. We found that transgenic expression of the mutant protein (DVAPT48I) recapitulates major hallmarks of the disease such as aggregate formation, ER fragmentation and upregulation of Hsp70 and neurodegeneration of the adult fly eye. Expression of DVAPT48I in neurons induces the formation of aggregates both in the neuronal cell bodies and the nerves of the larval motor system. In controls, DVAP staining appears dispersed throughout the cytoplasm of neuronal cell bodies while in DVAPT48I

transgenic brains, DVAP immunoreactivity is associated with intracellular aggregates of variable sizes. (Figure 1E-H). We also observed a disruption of ER morphology, transgenic expression of DVAP containing the pathogenic mutation induces ER fragmentation (Figure 1I-N) while an up-regulation of Hsp70 clearly indicates an accumulation of unfolded or aberrantly folded proteins. In control neuronal cell bodies, Hsp70 staining appears faint and uniformly distributed throughout the cell. In DVAPT48I transgenic neurons, Hsp70 is up-regulated and forms inclusions closely associated with DVAP aggregates (Figure 1O-T). Targeting the expression of the same protein in the adult nervous system and in particular in the eye also induces neurodegeneration characterized by smaller eyes, loss or aberrantly oriented bristles and fused ommatidia. While the adult *Drosophila* eye is composed of an ordered array of ommatidia and interspersed bristles, transgenic eyes appear smaller, with missing or aberrantly oriented bristles (black arrowhead) and fused ommatidia (white arrowhead) (Figure 1A-D).

Expression of tagged proteins in a cell culture system confirms that the aggregates are composed of both the mutant and the wild-type protein. DVAP normally distributes throughout the cytoplasm forming a reticulum as is expected for an ER-associated protein. A concomitant transfection with a plasmid expressing a myc-tagged mutant protein depletes the wildtype (wt) protein from its normal localization. We also demonstrate that the presence of the mutant protein is necessary for the formation of aggregates. Co-transfection of wt DVAP with the DVAPT48I depletes the wt protein and induces the formation of aggregates. These aggregate are also immunoreactive for the mutant protein indicating that the mutant protein is sequestered in these inclusions (Figure 2A-G).

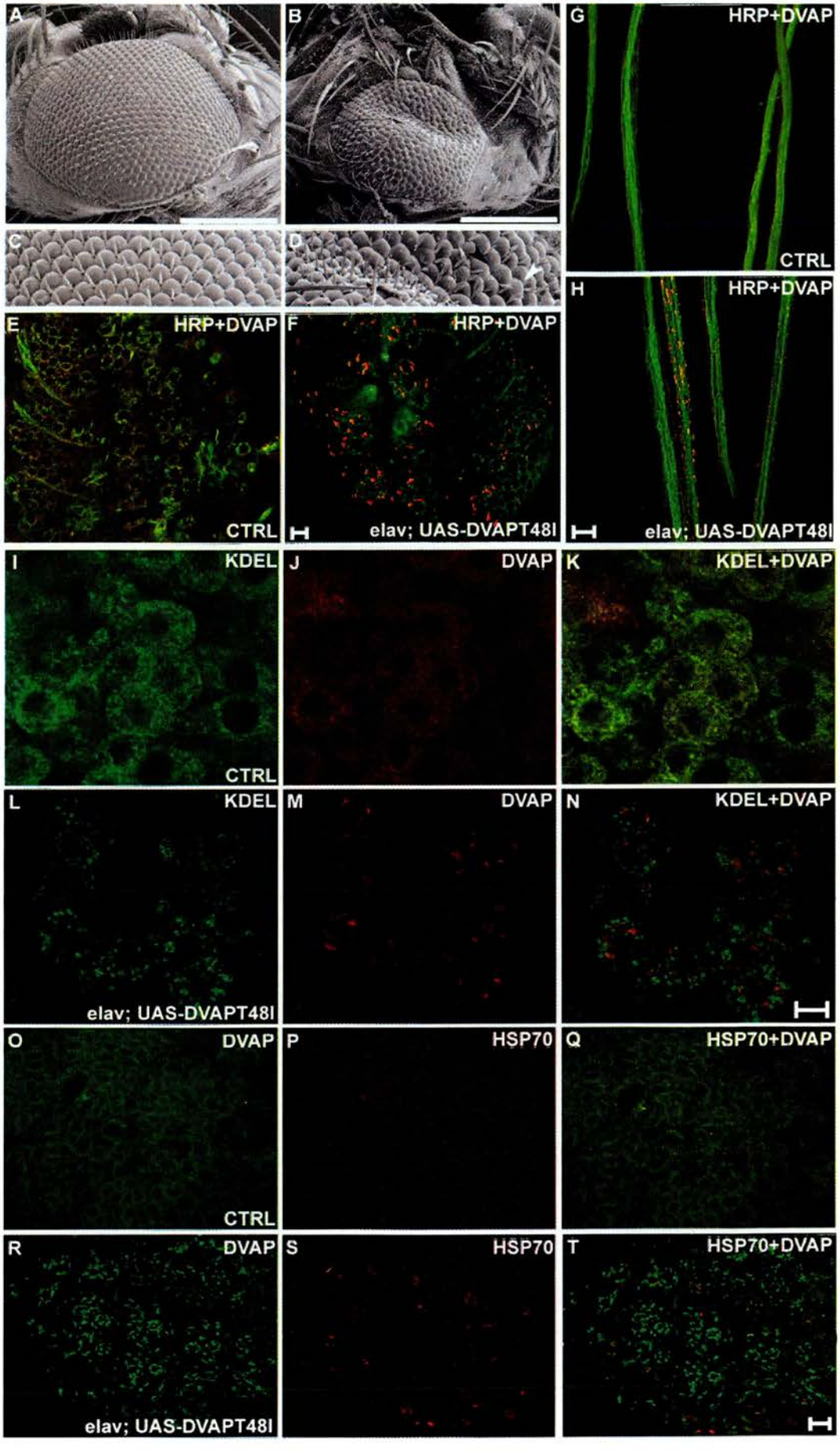
A
B
C
D
G
HRP+DVAP
CTRL
H
HRP+DVAP
E
HRP+DVAP
CTRL
F
HRP+DVAP
elav; UAS-DVAPT48I
elav; UAS-DVAPT48I
I
KDEL
CTRL
J
DVAP
K
KDEL+DVAP
L
KDEL
elav; UAS-DVAPT48I
M
DVAP
N
KDEL+DVAP
O
DVAP
CTRL
P
HSP70
Q
HSP70+DVAP
R
DVAP
elav; UAS-DVAPT48I
S
HSP70
T
HSP70+DVAP

Figure 1. Characterization of the disease in transgenic flies expressing DVAPT48I, the DVAP mutant allele that causes typical ALS in humans.
(A) Scanning electron micrographs of controls and (B) transgenic adult fly eyes expressing the *UAS-DVAPT48I* transgene under the control of the eye-specific driver, *eyeless-Gal4.* (C) and (D) are higher magnifications of (A) and (B) respectively. (E-H) Brains and nerve fibers of third instar larvae were stained with antibodies for DVAP (red) and with antibodies for the neuronal cell surface marker anti-HRP (green). (E) Brains of control larvae and (F) brains of larvae expressing transgenic DVAPT48I. Nerve fibers of control larvae (G) and transgenic larvae (H) were stained with anti-HRP (green) and anti-DVAP antibodies in red. In control nerves a faint and uniform staining for DVAP is observed while in transgenic nerves large aggregate strongly immunoreactive for DVAP accumulate along the nerves. In (I-K) control brains and (L-N) brains from transgenic larvae were stained with anti-DVAP antibodies (red) and with antibodies specific for KDEL, a Endoplasmic reticulum (ER) marker (green). (O-Q) Control brains stained with DVAP (green) and Hsp70 antibodies (red). (R-T) T48I transgenic brains stained with the same antibodies. Scale bars in (A) and (B) are 200μm. The other ones are 10μm.

Studies have shown that CERT interacts with VAPs via its FFAT motifs (Kawano *et al.*, 2006) and we also demonstrate that DVAP-33A colocalizes with dCERT (*Drosophila* CERT). Using antibodies specific for DVAP and dCERT we observe that DVAP and dCERT colocalize in larval tissues, including brains (data not shown). The colocalization studies have also been confirmed in a cell culture system as co-expressed tagged versions of DVAP and dCERT in COS7 cells show that DVAP and dCERT colocalize (Figure 2H-M). The extensive colocalization of dCERT and DVAP suggest that these proteins may interact and effects of the T46I and P56S mutations on the ability of VAP to bind CERT, the localization of CERT and lipid metabolism are currently being investigated.

Taken together the data reported in our study lead us to several important conclusions. Firstly, the identification of a new mutation in hVAPB confirms and reinforces the fact that hVAPB is indeed a causative gene of ALS. Secondly, the newly identified mutation in an unrelated family is the cause of the disease because major pathological hallmarks are recapitulated in a *Drosophila* system. Thirdly, colocalization of DVAP-33A with dCERT in cell culture suggest that the interaction is conserved across species and that VAP could play a part in regulating lipid metabolism and homeostasis through lipid regulators such as Sac1 and CERT. These observations in turn imply a significant role of lipid metabolism in ALS

pathogenesis. Interaction of CERT with VAP has previously been proposed to be important for the correct localization of CERT and for the stimulation of CERT-dependent ceramide transport and sphingomyelin synthesis (Perry and Ridgeway, 2006). Studies on the role of these lipid regulators at the synaptic level could lead us to understand how lipid dysfunction could result in motor neuron degeneration. This project is currently ongoing in our lab as a result of collaboration with the group of Prof. Jacqueline de Belleroche at the Imperial College London.

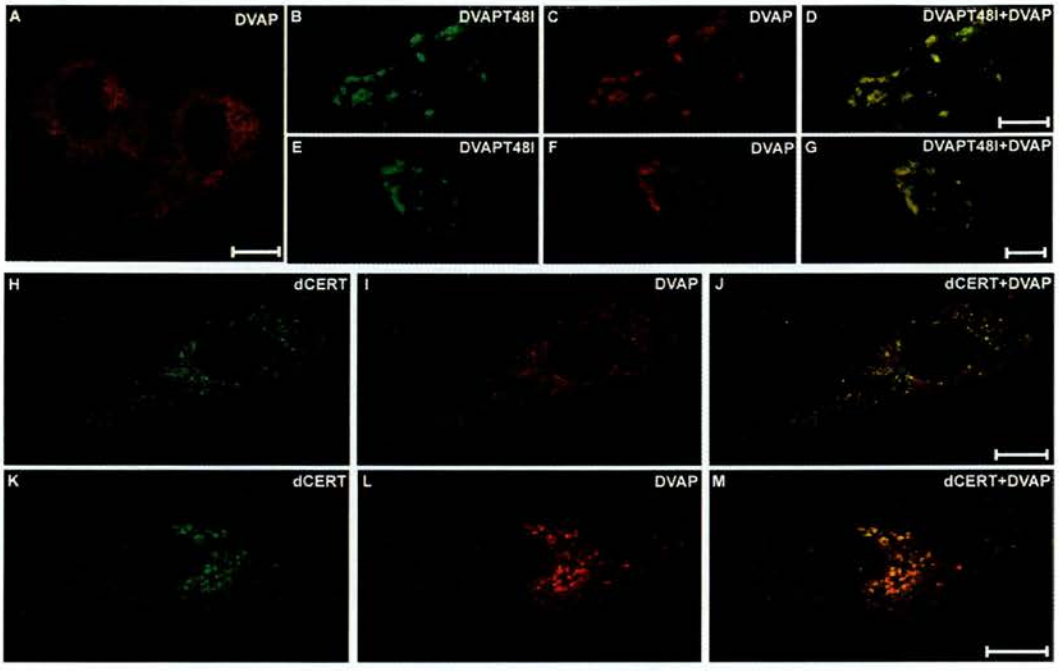

Figure 2 (A-G) Aggregates, an hallmark of the disease in flies, are composed of both wild-type and mutant DVAP.
COS7 cells transfected with plasmids expressing DVAP-FLAG and DVAPT48I-myc were stained with antibodies specific for the two tags. COS7 cells transfected with a plasmid expressing DVAP-FLAG and stained with anti-FLAG antibodies are shown in (A) as a control.

Figure 2 (H-M) dCERT and DVAP colocalize in a cell culture system.
COS7 cells were co-transfected with plasmids expressing DVAP-FLAG and dCERT-myc proteins. Co-transfected cells were stained with antibodies specific for both tags to visualize the proteins.

Materials and Methods

Fly stocks, genetics and molecular techniques

elav-Gal4 and *eyeless-Gal4 drivers* were obtained from Bloomington *Drosophila* Stock Center.

The T48I amino acid change was introduced into *DVAP-33A* cDNA cloned in pBluescript (G. Pennetta) by site-directed mutagenesis using Quick Change Site Directed Mutagenesis Kit (Stratagene) and following manufacturer's instructions. The introduction of the point mutation was verified by direct sequencing of the corresponding clone. The *DVAP-33A* cDNA carrying the mutation was isolated by PCR amplification and cloned into the pUAST vector using EcoRI- KpnI linkers. All transgenic lines were established by following standard protocols (Spradling and Rubin, 1982). For expression in a cell culture system, theT48I DVAP-33A cDNA was amplified by PCR and cloned into pCMV-myc vector (Clontech) by using EcoRI-KpnI linkers. DVAP-33A-FLAG tagged protein was expressed in cell culture by cloning the *DVAP-33A* cDNA in frame with the FLAG tag in pCMV-Tag 2 (Stratagene). The cloning was performed by PCR amplification using EcoRI-SalI linkers. *dCERT* cDNA was retrieved from the GH07688 cDNA clone obtained from BDGP (http://flybase.bio.indiana.edu/). *dCERT* cDNA was cloned in frame with the myc-tag in the pCMV-myc vector (Clontech) using EcoRI-KpnI linkers. Basic molecular biology techniques were performed according to (Ausubel *et al.*, 1998).

COS7 cell transfection and immunocytochemistry

COS7 cells were cultured in DMEM medium (Gibco) containing 10% FCS and 1% Penicillin/Streptamycin. One day before transfection, cells were plated at 150 000 cells/ml on poly-L-Lysine coated cover slips (BD Biosciences). Cells were transfected with Fugene 6 Transfection Reagent (Roche) according to manufacturers protocol and grown for 24 hours. Cells were fixed in 4% paraformaldehyde for 20 minutes at room temperature. Slides were blocked in 10% NGS and labelled with primary antibody for 2 hours at room temperature.

Immunohistochemistry and confocal immunofluorescence

Wandering theird instar larva brains were dissected in 1X PBS and fixed in Bouin's Fixative for 5 minutes. Rabbit anti-c-myc (Sigma) was used at 1:500, Mouse anti-FLAG (Sigma) was used at 1: 200, Mouse anti-Hsp70 (Affinity BioReagents) at 1:200, Mouse anti-KDEL (Stressgen) at 1:50, Rabbit anti-HRP(Jackson Immunoresearch) at 1:500 and Guinea pig anti-DVAP (G.Pennetta) at 1:1000. Larval nerves, tissues and COS7 cells were imaged using an Axiovert Zeiss Microscope.

Scanning Electron Microscopy (SEM)

SEM was done according to methods described in the main text of the thesis.

References

Acharya, U., Acharya, J.K. (2005). *Cell Mol Life Sci.* **62:** 128-142.

Ausubel F.M., Brent R., Kingston R.E., Moore D.D., Seidman J.G., Smith A.J., Struhl K. Current Protocols in Molecular Biology (1998) New York: John Wiley & Son.

Dupuis, L., Oudart, H., René, F., Gonzalez de Aguilar, J.L., Loeffler, J.P. (2004). *Proc Natl Acad Sci U S A.* **101:** 11159-11164.

Dupuis, L., Corcia, P., Fergani, A., Gonzalez de Aguilar, J.L, Bonnefont-Rousselot, D., Bittar, R., *et al.* (2008). *Neurology.* **70:** 1004-1009.

Kaiser, S.E., Brickner, J.H., Reilein, A.R., Fenn, T.D., Walter, P., Brunger, A.T. (2005). *Structure*. **13:**1035-1045.

Kawano, M., Kumagai, K., Nishijima, M., Hanada, K. (2006). *J Biol Chem.* **281:** 30279-30288.

Loewen, C.J., Roy, A., Levine, T.P. (2003). *EMBO J.* **22:** 2025-2035.

Loewen, C.J., Levine T.P. (2005). *J Biol Chem.* **280:** 14097-14104.

Marques, V.D., Barreira, A.A., Davis, M.B., Abou-Sleiman, P.M., Silva, W.A. Jr, Zago, M.A., *et al.* (2006). *Muscle Nerve.* **34:** 731-739.

Nishimura, A.L., Mitne-Neto, M., Silva, H.C., Richieri-Costa, A., Middleton, S., Cascio, D., *et al.* (2004). *Am. J. Hum. Genet.* **75:** 822-831.

Nishimura, A.L., Al-Chalabi ,A., Zatz, M. (2005). *Hum Genet.* **118:** 499-500

Perry, R.J., Ridgway, N.D. (2006). *Mol Biol Cell.* **17:** 2604-2616.

Rohrbough, J., Broadie, K. (2005). *Nat Rev Neurosci.* **6:** 139-150.

Spradling A.C., Rubin G.M. (1982) **218:**341–347.

Teuling, E., Ahmed, S., Haasdijk, E., Demmers, J., Steinmetz, M.O., Akhmanova, A., *et al.* (2007). *J Neurosci.* **27:** 9801-9815.

Wyles, J.P., McMaster, C.R., Ridgway, N.D. (2002). *J Biol Chem.* **277**: 29908-29918.

Yan, D., Olkkonen, V.M. (2008). *Int Rev Cytol.* **265:** 253-285.

Acknowledgements

I thank G. Pennetta and M. Marescotti for designing the cloning strategy and performing the molecular cloning of pUAST-DVAPT48I, pCMV-myc-dCERT, pCMV-DVAP-FLAG and pCMV-DVAPT48I-myc constructs.

(1997) Rescue of cardiac alpha-actin-deficient mice by enteric smooth muscle gamma-actin. *Proc. Natl. Acad. Sci. USA*, **94**, 4406–4411.
29. Abdelwahid, E., Pelliniemi, L.J., Szucsik, J.C., Lessard, J.L. and Jokinen, E. (2004) Cellular disorganization and extensive apoptosis in the developing heart of mice that lack cardiac muscle alpha-actin: apparent cause of perinatal death. *Pediatr. Res.*, **55**, 197–204.
30. Anderson, R.H., Brown, N.A. and Webb, S. (2002) Development and structure of the atrial septum. *Heart*, **88**, 104–110.
31. Boheler, K.R., Carrier, L., de la Bastie, D., Allen, P.D., Komajda, M., Mercadier, J.J. and Schwartz, K. (1991) Skeletal actin mRNA increases in the human heart during ontogenic development and is the major isoform of control and failing adult hearts. *J. Clin. Invest.*, **88**, 323–330.
32. Suurmeijer, A.J., Clement, S., Francesconi, A., Bocchi, L., Angelini, A., Van Veldhuisen, D.J., Spagnoli, L.G., Gabbiani, G. and Orlandi, A. (2003) Alpha-actin isoform distribution in normal and failing human heart: a morphological, morphometric, and biochemical study. *J. Pathol.*, **199**, 387–397.
33. Garner, I., Minty, A.J., Alonso, S., Barton, P.J. and Buckingham, M.E. (1986) A 5′ duplication of the alpha-cardiac actin gene in BALB/c mice is associated with abnormal levels of alpha-cardiac and alpha-skeletal actin mRNAs in adult cardiac tissue. *EMBO J.*, **5**, 2559–2567.
34. Nowak, K.J., Sewry, C.A., Navarro, C., Squier, W., Reina, C., Ricoy, J.R., Jayawant, S.S., Childs, A.M., Dobbie, J.A., Appleton, R.E. *et al.* (2006) Nemaline myopathy caused by absence of alpha-skeletal muscle actin. *Ann. Neurol.*
35. Gelernter-Yaniv, L. and Lorber, A. (2007) The familial form of atrial septal defect. *Acta Paediatr.*, **96**, 726–730.
36. Zetterqvist, P., Turesson, I., Johansson, B.W., Laurell, S. and Ohlsson, N.M. (1971) Dominant mode of inheritance in atrial septal defect. *Clin. Genet.*, **2**, 78–86.
37. Klar, J., Gedde-Dahl, T., Jr, Larsson, M., Pigg, M., Carlsson, B., Tentler, D., Vahlquist, A. and Dahl, N. (2004) Assignment of the locus for ichthyosis prematurity syndrome to chromosome 9q33.3–34.13. *J. Med. Genet.*, **41**, 208–212.
38. Trybus, K.M. (2000) Biochemical studies of myosin. *Methods*, **22**, 327–335.
39. Bing, W., Knott, A. and Marston, S.B. (2000) A simple method for measuring the relative force exerted by myosin on actin filaments in the in vitro motility assay: evidence that tropomyosin and troponin increase force in single thin filaments. *Biochem. J.*, **350** (Pt 3), 693–699.
40. Kinose, F., Wang, S.X., Kidambi, U.S., Moncman, C.L. and Winkelmann, D.A. (1996) Glycine 699 is pivotal for the motor activity of skeletal muscle myosin. *J. Cell. Biol.*, **134**, 895–909.
41. Becker, D.L., McGonnell, I., Makarenkova, H.P., Patel, K., Tickle, C., Lorimer, J. and Green, C.R. (1999) Roles for alpha 1 connexin in morphogenesis of chick embryos revealed using a novel antisense approach. *Dev. Genet.*, **24**, 33–42.
42. Becker, D.L. and Mobbs, P. (1999) Connexin alpha1 and cell proliferation in the developing chick retina. *Exp. Neurol.*, **156**, 326–332.

Human Molecular Genetics, 2008, Vol. 17, No. 2 **266–280**
doi:10.1093/hmg/ddm303
Advance Access published on October 18, 2007

hVAPB, the causative gene of a heterogeneous group of motor neuron diseases in humans, is functionally interchangeable with its *Drosophila* homologue *DVAP-33A* at the neuromuscular junction

Andrea Chai[1], James Withers[1], Young Ho Koh[2,4], Katherine Parry[1], Hong Bao[3], Bing Zhang[3], Vivian Budnik[2] and Giuseppa Pennetta[1,*]

[1]Center for Neuroscience Research, Royal (Dick) School of Veterinary Studies, University of Edinburgh, Summerhall, Edinburgh EH9 1QH, UK, [2]Department of Neurobiology, University of Massachusetts Medical School, Worcester, MA 01605-2324, USA, [3]Department of Zoology, University of Oklahoma, Norman, OK 73019, USA and [4]Ilsong Institute of Life Science, Hallym University, Anyang, Kyunggi-do 431-060, Korea

Received September 3, 2007; Revised and Accepted October 10, 2007

Motor neuron diseases (MNDs) are progressive neurodegenerative disorders characterized by selective death of motor neurons leading to spasticity, muscle wasting and paralysis. Human VAMP-associated protein B (*hVAPB*) is the causative gene of a clinically diverse group of MNDs including amyotrophic lateral sclerosis (ALS), atypical ALS and late-onset spinal muscular atrophy. The pathogenic mutation is inherited in a dominant manner. *Drosophila* VAMP-associated protein of 33 kDa A (DVAP-33A) is the structural homologue of hVAPB and regulates synaptic remodeling by affecting the size and number of boutons at neuromuscular junctions. Associated with these structural alterations are compensatory changes in the physiology and ultrastructure of synapses, which maintain evoked responses within normal boundaries. *DVAP-33A* and *hVAPB* are functionally interchangeable and transgenic expression of mutant DVAP-33A in neurons recapitulates major hallmarks of the human diseases including locomotion defects, neuronal death and aggregate formation. Aggregate accumulation is accompanied by a depletion of the endogenous protein from its normal localization. These findings pinpoint to a possible role of hVAPB in synaptic homeostasis and emphasize the relevance of our fly model in elucidating the patho-physiology underlying motor neuron degeneration in humans.

INTRODUCTION

Motor neuron diseases (MNDs) encompass a group of inherited disorders characterized by the selective dysfunction and death of motor neurons leading to spasticity, hyperreflexia, generalized weakness, muscle atrophy and paralysis (1). The best characterized and the most common of these diseases is amyotrophic lateral sclerosis (ALS) with a prevalence of approximately 5/100 000 individuals. The majority of ALS cases are sporadic while only ~10% are familial, manifesting a variety of inheritance patterns with linkage to multiple independent chromosome loci (2). Among the familial cases, ~20% are caused by dominantly inherited mutations in the protein encoded by the gene Cu/Zn superoxide dismutase 1 (*SOD1*) (3).

In 2004, a genetic linkage study mapped the locus responsible for a group of MNDs to chromosomal region 20q13.3 (ALS8). The disease affects both sexes equally and the clinical onset occurs between the third and fifth decade. Most patients have lower motor neuron symptoms but some show bulbar involvement (4). Mutation screening led to the

*To whom correspondence should be addressed at: Tel: +44 (0)1316506144; Fax: +44 (0)1316506576; Email: g.pennetta@ed.ac.uk

identification of a Proline to Serine substitution (P56S) at codon 56 in human VAMP-associated protein B (hVAPB) (5). In a branch of the same large family the P56S mutation has been shown to cause a lower motor neuron disorder accompanied by autonomic involvement and dyslipidemia (6). The mutated Proline is present in a stretch of amino acids that is very highly conserved from yeast to man in all VAP homologs.

hVAPB is a type II integral membrane protein that belongs to a highly conserved family of proteins. VAP proteins have been implicated in glucose transport trafficking, expression of phospholipid biosynthetic genes, regulation of synaptic growth, neurotransmitter release and ER-Golgi and intra-Golgi transport (7–11). These seemingly different functions have been investigated in different species and cell types and they are possibly mediated by different members of the same family.

The overall structure of all VAP proteins is similar and consists of a cytoplasmic N-terminal region and a *trans*-membrane domain at the C-terminus. The N-terminal domain shares a high degree of structural similarity with the *Caenorhabditis elegans* major sperm proteins (MSPs) (12). MSPs are highly abundant proteins expressed in the amoeboid nematode sperm. The movement of these cells is driven by the assembly of MSP proteins into fibrous networks (13). MSP proteins have also been shown to function as signaling molecules as they antagonize ephrin/Eph receptor signaling in order to promote oocyte meiotic maturation and ovarian muscle contractions in *C. elegans* (12).

DVAP-33A (*Drosophila* VAMP-associated protein of 33 kDa A) exhibits significant homology with hVAPB. DVAP-33A regulates bouton budding at larval neuromuscular junctions (NMJs) in a dosage-dependent manner. It is required for structural remodeling of synapses where it controls microtubule cytoskeleton dynamics. We have previously proposed that synapse formation is dependent on DVAP-33A in a process similar to budding in yeast (9). Recently, it has been shown that, MSP localizes to membranes and can generate the protrusive force necessary to induce vesicle budding from male germ cells in *C. elegans* (14).

To better understand the pathophysiology underlying VAP-induced MNDs in humans, we have undertaken a functional characterization of VAP proteins in flies. In *Drosophila*, structural remodeling induced by loss-of-function and overexpression of *DVAP-33A* is paralleled by functional and ultrastructural compensation at the synapse. We show that hVAPB and DVAP-33A are functionally interchangeable and that transgenic expression of mutant VAP in neurons recapitulates several hallmarks of the human disease including locomotion defects, neuronal apoptosis and aggregate deposition. Interestingly, aggregate accumulation is associated with a strong reduction in the abundance of the endogenous protein at its normal localization. Taken together these data underline a possible role for hVAPB in synaptic homeostasis and highlight the importance of this fly model in elucidating the pathomechanism of VAP-induced motor neuron degeneration in humans.

RESULTS

Homeostatic regulation of neurotransmitter release at NMJs with altered expression of DVAP-33A

Hypomorphic and null mutations in *DVAP-33A* cause a severe decrease in bouton number and an increase in bouton size. Conversely, overexpression of *DVAP-33A* in neurons induces a highly significant increase in the number of boutons with a concomitant decrease in their size (Supplementary Material, Fig. S1). Since the number and size of synaptic contacts between a neuron and its target may affect synaptic strength, we investigated whether these structural changes have any consequences on synaptic physiology. We focused our electrophysiological analysis on $DVAP\text{-}33A^{\Delta 166}$ partial loss-of-function mutants as many more of them survive to the third instar larval stage than null mutants though both mutants exhibit very similar phenotypes. As shown in Figure 1A and B, the amplitude of the evoked junctional potentials (EJPs) is not significantly different ($P > 0.05$) in synaptic terminals exhibiting fewer and larger boutons (36 ± 2 mV) relative to controls (37 ± 2 mV). To determine whether other aspects of synaptic transmission are altered in mutants, we studied the properties of miniature EJPs (mEJPs). We found an increase in the mean frequency of mEJPs in mutants when compared with controls (3.80 ± 0.24 Hz versus 2.00 ± 0.11 Hz, $P < 0.001$) (Fig. 1E). In addition, as shown in Figure 1E and F, the mean mEJP amplitude is increased in partial loss-of-function mutants compared with controls (1.30 ± 0.02 mV in $DVAP\text{-}33A^{\Delta 166}$ versus 0.80 ± 0.01 mV in controls). This difference in quantal size is significant ($P < 0.001$) and is also observed in null mutants (data not shown). We calculated the quantal content by dividing the mean EJP size by the mean of the mEJP size and found a decrease in quantal content of ~40% in mutants compared with controls (44.90 ± 0.9 in controls versus 26.91 ± 0.5 in mutants, $P < 0.001$).

In *Drosophila*, the UAS/GAL4 system allows the temporal and tissue-specific expression of a transgene by using a variety of GAL4 drivers (15). We overexpressed DVAP-33A in neurons by using the pan-neural driver *elav-GAL4*. In synaptic terminals overexpressing *DVAP-33A*, the EJP amplitude is not significantly changed compared with controls (32 ± 3 mV versus 33 ± 2 mV, $P > 0.05$) (Fig. 1C and D). Conversely, there is a significant decrease in quantal size in these mutants (0.59 ± 0.05 mV versus 0.90 ± 0.06 mV in controls, $P < 0.05$) (Fig. 1G). Interestingly, cumulative amplitude histograms indicate that the entire mEJP amplitude distribution is shifted towards larger values in mutants (Fig. 1F) and towards smaller values in animals overexpressing DVAP-33A (Fig. 1G). A significant increase in quantal content accompanies the increase in bouton number as the quantal content in DVAP-33A overexpressing larvae is 54.13 ± 1.5 compared with 36.66 ± 0.8 in controls ($P < 0.05$). Thus, changes in quantal size are responsible for maintaining normal synaptic transmission in loss-of-function and overexpression paradigms.

Ultrastructural remodeling at NMJs lacking and overexpressing DVAP-33A

To determine whether ultrastructural remodeling at the synapse accompanies the previously described functional

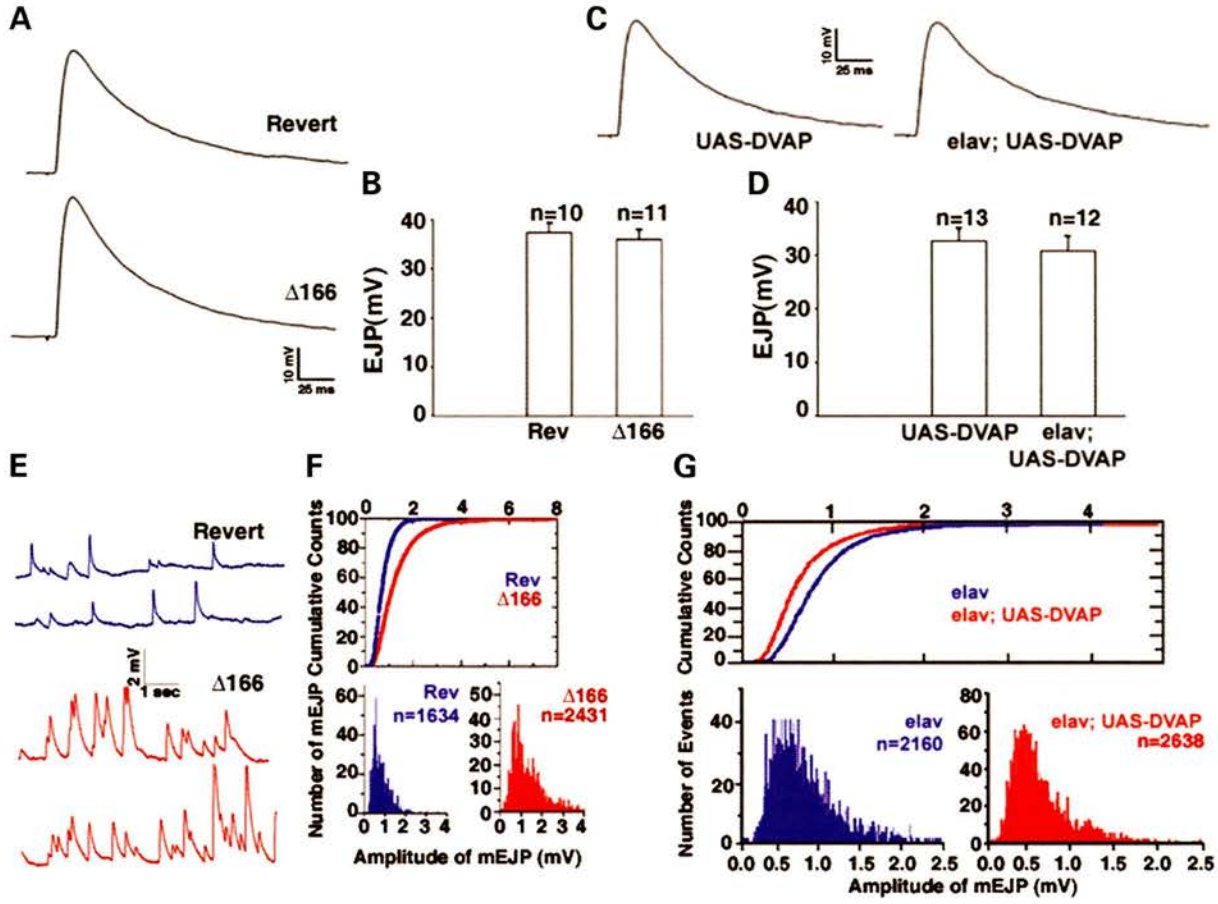

Figure 1. Electrophysiological analysis of larvae lacking and overexpressing *DVAP-33A*. (**A**) Examples of single traces showing EJPs in *DVAP-33A* mutants (Δ166) and controls (Revert); (**B**) summary of EJP amplitudes for $DVAP\text{-}33A^{\Delta 166}$ mutants ($n = 11$) and controls (Rev. $n = 10$); (**C**) representative traces of EJPs in synaptic terminals overexpressing DVAP-33A (elav; UAS-DVAP) and controls (UAS-DVAP); (**D**) summary of EJP amplitudes for overexpression mutants ($n = 12$) and controls ($n = 13$). Note that evoked neurotransmitter release is normal in both *DVAP-33A* loss-of-function and overexpression mutants; (**E**) representative traces of mEJPs for *DVAP-33A* mutants and controls; (**F**) cumulative distribution of total mEJP amplitudes in *DVAP-33A* mutants and in controls. Histograms of mEJPs for Rev. and Δ166 are shown; (**G**) cumulative distribution and histograms of total mEJP amplitudes for terminals overexpressing DVAP-33A (elav; UAS-DVAP) and for controls (elav). *DVAP-33A* mutations significantly increase the frequency and the amplitude of mEJPs while *DVAP-33A* overexpressing mutants exhibit a significant decrease in mean mEJP amplitude. Error bars represent SEM.

compensation, we performed a serial section TEM (transmission EM) analysis of terminals lacking and overexpressing DVAP-33A. As shown in Figure 2, boutons from $DVAP\text{-}33A^{\Delta 166}$ animals display an increase in the number of active zones: 2.0 ± 0.2 active zones per bouton cross-sectional area versus 0.8 ± 0.3 in controls (Fig. 2A–C and E). Although overexpression of DVAP-33A does not affect the number of active zones per surface area, other features clearly differentiate these boutons from wild-type (wt) terminals. As shown in Figure 2D, there are substantially more boutons which are significantly smaller in size when compared with wt boutons (Fig. 2A). In addition, these boutons appear to contain fewer vesicles. As reported in Figure 2F, in every small bouton resulting from DVAP-33A overexpression, more than 80% of the bouton cross-sectional area is devoid of synaptic vesicles, whereas in controls, numerous vesicles are packed in each bouton leaving only 40–50% of the bouton area devoid of synaptic vesicles. No change in the size of synaptic vesicles was observed in any of the genotypes (data not shown). In summary, analysis by TEM of $DVAP\text{-}33A^{\Delta 166}$ mutant synapses, containing larger and fewer varicosities, reveals a compensatory increase in the number of active zones per bouton. In contrast, in synaptic terminals overexpressing DVAP-33A, which contain more boutons that are smaller in size, the density of the vesicles per bouton is decreased. These data indicate that synapses can undergo structural remodeling, whereby active zones are concentrated in a reduced number of boutons while the pool of vesicles can be diluted in an increased number of boutons to maintain functional and structural homeostasis.

DVAP-33A is the functional homolog of *hVAPB*

In *Drosophila* there are three proteins (CG33523, CG7919 also named *farinelli* and CG5014 which is *DVAP-33A*) with significant homology and structural similarity to hVAPB. *Farinelli*, expressed specifically in testes and in larval fat body, is required for male fertility. The proteins encoded by CG33523 and *DVAP-33A* are ubiquitously expressed but the CG33523 protein is only 34% similar while DVAP-33A is

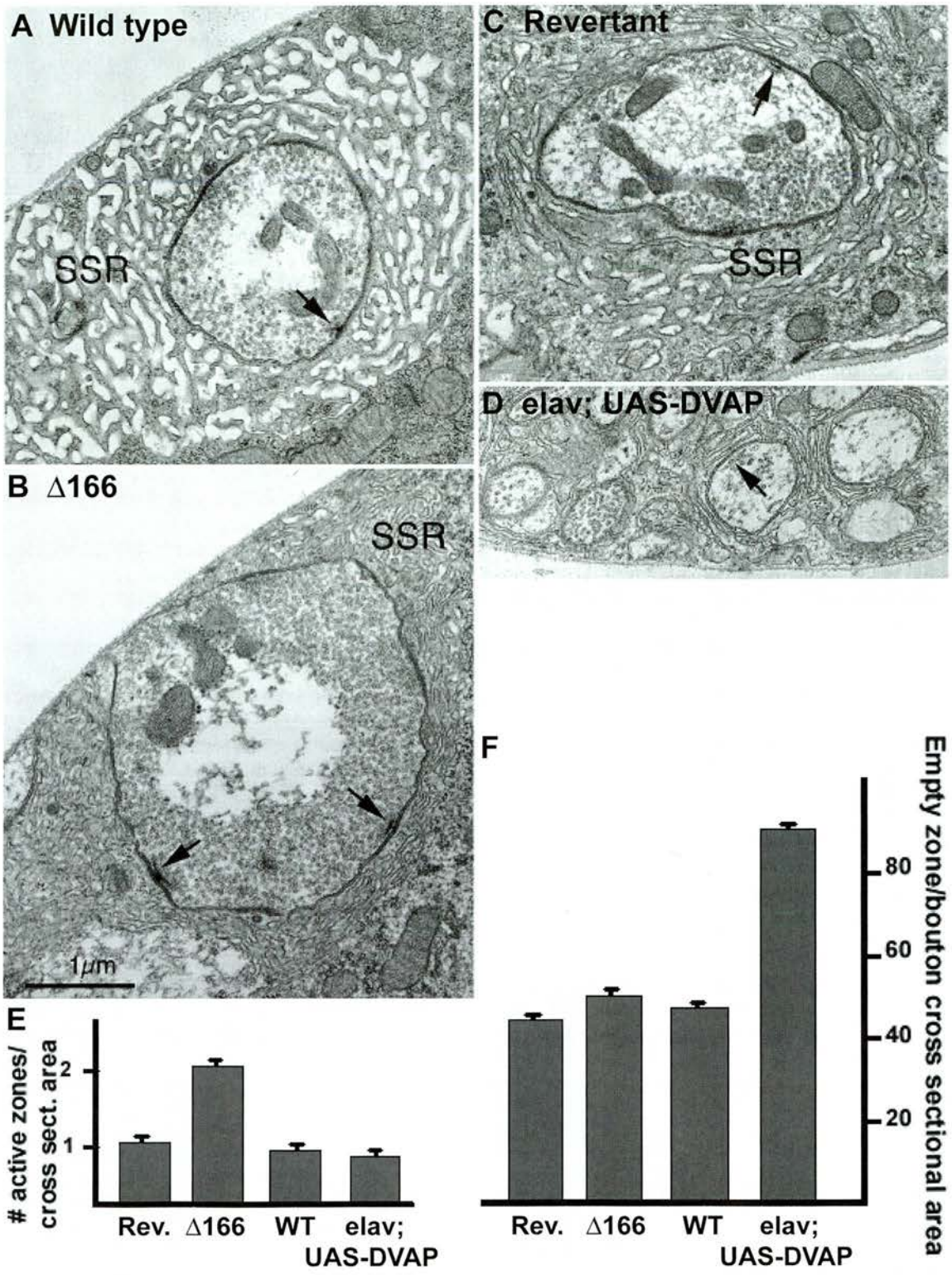

Figure 2. Nerve terminal ultrastructure of *DVAP-33A* mutants. (**A** and **C**) Electron micrographs of control NMJs: Canton S in (A) and Revertant in (C); (**B**) electron micrographs of *DVAP-33A*$^{\Delta 166}$ hypomorphic mutant NMJs (Δ166); (**D**) electro-micrographs of *DVAP-33A* (elav; UAS-DVAP) overexpressing NMJs. Presynaptic active zones (arrow) and subsynaptic reticulum (SSR) are indicated. Arrow in (D) indicates synaptic vesicles; (**E** and **F**) morphometric analysis of Δ166 mutants and *DVAP-33A* overexpressing terminals. Nerve terminals were sectioned and analyzed for the number of active zones per bouton cross-sectional area (E), and for the bouton area devoid of synaptic vesicles (empty area) (F). *DVAP-33A* mutants exhibit an increase in the number of active zones per bouton, whereas in the overexpression the density of vesicles per bouton is decreased. At least 11 boutons per animals were analyzed. Error bars represent SEM.

62% similar to hVAPB. The degree of homology and the pattern of expression suggest that DVAP-33A is likely to be the *Drosophila* ortholog of hVAPB. DVAP-33A and hVAPB also share a common three-partite domain organization: an MSP homology domain (Supplementary Material, Fig. S2A and C) containing a stretch of 16 amino acids conserved from yeast to man (Supplementary Material, Fig. S2B), a coiled-coil domain (Supplementary Material, Fig. S2A and C), and a *trans*-membrane domain at the C-terminus (Supplementary Material, Fig. S2A and C).

Given the degree of homology between DVAP-33A and hVAPB, we tested whether the human gene can functionally substitute for the loss of *DVAP-33A*. We generated transgenic flies carrying the *UAS-hVAPB* cDNAs and tested several independent transgenic lines. We have previously shown that the synaptic bouton phenotype associated with *DVAP-33A* loss-of-function mutations can be rescued by driving the expression of the wt protein in neurons (9). We therefore used the same GAL4 drivers to test the ability of hVAPB to functionally replace DVAP-33A. The *hVAPB* gene was expressed using the *C164-GAL4* (16) and *D42-GAL4* (17) drivers in null ($DVAP\text{-}33^{\Delta 448}$, $DVAP\text{-}33^{\Delta 20}$) and hypomorphic ($DVAP\text{-}33^{\Delta 166}$) mutant backgrounds. Although DVAP-33A is expressed ubiquitously and its zygotic loss results in larval lethality with rare adult escapers ($\sim$1%), the lethality associated with the loss or partial loss of *DVAP-33A* can be rescued with both drivers in combination with several *UAS-hVAPB* transgenes. We often obtained the expected Mendelian ratio. Rescued flies were fertile and did not show any obvious morphological or behavioral defects. We next investigated whether *hVAPB* can rescue the morphological and electrophysiological phenotypes associated with *DVAP-33A* loss-of-function mutations. We found that in synapses expressing *hVAPB* under the control of *C164-Gal4* or *D42-Gal4* in $DVAP\text{-}33A^{\Delta 448}$ null background, the number of synaptic boutons is similar to controls (284 ± 11 boutons versus 278 ± 12 boutons in controls, $P > 0.05$, Fig. 3A and B). Moreover, electrophysiological analysis of the same synapses shows that the EJPs (36 ± 2 mV versus 37 ± 2 mV in controls; $P > 0.05$) and mEJPs (0.83 ± 0.02 mV versus 0.89 ± 0.03 mV in controls; $P > 0.05$) are both similar to controls (Fig. 3C and D). Hence, the lethality, aberrant NMJ morphology and increased mEJP amplitude associated with loss of DVAP-33A, are rescued by targeting the expression of *hVAPB* in neurons. These data indicate that the human and the *Drosophila* protein share a common structure and perform homologous functions.

Transgenic expression of hVAPB mimics DVAP-33A overexpression

As shown in Supplementary Material, Figure S1D, neuronal overexpression of *DVAP-33A* using the pan-neural *elav-GAL4* driver causes a dramatic increase in the number of boutons as well as a decrease in their size. Despite these morphological changes, a homeostatic mechanism maintains muscle EJPs within normal values (Fig. 1C, D and G). To assess whether transgenic expression of the human protein in neurons has similar effects on synaptic structure and function, we used the same *elav-Gal4* driver. As shown in Figure 3E and F, we observed a dramatic increase ($P < 0.001$) in the number of boutons (535 ± 16) with a concomitant decrease in bouton size when compared with controls (297 ± 7). Similar to the overexpression of DVAP-33A, expression of hVAPB in a wt background also causes a reduction in the average mEJP amplitude. In this case, however, a 50% reduction in the mEJP size (0.48 ± 0.01 mV versus 0.82 ± 0.01 mV in controls; $P < 0.001$, Fig. 3H) and about a 10% reduction in the EJP amplitude (29.0 ± 0.8 mV and 35.0 ± 0.7 mV in controls; $P < 0.001$, Fig. 3G) were observed. Although there is a small decrease in the amplitude of the evoked response, the decrease in quantal size allows a nearly normal post-synaptic response. Hence, the experiments in both loss-of-function and transgenic expression indicate that hVAPB and DVAP-33A can substitute for each other's function.

Expression levels of VAP proteins affect the abundance of specific receptor subunits and the volume of post-synaptic receptor clusters

In *DVAP-33A* loss-of-function mutations, an increase in quantal size ensures functional homeostasis despite a significant decrease in bouton number (Supplementary Material, Fig. S1 andFig. 1). This increased response to spontaneous release of neurotransmitter is usually due to changes in the composition or sensitivity of post-synaptic glutamate receptors. Neurotransmitter is released from presynaptic specializations termed active zones. In wt animals, glutamate receptors are clustered in puncta that lie opposite the presynaptic active zones, placing them in an ideal position to detect neurotransmitter released. To date, five ionotropic glutamate receptor subunits have been identified at the *Drosophila* NMJ: GluRIIA, GluRIIB (18,19), GluRIII (20,21), GluRIID and GluRIIE (21,22). We used previously characterized antibodies to assess glutamate receptor abundance and distribution in synapses lacking DVAP-33A. A significant increase in cluster count ($P < 0.05$) and a marked increase in the average cluster volume for GluRIIA were observed ($P < 0.01$, Fig. 4A–C). For all the other subunits a small but statistically significant decrease in cluster count was found ($P < 0.05$, Fig. 4C). GluRIIB and GluRIII also exhibit a marked reduction in the average cluster volume (30% reduction for GluRIIB, Fig. 4C; 46% for GluRIII, Fig. 4C–E, $P < 0.001$) while cluster size for GluRIID is similar to controls (Fig. 4C). The staining intensity of every subunit does not differ significantly between controls and mutants (data not shown).

A striking physiological feature of transgenic expression of VAP proteins in neurons is a significant decrease in quantal size (Figs 1G and 3H). We investigated whether the decrease in quantal size was associated with changes in the post-synaptic glutamate receptors as well. We focused our analysis on synapses expressing transgenic hVAPB in neurons, which exhibit a greater reduction in quantal size (Fig. 3H). A marked decrease ($P < 0.001$) in GluRIIA abundance compared with controls was observed (Fig. 5A–G). This decrease was specific for GluRIIA as no difference in expression levels between controls and mutants was found for any other subunits (data not shown). Moreover, synapses expressing transgenic hVAPB exhibit a reduction in the average cluster

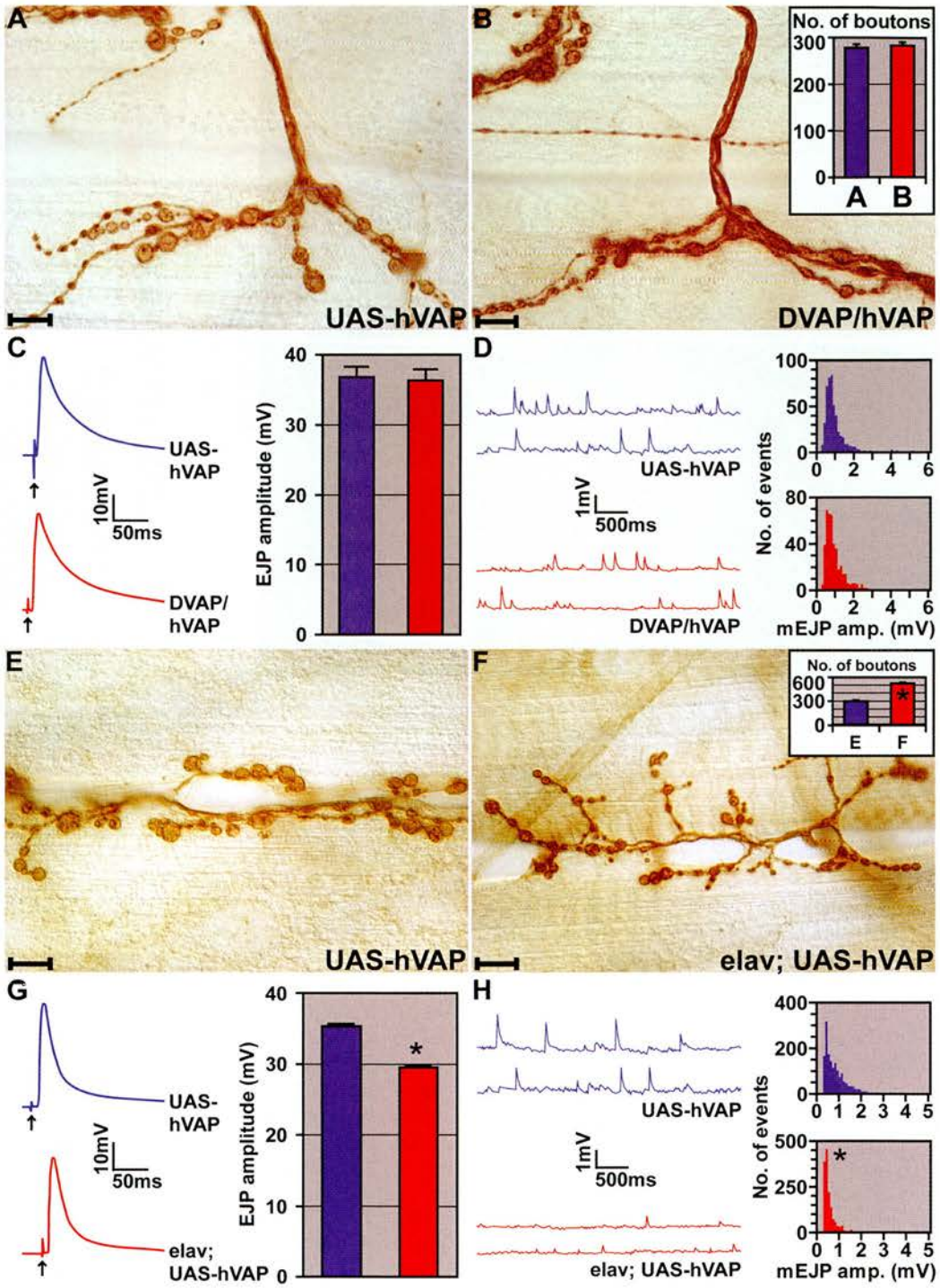

Figure 3. hVAPB and DVAP-33A are functional homologs. (**A**) Anti-HRP stainings of control NMJs (UAS-hVAP). (**B**) NMJs expressing hVAPB in *DVAP-33A* mutant background (DVAP/hVAP). In the inset, total number of boutons on muscles 12 and 13 for controls (blue) and NMJs expressing DVAP/hVAP (red). (**C**) Examples of single traces showing EJPs in controls and NMJs expressing DVAP/hVAP. In the inset, summary of EJP amplitudes for the corresponding genotypes. (**D**) Representative traces of mEJPs of control and DVAP/hVAP animals. In the inset, histograms of mEJP amplitudes for control and DVAP/hVAP NMJs are shown. Defects in synaptic function and morphology in *DVAP-33A* loss-of-function mutations are rescued by neuronal-specific expression of hVAPB. (**E**) Anti-HRP stainings of control NMJs (UAS-hVAP). (**F**) NMJs with transgenic expression of hVAPB in a wt background for *DVAP-33A* (elav; UAS-hVAP). In the inset, the total number of boutons on muscles 12 and 13 is reported for controls (blue) and elav; UAS-hVAP larvae (red). (**G**) Examples of traces of EJP amplitudes for control and elav; UAS-hVAP NMJs. In the inset, a summary of EJP amplitudes for the corresponding genotypes. (**H**) Representative traces of mEJP amplitudes for controls and elav; UAS-hVAP synapses. In the inset, histograms of mEJP amplitudes for controls and synapses expressing transgenic hVAPB are shown. Transgenic expression of hVAPB in neurons induces an increase in the number of smaller boutons, a small but significant decrease in the evoked response and a decrease in mini amplitude. UAS-hVAPB transgenic lines without the driver were used in all the control experiments reported in this figure. '*' denotes statistically significant changes. $n = 11$ per genotype. Error bars are SEM. Scale bars = 10 μm.

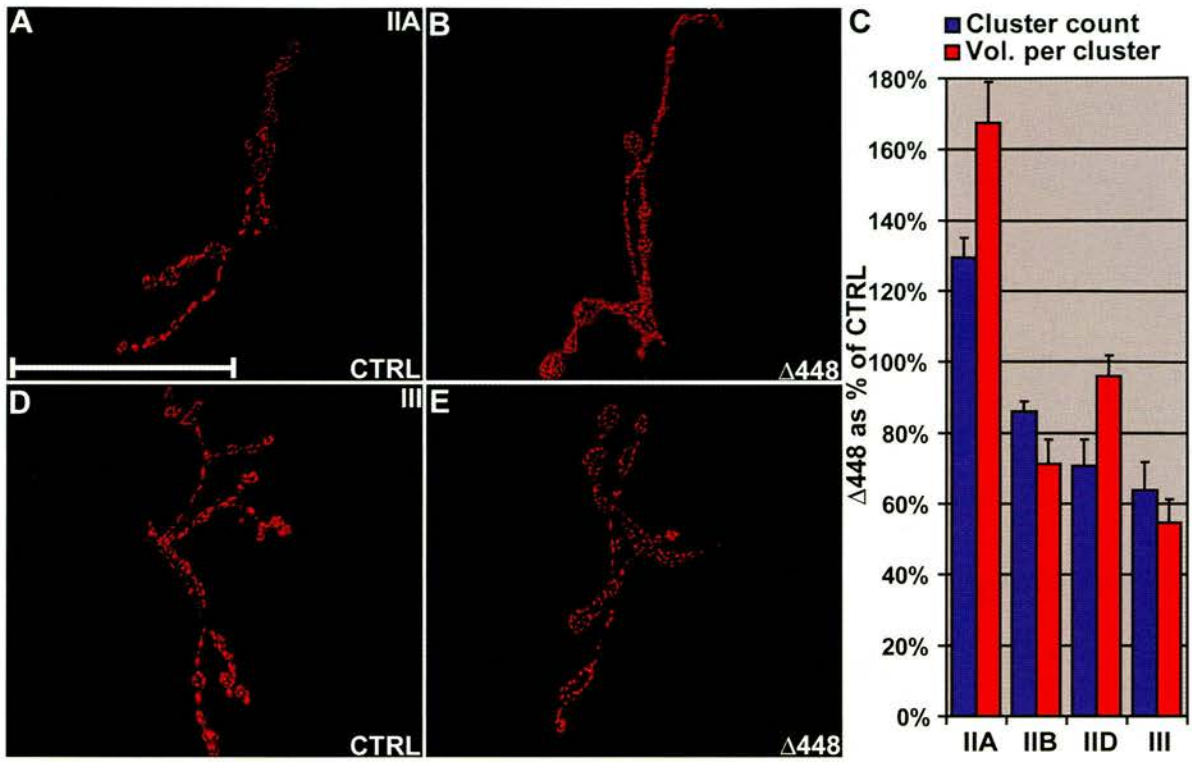

Figure 4. DVAP-33A loss-of-function mutations affect subunit abundance and cluster size of post-synaptic glutamate receptors. (**A**) Volume renderings of controls stained with anti-GluRIIA antibodies. (**B**) Mutant synapses for *DVAP-33A* (Δ448) stained with the same antibodies as in (A). (**D**) Control synapses stained with anti-GluRIII antibodies. (**E**) Δ448 synapses stained with the same antibodies as in (D). (**C**) Morphometric analysis of Δ448 NMJs reporting cluster count and mean cluster volume for every GluR subunit as percentages of control values. A striking increase in the average cluster volume for GluRIIA subunit is observed in *DVAP-33A* mutants. The revertant line generated by precise excision of the original P-element was used as a control in this experiment (9). Data in (C) are shown as mean ± SEM and $n = 5$ larvae for every analyzed genotype. Scale bar = 50 μm.

volume for the subunit GluRIIA ($P < 0.001$ Fig. 5H–J), subunit GluRIIB and GluRIII ($P < 0.05$ in both cases, Fig. 5J). Cluster count on the other hand, does not change significantly ($P > 0.05$) except for the subunit GluRIII where a small but statistically significant increase is observed ($P < 0.05$, Fig. 5J). No significant changes ($P > 0.05$, Fig. 5J) in cluster count and average cluster volume were reported for the subunit GluRIID.

Taken together, these data indicate that changes in the expression levels of VAP proteins regulate quantal size by shaping the post-synaptic glutamate receptor field and the abundance of specific subunits. Moreover, our data indicate that VAP proteins are components of a *trans*-synaptic signal as their presynaptic expression affects the post-synaptic sensitivity to neurotransmitters.

hVAPB carrying the ALS8 mutation rescues the *DVAP-33A* mutant phenotype

The Proline residue that is changed into a Serine in ALS8 patients is conserved and contained in a stretch of 16 amino acids that is virtually identical in all VAP proteins (5). Such a high degree of conservation suggests that this region plays a crucial role in the function of VAP proteins and mutations affecting this region are likely to have similar consequences in all VAP homologues. To help define the nature of the ALS8 mutation, we expressed mutant VAP proteins in a null background for *DVAP-33A*. We generated flies carrying *UAS-hVAPBP56S* (the human VAP mutant) transgene and flies carrying the *UAS-DVAPP58S* (the *Drosophila* mutant VAP) transgene. We tested the ability of these transgenes to rescue the mutant phenotypes associated with the loss of *DVAP-33A*. Lethality was rescued when the *hVAPBP56S* transgene was driven by the *D42-Gal4* and *C164-GAL4* drivers in a null background ($DVAP\text{-}33A^{\Delta 20}$ and $DVAP\text{-}33A^{\Delta 448}$, denoted as DVAP/hVAPmt in Fig. 6). In addition, as shown in Fig. 6A and B, the number of boutons is not significantly different in flies expressing the human mutant protein (*C164-Gal4; UAS-hVAPmt*; bouton number: 290 ± 11) compared with controls (*UAS-hVAPmt*; bouton number: 304 ± 11; $P > 0.05$). Moreover, no significant difference in EJPs was observed in flies expressing hVAPBP56S (36 ± 2 mV) compared with controls (34 ± 2 mV, $P > 0.05$, Fig. 6C). Finally, flies expressing hVAPBP56S exhibit quantal sizes (0.89 ± 0.02 mV) similar to those of control animals (0.83 ± 0.03 mV, $P > 0.05$, Fig. 6D). Similar data with respect to viability, morphological and electrophysiological properties were also observed with the *UAS-DVAPP58S* transgene expressed in *DVAP-33A* mutant background (data not shown). The fact that both the human and fly protein carrying the pathogenic mutation can substitute for the function of DVAP-33A indicates that the pathogenic allele retains wt properties.

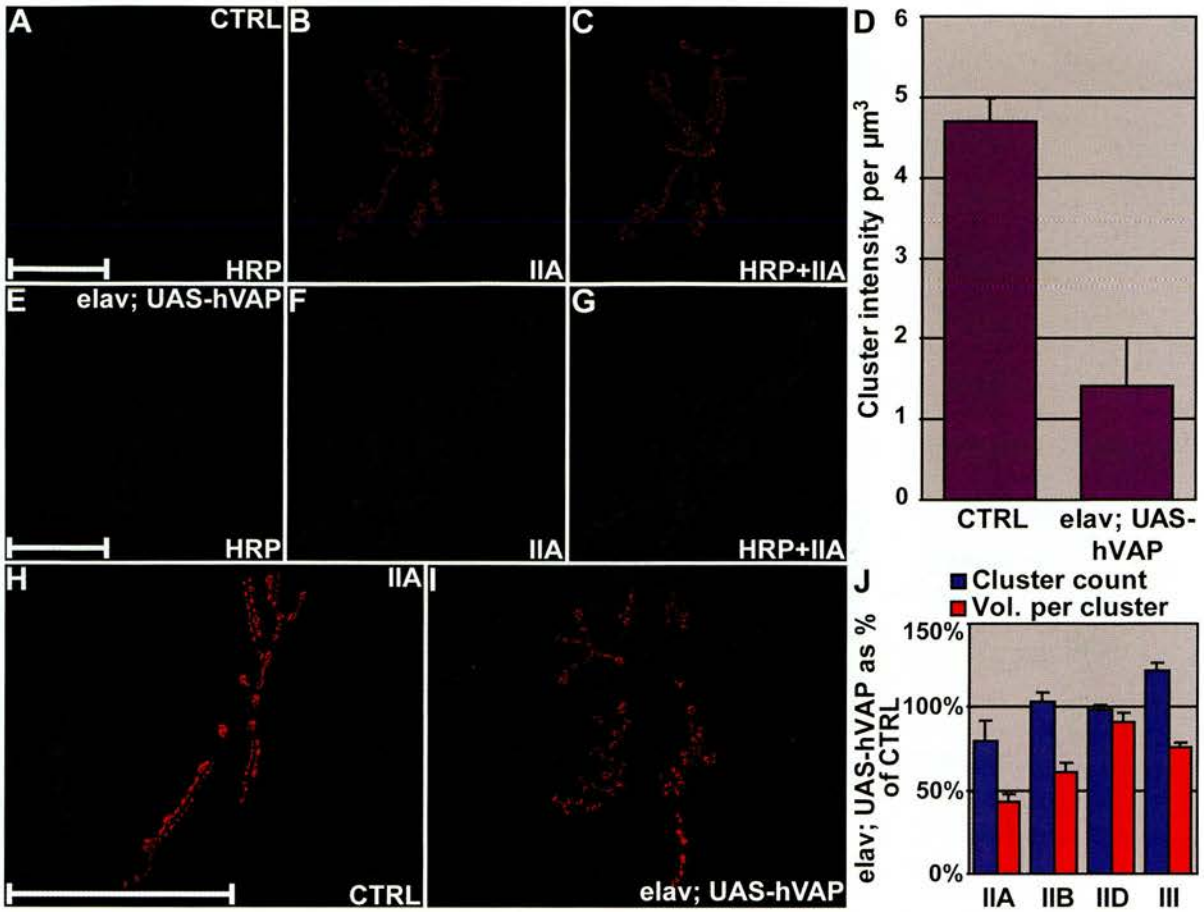

Figure 5. Neuronal expression of VAP proteins affects post-synaptic glutamate receptor composition. (**A–C**) GluRIIA subunit localization (red) at control NMJs visualized by using the neuronal cell surface marker anti-HRP (green). (**E–G**) Synapses expressing transgenic hVAPB (elav; UAS-hVAP) stained using the same antibodies as in (A–C). (**D**) Quantification of the fluorescence intensity per volume unit of GluRIIA clusters in controls and in elav; UAS-hVAP synapses. (**H** and **I**) Synapses of relevant genotypes stained with anti-GluRIIA antibodies are shown as an example. Volume renderings of clusters immunoreactive to GluRIIA are presented irrespective of their signal intensity. (**J**) Morphometric analysis of cluster count and mean cluster volume for every GluR subunit in elav; UAS-hVAP synapses are presented as percentages of control values. Neuronal expression of VAP proteins induces a decrease in the expression levels of GluRIIA and a reduction in the receptor field size. NMJ of Canton S larvae were used as controls. Data in (D) and (J) are shown as mean ± SEM and in (D) the intensity is presented in arbitrary units. $N = 5$ larvae for every analyzed genotype. Scale bars = 50 µm.

Transgenic expression of the *Drosophila* mutant protein in neurons recapitulates several hallmarks of the human disease

Expression of hVAPB and hVAPBP56S in neurons rescues the lethality, morphological and electrophysiological phenotypes associated with *DVAP-33A* loss-of-function mutations. This suggests that the human and the fly proteins perform similar functions and that the pathogenic allele retains crucial properties of the normal protein. One of the most common features of VAP homologues is their ability to self-oligomerize (11,23,24). To test whether the fly and the human VAPs exhibit this ability, we employed the yeast two-hybrid system. We found that DVAP-33A as well as its human counterpart can form homodimers, supporting the data that the human protein and the fly protein are functionally interchangeable (Supplementary Material, Fig. S3). We also found that the human and the *Drosophila* proteins carrying the ALS8 mutation can self-oligomerize, supporting the evidence that both mutant proteins retain at least part of the functional properties of the wt protein (Supplementary Material, Fig. S3). Surprisingly, we observed that, although both the human and *Drosophila* protein can interact with their respective mutant protein, there was no significant interaction between proteins from different species (e.g. the human mutant protein does not interact with the wt *Drosophila* protein although the same protein strongly interacts with the human wt protein, Supplementary Material, Fig. S3B and C). This observation suggests that the best way to model the human disease inherited in a dominant manner is to use the *Drosophila* system where the *Drosophila* mutant protein will be expressed in the presence of the fly wt protein.

One of the earliest and most common symptoms of MND in humans is paralysis and impaired movements. Similarly, we found that transgenic larvae expressing DVAPP58S in neurons were sluggish and uncoordinated. We therefore performed a quantitative analysis of their locomotion behavior. Forward locomotion in larvae consists of contractions of the posterior end alternating with extension of the anterior body

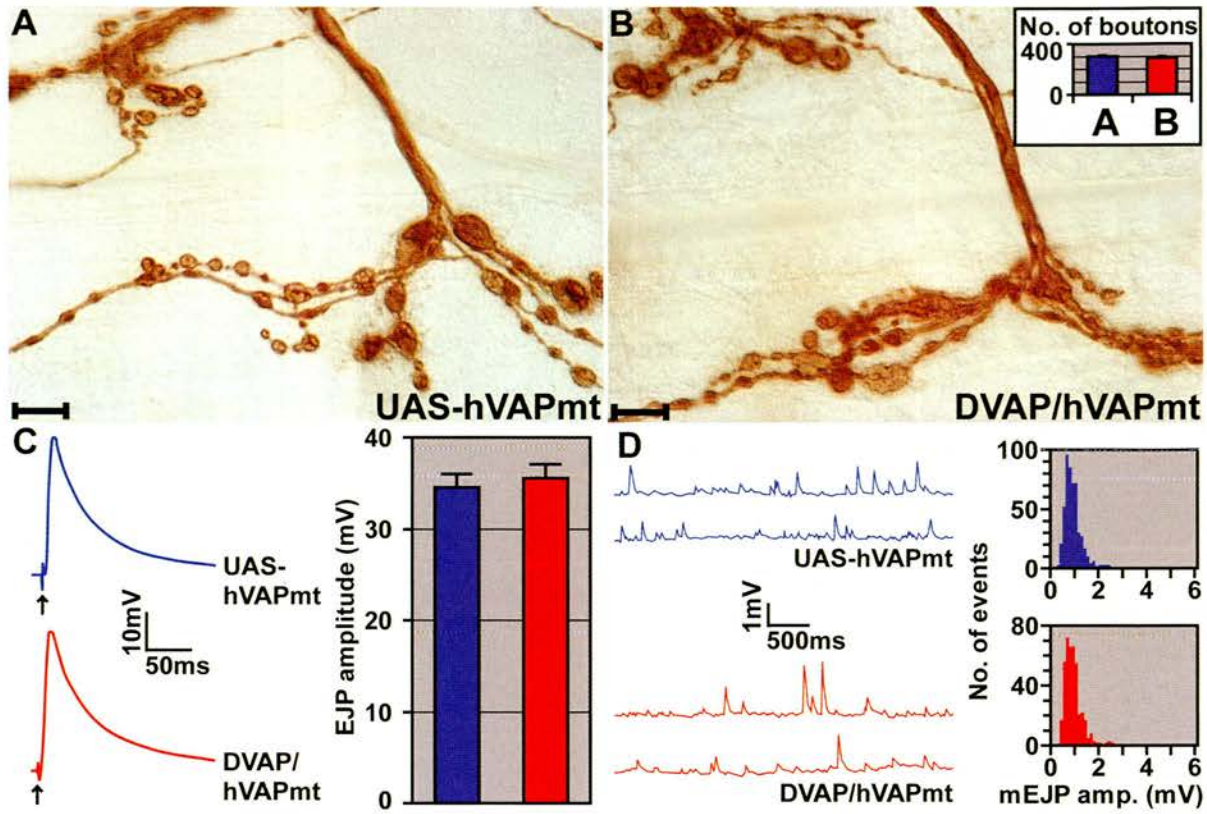

Figure 6. hVAPP56S rescues the mutant phenotypes associated with *DVAP-33A* mutations. (**A**) Anti-HRP stainings of control NMJs (UAS-hVAPmt). (**B**) NMJs expressing mutant hVAPB in *DVAP-33*A mutant background (DVAP/hVAPmt). In the inset, the total number of boutons on muscles 12 and 13 for the same genotypes is reported. (**C**) EJP traces are reported for control and DVAP/hVAPmt NMJs. In the inset, a summary of EJP amplitudes is reported for the respective genotypes. (**D**) Representative traces of mEJP amplitudes for control and DVAP/hVAPmt NMJs. In the inset, histograms of mEJP amplitudes are shown for the corresponding genotypes. Defects in synaptic function and morphology in *DVAP-33A* loss-of-functions are rescued by neuronal-specific expression of hVAPB carrying the ALS8 mutation. UAS-hVAPmt transgenic lines without the driver were used in the control experiments reported in this figure. $n = 10$ larvae for every genotype. Error bars are SEM. Scale bars = 10 μm.

regions (25,26). Third instar larvae expressing transgenic DVAPP58S and control larvae reared in the same environmental conditions were observed on an agarose substrate for a period of at least 2 min. The frequency of strides in Hz (number of events per second) was calculated by dividing the number of strides by their duration.

Unexpectedly, transgenic larvae expressing DVAPP58S revealed significant heterogeneity in the mobility phenotype compared with controls. As shown in Figure 7A, 34% of the larvae are completely paralyzed or exhibit very few peristaltic contractions while the majority has a frequency of strides that is only 30% of the wt value. In controls, the frequency of strides is homogeneous (0.85 ± 0.01 Hz). The difference in frequency distribution between mutants and controls is statistically significant ($P < 0.001$, see legend of Fig. 7 and Materials and Methods for details).

Motor neuron death is one of the hallmarks of MND both in human patients and murine models (2). We therefore performed TUNEL analysis to assess whether transgenic expression of DVAPP58S causes neuronal apoptosis. Significantly enhanced neuronal death was observed in the central neurons of larvae expressing transgenic DVAPP58S compared with controls (Fig. 7B and C).

In mouse models for ALS expressing pathogenic SOD1, the paralytic phenotype and the neuronal cell death have been associated with the formation of aggregates that are strongly immunoreactive with SOD1 antibodies (27). Similarly, aggregates containing pathogenic SOD1 have been reported for sporadic and familial cases of ALS in humans (28). To test whether this feature is also common to VAP-induced MNDs, we performed Western analysis on whole tissue extracts of third instar larvae. Although DVAP-33A migrates exclusively as a monomer in SDS-PAGE of controls, in DVAPP58S transgenic lines an immunoreactive smear with a significant reduced mobility was observed (data not shown). The presence of these higher molecular weight species is suggestive of the ability of the protein to form aggregates. To identify where these aggregates accumulate and whether there are regional differences in the localization of the endogenous protein, we performed confocal analysis on larval brains, nerve fibers and neuromuscular synapses of *DVAPP58S* transgenic animals stained with antibodies specific for DVAP-33A. In control nerves, we observed faint but uniform staining while in the nerves of *DVAPP58S* transgenic larvae, highly immunoreactive aggregates of variable sizes were found (Fig. 8A and B). Large aggregates accumulate in the region of the nerves

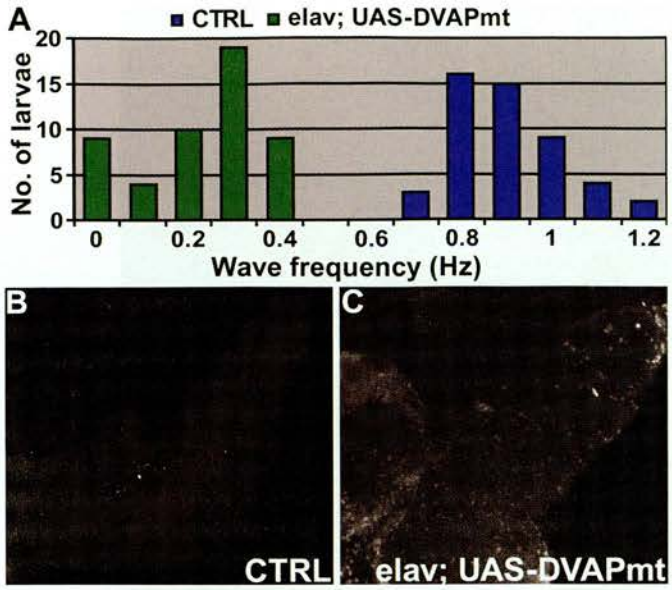

Figure 7. Transgenic expression of DVAPP58S in neurons induces locomotion defects and neuronal cell death. (**A**) Summary of the frequency of peristaltic waves for elav; UAS-DVAPmt larvae (green) and for controls (blue). $n = 49$ for controls and $n = 51$ for elav; UAS-DVAPmt. Differences between genotypes were highly significant ($P < 0.001$, accordingly to the non-parametric Mann–Whitney U test when the data sets relative to elav; UAS-DVAPmt were compared with controls. In this experiment, the UAS-DVAPP58S transgenic line without the driver was used as a control. (**B**) Neuronal cell death in UAS-DVAPP58S/+ control brains. (**C**) Neuronal cell death within larval brains expressing transgenic DVAPP58S.

proximal to the brain and in their terminal tracts just before motor nerves sprout on the muscles to form the synaptic arbor (Fig. 8B). In between these regions, the deposition of aggregates was less prominent (Fig. 8C). In neuronal cell bodies of *DVAPP58S* larval brains, we also observed aggregate formation and the wt protein associated with the plasma membrane decreased to nearly undetectable levels (compare Figs 8E with D). Similarly, at neuromuscular synapses of *DVAPP58S* transgenic larvae, DVAP-33A positive immuno-reactivity was virtually undetectable (less than 8% of the wt level, Figs 9A–C and G–J). This phenomenon was consistently observed in all five DVAPP58S transgenic lines examined. Conversely, in DVAP-33A overexpressing lines the protein is correctly targeted to the NMJ even when protein levels are 4-fold the wt level (Fig. 9A–F and J). No aggregates were found in the neuronal cell bodies and nerve fibers of DVAP-33A overexpressing lines (data not shown and compare arrow in Fig. 9E with arrow in Fig. 9H). Taken together, these data indicate that transgenic expression of DVAPP58S in neurons induces the formation of DVAP-33A immuno-reactive aggregates and a depletion of the endogenous protein from its normal localization. At the *Drosophila* NMJ, decreasing the level of DVAP-33A induces a decrease in the number of boutons and an increase in their size (Supplementary Material, Fig. S1). As a consequence of the decreased synaptic level of DVAP-33A, the number of boutons at the *DVAPP58S* transgenic synapses was only 40% of the wt number (122 ± 3 as compared with 283 ± 12 in controls, $P > 0.001$, data not shown, but compare Fig. 9A with G). Although not directly quantified, an increase in bouton size was also observed (data not shown). A number of other abnormalities such as muscle wasting and synaptic degeneration were often observed at these NMJs. A detailed analysis of these phenotypes is reported in Supplementary Material, Fig. S4. Taken together these data indicate that neuronal expression of DVAPP58S in the presence of the wt protein recapitulates several hallmarks of the human disease including locomotion defects, neuronal cell death and aggregate formation. It is noteworthy that aggregate accumulation is associated with a depletion of the endogenous protein from its normal localization and a consequent decrease in its function.

DISCUSSION

Recently, *hVAPB* has been shown to be the causative gene of late-onset autosomal dominant forms of motor neuron disorders, including typical and atypical ALS and late-onset spinal muscular atrophy (5, 6). The pathogenic mutation predicts a substitution of a Serine for a conserved Proline (P56). We decided to study the role of hVAPB in MNDs using *Drosophila* genetics.

One of the hallmarks associated with loss-of-function and neuronal overexpression of *DVAP*-33A is decreased and increased bouton formation at the NMJ, respectively. Despite this structural alteration, synaptic transmission is maintained within a wt range. At the mechanistic level, muscles respond to a decreased number of boutons and quantal content by upregulating quantal size; conversely muscles compensate an increase in number of boutons and quantal content by downregulating quantal size. Compensatory changes in quantal size during synaptic homeostasis are thought to be determined, largely, by the properties of transmitter receptors. At the *Drosophila* NMJ, there are two classes of glutamate receptors: one set containing the subunit IIA and another one containing the subunit IIB (29). In *DVAP-33A* loss-of-function mutations, the increase in quantal size is associated with an increase in the number and average cluster volume of subunit IIA. Conversely, the decrease in quantal size in the oversprouting mutants is accompanied by a decrease in the level of post-synaptic receptor subunit IIA and a reduction in the average cluster volume for several subunits. In agreement with our data, the IIA subunit receptors have been shown to affect quantal size and receptor channel open time (18,30). Similar to our oversprouting mutants, in synapses lacking the receptor subunit IIA, a homeostatic increase in neurotransmitter release compensates for the reduction in quantal size and the evoked response is maintained within normal values (18,30). These data indicate that expression levels of VAP proteins play a crucial role in synaptic homeostasis by coordinating structural remodeling and post-synaptic sensitivity to neurotransmitter to ensure synaptic efficacy.

Interestingly, expression of hVAPB in neurons rescues lethality, morphological and electrophysiological phenotypes associated with *DVAP-33A* loss-of-function mutations. Moreover, neuronal expression of hVAPB in a wt background induces phenotypes similar to the overexpression of DVAP-33A. These data clearly indicate that DVAP-33A and

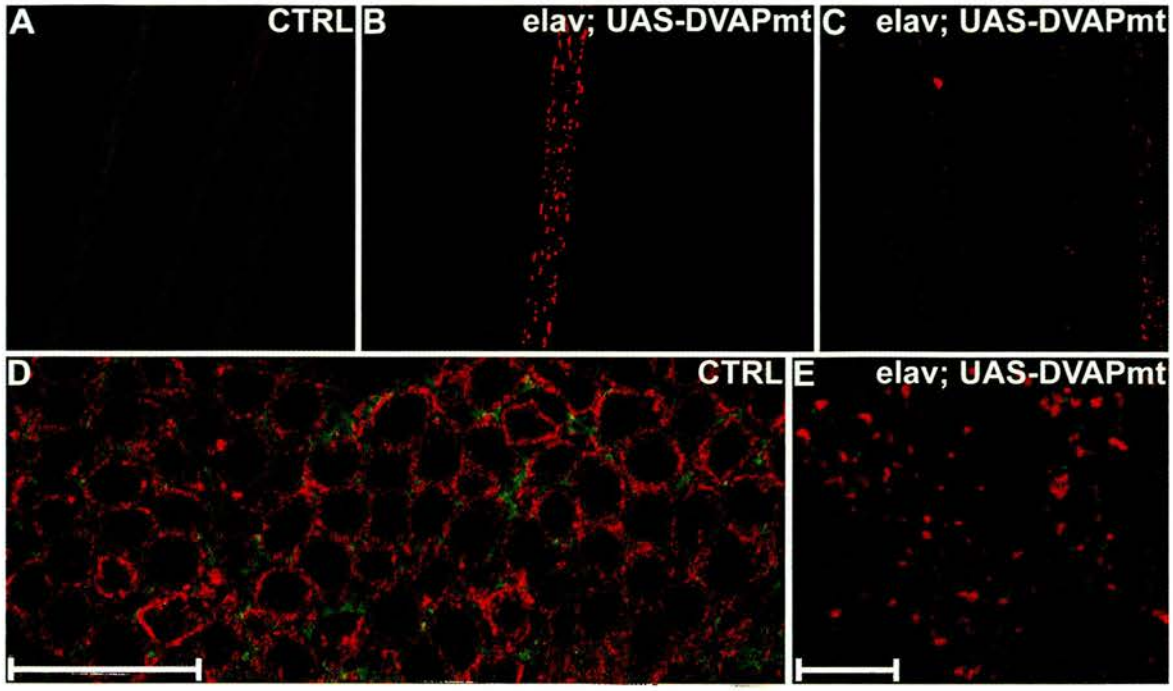

Figure 8. Aggregates strongly immunoreactive for DVAP-33A are markers of the disease in flies. Nerve fibers and brains of third instar larvae were stained with antibodies for DVAP-33A (red) and with antibodies for the neuronal cell surface marker anti-HRP (green). (**A**) Nerve fibers of control larvae. (**B** and **C**) Nerve fibers of larvae expressing transgenic DVAPP58S (elav; UAS-DVAPmt). In control nerves, a faint but uniform staining is observed (A). Conversely, in *DVAPP58S* transgenic nerves, large aggregates accumulate in the region of the nerves proximal to the brain and in their terminal tracts just before motor nerves contact the muscles (B). In between these regions, the deposition of aggregates was less prominent (C). (**D**) Brains of control larvae stained with anti-HRP (green) and anti DVAP-33A antibodies (red). (**E**) Brains of larvae expressing transgenic DVAPP58S (elav; UAS-DVAPmt) using the same antibodies. DVAP-33A associates mainly with the plasma membrane of neuronal cell bodies (D). On the contrary, in *DVAPP58S* transgenic brains, the DVAP-33A immunoreactivity is associated with intracellular aggregates of variable sizes (E). The anti DVAP-33A antibodies used in this report do not discriminate between the wt and the mutant protein. By western analysis, these antibodies recognize a band of similar size to the wt protein in protein extracts from NMJs expressing DVAPP58S in a null background for the endogenous protein (data not shown). In (D) and (E), single sections of confocal images are shown. Canton S larvae were used as controls in the experiments reported in this figure. Scale bars = 20 μm.

hVAPB perform homologous functions at the synapse and as a consequence, information gained by studying DVAP-33A is expected to be relevant for hVAPB function as well. Surprisingly, neuronal expression of mutant VAP proteins also rescues all phenotypes associated with mutations in *DVAP-33A*. Two alternative scenarios could be proposed to explain these data: the mutation is irrelevant for the ALS8 pathogenesis or the mutant allele has a pathogenic effect while retaining certain functional properties of the wt protein. We strongly favor the second hypothesis for the following reasons. First, the P56S mutation in hVAPB has been reported to be causative for an inherited form of MNDs in humans. This mutation affects nine related families totaling 1500 individuals of which 200 suffer from motor neuron disorders (31). Second, we have generated a genetic model for MNDs where the expression of the aberrant VAP recapitulates major hallmarks of the human disease, clearly indicating that the mutation has a pathogenic effect. Third, our data and data published by others (23) suggest that both the *Drosophila* and the human mutant proteins retain some functional wt properties such as the ability to self-oligomerize. However, neuronal expression of the pathogenic protein induces aggregate formation and depletes the wt protein from its normal localization. These effects are not observed when the wt protein is overexpressed, suggesting that the mutant protein has acquired a new, potentially toxic property.

Indeed, one of the most common features of MNDs and nearly all neurodegenerative diseases is the accumulation of aggregates that are intensively immuno-reactive to disease-related proteins (2). Each disease, however, differs with respect to the anatomical location and morphology of the aggregates. The major component of the aggregates is usually the protein encoded by the gene mutated in the familial forms, which is also unique to each disease. Despite this diversity, a bulk of circumstantial evidence support the hypothesis that aggregates are typical hallmarks of neurodegenerative diseases and have a toxic effect on neurons (32). While no autopsy material is available for familial cases with the P56S mutation, SOD1-positive inclusions have been reported in human sporadic and familial ALS cases as well as in SOD1 mouse models (28). We found the presence of aggregates that are intensively immuno-reactive for DVAP-33A both in neuronal cell bodies and in nerve fibers of our MND model. Interestingly, hVAPB carrying the pathogenic mutation has also been shown to undergo intracellular aggregation when expressed in a cell culture system (23). However, similarities between human disease and our fly model are not limited to aggregate formation as flies expressing transgenic VAP proteins carrying the ALS8

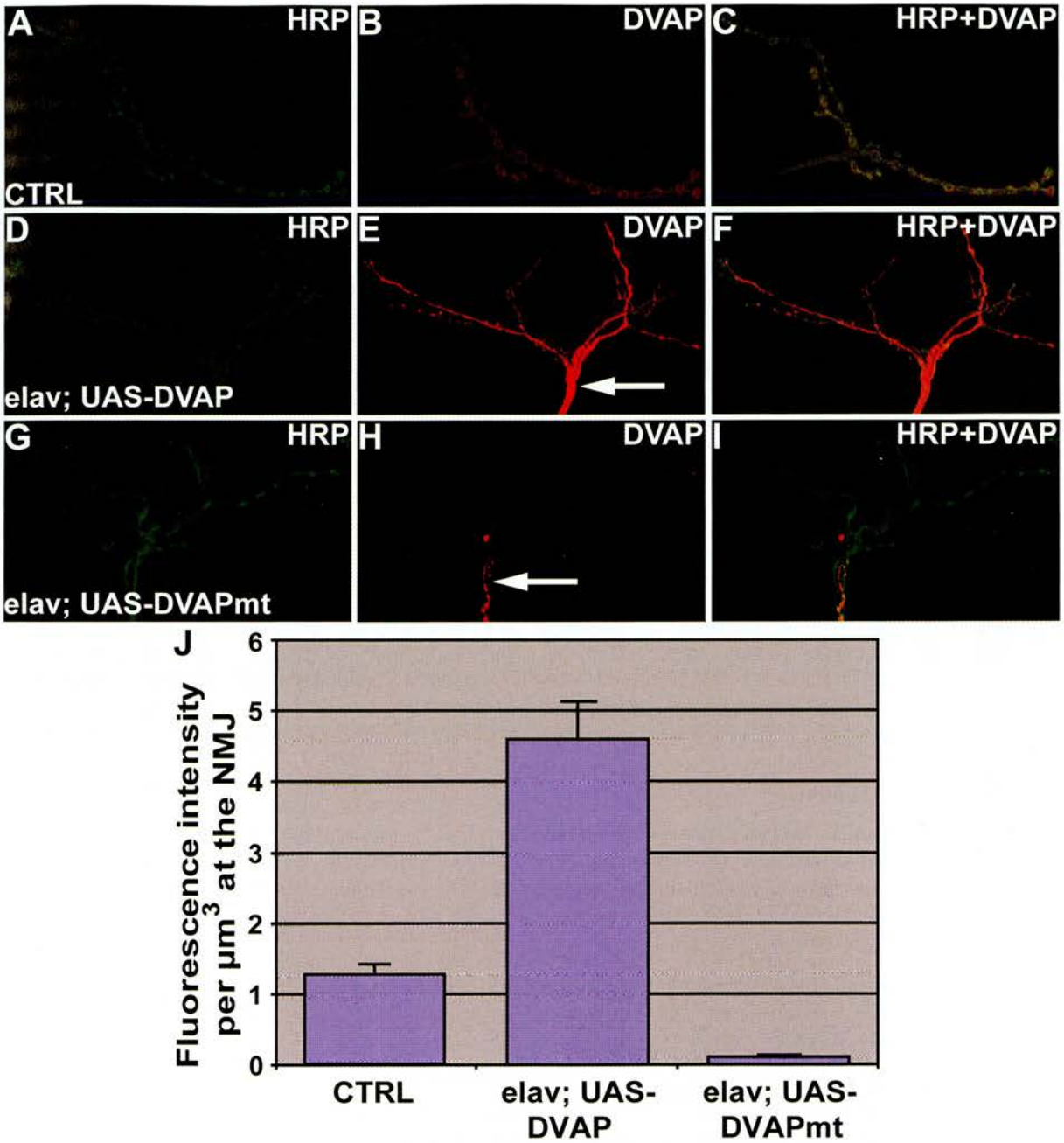

Figure 9. Transgenic expression of DVAPP58S affects synaptic levels of the endogenous protein. NMJs were stained with antibodies specific for DVAP-33A (red, DVAP) and for anti-HRP (green) to visualize the synapses. (**A–C**) Control NMJs. (**D–F**) NMJs overexpressing DVAP-33A (elav; UAS-DVAP). (**G–I**) NMJs expressing transgenic DVAPP58S (elav; UAS-DVAPmt). (**J**) Quantification of synaptic DVAP-33A fluorescence intensity for the reported genotypes. Note that despite a 4× increase in the level of expression of DVAP-33A, the protein is located at the synapse and no aggregates are visible in the nerves of these transgenic lines expressing the wt protein (arrow in E). In *DVAPP58S* transgenic lines, aggregates are evident in the terminal part of the nerve (arrow in H) and the endogenous protein at the synapse is nearly undetectable (H and J). Canton S larvae were used as controls in the experiment reported in this figure. In (J) fluorescence intensity is presented in arbitrary units. Scale bar = 10 µm.

mutation, exhibit other hallmarks of the human disease such as neuronal cell death, muscle wasting and defective locomotion behavior.

Although it remains to be established whether the VAP protein in the aggregates represents the mutant protein, the endogenous protein or a mixture of both, we clearly observe a regional decrease in the level of the endogenous protein. The DVAP-33A protein that is normally associated with the plasma membrane in neuronal cell bodies and at the neuromuscular synapses is nearly undetectable in *DVAPP58S* transgenic animals. As a consequence of the decrease in synaptic levels of the endogenous protein, a decrease in the number of boutons is observed. We have previously shown that DVAP-33A regulates bouton formation at the synapse in a

dosage-dependent manner (9). Despite these structural alterations a homeostatic mechanism is established to maintain synaptic efficacy within functional boundaries. We speculate that the depletion of the endogenous protein from its normal localization and the formation of aggregates would affect the homeostatic mechanism linking structural remodeling and synaptic efficacy controlled by DVAP-33A. Although not directly tested in our model, experiments in cell culture show that overexpression of mutant hVAPB induces formation of aggregates in which the endogenous wt protein is recruited (23,33). This would suggest that the pathogenic allele functions as a dominant negative. However, the depletion of the endogenous protein from its normal localization cannot be the principal mechanism of the disease as mutants lacking DVAP-33A do not develop MND. It is therefore possible that the pathogenic allele has acquired an abnormal, new toxic activity. Similar to what has been proposed for other neurodegenerative diseases, the formation of aggregates may directly interfere with critical cellular processes and /or compromise the ability of the system to keep up with the degradation of aggregated proteins (34).

Taken together these data offer experimental support to the hypothesis that VAP proteins play a conserved role in synaptic homeostasis and emphasize the relevance of this fly model in fostering our understanding of the molecular mechanisms underlying VAP-induced motor neuron degeneration in humans.

MATERIALS AND METHODS

Genetics and molecular techniques

DVAP-33A$^{\Delta 166}$ is an hypomorphic mutation obtained by imprecise excision of *P{ry*$^{+t7.2}$ *= lArB}47*, a *P* element inserted 600 bp upstream of the AUG (9). A revertant line generated by precise excision of the same *P* element was used as a control for loss-of-function mutations.

Site-directed mutagenesis on *DVAP-33A* and *hVAPB* cDNAs was performed using Quick Change Site Directed Mutagenesis Kit (Stratagene). All transgenic lines were established by following standard protocols (35). Basic molecular biology techniques were performed according to (36) and Western Blots on single dissected NMJ according to (9).

To test the ability of the hVAPB protein to rescue the lethality associated with *DVAP-33A* mutations, female flies, *DVAP-33A*$^{\Delta 448}$*/FM7; +/+; UAS-hVAPB/TM3*, were mated to males contributing the *C164-Gal4* or *D42-Gal4* drivers. *DVAP-33A*$^{\Delta 448}$*/Y; C164-Gal4/+; UAS-hVAPB/+* adult, non-FM7, males were identified and counted. The specificity of the rescue was confirmed by the absence of *DVAP-33A*$^{\Delta 448}$*/Y; C164-Gal4/+; +/TM3* males. A similar protocol was used to test the ability of *hVAPBP56S* and *DVAPP58S* to rescue the lethality associated with *DVAP-33A* mutations. In all cases, the rescue was confirmed by using all *DVAP-33A* mutant alleles in combination with several transgenic lines expressing *hVAPB*, *hVAPBP56S* or *DVAPP58S*.

For the analysis of the morphological and physiological rescue, the following crosses were performed. *yw/Y; C164-GAL4/C164-GAL4* males were crossed to *DVAP-33A*$^{\Delta 448}$*/FM7; +/+; UAS-hVAPB/UAS-hVAPB* females. *DVAP-33A*$^{\Delta 448}$*/Y; C164-Gal4/+; UAS-hVAPB/+* males were identified as y^+ third-instar larvae lacking the *FM7* chromosome. A similar genetic scheme was applied to test the ability of *Drosophila* and human mutant proteins to rescue the morphological and physiological phenotypes. To characterize the transgenic expression phenotype, the *Gal4* drivers were crossed with transgenic lines. Embryos were collected for 20–24 h and then transferred to a water-bath at 30°C.

Immunohistochemistry, imaging and morphometric analysis

Stainings of third instar larval NMJs and analysis of the morphological phenotype was performed as described in (9). For the phalloidin staining the NMJs were fixed in 4% paraformaldehyde and the phalloidin treatment was performed accordingly to the manufacturer's instructions (Molecular Probes). NMJ stainings with antibodies specific for the glutamate receptor subunits were performed according to (20), except for the subunit IID where the protocol described in (21) was used. Larval NMJs were imaged using an Axiovert Zeiss Microscope. The same confocal gain settings were applied to control and mutant NMJs. A complete Z-stack was acquired for every NMJ and rendered on a 3D projection. For the morphometric analysis, images were initially trimmed using the Zeiss LSM Image Examiner 3.2.0.70 software (Carl Zeiss, 2002). Cluster counting and volume estimation were performed with the software package Imaris 4.7.2 (Bitplane AG, 2006). The minimum cluster radius was set to 0.4 μm and background object subtraction was used when applying the 'spot detection' function. The total cluster volume was found by fitting a 3D surface to the clusters with the iso-surface tool and no additional Gaussian smoothing or re-sampling steps were applied. The average volume of a single cluster was calculated by dividing the total cluster volume by the total number of clusters. Appropriate intensity thresholds were selected to properly identify clusters and ignore background intensities for both tools in the Imaris package. Statistical analysis was performed using a two-tailed Student's *t*-test.

Electrophysiology

Intracellular recordings were performed in HL3 saline (37). Spontaneous mEJPs were obtained by intracellular recording from muscles bathed in HL3 saline containing low calcium concentration (0.3 mM) and 3 μM tetrodotoxin. For evoked transmitter release, 1 mM Ca^{2+} was added to the HL3 saline. Electrical signals were amplified through an Axoclamp 2B amplifier (Axon Instruments), digitized and recorded by a computer equipped with pClamp8 software (Axon Instruments). Quantal content was calculated by the method of dividing the size of the mean EJP with the size of the mean mEJP.

Analysis of the amplitude and frequency of mEJPs was performed using Mini Analysis (Synaptosoft, Inc.). mEJPs with slow time course arising from neighboring electrically coupled muscle cells were excluded from analysis (38). No significant differences were found in muscle resting potentials or muscle input resistance among different genotypes. The unpaired Student's *t*-test was used for data statistics.

Additionally, the Kolmogorov–Smirnov test was used when comparing quantal size analysis of different genotypes for the data reported in Figure 1 while one-way ANOVA (analysis of variance) was used for statistical analysis of different genotypes in the remaining figures.

Ultrastructural analysis

Body wall muscles were prepared for TEM as in (39). Synaptic boutons were serially sectioned and photographed at 10 000–30 000× using a JEOL 100S TEM. For morphometric analysis, the cross-section corresponding to the bouton midline (cross-section of largest diameter) was identified, the negative scanned at 60 000×, and used for quantification using NIH image (Version 1.62) as in (40). Number of active zones was determined by counting the number of T-bar structures (complete or partial) observed at the cross-sectional area. To measure the area of empty zones (devoid of synaptic vesicles) in the cross-sectional area of synaptic boutons, the boundary of synaptic vesicle pools was digitalized and the enclosed area was calculated by using the Measure function of NIH image. Serial sections taken from 11 synaptic boutons of two independent preparations for each genotype were used for EM analysis. Statistical analysis was performed using a two-tailed Student *t*-test.

Larval locomotion behavior

Wandering third instar larvae were collected from the vial and washed briefly in distilled water to remove traces of food. Each larva was transferred to the centre of a 9 cm Petri dish containing grape juice medium. The larva was then allowed to adjust to the Petri dish environment and the counting of the peristaltic waves was started only after observing the first wave of contractions. The contraction waves were counted for at least 2 min per larva and their number divided by the time in seconds to obtain the frequency of contractions expressed in Hz. The Lillefors test was applied to check for normality in the distribution of the different datasets. Since the data concerning the elav; UAS-DVAPmt failed to pass the test for normality, the non-parametric Mann–Whitney U test was used to compare the datasets.

Tunel staining for apoptosis detection

Larval brains were carefully dissected and fixed in 4% paraformaldehyde for 15 min. Detection of apoptotic neuronal cells was performed using the fluorescein cell death kit (Promega) following manufacturer's instructions.

SUPPLEMENTARY MATERIAL

Supplementary Material is available at HMG Online.

ACKNOWLEDGEMENTS

We thank H. Bellen, in whose laboratory this project was initiated, for helpful comments on a previous version of this manuscript. We are grateful to P. Brophy for his constant support and scientific advice. We thank C. O'Kane and R. Ribchester for their input and criticisms. We also thank A. DiAntonio and S. Sigrist for providing the glutamate receptor antibodies and T. Gillispie for the confocal analysis. The hVAPB cDNA was obtained from MRC, Gene Service, Cambridge (UK).

Conflict of Interest statement. None declared.

FUNDING

This research was supported by grants from the Wellcome Trust, the Scottish Motor Neuron Disease Association and the Royal Society to G.P., in part by a NIH grant (ES014441) to B.Z. and in part by a NIH grant (NS030072) to V.B. J.W. is supported by an EPSRC/MRC pre-doctoral fellowship at the School of Informatics and K.P. by a MRC pre-doctoral fellowship.

REFERENCES

1. Talbot, K. (2002) Motor neurone disease. *Postgrad. Med. J.*, **78**, 513–519.
2. Bruijn, L.I., Miller, T.M. and Cleveland, D.W. (2004) Unraveling the mechanisms involved in motor neuron degeneration in ALS. *Annu. Rev. Neurosci.*, **27**, 723–749.
3. Rosen, D.R., Siddique, T., Patterson, D., Figlewicz, D.A., Sapp, P., Hentati, A., Donaldson, D., Goto, J., O'Regan, J.P., Deng, H.X. *et al.* (1993) Mutations in Cu/Zn superoxide dismutase gene are associated with familial amyotrophic lateral sclerosis. *Nature*, **362**, 59–62.
4. Nishimura, A.L., Mitne-Neto, M., Silva, H.C., Oliveira, J.R., Vainzof, M. and Zatz, M. (2004) A novel locus for late onset amyotrophic lateral sclerosis/motor neurone disease variant at 20q13. *J. Med. Genet.*, **41**, 315–320.
5. Nishimura, A.L., Mitne-Neto, M., Silva, H.C., Richieri-Costa, A., Middleton, S., Cascio, D., Kok, F., Oliveira, J.R., Gillingwater, T., Webb, J. *et al.* (2004) A mutation in the vesicle-trafficking protein VAPB causes late-onset spinal muscular atrophy and amyotrophic lateral sclerosis. *Am. J. Hum. Genet.*, **75**, 822–831.
6. Marques, V.D., Barreira, A.A., Davis, M.B., Abou-Sleiman, P.M., Silva, W.A., Jr, Zago, M.A., Sobreira, C., Fazan, V. and Marques, W., Jr (2006) Expanding the phenotypes of the Pro56Ser *VAPB* mutation: proximal SMA with dysautonomia. *Muscle Nerve*, **34**, 731–739.
7. Foster, L.J., Weir, M.L., Lim, D.Y., Liu, Z., Trimble, W.S. and Klip, A. (2000) A functional role for VAP-33 in insulin-stimulated GLUT4 traffic. *Traffic*, **1**, 512–521.
8. Kagiwada, S., Hosaka, K., Murata, M., Nikawa, J. and Takatsuki, A. (1998) The *Saccharomyces cerevisiae SCS2* gene product, a homolog of a synaptobrevin-associated protein, is an integral membrane protein of the endoplasmic reticulum and is required for inositol metabolism. *J. Bacteriol.*, **180**, 1700–1708.
9. Pennetta, G., Hiesinger, P.R., Fabian-Fine, R., Meinertzhagen, I.A. and Bellen, H.J. (2002) *Drosophila* VAP-33A directs bouton formation at neuromuscular junctions in a dosage-dependent manner. *Neuron*, **35**, 291–306.
10. Skehel, P.A., Martin, K.C., Kandel, E.R. and Bartsch, D. (1995) A VAMP-binding protein from *Aplysia* required for neurotransmitter release. *Science*, **269**, 1580–1583.
11. Soussan, L., Burakov, D., Daniels, M.P., Toister-Achituv, M., Porat, A., Yarden, Y. and Elazar, Z. (1999) ERG30, a VAP-33-related protein, functions in protein transport mediated by COPI vesicles. *J. Cell. Biol.*, **146**, 301–311.
12. Kuwabara, P.E. (2003) The multifaceted *C. elegans* major sperm protein: an ephrin signaling antagonist in oocyte maturation. *Genes Dev.*, **17**, 155–161.
13. Roberts, T.M. and Stewart, M. (1995) Nematode sperm locomotion. *Curr. Opin. Cell Biol.*, **7**, 13–17.
14. Kosinski, M., McDonald, K., Schwartz, J., Yamamoto, I. and Greenstein, D. (2005) *C. elegans* sperm bud vesicles to deliver a meiotic maturation signal to distant oocytes. *Development*, **132**, 3357–3369.

15. Brand, A.H. and Perrimon, N. (1993) Targeted gene expression as a means of altering cell fates and generating dominant phenotypes. *Development*, **118**, 401–415.
16. Torroja, L., Packard, M., Gorczyca, M., White, K. and Budnik, V. (1999) The *Drosophila* beta-amyloid precursor protein homolog promotes synapse differentiation at the neuromuscular junction. *J. Neurosci.*, **19**, 7793–7803.
17. Elia, A.J., Parkes, T.L., Kirby, K., St George-Hyslop, P., Boulianne, G.L., Phillips, J.P. and Hilliker, A.J. (1999) Expression of human FALS SOD in motorneurons of *Drosophila*. *Free Radic. Biol. Med.*, **26**, 1332–1338.
18. Petersen, S.A., Fetter, R.D., Noordermeer, J.N., Goodman, C.S. and DiAntonio, A. (1997) Genetic analysis of glutamate receptors in *Drosophila* reveals a retrograde signal regulating presynaptic transmitter release. *Neuron*, **19**, 1237–1248.
19. Schuster, C.M., Ultsch, A., Schloss, P., Cox, J.A., Schmitt, B. and Betz, H. (1991) Molecular cloning of an invertebrate glutamate receptor subunit expressed in *Drosophila* muscle. *Science*, **254**, 112–114.
20. Marrus, S.B., Portman, S.L., Allen, M.J., Moffat, K.G. and DiAntonio, A. (2004) Differential localization of glutamate receptor subunits at the *Drosophila* neuromuscular junction. *J. Neurosci.*, **24**, 1406–1415.
21. Qin, G., Schwarz, T., Kittel, R.J., Schmid, A., Rasse, T.M., Kappei, D., Ponimaskin, E., Heckmann, M. and Sigrist, S.J. (2005) Four different subunits are essential for expressing the synaptic glutamate receptor at neuromuscular junctions of *Drosophila*. *J. Neurosci.*, **25**, 3209–3218.
22. Featherstone, D.E., Rushton, E., Rohrbough, J., Liebl, F., Karr, J., Sheng, Q., Rodesch, C.K. and Broadie, K. (2005) An essential *Drosophila* glutamate receptor subunit that functions in both central neuropil and neuromuscular junction. *J. Neurosci.*, **25**, 3199–3208.
23. Kanekura, K., Nishimoto, I., Aiso, S. and Matsuoka, M. (2006) Characterization of amyotrophic lateral sclerosis-linked P56S mutation of vesicle-associated membrane protein-associated protein B (VAPB/ALS8). *J. Biol. Chem.*, **281**, 30223–30233.
24. Weir, M.L., Xie, H., Klip, A. and Trimble, W.S. (2001) VAP-A binds promiscuously to both v- and tSNAREs. *Biochem. Biophys. Res. Commun.*, **286**, 616–621.
25. Fox, L.E., Soll, D.R. and Wu, C.F. (2006) Coordination and modulation of locomotion pattern generators in *Drosophila* larvae: effects of altered biogenic amine levels by the tyramine beta hydroxlyase mutation. *J. Neurosci.*, **26**, 1486–1498.
26. Wang, J.W., Soll, D.R. and Wu, C.F. (2002) Morphometric description of the wandering behavior in *Drosophila* larvae: a phenotypic analysis of K+ channel mutants. *J. Neurogenet.*, **16**, 45–63.
27. Hart, P.J. (2006) Pathogenic superoxide dismutase structure, folding, aggregation and turnover. *Curr. Opin. Chem. Biol.*, **10**, 131–138.
28. Bruijn, L.I., Houseweart, M.K., Kato, S., Anderson, K.L., Anderson, S.D., Ohama, E., Reaume, A.G., Scott, R.W. and Cleveland, D.W. (1998) Aggregation and motor neuron toxicity of an ALS-linked SOD1 mutant independent from wild-type SOD1. *Science*, **281**, 1851–1854.
29. DiAntonio, A. (2006) Glutamate receptors at the *Drosophila* neuromuscular junction. *Int. Rev. Neurobiol.*, **75**, 165–179.
30. DiAntonio, A., Petersen, S.A., Heckmann, M. and Goodman, C.S. (1999) Glutamate receptor expression regulates quantal size and quantal content at the *Drosophila* neuromuscular junction. *J. Neurosci.*, **19**, 3023–3032.
31. Nishimura, A.L., Al-Chalabi, A. and Zatz, M. (2005) A common founder for amyotrophic lateral sclerosis type 8 (ALS8) in the Brazilian population. *Hum. Genet.*, **118**, 499–500.
32. Caughey, B. and Lansbury, P.T. (2003) Protofibrils, pores, fibrils, and neurodegeneration: separating the responsible protein aggregates from the innocent bystanders. *Annu. Rev. Neurosci.*, **26**, 267–298.
33. Teuling, E., Ahmed, S., Haasdijk, E., Demmers, J., Steinmetz, M.O., Akhmanova, A., Jaarsma, D. and Hoogenraad, C.C. (2007) Motor neuron disease-associated mutant vesicle-associated membrane protein-associated protein (VAP) B recruits wild-type VAPs into endoplasmic reticulum-derived tubular aggregates. *J. Neurosci.*, **27**, 9801–9815.
34. Shao, J. and Diamond, M.I. (2007) Polyglutamine diseases: emerging concepts in pathogenesis and therapy. *Hum. Mol. Genet.*, **16**, R115–R123.
35. Spradling, A.C. and Rubin, G.M. (1982) Transposition of cloned P elements into *Drosophila* germ line chromosomes. *Science*, **218**, 341–347.
36. Ausubel, F.M., Brent, R., Kingston, R.E., Moore, D.D., Seidman, J.G., Smith, A.J. and Struhl, K. (1998) *Current Protocols in Molecular Biology*, John Wiley & Son, New York.
37. Stewart, B.A., Atwood, H.L., Renger, J.J., Wang, J. and Wu, C.F. (1994) Improved stability of *Drosophila* larval neuromuscular preparations in haemolymph-like physiological solutions. *J. Comp. Physiol. [A]*, **175**, 179–191.
38. Zhang, B., Koh, Y.H., Beckstead, R.B., Budnik, V., Ganetzky, B. and Bellen, H.J. (1998) Synaptic vesicle size and number are regulated by a clathrin adaptor protein required for endocytosis. *Neuron*, **21**, 1465–1475.
39. Koh, Y.H., Popova, E., Thomas, U., Griffith, L.C. and Budnik, V. (1999) Regulation of DLG localization at synapses by CaMKII-dependent phosphorylation. *Cell*, **98**, 353–363.
40. Budnik, V., Koh, Y.H., Guan, B., Hartmann, B., Hough, C., Woods, D. and Gorczyca, M. (1996) Regulation of synapse structure and function by the *Drosophila* tumor suppressor gene *dlg*. *Neuron*, **17**, 627–640.